



HAL
open science

Filamentary plasma discharge inside water : initiation and propagation of a plasma in a dense medium

Paul Ceccato

► **To cite this version:**

Paul Ceccato. Filamentary plasma discharge inside water : initiation and propagation of a plasma in a dense medium. Engineering Sciences [physics]. Ecole Polytechnique X, 2009. English. NNT : . pastel-00005680

HAL Id: pastel-00005680

<https://pastel.hal.science/pastel-00005680>

Submitted on 11 Jan 2010

HAL is a multi-disciplinary open access archive for the deposit and dissemination of scientific research documents, whether they are published or not. The documents may come from teaching and research institutions in France or abroad, or from public or private research centers.

L'archive ouverte pluridisciplinaire **HAL**, est destinée au dépôt et à la diffusion de documents scientifiques de niveau recherche, publiés ou non, émanant des établissements d'enseignement et de recherche français ou étrangers, des laboratoires publics ou privés.

PhD report of Paul CECCATO

« Pour le titre de docteur en physique de l'Ecole Polytechnique
Mention physique et applications
Ecole doctorale EDX

MICROPLASMAS DE CAVITATION EN MILIEU FLUIDE CONDENSE :
APPLICATION A LA PURIFICATION DE L'EAU »

Filamentary plasma discharge inside water : initiation and propagation of a plasma in a dense medium

Jury members:

- Anne Bourdon EM2C Ecole Centrale France
- Bill Graham Queen's University Belfast UK
- Svetlana Starikovskaya LPP Ecole Polytechnique France

Referee members:

- Peter Bruggeman Eindhoven University of Technology Netherlands
- Olivier Lesaint G2E Université Grenoble France

Achieved at the LPP laboratory in Ecole Polytechnique Palaiseau (Paris) France
2006-2009

supervisor: Antoine Rousseau



Thanks

Thanks first to all to the cold plasma team

Thanks Antoine Rousseau for the PhD thesis funding

Thanks Olivier Guaitella for the experimental and moral support

Thanks Joseph Youssef for sharing the experimental room

Thanks Philippe Auvray for help

Thanks Jean Larour for multiple technical solutions and discussions

Thanks Pierre Ledellieu for dedicated experimental work

Thanks Mikael Baudier for reactor design and realisation

Thanks all laboratory personnel in a general way

Thanks Lucas Shaper for a challenging experimental campaign

Thanks to Svetlana Starikovskaya, Olivier Lesaint, Peter Bruggeman to have read this report and made useful comments,

Thanks to the other members of the jury

Thanks Bill Graham for you enthousiasm

Thanks to Dr Bruggeman, Dr Locke, Dr Lukes, Dr Graham, Dr Babaeva, Dr Lesaint, Dr Beroual, Dr Koslov for interest and usefull discussions in internationnal scientific conferences.

Did I missed someone?

Summary:

This thesis presents an experimental study of a filamentary microplasma discharge inside liquid water. Such plasmas are used for liquid electrical insulations tests and for pollution control of water. Plasmas inside dense media are less understood than discharge inside gases. The purpose of the present thesis is to understand the physical mechanisms responsible for initiation and propagation of the discharge. A point to plane electrode configuration submerged in water has been constructed and was submitted to a high voltage pulse. Filaments inception and propagation and several discharges modes have been characterized with electrical measurements and time resolved nanosecond imaging. A Shadow diagnostic using 2 iCCDs was implemented to study the gas content and the shock wave emission from the discharge. The influence of the applied voltage polarity and the water conductivity was investigated. Spectroscopic measurements were performed on the OH emission band and the hydrogen emission lines.

At positive high voltage the growth of the discharge begins by the nucleation of a microbubble at the needle electrode within a few microseconds at an applied voltage of 40kV, a hemispheric tree like filamentary structure grows at 3km/s during 100ns and is followed by the propagation of second filamentary structure ten time faster. This continuous propagation on a nanosecond time scale is followed by a stepwise propagation in case of distilled water. When the filaments reach the opposite electrode electrical breakdown occurs. At negative polarity the discharge is much slower 600m/s. The morphology of the gas cavity is driven by interface instability. Curiously, water conductivity has no influence at positive voltage polarity and even inhibits the propagation of the plasma filaments at negative voltage polarity.

This thesis made possible to achieve a better understanding of the detailed phenomenology of electrical discharges in water.

Résumé:

Il s'agit de l'étude expérimentale d'un microplasma dans l'eau liquide. Ce type de plasma est rencontré dans les domaines de l'isolation électrique par liquides diélectrique ou la dépollution de l'eau. Les plasmas en milieu liquide sont bien moins connus et maîtrisés qu'en milieux gazeux. L'objectif de cette thèse est de comprendre les mécanismes physiques sous jacents à l'initiation et à la propagation de la décharge. Un réacteur pointe/plan a été réalisé et soumis à un pulse de haute tension. L'initiation et la propagation des différents modes de décharge plasma à travers le milieu liquide ont été caractérisés par des diagnostics électrique et d'imagerie rapide nanoseconde. Un diagnostic d'ombroscopie à deux iCCD a également été réalisé afin d'observer le contenu gazeux non lumineux de la décharge et l'émission d'ondes de choc. Nous avons principalement testé l'influence de la polarité de la tension appliquée ainsi que l'influence de la conductivité de l'eau. Des mesures spectroscopiques ont été réalisées sur la bande d'émission de OH et les lignes de l'hydrogène.

En polarité positive, une bulle micrométrique est nucléé à la pointe en quelques microsecondes puis une décharge filamentaire se propage à 3km/s durant typiquement 100ns, suivie par une décharge dix fois plus rapide. A basse conductivité, cette propagation continue est suivie par une propagation par bonds. Le claquage de l'intervalle de liquide est obtenu quand les filaments parviennent à la contre-électrode. La décharge en polarité négative est beaucoup plus lente à 600m/s. Curieusement la conductivité de l'eau n'a aucune influence sur la décharge en polarité positive et inhibe la propagation en polarité négative.

Cette étude apporte une meilleure compréhension de la phénoménologie détaillée de la décharge plasma dans l'eau.

Filamentary plasma discharge inside water : initiation and propagation of a plasma in a dense medium

| | | |
|------|--|-----|
| 1 | General introduction | |
| 1.1 | The plasma state..... | 6 |
| 1.2 | Cold plasmas in industry..... | 7 |
| 1.3 | Filamentary plasmas | 7 |
| 1.4 | Pollution control by plasma processes in gases | 7 |
| 1.5 | Plasmas in water | 8 |
| 1.6 | Purpose of the present thesis..... | 12 |
| 1.7 | Brief overview of this report..... | 12 |
| 2 | Discharges inside water, state of the art, synthesis and discussion | |
| 2.1 | Electrode configurations: homogeneous field, inhomogeneous fields, small gaps and large gaps, streamer, spark, arcs..... | 15 |
| 2.2 | Chemical yield of plasma inside water | 20 |
| 2.3 | Discharges modes and classification | 26 |
| 2.4 | Influence of experimental parameters: parametric experimental studies performed in literature | 35 |
| 2.5 | Electrostatic considerations | 45 |
| 2.6 | The liquid state and its ability to withstand electron avalanches: from gases to liquids and vice versa..... | 48 |
| 2.7 | Bubble processes..... | 63 |
| 2.8 | Interface processes | 72 |
| 2.9 | Summary on the mechanisms for initiation and propagation | 77 |
| 2.10 | Purpose of this work: a fine time resolved study of the case of water..... | 80 |
| 3 | experimental setup and experimental procedures | |
| 3.1 | Reactors..... | 82 |
| 3.2 | Electrical | 88 |
| 3.3 | Emission imaging..... | 93 |
| 3.4 | Transmission imaging..... | 98 |
| 3.5 | Spectroscopy | 103 |
| 4 | The positive polarity | |
| 4.1 | General description of the positive mode: primary mode, secondary mode, reillumination, post discharge | 108 |
| 4.2 | Electrical characterization, discharge current | 111 |
| 4.3 | Initiation of the discharge for positive polarity..... | 115 |
| 4.4 | Propagation of the positive mode | 122 |
| 4.5 | Discussion and conclusions on the positive mode..... | 153 |
| 5 | The slow negative mode | |
| 5.1 | The QUB low voltage discharge..... | 157 |
| 5.2 | The HV point to plane negative mode | 163 |
| 5.3 | Conclusions on the negative polarity modes | 180 |
| 6 | General conclusions on the negative and the positive modes | |
| 7 | references | |
| 7.1 | Plasma discharges inside water and liquids dielectrics..... | 186 |
| 7.2 | Streamers in gases, DBD, ozone production | 199 |
| 7.3 | Soft matter, bubble motion | 201 |
| 7.4 | Electrotechnical..... | 202 |

| | | |
|-------|---|----|
| 1 | General introduction | |
| 1.1 | The plasma state..... | 6 |
| 1.2 | Cold plasmas in industry..... | 7 |
| 1.3 | Filamentary plasmas | 7 |
| 1.4 | Pollution control by plasma processes in gases | 7 |
| 1.4.1 | Some history | 7 |
| 1.4.2 | Principle of pollution control by plasma discharge | 8 |
| 1.4.3 | Applications of plasmas for environment purpose | 8 |
| 1.5 | Plasmas in water | 8 |
| 1.5.1 | Plasma in dielectric liquids in general : HV lines, switches and power transformers | 8 |
| 1.5.2 | Plasma in water for pollution control..... | 10 |
| 1.5.3 | Plasma in water for medical application..... | 10 |
| 1.5.4 | Physical aspects of plasmas inside liquids..... | 10 |
| 1.6 | Purpose of the present thesis..... | 12 |
| 1.7 | Brief overview of this report..... | 12 |

1 General introduction

1.1 The plasma state

Plasma is an **ionized gaseous state** of the matter that reacts to electromagnetic stimulations. It has electromagnetic, chemical and fluid properties. Plasmas are widely spread in nature and are one of the main constituent of the universe: interstellar and stellar matter are mostly plasma state. On earth “natural plasmas” are not so common and are mostly produced artificially: they are naturally present only on the high atmosphere and in lightening. **Artificial plasmas** on the opposite are widely spread in multiple domains, and are used in a daily basis for high techs industrial processes such as microelectronic industry, surface treatment, propulsion....

From the physical point of view, the plasma state has very wide phenomenology and can be studied from many points of view: **atomic and molecular physics for collisions and spectroscopy, Hamiltonian physics and chaos theories, fluid motion and diffusion, electromagnetic properties and space charge separations, chemical processes**. The plasma state is highly **non linear** since the particles motion is dictated by the electromagnetic fields through Laplace and Coulomb forces, the individual motion of particles leads to charges and current distributions, and those distribution are the cause of the electromagnetic fields. Thus, most of the time the plasma state is non linear (ionization and chemistry), self organised (space charge separation, electric potential reorganisation) or turbulent.

The generic denomination of “ionized matter” can easily make one forget that the plasma state exists in an very wide range of physical parameters: from high pressure of hundreds of atmosphere to ultravacuum, from purely electrostatic to highly magnetised, steady state or pulsed, wave/particles interaction, thermal or non thermal.... Several classifications can be distinguished: as a function of **pressure, degree of ionization, electronegativity, magnetisation, electron temperature**... Each family of plasma state has its own set of physical parameters, in the case of non thermal plasma the electron temperature, the electronegativity, and the neutral density are the most relevant parameters.

The **chemically reactive** plasmas have a typical electronic temperature of several **eV** to achieve ionization, excitation and dissociation reactions. Those types of plasmas can be homogeneous or inhomogeneous depending on the operating pressure.

1.2 Cold plasmas in industry

Microelectronic industry uses plasma in a daily basis and modern microelectronics and personal computers would simply not exist without plasma physics. Many common multimedia goods are directly related to the plasma industry: flat screens, CPU, GPU, motherboard chipsets, phones, RAM... This microelectronic industry uses plasma reactors for etching of silicon wafers or deposition of thin layers to create active surfaces such as solar panels. The plasma sources are CCP or ICP reactors that use respectively capacitive and inductive coupling.

Lightning industry has largely invested in plasma technology and energy efficient bulbs without toxic compound are now available for the market.

A growing branch of the plasma industry is the **surface treatment** of metal and polymers. The surface energy modification by plasma treatment is of most importance for wetting of polymer surfaces in food industry.

A yet to come commercial application of plasma is the **pollution control** and **sterilization** applications. Car manufacturers have dedicated years of research and development to treat car exhausts by plasma, to realise plasma assisted combustion in engines, and to treat the indoor air. The sterilization of medical tools by plasmas or the plasma scalpels are just at the beginning or their commercial implementation. Pollution control by plasma is also not yet implemented in Europe. Japan has some advance and several fish industries are already using tens of kW installations dedicated to odour removal by combination of a catalytic and a plasma stage. The indoor air treatment by plasma is not yet successfully implemented as a truly working prototype that has a real pollution removal efficiency and a real benefit influence on human health.

1.3 Filamentary plasmas

Low cost **industrial** plasma processing requires working at **atmospheric pressure** in order to avoid any vacuum system. However, at atmospheric pressure, the discharge physics is driven by a mechanism called the streamer mechanism that lead to filamentary plasma structure. The **Townsend** mechanism that usually causes homogenous plasma is unfortunately only valid for low pressure**size* (Pd) values. For high Pd values the space charge generated by the primary **electron avalanches** begins to self organise and gives a **filamentary** plasma structure [Kogelshatz]. This filamentation is a universal feature of atmospheric pressure non thermal plasmas. It can only be avoided in some very specific cases (UV irradiations, noble gases, high electron secondary emission [Fassines] [Marode]) that are not much relevant for industrial applications (except the new pulsed repetitive nanosecond discharges [Pai]). The **non homogeneous** treatment obtained can be a difficulty for surface treatment where homogeneity of the processed area is an important requirement.

1.4 Pollution control by plasma processes in gases

1.4.1 Some history

The first industrial scale application of non thermal plasmas in France dates back to the beginning of the 20th century, it was used in Paris for **drinking water** cleaning [Kogelshatz]. Plasma was even used well before, in the 19th century, for **ozone generation** and its supposed medical virtues on (unfortunates) patients.

1.4.2 Principle of pollution control by plasma discharge

Plasmas are a physical way to **produce chemically active species** from a neutral medium and using only electrical input power. In air filamentary plasmas produce very high reduced electric field that dissociates O₂ molecules by electron impact. This dissociation is much more efficient with filamentary plasmas than in a homogeneous one. The atomic oxygen resulting from electron impact dissociation has very high oxidative properties. In humid air electron impact can also produce **atomic oxygen** and **hydroxyl radical** by **dissociative excitation**. O and OH are transient chemical species that have very **strong oxidative properties** compared to classical neutral oxidant molecules. The plasma can also produce more complex ionic species such as O₂⁻ or N₄⁺. Those chemical radicals can then diffuse and react with any organic molecule. The organic molecule is thus split and transformed into organic smaller molecules called **byproducts** (for polymerisation application it is the opposite). Those intermediates can also react and be ultimately destroyed and **mineralised** into CO, CO₂ and H₂O. The CO₂/CO ratio needs to be maximal in order to avoid the toxic CO molecule. CO₂ is produced but it is the natural purpose of depollution: one want to destroy a complex toxic organic molecule into neutral CO₂ with is completely harmless for human **health** (at moderate concentration and neglecting global warming of course).

1.4.3 Applications of plasmas for environment purpose

- Ozonizer are widely known and used for decades
- Indoor air cleaning for car or buildings,
- Waste treatment by plasma torches and vitrification of nuclear solid waste
- Treatment of industrials gas waste
- Liquid waste treatment, water cleaning, dye removal
- Sterilisation for drinking water

1.5 Plasmas in water

1.5.1 Plasma in dielectric liquids in general : HV lines, switches and power transformers

Discharges in liquids have historically been studied by the **electrical engineering** community for **pulsed power** applications and high voltage insulation [Elizondo2003][Woodworth2003]. Discharges in **organic insulating liquids** are well known as “**partial discharges**”. Any low conductive liquid can be considered as a conductor or as an insulating medium depending on the timescale. The relevant time is the **Maxwell relaxation time** that is the ratio of the dielectric **permittivity** and the electrical **conductivity**. From the practical point of view an insulating liquid is characterized by its **dielectric strength**. This strength quantifies the voltage the medium is able to sustain without **breakdown**, it is a property related to the liquid nature, the applied voltage level and duration, and the interelectrode gap. The dielectric behaviour combined to the large dielectric permittivity are the reason why distilled water has been widely used as an insulating media for **high voltage pulse forming lines** on microsecond timescale in many pulse power systems as shown in **fig 1.1** and **fig 1.2**. The lines can sustain heavy electric stress and are quite compact due to the propagation velocity of the voltage wave in a water line. Applications of

those pulse forming lines are pinch machines, X diodes, railguns, etc. [Martin] [Rossi] [McGregor][Mesyat]

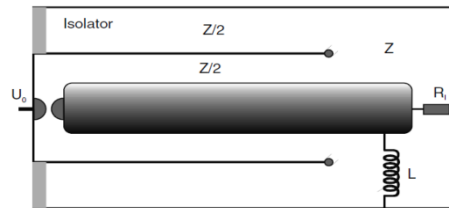


fig 1.1 schematic representation of a classical blumlein line, the liquid insulator between the center high voltage conductor and the ground external part can be distilled water because of its dielectric permittivity and its breakdown strength, [Power systems2006].

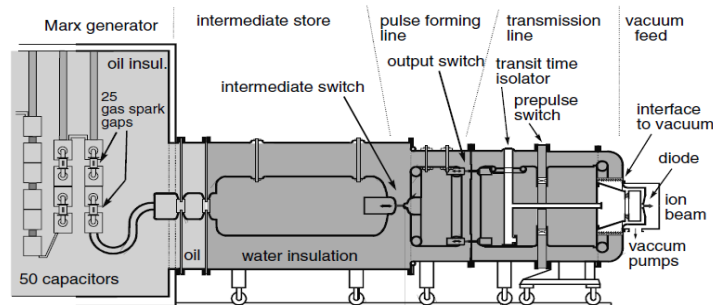


fig 1.2 schematic illustration of the 1.5TW pulse generator KALIF, 1.7MV, pulse duration 50ns, pulse energy 75kJ, electrical efficiency 30%, insulation is realized by oil in the Marx generator stage and by distilled water in the pulse transmission line, [Power systems2006].

The dielectric strength of usual dielectric liquids is better than insulating gases at a pressure of a few bar. Liquids are used for insulation not gases. Liquids can also be used for **closing switches** used as dielectrics for **spark gap** switches in pulsed power systems. Most pulsed power supply require a switching element with high voltage hold off level, high recovery rate, high frequency repetition rate, high current, short rise time, etc. The liquid plays the same role as pressurised gases such as air or SF₆ but have a significantly higher hold off voltage. The recovery is limited by the quenching of the gas channel by the liquid flow or by its hydrodynamic collapse. The electrode configuration is often symmetrical with sphere to sphere or plane to plane electrodes and short gap from 100μm to several cm. the shorter the interelectrode gap the lower the stray inductance of the arc and consequently the stray inductance of the switch itself to obtain better rise time. [Akiyama] [Ushakov]

Power transformers or electrical distribution in industry works in **AC** modes and are usually insulated with organic liquids such as castor oil, mineral oil, or classical **transformer oil** [Beroual]. Due to recent environmental issues, those insulating material are progressively replaced by ester liquids and an intense work of electrical characterisation of this new insulating material is being carried out by several electrical network industries in Europe and Canada [Fofana]. At the moment the power transformer community is moving from oils toward **esters**. The main scientific problems in this domain are the characterization of the dielectric strength, the ageing of the molecular liquid leading to a degradation of the **dielectric strength**, the **electroosmotic flows**, and the **tribo-charging** that can lead to electrical **failures**. The **ageing** of the material is mainly chemically induced. The partial discharges that occur in the organic liquids release by-products that have a lower molecular weight (number of carbon molecules) and thus a lower vaporization temperature and produce bubble **impurities** inside the medium. Those by-product molecules also have a different electronic affinity, ionisation potential, chemical reactivity and thermodynamic properties compared to the original long carbon chain molecules. Hence the ageing of the liquid due to partial discharges or time can lead to a modified

breakdown strength. The role of dissolved gas microbubbles and fibers impurities is of particular importance to avoid breakdown. Playing with surfactant, the hydrostatic pressure, or gas circulation over the liquid free surface can help. The control of dissolved gases can be made by forced liquid motion and the electroosmotic flow can help in this respect. The electroosmotic flow is an equivalent of the ionic wind in gas phase. The EHD flow arises from charged particles dissolved in the bulk liquid and accelerated by the applied electric field. [Beroual] [Fofana] [Atten] [Moreau] [Touchard]

1.5.2 Plasma in water for pollution control

Plasma discharges in water have a promising potential for pollution control in liquids. Hot electrons created in the non thermal plasma can **dissociate water** molecules and produce OH, H and O radicals from water molecule dissociation. Those **radicals** can diffuse in the surrounding liquid and be used for the removal of dissolved organic compound in a non selective way. They are able to **oxidize** any organic molecule into “harmless” carbon dioxide. The objectives of pollution control by plasma processes in liquids are to **remove dissolved organic compounds**.

The chemical reactivity of plasma inside water is very similar to plasma inside gases. This time, fast electrons are accelerated by high electric field collide on the water molecule. Electron impact dissociation of the water molecule leads to hydroxyl radical production. This hydroxyl radical has even higher oxidative properties than atomic oxygen and is also a short lived species that can diffuse and react with any organic molecules. The OH radical can recombine into H₂O₂ which is its stable form and is very similar to ozone in air plasmas. [Locke] [Lukes] [Grymonpre]

The objectives are the same as for gas pollution control: characterization of the radical production yield in function of the input power and optimisation of reactions paths and selectivity toward total oxidation.

1.5.3 Plasma in water for medical application

The **oxidative properties of plasma inside liquid** mean that plasma will obviously have some efficiency over biological proteins. OH can be used to etch the membrane of biological cells or to destroy viruses in order to perform liquid sterilization. In this respect plasma treatment is equivalent to UV irradiation [Locke].

The **shock wave** produced by arc discharge inside a liquid can be used for sonar systems or medical application. In this case the problem is to optimise the source shape. For military applications the source need to be punctual and thus the main problem is the electrode erosion [Fry1999]. For medical application as calculus fragmentation or tumour destruction, the problem is to focus the waves precisely to a specific region inside the biological tissues. The composite electrode developed in Prague for this purpose with ceramic plasma spraying enables to design any shape of source from cylindrical to paraboloidal, the obtained result is similar to alternative ultrasonic method [Lukes][Sunka].

Another medical application of plasma is to use the plasma as an **etching tool** for biological tissues. This plasma scalpel in saline liquid is able to etch flesh and clean wounds during surgical interventions. Such a tool is widely used in all US hospitals [Stalder] [Graham] [Shaper].

1.5.4 Physical aspects of plasmas inside liquids

In a general way, **plasma discharges inside liquids combine gas discharge physics, fluid thermodynamic properties and fluid or interface motion**.

In liquids the plasma **phenomenology** is wider than in gases because of the number of physical processes that can contribute to the discharge:

- **bulk processes** related to the liquid nature of the medium and its electronic state
- **surfaces processes** at the electrode/liquid interface
- **interface processes** at the plasma/liquid interface

The case of water is special among other liquids. Water presents a **low molecular weight** but differs strongly from liquefied noble gases at high pressure from the electronic state point of view. Water is a **highly polar** liquid and the **conductivity** is in competition with the dielectric behaviour of the medium. This last property is likely to explain the difference between plasma discharges in classical insulating liquid and discharges inside water.

In gases, the physical mechanisms of plasma discharge are well known and are based on the electron avalanche mechanism by Townsend mechanism [Raizer] at low pd (pressure*gap) values and streamer mechanism at high pd values. The problem with liquids is that the high density of such medium prevents electrons to accelerate and undergo dissociative collisions unless the electric field is several orders of magnitude higher compared to plasmas at atmospheric pressures [Atrazev] [Joshi] [Ushakov]. **Electron avalanches are almost impossible inside a liquid because of low mobility and high recombination rate** and one need to explain why plasma discharge occurs whereas the electronic state of the liquid is unfavourable. A **phase change** can be required prior to electron avalanches. Thus thermodynamics can play a role and can be coupled to gas discharge physics. Breakdown of liquids seems to have more in common with the **breakdown of solids** than gases.

1.6 Purpose of the present thesis

The present study is an attempt to **clarify the initiation and propagation mechanisms** of a plasma discharge inside water. **Electrical diagnostics and fast imaging** has been performed in order to characterise the discharge and its growth as a function of several parameters and in particular the water conductivity. The experimental behaviour of the discharge will give some insight about the physical mechanisms responsible for the propagation of the discharge inside the liquid.

1.7 Brief overview of this report

- State of art:
 - Configurations of plasma inside liquids and different modes
 - liquid state and electrons
 - mechanisms responsible for plasma discharges
 - Attempts of streamer-like fluid numerical simulations
 - Electrostatic stress
 - Thermal processes and bubbles
 - Interfaces
- Experimental setup
 - Point to plane reactor with pulsed high voltage
 - Fast imaging: 1iCCD,2iCCD streak camera, shadow imaging
- Experimental results on the positive mode
 - Initiation of the discharge
 - Propagation velocity of the primary mode and the secondary mode
 - Influence of the water conductivity
 - Reilluminations at low water conductivity
 - Shock wave emission
 - Channel expansion in post discharge
- Experimental results on the negative mode
 - Comparison with the positive mode
- Synthesis and discussion: contribution of this study to a better understanding of plasma inside liquids

| | | |
|---------|---|----|
| 2 | Discharges inside water, state of the art, synthesis and discussion | |
| 2.1 | Electrode configurations: homogeneous field, inhomogeneous fields, small gaps and large gaps, streamer, spark, arcs..... | 15 |
| 2.2 | Chemical yield of plasma inside water | 20 |
| 2.3 | Discharges modes and classification | 26 |
| 2.3.1 | Contact glow electrolysis: a specific mode?..... | 27 |
| 2.3.2 | Fast modes vs slow modes classification?..... | 28 |
| 2.3.3 | Positive vs negative modes classification? | 30 |
| 2.3.4 | An example: Positives modes reported in oil liquids..... | 32 |
| 2.4 | Influence of experimental parameters: parametric experimental studies performed in literature | 35 |
| 2.4.1 | Influence of applied voltage polarity | 35 |
| 2.4.2 | Influence of electric field/applied voltage level..... | 35 |
| 2.4.3 | Influence of the dielectric permittivity of the liquid..... | 37 |
| 2.4.4 | Influence of applied voltage pulse duration..... | 37 |
| 2.4.5 | Influence of the gap: reactor impedance..... | 38 |
| 2.4.6 | Influence of the conductivity of the liquid..... | 39 |
| 2.4.7 | Influence of applied pressure | 40 |
| 2.4.8 | Influence of the liquid viscosity..... | 41 |
| 2.4.9 | Influence on the surface tension | 42 |
| 2.4.10 | Influence of liquid molecular structure..... | 42 |
| 2.4.11 | Influence of additives: electronic affinity and ionisation potential | 43 |
| 2.4.12 | Brief summary on the influence of experimental parameters..... | 44 |
| 2.5 | Electrostatic considerations | 45 |
| 2.6 | The liquid state and its ability to withstand electron avalanches: from gases to liquids and vice versa..... | 48 |
| 2.6.1 | Plasma discharge in gases..... | 48 |
| 2.6.1.1 | The Townsend gas discharge theory..... | 48 |
| 2.6.1.2 | The gas streamer theory | 50 |
| 2.6.2 | Electron avalanches in liquid phase: the liquid state, ionization, recombination | 56 |
| 2.6.2.1 | Conduction in dielectric liquids according to semiconductor analogy: electronic state and mobility | 56 |
| 2.6.2.2 | The dense gas approximation: field ionization, collisional ionization, electron energy losses | 58 |
| 2.6.2.3 | Gas content of the liquid, dissolved gas and microbubbles: impurities explain discharge propagation and morphology? | 61 |
| 2.7 | Bubble processes..... | 63 |
| 2.7.1 | Bubble motion..... | 63 |
| 2.7.1.1 | Rayleigh motion: natural oscillation frequency..... | 63 |
| 2.7.1.2 | Inertia-limited bubble expansion | 65 |
| 2.7.1.3 | Viscosity-limited bubble expansion..... | 66 |
| 2.7.2 | Bubble nucleation: electrostatic crack mechanism | 66 |
| 2.7.2.1 | Electro-thermally induced “holes” in the liquid “lattice” | 66 |
| 2.7.2.2 | Electrostatic stress and crack formation | 67 |
| 2.7.2.3 | Bubble elongation by electrostatic pressure | 70 |
| 2.7.3 | Bubble nucleation: Local joule heating and the microexplosive nucleation | 71 |
| 2.8 | Interface processes | 72 |

| | | |
|---------|---|----|
| 2.8.1 | Double layers : what happens at the interfaces according to electrochemistry | 72 |
| 2.8.2 | Charge injection from the metal electrode into the liquid | 74 |
| 2.8.2.1 | Cathode electronic processes | 74 |
| 2.8.2.2 | Anode electronic processes..... | 76 |
| 2.8.3 | Surface state: field injection, electrode melting, microdischarge, oxide layer breakdown and formation of a plasma spot close to the metal electrode | 77 |
| 2.9 | Summary on the mechanisms for initiation and propagation | 77 |
| 2.9.1 | Initiation mechanisms | 77 |
| 2.9.2 | Propagation mechanism | 78 |
| 2.10 | Purpose of this work: a fine time resolved study of the case of water..... | 80 |

2 Discharges inside water, state of the art, synthesis and discussion

This chapter presents:

- the several types of existing water discharges
- the experimental studies performed in literature
- electronic processes inside liquids
- bubble processes
- interfacial processes

We focus on all mechanisms relevant to explain the initiation and the propagation of a plasma discharge in a dense liquid medium.

Warning: this chapter is based on a little more than 500 papers read during the present PhD thesis. It can be found to be somehow oversized and without any obvious link with the following experimental work. However this chapter is representative of the time I spent to identify a relevant PhD topic and to dig the physical aspects behind this peculiar plasma discharge. It should be understood as short lecture on plasma inside liquids.

2.1 *Electrode configurations: homogeneous field, inhomogeneous fields, small gaps and large gaps, streamer, spark, arcs*

Here is an exhaustive presentation of the different electrode configuration used in literature to produce plasmas inside liquids based on [Locke2006] and [bruggeman2009] reviews.

Depending on the electrode configuration and in a more general way depending on the particular experimental setup, a wide phenomenology of plasma discharges inside liquids can be observed. For example for a given pulse duration the following setup in **fig 2.1** will lead to streamer or spark discharge. Both types of filaments can coexist at the same time.

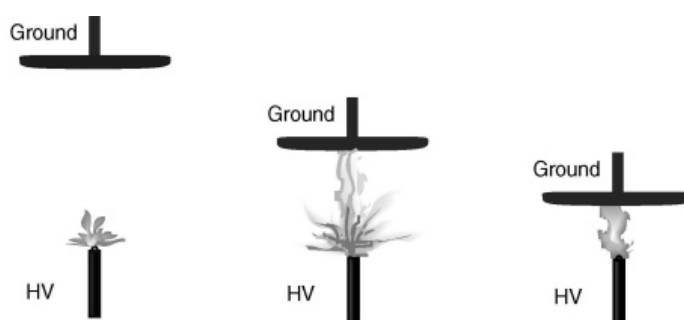


fig 2.1 streamer, spark, and arc regime in point to plane configuration [Locke2006].

The plasma in water grows as a partial discharge starting from the electrode and can be described as corona-like. The discharge is partial because it does not bridge the gap and is not a full breakdown of the gap. If the plasma is able to reach the opposite electrode, a conductive channel bridges the interelectrode gap and the power supply begins to supply as much current as it can. It will lead to a spark or an arc depending on the power supply. This spark is transient and thermalize into and arc only is the spark duration is long enough to allow time for the plasma channel fully thermalize (typically some microseconds).

One can distinguish between **breakdown in homogenous electric field** with symmetrical electrode configuration, and **breakdown in inhomogeneous electric field** with strongly asymmetric electrode configuration such as point to plane. Homogeneous electric field is difficult to achieve for long (cm) gaps at a level sufficient for plasma initiation. One needs to notice that short gaps in the range of hundreds of micrometers (often reported in literature as homogeneous field case) leads also to a different phenomenology compared to what can be observed in large gaps in the centimeter scale because initiation phenomena dominate over propagation phenomena. Some people classify breakdown in homogeneous versus inhomogeneous field, short gap versus long gap, short applied voltage pulses versus long pulses [Ushakov]. In fact we think that this classification is too close to the experimental point of view and a better classification has been made that distinguishes slow modes and fast modes, with initiation and propagation stages, and polarity effects [Beroual][Lesaint][Kolb]. This classification is quite universal and can be applied for most of the dielectric liquids. This latter classification will be presented in the following section.

Different kinds of discharge can be produced by playing with the power supply, the electrode inhomogeneity, the interelectrode gap, the presence of a gas or of a solid layer...

As a general rule, given the very high inception field of discharge in an insulating liquid or in water, one must rely on local electric field enhancement with low curvature radius electrode in order to ignite a plasma discharge. **Point to plane** and **cylinder to plane** are widely spread electrode configurations in gas phase discharges and are also employed in liquid discharges. The enhanced electrical field obtained with a 100 μ m wire and typical 50kV voltage for usual centimetre gap configuration allows to reach the MV/cm required for most of liquid discharge inception. The point to plane allows the study of a punctual source of chemical radical [Lukes] [Sun] from the chemical point of view or a single plasma filament emission point from the physical point of view. The wire to cylinder shown in **fig 2.11** allows to study the behaviour of several simultaneous adjacent plasma filaments and to scale up the discharge power and the treated volume of liquid [Akiyama].

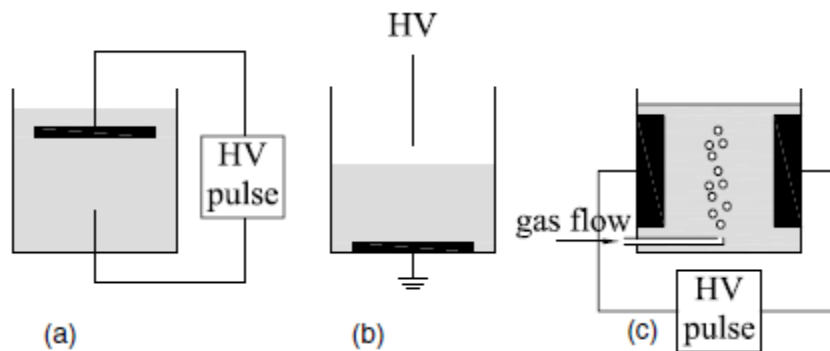


fig 2.2 plasma underwater, overwater, inside bubbles [bruggeman2009].

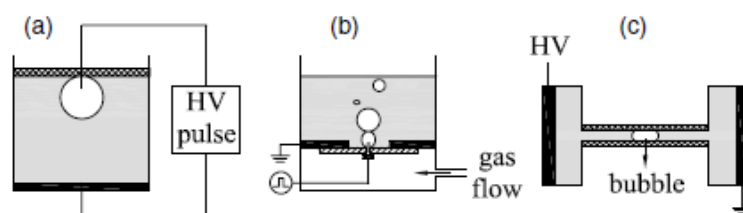


fig 2.3 capillary discharge reactor configurations [bruggeman2009].

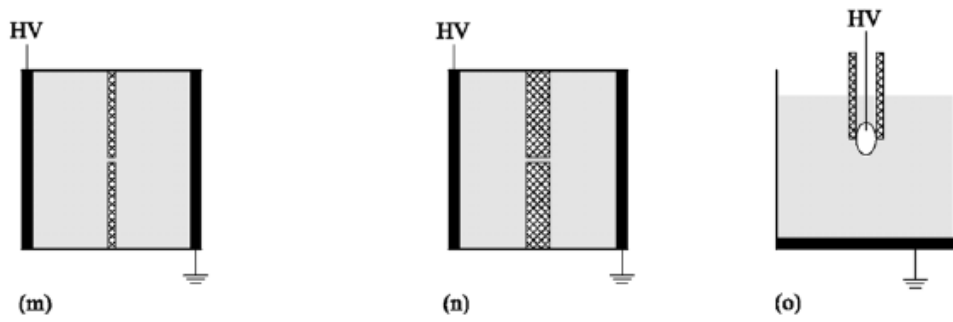


fig 2.4 diaphragm discharge reactor configuration [bruggeman2009].

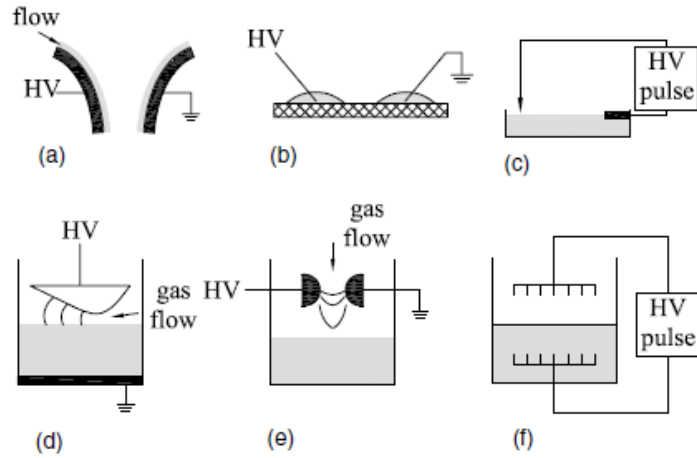


fig 2.5 several plasma overwater reactor configuration [bruggeman2009].

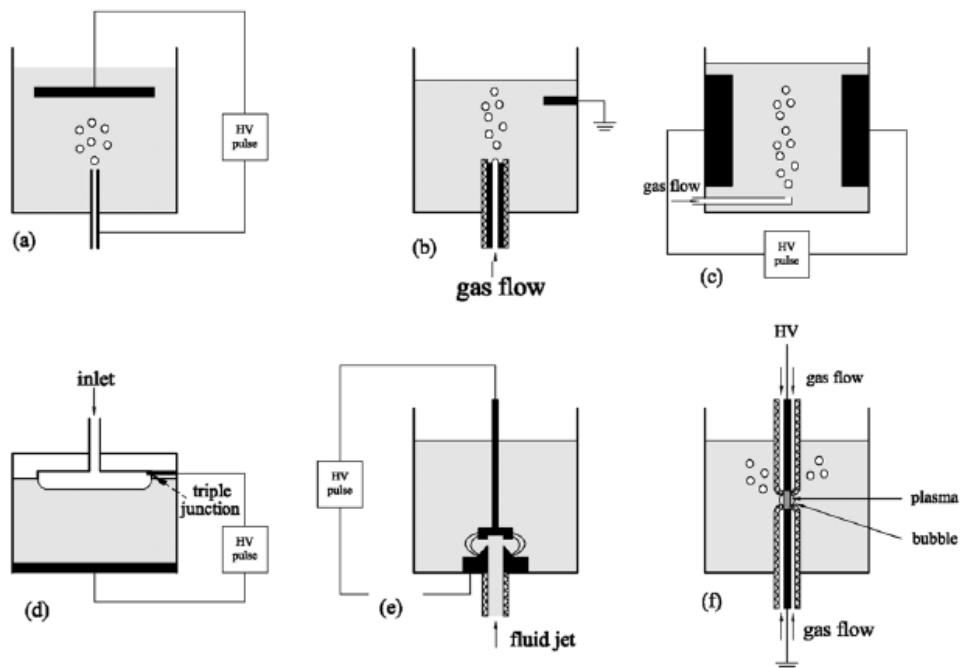


fig 2.6 gas injection reactor configuration [bruggeman2009].

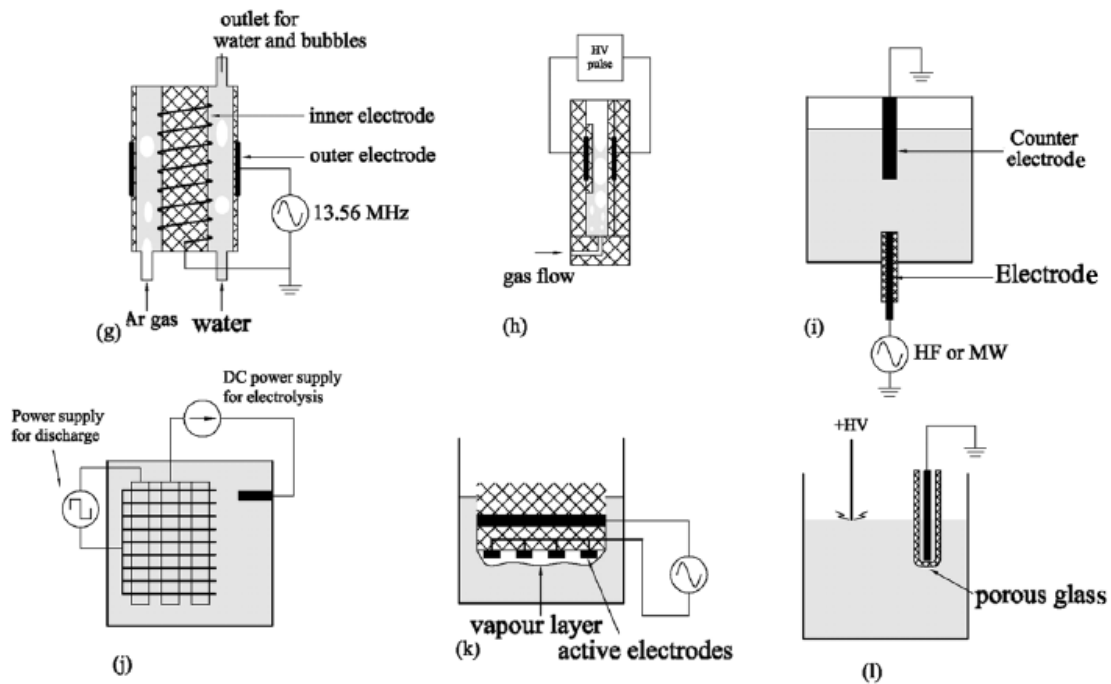


fig 2.7 glow discharge electrolysis reactors[bruggeman2009].

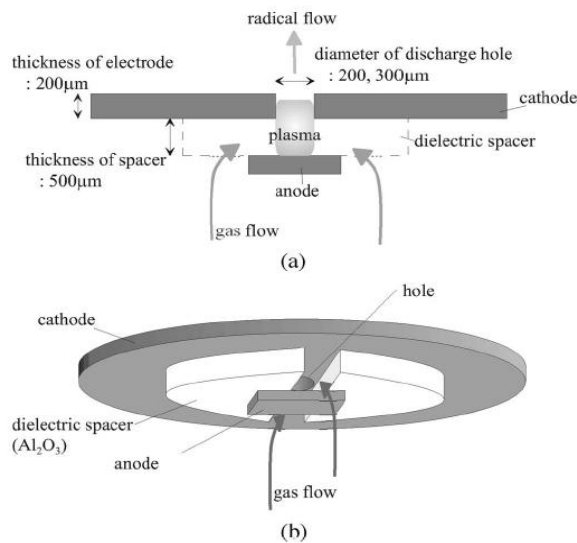


fig 2.8 microplasma discharge inside water with gas injection by the bottom of the microhole configuration, operating voltage of some hundreds of V [Yamatake2006].

Local electric field amplification can also be obtained at the junction of a dielectric layer and a metal. The **composite electrode** shown in fig 2.9 [Lukes] [Sunka] is a way to achieve local field amplification and large plasma volume at the same time as in the wire to cylinder case. The ceramic presence induces new chemical processes due to the ceramic adsorption properties, reactivity and porosity. It induces also new physical processes such as double layers [Sunka], and field screening as in a DBD. Such reactor can be operated at high power without observed electrode erosion and is close to industrial requirements [Lukes].

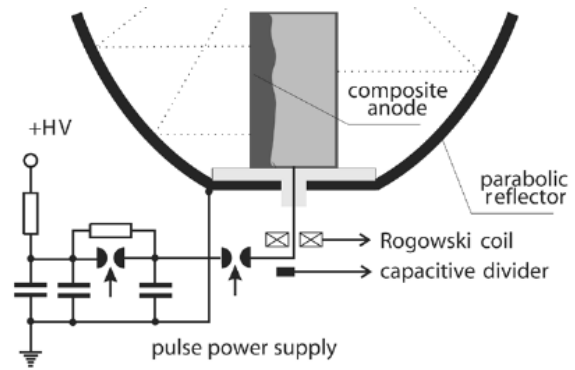
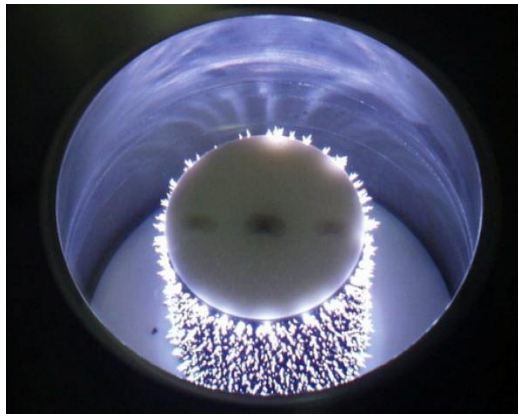


fig 2.9 cylinder to cylinder geometry, 2cm gap, composite electrode coated with porous ceramics by thermal plasma spraying, 20kV applied voltage, tap water, this configuration is a very good candidate for large scale water treatment by plasma discharges or shock wave emission [Lukes][Sunka], parabolic focalization of the emitted shock waves [Sunka2004], see also [Carnell1997].

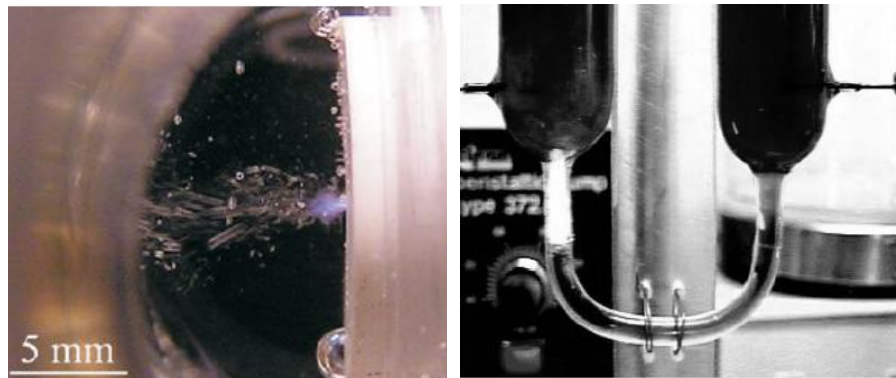


fig 2.10 diaphragm discharge, capillary of 5mm*0.5mm, 50 μ S/cm, 25W, [Baerdemaeker2007][Krema][Stara], capillary discharge [Maximov2006] [Nikiforov2007] [Leys].

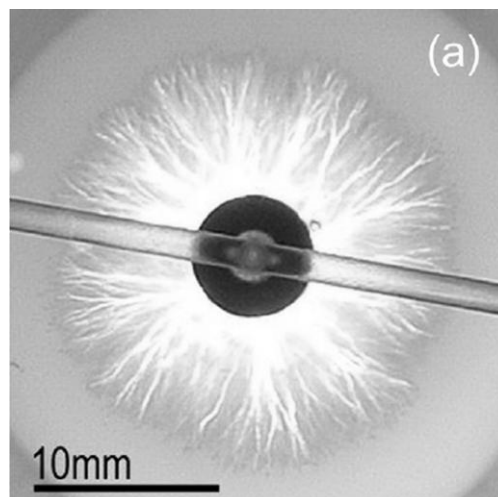


fig 2.11 wire to cylinder discharge in distilled water, tungsten wire diameter is 50 μ m, 80kV 400ns voltage pulse, [Kolb2008].

A **plasma discharge over an insulating liquid** such as in fig 2.2 or in fig 2.5 is easier to obtain from an electrotechnical point of view and can be useful to describe processes occurring at the plasma/liquid interface. It can also be used to treat the liquid with the absorption of the chemical products from the gas phase discharge and specific chemical reactivity at the gaseous

plasma/liquid interface. This configuration has been proved to be the most efficient for liquid pollution control by plasma processes [Bruggeman][Lesaint]. In corona over water, the plasma occurs in the gas phase and is filamentary depending on the working gas pressure. The liquid is equivalent to a series resistance and carries the discharge current through ionic mobility of solvated ions. In the DBD setup of plasma over liquid, the liquid can be used as an insulating layer if its conductivity is sufficiently low and if the voltage timescale is short enough. There can be adsorbed charged species on the liquid interface in this configuration that accumulate on the liquid surface and screen the electric field in the gap as in well known dielectric barrier discharges.

The combination of a plasma over and inside the liquid at the same time can be performed in an **hybrid reactor**. Such reactor needs to be designed carefully in order to control the amount of injected energy in the gas part and the liquid part. This kind of reactor has some advantages from the chemical point of view because of synergy between the two discharges.

The **arc** and the **gliding arc over water** in **fig 2.5** are similar to the corona over water case: the discharge is produced in a gas phase [Yan]. The plasma regime is thermal in this latter case. For a blown gliding arc, the post discharge region of the plasma is in contact with the liquid. On the contrary, for a gliding arc with water electrode there is direct contact of the plasma column with the liquid leading to a plasma/liquid active interface. The liquid nature of one electrode leads to different arc root constriction. In the same order of idea, plasma torches can be stabilised with water boundaries [Sunka].

The **contact glow electrolysis** [Yerokin] [Denaro1958] shown in **fig 2.7** is a thermal plasma layer around an immersed electrode in a highly conductive electrolyte (saline). This glow mode is obtained when an electrolysis is forced at high current regime as presented in more details in a following section. At high electrolysis current, a gaseous layer forms due to high local joule heating around the electrode and redox reactions. The plasma layer forms in this gas envelope. A stable mode is difficult to obtain. This configuration is widely claimed to realize cold fusion because of non faradic yield [Sengupta1998] due to the plasma presence in the system. More seriously the contact glow discharge electrolysis gives an insight on a plasma interaction with a liquid layer. This type of discharge has been extensively studied by the electrochemistry community in the 1950s with several electrode materials and geometries and several electrolytes. The main processes observed to occur at the plasma/liquid interface are ion impact into the liquid and not redox chemical reactions. The chemistry initiated by such discharge is similar to radicals obtained in α radiolysis chemistry [Yerokin] [Grymonpre].

The **diaphragm discharge** shown in **fig 2.4** is an “electrodeless” configuration: a small diameter dielectric opening separates the electrodes and the discharge is not in contact with any metal electrode. A strong current flow through this opening and joule heating nucleate a gas bubble, as soon as this gas bubble nucleates, the discharge can occur. The bubble expands or grows and the bubble is expelled from the opening and the discharge is quenched. The operating mode of such a discharge is always pulsed from the plasma point of view but can be obtained with DC voltage. The diaphragm discharge itself consists of a hole in a thin dielectric. At the opposite, the capillary discharge shown in **fig 2.3** uses a long tube, the current is concentrated in the tube, joule heating of the liquid occurs and a gas bubble is nucleated, the discharge occurs in this gas bubble. The diaphragm discharge can be used for liquid treatment or micropumping. This kind of experiment can be used to observe a slow mode, its initiation by gas bubble nucleation, the bubble motion, and the interaction between a filamentary plasma and a bubble interface [Bruggeman][Clupek][Maximov].

2.2 Chemical yield of plasma inside water

This section presents basic considerations about the chemical efficiency and chemical applications of underwater plasmas based on reviews [Bruggeman2009] [Locke2006] and papers

from [Grymonpre][Clements][Joshi][Lukes][Sun][Malik][Sato][Gogate][Wen][Tezuka] [Sugianto] [Skiguchi2003][Sahni2006][Namihira2003][Akiyama] [Katsuki] [Lisitsyn1999] [Lee] [Kuraika2004] [Hoeben1999][He2005][Mizeraczyk2006][Appleton][Yang][Sugianto][sahni2006][Perkowski2003] [Njatawidjaja2001][Mikula1997][Denat][kuraika2004][Glaze1982][Bing2005][Abou-Ghazala2002] [Adelhelm1999][Gao][He2005] [Hiroki2002] [Ihara1999] [Namihira2003]

We have already mentioned several times that water discharges can be applied for **water sterilisation or cleaning**. However their main field of expertise could be the treatment of pollutant impossible to destroy by conventional chemical or biological methods. Degradation of dye have been intensively studied from decades as it is widely spread aqueous liquid waste in textile industry [Sun]. In order to understand the fundamentals of plasma chemical efficiency underwater, simpler test molecules have been used by many authors [Locke2006] [Lukes][Sun][Malik][Sato]. One of the most commonly used is phenol since its chemistry is very well known and the by-products can be easily identified [Lukes].

From the chemical point of view underwater plasmas are able to produce:

- Production of oxidative species
- Flux of charged or heavy particles
- Pulsed electric field [Dickens2003]
- UV irradiation
- Shock waves
- Thermal effects (plasma underwater are usually quite hot “non thermal” plasmas)
- Those different effects play simultaneously a role in the global chemical yield of the discharge and synergy has been observed especially in hybrid reactors .

| Species | Oxidation potential (V) |
|-------------------------------|-------------------------|
| F ₂ | 3.03 |
| OH [•] | 2.80 |
| O [•] | 2.42 |
| O ₃ | 2.07 |
| H ₂ O ₂ | 1.78 |
| O ₂ H [•] | 1.70 |
| Cl ₂ | 1.36 |

fig 2.12 oxydation potentials [Lukes].

A detailed schematic of the chemistry relative to plasma inside or over water can be found in the recent review [Bruggeman2008] and is reproduced in **fig 2.14**.

Regarding the chemical species produced by the plasma itself, a plasma discharge in water produces locally many primary molecules from the water molecule dissociation. The water molecule is dissociated by inelastic electronic collision in the vaporised liquid or heavy ionic bombardment directly on the plasma/liquid interface. The mechanism of water dissociation in water is closely related on the discharge propagation mechanism. Water discharge is known to produce H, OH and O radicals. This primary source of radicals is often localised in a small region related to the size of the plasma discharge. Those radicals are highly reactive. Their **oxidation potentials** are one order of magnitude higher than usual chemical substances used to sterilise or to remove pollutants from the liquid phase such as peroxide, ozone or simply oxygen as shown in **fig 2.12**. Those short live radicals initiate a whole set of secondary reactions: pollutant oxidation, production of long live oxidant species and recombination/termination reactions. The **radicals or ions such as H O, OH, HO₂⁻ and O₂⁻** only have a localised action but the long live **species as H₂O₂ and O₃** can diffuse and react in the entire volume as illustrated by **fig 2.13** and **fig 2.14**.

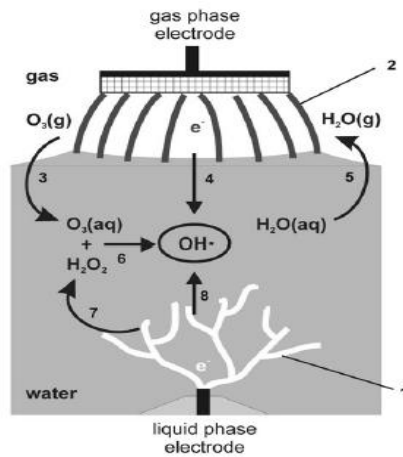


fig 2.13 production of active chemical species in a hybrid reactor [Lukes].

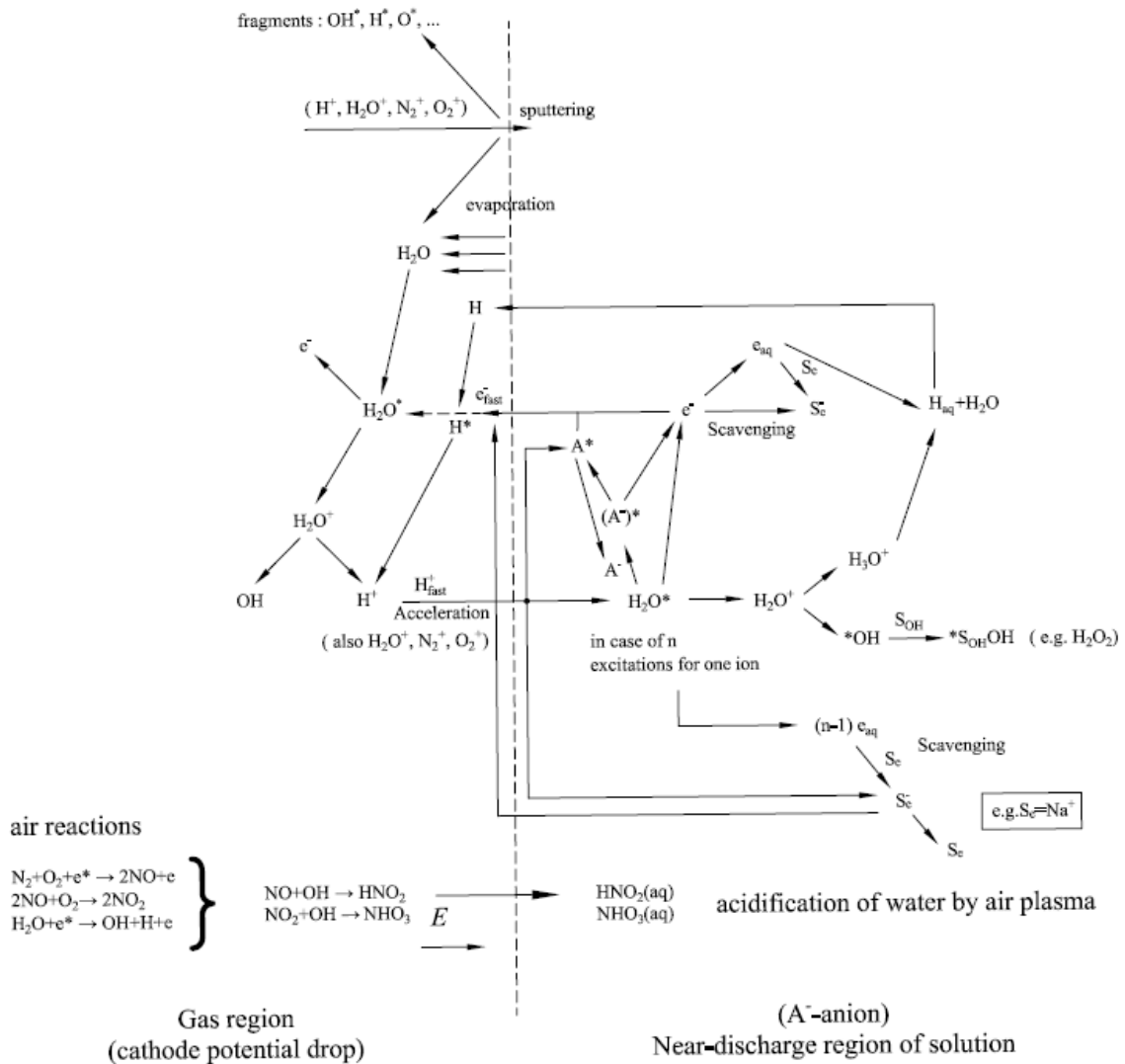


fig 2.14 chemical radical production path in water plasma discharges [Bruggeman2009].

A discharge over the liquid interface used as a ground plane produce chemical reactive such as O radical in dry air (OH in humid air) and its stable form O_3 that can cross the interface and oxidise the pollutant in the liquid phase. The weak point of those methods is the weak surface exchange between the plasma inside the gas phase and the liquid phase. The short live species

have almost no time to even reach the interface and even less chance to penetrate inside the liquid. The diffusion from the gas phase into the liquid phase can be realised by having a direct contact of the plasma and the liquid. The long lived species such as ozone will be able to diffuse into the liquid and achieve the desired oxidation. This ozone bubbling is known for a long time [Kogelshatz] but sometime ozone oxidative potential is not sufficient.

Simultaneous discharges in a gas phase and in the liquid phase have also been tested [Yang]. Those reactors are called hybrid series reactor and hybrid parallel reactor depending if the ground plane is at the gas/liquid interface or if the current must cross the interface [Sato] [Lukes]. A typical hybrid reactor is presented in **fig 2.13**. The reactions occurring in the liquid phase can be influenced by the reaction initiated by the plasma in the gas phase (and the other way around). For instance the short live species produced in the gas phase is O radical that gives the stable species O₃, in the liquid phase the short live species is OH radical that gives the stable species H₂O₂. When O₃ diffuse from the gas phase into the liquid, it reacts with H₂O₂ to give back OH radical. O₃ play a regeneration role as in the case of the Fenton reaction. However, the ozone production is quite quenched because of water vapour content of the humid air over the water surface. Conversely the H₂O present in the liquid will diffuse into the gas because of vapour saturation pressure of the liquid and lead to decomposition of O₃ into O radical and OH ion. Thus there is mutual enhancement of the gas phase reactivity and the liquid phase reactivity.

The presence of **UV emission** produced by the discharge itself is of special interest as it leads to photochemical reactions. UVs are able to oxide pollutant by direct photochemical attack or by water molecule dissociation. Regarding water sterilisation [Anpilov2002][Hancock2003], the UV are able to damage DNA or membrane of biological cells leading to cell death or apoptosis. This technique is already widely used in industry for sensitive liquid sterilisation and is in competition with ozone or chlorine treatment. The problem is that UV production by non thermal plasma is very inefficient unless excimer plasma mixtures are used. Arc discharges in water are quite thermal and are thus a quite more efficient way to produce UV through black body radiation instead of discrete line emission[Lukes].

The corona-like discharge produces moderate **shock waves** and the **arc** discharge produces very strong shock waves [Sunka]. These shocks can be used for solid waste treatment [Adelhelm1999] or solid fragmentation for oil duck drilling. Those shocks can also trigger some chemical reactions by violently compressing the gas content of the liquid. The chemical effect of the shock wave is widely described in sonoluminescence literature. Here the shock excitation is a dirac and there will be no resonance leading to the formation of a thermal plasma as in the case of sonoluminescence.

Arc discharge and non thermal discharges both produce the primary chemical radicals, but the arc also possesses a high gas **temperature**. This high temperature leads to pyrolysis of the pollutant in the discharge region. This is a pure thermal action. Some authors [Akiyama] reported that the energetic efficiency of an arc discharge for pollution control was higher compared to corona-like underwater plasmas. This result is quite surprising and is contradictory to the usual results obtained for pollution control in gases. This result can be explained as the following: The several reactivity sources of and arc discharge (radicals, thermal, UV, shock waves) leads to simultaneous reaction paths that can participate independently to the final total mineralization of the pollutant or there can be synergetic influence between those reaction paths (the by-products from one reaction path can be used in an other reaction path).

The **Fenton reaction** involves catalytic regeneration of OH radical from H₂O₂ molecule by ferrous solvated ions [Lukes]. This reaction is of particular importance when using electrodes containing iron. The primary active chemical radical produced by the plasma discharge in water is OH and the stable form of OH is H₂O₂ which is also a very good non selective oxidant. Unfortunately the oxidation potential of H₂O₂ is lower than OH and not all pollutant are destroyed by H₂O₂. However, when ferrous ions are introduced in the liquid the Fenton reaction occurs: the ferrous ion reacts with H₂O₂ to give back OH, it is thus a regeneration process.

Thanks to this Fenton reaction and H_2O_2 diffusion, OH becomes available over a large volume of liquid and this increases tenfold the yield. The ferrous ion can originate from electrode redox dissolution or erosion in the liquid, this fact must be taken into account when performing chemical measurement. This ion can also be manually added in the liquid. An example of the influence of dissolved ferrous ions on the destruction yield of phenol is given by **fig 2.18**.

The main problem from the chemical point of view is to:

- Optimise the primary radical production: the reaction rate of primary reactions can be enhanced by a more efficient discharge with higher reduced field and thus higher electron velocity, the volume of the discharge and its duration are also important to avoid to recombine without being able to use the radicals we have just produced as shown by the saturation in the **fig 2.15**.
- Optimise diffusion of the reactants: this diffusion of radicals and the subsequent diffusion of H_2O_2 and O_3 are important to treat a large volume of liquid and avoid termination reaction. Indeed those termination reactions decrease the energetic yield.
- Optimise reaction path: the reactions between by-products can have a synergetic effect that is to say lead to a more complete total oxidation of the pollutant. In addition, other simultaneous reactions can occur and lead to better total oxidation (UV, Fenton reaction).

The plasma is often very efficient for pollution removal but the yield and the selectivity are quite poor. The addition of a catalyst is required to enhance the yield or to enhance the selectivity toward total oxidation/mineralization. The addition of a catalytic media has been tested by several authors:

- Additives
- Solid porous catalyst
- Suspended solid catalyst

The usual catalysts are:

- photocatalyst such as TiO_2
- ceramics or zeolites
- activated carbon
- Metal particles or nano particles

As in gas discharges the introduction of catalyst can influence the final chemical yield in several ways:

- porosity effect that concentrate the pollutant in a localised region of the liquid, or increase of the residence time of the pollutant by adsorption on the pollutant
- activation of the catalyst that convert by-products or the pollutant itself
- modification of the discharge properties and thus modification discharge chemical reactivity

The reactor can be operated in flow mode to quantify the efficiency of a chemical process or as a closed system to study the order of the chemical reaction responsible for the test molecule mineralization. The chemical methods often used for analytical chemistry of water pollution control are:

- liquid chromatography (HPLC),
- gas chromatography (GC)
- colorimetric titration,
- pH measurement

Those methods are described in details in [Lukes PhD thesis].

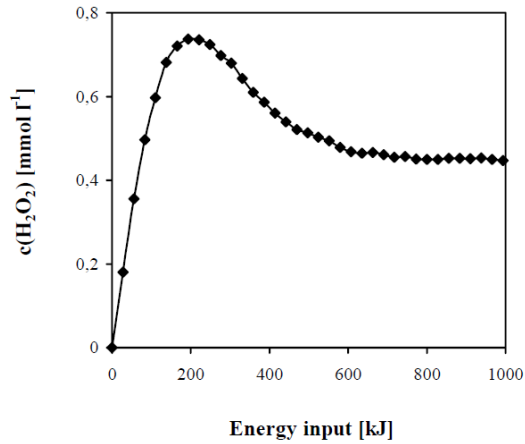


fig 2.15 production of H₂O₂ in H₂SO₄ (0.6mmol/L) solution with initial conductivity of 50mS/m, 24.5kV, 30Hz repetition frequency, 10.2nF capacitor, 92W continuous electrical power, point to plane electrode configuration [Lukes PhD], the linear production region is useful to quantify the chemical yield of the discharge, the saturation occurs because of recombination and termination reactions.

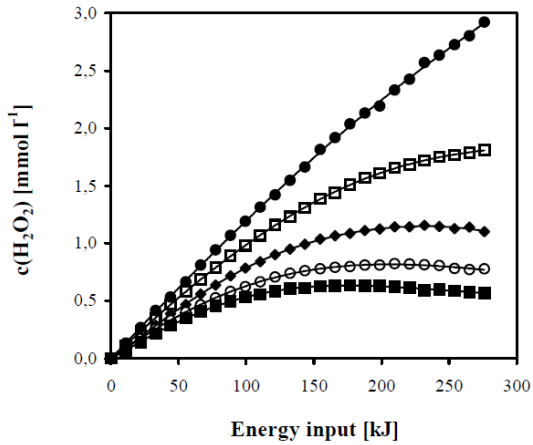


fig 2.16 effect of the initial solution conductivity on the production of H₂O₂ in H₂SO₄ solution at 92W, filled circles 10mS/m (19kV, 50Hz), respectively 20mS/m (20.5kV, 43Hz), 30mS/m (21.5kV, 39Hz), 40mS/m (23kV, 34Hz), 50mS/m (24.5kV, 30Hz), [Lukes PhD], the solution initial conductivity has a huge influence on the discharge chemical efficiency.

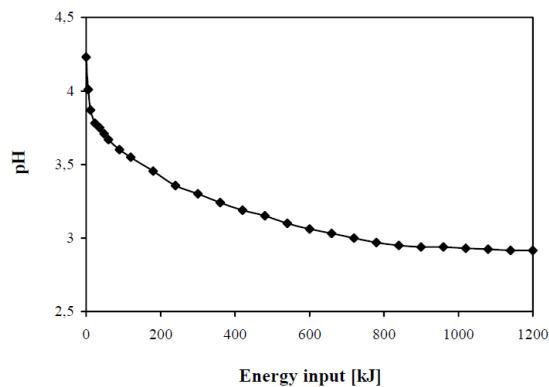


fig 2.17 change of pH value of the solution during degradation of 1mmol/L phenol by the corona discharge in presence of 0.5mmol/L Fe(ClO₄)₂, initial solution conductivity of 10mS/m, power input 100W, applied voltage 20kV, 50Hz, [Lukes PhD], pH drift is due to solvated ions resulting from the byproducts of phenol degradation and from released material in the solution because of electrode erosion.

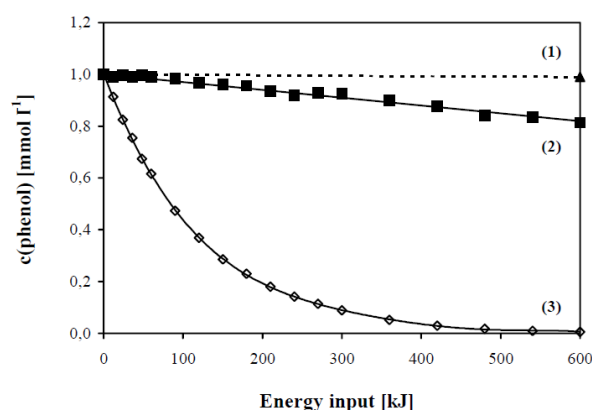


fig 2.18 phenol removal for (1) electrolysis only in 1mmol/l of NaCl, (2) corona discharge in 1mmol/L NaCl, (3) corona discharge in 0.5mmol/L of FeCl₂, power input of 100W, applied voltage 20kV, 50Hz,, initial solution conductivity of 11mS/m, phenol concentration of 1mmol/L, [Lukes PhD], fenton reaction has a huge synergetic effect on phenol degradation by plasma discharge.

Usually, the power input of the discharge is measured with electrical diagnostics and compared to the mineralization efficiency [Lukes] [Sato]. Thus the chemical yield of the discharge can be quantified as a function of electrical parameters, electrode configuration, duty cycle, molecule concentration, mixing of molecules... However, the power input is a global parameter that includes the energy lost due to heat dissipation in the liquid, evaporation of the liquid to create the plasma gas cavity, formation of the plasma itself, and at last the energy really spent for particle acceleration and dissociation used for the chemical reactions.

The main conclusion from chemical studies is that underwater plasmas are efficient for liquid treatment with a yield similar to the yield per molecule obtained in gas phase plasma treatment. Best energy efficiency is obtained by using a plasma over water. However, this **energy efficiency** is still in the **kWh/g of pollutant** range and must be associated to another complementary process for commercial use. Typically, for liquid treatment a first plasma stage followed by biodegradation stage seems to be good solution.

The other obstacle is the electrotechnical difficulty of the power supply: security is a problem due to the voltage level required, erosion of the electrodes due to the local high power level. Because of those unsolved difficulties, the use of conventional chemical method is much easier and is systematically chosen in industry. There is not yet widely commercial pulsed high voltage power supply developed for liquid discharges. However, some prototypes using magnetic compression have already been developed in gas phase treatment units.

The above figures from [Lukes] illustrate the obvious importance of the water conductivity for the chemical efficiency of the process and justify a physical study of the plasma discharge in water as a function of conductivity.

No chemical measurements have been performed in this thesis. The first orientation of this thesis topic was at first the pollution control efficiency of plasmas inside water but quickly the topic of the thesis changed into a purely physical study.

2.3 Discharges modes and classification

A wide phenomenology of plasma discharge can be observed depending on liquid nature and experimental conditions. Here we report the several modes observed and the previous classification attempts.

2.3.1 Contact glow electrolysis: a specific mode?

Historically, **contact glow electrolysis** is one of the first plasma inside water mode discovered. In electrochemistry, the high current regime of an electrolysis leads to the formation of a plasma layer nearby the high voltage electrode [Yerokin][Denaro][Sengupta][Zakharov][Gao].

This plasma is a thermal glow and is obtained by low voltage DC voltage in reactors with one electrode of reduced radius of curvature or with a reduced area as shown in **fig 2.21**. The plasma discharge is obtained by using asymmetric electrodes, the discharge will occur on the electrode with the smaller area where heating is more important. Local joule heating occurs at this electrode because of current constriction and higher electric fields. This leads to a vaporization of the saline liquid around the electrode and a thermal plasma is formed between the electrolyte interface and the metal.

The gas layer around the electrode can have two sources:

- charge exchange electrolysis (redox) and subsequent production of a gas product, a basic schematic of a redox cell is given in **fig 2.19**
- ion conduction inside the liquid due to solvated ions impurities and subsequent vaporization by local joule heating

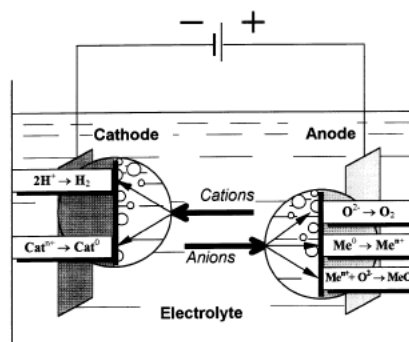


fig 2.19 redox chemical reactions at the anode side and the cathode side in classical electrolysis [Yerokin1999].

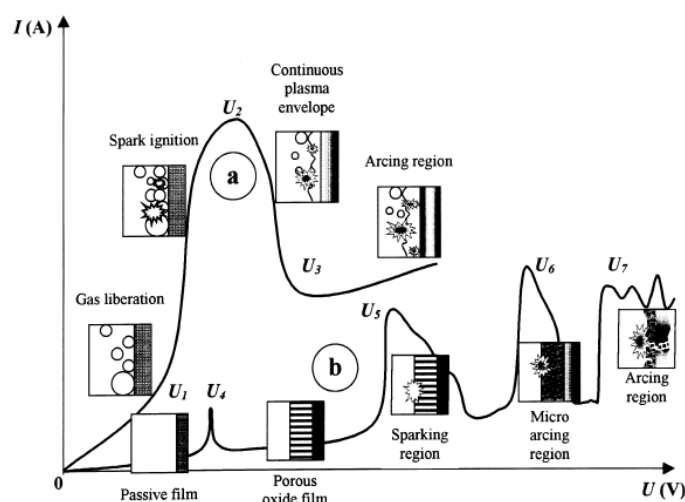


fig 2.20 contact glow plasma electrolysis regimes on the dissolution side and the passivation side [Yerokin1999].

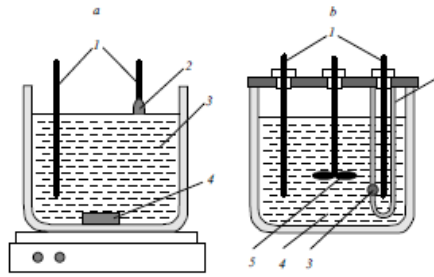


fig 2.21 typical reactor configuration for plasma electrolysis [Zakharov2007].

It can be a glow discharge or an arc depending on the current flowing through the discharge and the gap. The plasma glow electrolysis has been widely explored and several stable and instable operation modes have been identified with current/voltage plots as shown in fig 2.20.

As usual in electrolysis, there is dissolution of the metal at one side and deposition on the other side. At the electrode where there is deposition of a non conductive material, the layer is first porous and let the current go through this deposited dielectric layer. When the layer begins to be quite insulating, the current can cross this layer only by breakdown and arcing through this layer. Thus at high current and after some time the deposition on an electrode by electrolysis is followed by an arcing regime.

At the electrode where there is erosion and gas production, the plasma discharge occurs directly into those bubbles. At high current a steady gas layer with a quite glow discharge can exist. At even higher current there is an arcing regime. The electrode surface endures strong heating and can even melt locally under the intense heating at the root of the arc filament. The arcing electrolysis is not always a problem: it can be used for the surface processing of a metal and deposition of porous layer with a very high deposition velocity. The stable regime is difficult to obtain because the gas layer can easily move and thus the gap and the pressure does not remain constant for the plasma discharge. The stable regime can only be obtained for a given electrode geometry and a given electrolysis current and a given electrolyte. The use of a repetitive pulsed power supply allow to play on the duty cycle and thus to obtain a controlled gas layer and a glow discharge without arcing. Such a plasma device is being implemented for medical application such as skin etching and biological tissues etching or wound cleaning [Stalder].

This kind of discharge is very useful to understand the fundamental interaction of positive ion or negative ion flux incoming from the plasma and impacting on the liquid. Those impact ionization processes differ from the classical electron exchange of redox chemical reactions and thus induce non faradic yield in the charged particle balance. The chemical reactions induced inside the liquid are completely different if there is positive ion flux or electron flux [Yerokin] [Bruggeman]. Such difference is important when considering positive and negative plasma discharge modes. It is not sure if contact glow electrolysis is a special mode with specific mechanism or if it can be identified to a slow mode as discussed in the following sections.

2.3.2 Fast modes vs slow modes classification?

The plasma discharges in liquids are often classified as **short pulse breakdown** or **long pulse breakdown**. In fact this kind of classification in [Ushakov] comes from the experimental community of switches [McDonald] as shown in fig 2.22 and partial discharges [Pompilli2005] respectively. In reality, this classification is based on the **time delay to breakdown** which is related to the three following parameters: the discharge **initiation time**, the discharge **propagation velocity**, and the electrode configuration. Short pulse breakdown are of course systematically associated to fast plasma discharge as in fig 2.24, and respectively long pulse

breakdown are associated to slow plasma discharge as shown in **fig 2.23**. Given this obvious relation a more physical classification into fast and slow mode can be performed. The several modes can be distinguished by their propagation velocity which is a quite relevant criterion as it corresponds to different physical propagation mechanisms. Fast mode would be associated to accelerated charges and slow modes would be associated to phase change processes or fluid motion. Those slow and fast modes are sometimes qualified as subsonic and supersonic mode [Touya2006] as shown in **fig 2.23** and in **fig 2.24**.

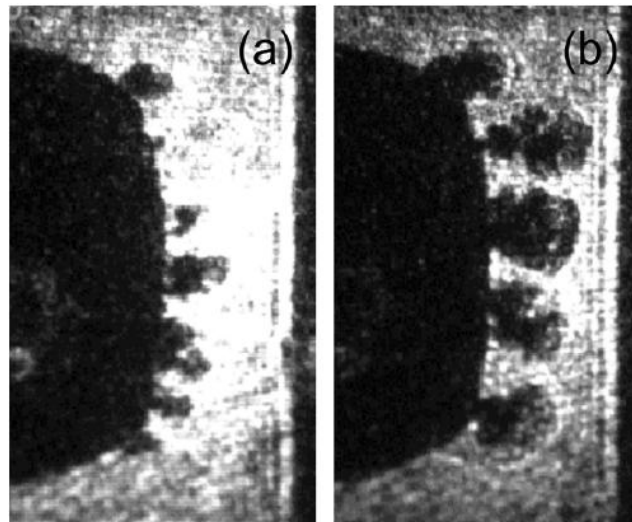


fig 2.22 short gap/short pulse discharge, shadowgraph of “dark” non luminous streamers, pin radius is 0.8mm, 200ns voltage pulse, 60ns and 150ns delay, [Kolb2008], see also [Schoenbach2008].

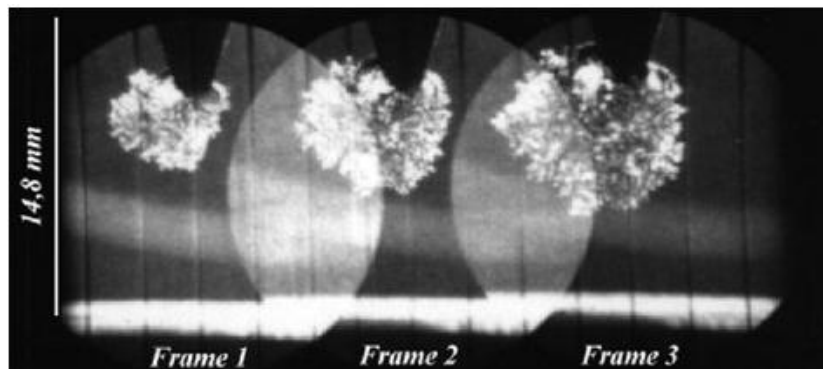


fig 2.23 image converter pictures showing subsonic positive discharge growth in tap water, gap is 1cm, tip radius is 1.5mm, 317 μ s, 425 μ s and 538 μ s delay, 25kV, [Touya2006].

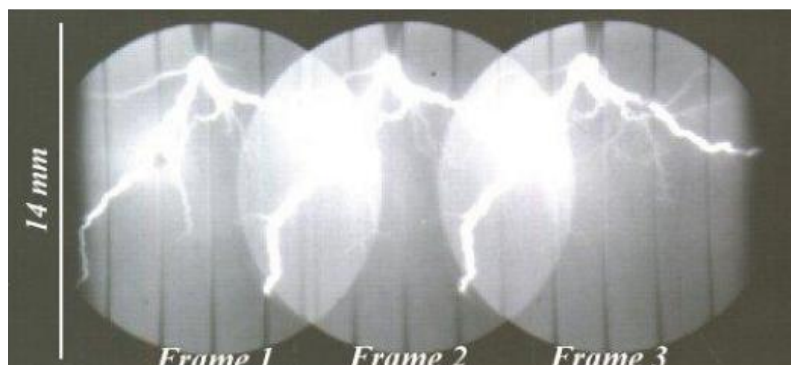


fig 2.24 image converter pictures showing supersonic positive discharge growth in water, gap is 2.8cm, pin radius is 150 μ m, 200Ns gate, 252ns 1.85 μ s 3.7 μ s delay, 30kV, 220 μ S/cm , [Touya PhD].

2.3.3 Positive vs negative modes classification?

In a general way, the positive and the negative applied voltage polarity lead to very different discharge phenomenology [Beroual] [Lesaint] [Kolb] [Ushakov]. The positive polarity mode is often more filamentary and the negative mode more bush-like with more gas content and a bubbly shape whatever the liquid considered. An example of positive discharge and negative discharge inside water is given in **fig 2.25**. On **fig 2.26** one can see that the classification is not so obvious in terms of morphology and description as “bush-like”, “tree-like”, “branchy”, “filamentary”, “streamers” are present in literature [Ushakov]. A **rigorous terminology** is not easy. For example the slow positive discharge (subsonic) presented in **fig 2.23** has a morphology similar to the negative discharge in **fig 2.25** (b).

The positive breakdown is often reported to happen at lower voltage than the negative breakdown. The breakdown strength is thus higher in the negative polarity. The propagation velocity is also one order of magnitude lower in the negative polarity whatever the liquid and whatever the experimental configuration.

An exhaustive review of shape and breakdown characteristics of discharge in many liquids is given by [Beroual] in **fig 2.26** for **negative polarity** and **fig 2.27** for **positive polarity**.

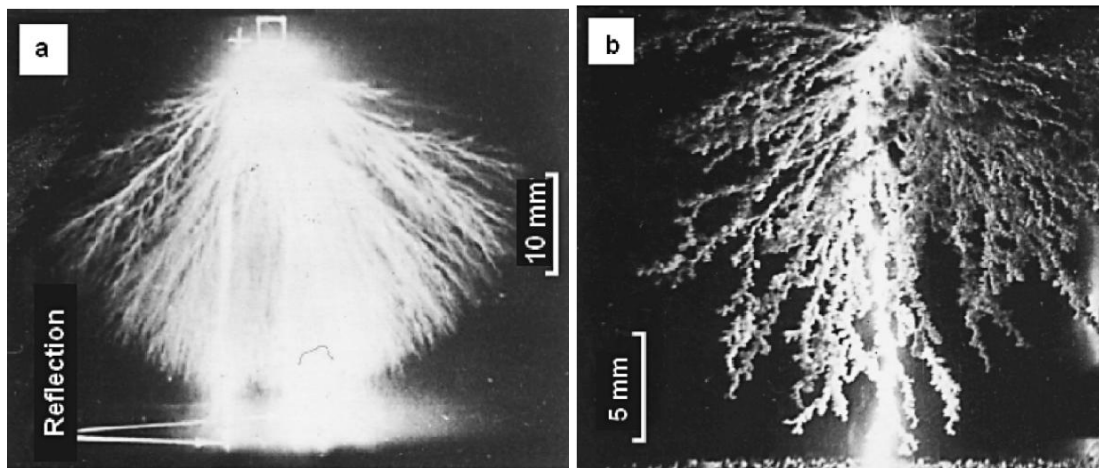


fig 2.25 still (time integrated) photographs of positive (a) and negative (b) discharge in water in point to plane configuration, [Ushakov].

Some nuances need to be given here. Some authors report fast filamentary discharges also at negative polarity [Ushakov]. The criterion for appearance of such unusual discharge at negative polarity is less clear than in positive discharge presented in next section. Consequently the mode classification needs to combine both applied voltage polarity and propagation velocity.

Table I: Negative Streamer

| Liquids | Ndl | Tip Radius | Gap Length | Voltage Waveform | kV | v_{max} / v_{av} km/s | Structure | Methods | Ref. |
|--|-----|-------------|------------|-------------------------------------|----------------------------------|--|--------------------------------------|-----------|------|
| n-pentane | W | 20 μ m | 4 mm | 2.3/1500 μ s | -45.9 | 0.40 / 0.07 | bush | Schn, ICC | 1 |
| n-hexane | W | 20 μ m | 4 mm | 2.3/1500 μ s | -48.1 | 0.60 / 0.11 | bush | Schn, ICC | 1,2 |
| n-heptane | W | 20 μ m | 4 mm | 2.3/1500 μ s | -48.1 | 0.50 / 0.13 | bush | Schn, ICC | 1 |
| n-octane | W | 20 μ m | 4 mm | 2.3/1500 μ s | -48.1 | 0.77 / 0.14 | bush | Schn, ICC | 1 |
| n-nonane | W | 20 μ m | 4 mm | 2.3/1500 μ s | -48.1 | 0.67 / 0.14 | bush | Schn, ICC | 1 |
| n-decane | W | 20 μ m | 4 mm | 2.3/1500 μ s | -50.4 | 0.75 / 0.16 | bush | Schn, ICC | 1 |
| n-hexane (5 MPa) | Stl | 35 μ m | 2.3 mm | 4 / 3 / 4 μ s | -156 | / 2.50 | tree | SG, ICC | 3 |
| n-hexane (+2% IMN) | W | 10 μ m | 10 mm | 1.1/225 μ s | -45.0 | 0.22 / 0.20 | bush | Schn, ICC | 4 |
| n-hexane (+2% CCl ₄) | W | 10 μ m | 10 mm | 1.1/225 μ s | -45.0 | 0.91 / 0.48 | filament | Schn, ICC | 4 |
| cyclo-hexane | W | 20 μ m | 4 mm | 2.3/1500 μ s | -52.7 | 0.35 / 0.17 | bush | Schn, ICC | 2 |
| cyclo-hexane (initiation) | W | 0.5 μ m | 4.7 mm | 0.2/540 μ s | -5.30 -6.18 -7.95 -9.71 | 0.037 / 0.014 0.043 / 0.013 0.057 / 0.019 0.051 / 0.021 | sphere hemi-sph pagoda bush | SG, ICC | 5,6 |
| c-hexane (+0.2% anthracene) | Stl | 3 μ m | 4 mm | 0.4 μ s step | -50.0 | / 0.19 | bush | SG, VCR | 7 |
| c-hexane (+1% CCl ₄) | Stl | 3 μ m | 4 mm | 0.4 μ s step | -50.0 | / 0.64 | tree | SG, VCR | 7 |
| CCl ₄ | W | 10 μ m | 4 mm | 2.2/190 μ s | -42.8 | / 8.40 | tree | Schn, ICC | 8 |
| 2-methyl-pentane | W | 20 μ m | 4 mm | 2.3/1500 μ s | -48.1 | 0.48 / 0.18 | bush | Schn, ICC | 9 |
| 2,3-dimethyl-butane | W | 20 μ m | 4 mm | 2.3/1500 μ s | -48.1 | 0.24 / 0.16 | bush | Schn, ICC | 9 |
| iso-octane | Stl | 35 μ m | 20mm | 4 / 3 / 4 μ s | -47.0 | / 0.26 | bush | SG, ICC | 10 |
| benzene | W | 20 μ m | 4 mm | 2.3/1500 μ s | -50.4 | 0.42 / 0.19 0.86 / 0.27 | bush tree | Schn, ICC | 2 |
| benzene (+1% CCl ₄) | W | few μ | 4 mm | 15ns/4 μ s | -40.0 | / 1.30 | tree | Schn, ICC | 11 |
| monochloro-benzene | W | 10 μ m | 4 mm | 2.2/190 μ s | -42.8 | / 0.45 | bush | Schn, ICC | 8 |
| toluene | Stl | 35 μ m | 10 mm | 4 / 3 / 4 μ s | -40.0 | 0.27 / 0.17 | bush | SG, ICC | 12 |
| toluene (5 MPa) | Stl | 35 μ m | 2.5 mm | 4 / 3 / 4 μ s | -100 | / 4.50 | tree | Schn, ICC | 13 |
| 1-hexene | W | 20 μ m | 4 mm | 2.3/1500 μ s | -48.1 | 0.21 / 0.14 | bush | Schn, ICC | 2 |
| 1,5-hexadien | W | 20 μ m | 4 mm | 2.3/1500 μ s | -48.1 | 0.32 / 0.27 | bush | Schn, ICC | 9 |
| cyclo-hexene | W | 20 μ m | 4 mm | 2.3/1500 μ s | -39.0 | 3.27 / 1.08 | tree | Schn, ICC | 9 |
| H ₂ O (2 · 20.3 M Ω .cm) | W | 20 μ m | 4 mm | 2.3/1500 μ s | -16.2 | 0.08 / 0.04 0.49 / 0.20 1.78 / 0.60 | sphere bush tree | Schn, ICC | 9 |
| L-Helium | W | 20 μ m | 4 mm | 2.3/1500 μ s | -30.0 | 7.05 / 3.97 | filament | Schn, ICC | 9 |
| L-Nitrogen | W | 20 μ m | 4 mm | 2.3/1500 μ s | -43.1 | 0.23 / 0.13 | bush | Schn, ICC | 9 |
| L-Nitrogen (initiation) | W | 1 μ m | 5 mm | 0.2/540 μ s | -17.6 -17.6 | 0.10 / 0.06 0.40 / 0.12 | bush filament | SG, ICC | 14 |
| PFPE | Stl | 35 μ m | 5 mm | 4 / 3 / 4 μ s | -49.0 | / 4.50 | tree | SG, ICC | 15 |
| PFPE (initiation) | W | 1 μ m | 5 mm | 0.2/540 μ s | -21.2 -33.6 | 0.35 / 0.21 3.29 / 1.35 | bush filament | SG, ICC | 16 |
| Si-Oil (10 cSt) | W | 8 μ m | 1.4 mm | 2 μ s pulse 30 μ s pulse | -22.0 | / 0.04 / 0.06 | bush tree | SG, SS | 17 |
| TFO | W | 20 μ m | 4 mm | 2.3/1500 μ s | -35.7 | 2.07 / 0.76 3.38 / 1.47 | bush tree | Schn, ICC | 18 |
| TFO (naphthenic) | Cu | 0.6 mm | 67 mm | 1/180 μ s | -343 | 50.0 / 16.0 | tree | LE, ICC | 19 |
| White-Oil (naphthenic) | Stl | 35 μ m | 10 mm | 4 / 3 / 4 μ s | -53.0 | / 0.20 | bush | SG, ICC | 10 |

IMN:1-methyl-naphthalene W:tungsten
 PFPE:perfluoro-polyether Stl:steel
 TFO:transformer oil Cu:copper

v_{max} :maximum speed Schn:Schlieren
 v_{av} :average speed SG:shadowgraph
 LE:light emission
 SS:single shot
 ICC:Image Converter Camera
 VCR:video recorder

fig 2.26 shape and breakdown characteristics in negative polarity for different liquids [Beroual].

Table II: Positive Streamer

| Liquids | Ndl mat | Tip Radius | Gap Length | Voltage Waveform | kV | v_{max} km/s | v_{av} km/s | Structure | Methods | Ref. |
|--|---------|-------------|------------|-------------------|----------------|----------------|---------------|------------------|-----------|------|
| n-pentane | W | 20 μ m | 4 mm | 2.3/1500 μ s | +30.9 +40.4 | 0.52 / 6.97 | 0.23 / 4.23 | bush tree | Schn, ICC | 1 |
| n-hexane | W | 20 μ m | 4 mm | 2.3/1500 μ s | +32.7 +45.1 | 0.48 / 7.61 | 0.21 / 3.86 | bush tree | Schn, ICC | 1,2 |
| n-heptane | W | 20 μ m | 4 mm | 2.3/1500 μ s | +42.8 | 6.32 / | 4.04 | tree | Schn, ICC | 1 |
| n-octane | W | 20 μ m | 4 mm | 2.3/1500 μ s | +48.7 | 6.20 / | 5.17 | tree | Schn, ICC | 1 |
| n-nonane | W | 20 μ m | 4 mm | 2.3/1500 μ s | +47.5 | 6.67 / | 4.28 | tree | Schn, ICC | 1 |
| n-decane | W | 20 μ m | 4 mm | 2.3/1500 μ s | +52.3 | 7.48 / | 5.15 | tree | Schn, ICC | 1 |
| dodecane | W | 1 μ m | 2.5 mm | 10/632 ns | +25.0 | 6.00 / | 3.09 | tree | SG, SS | 20 |
| hexadecane | W | 1 μ m | 2.5 mm | 10/632 ns | +24.0 | 4.00 / | 2.70 | tree | SG, SS | 20 |
| squalane | W | 1 μ m | 2.5 mm | 10/632 ns | +25.0 | 4.00 / | 2.06 | tree | SG, SS | 20 |
| n-hexane (5 MPa) | Stl | 35 μ m | 3.5 mm | 4 / 3 / 4 μ s | +117 | / | >18.0 | filament | SG, ICC | 3 |
| n-hexane (+0.1% 1MN) | W | 10 μ m | 10 mm | 1.1/225 μ s | +45.1 | / | 3.19 | tree | Schn, ICC | 4 |
| n-hexane (+5% DMA) | W | 10 μ m | 10 mm | 1.1/225 μ s | +45.1 | / | 2.78 | radial | Schn, ICC | 4 |
| cyclo-hexane | W | 20 μ m | 4 mm | 0.2/540 μ s | +45.1 | 0.33 / 3.22 | 0.24 / 2.54 | bush tree | Schn, ICC | 2 |
| cyclo-hexane (initiation) | W | 0.5 μ m | 4.7 mm | 0.12/830 μ s | +8.5 +29.1 | 0.22 / 2.85 | 0.13 / 1.53 | bush filament | SG, ICC | 5,6 |
| c-hexane (+0.98mol NB) | W | 1 μ m | 4 mm | 50ns/2 ms | +35.0 | / | 4.90 | filament | LE, VCR | 21 |
| c-hexane (+0.49mol TCE) | W | 1 μ m | 4 mm | 50ns/2 ms | +35.0 | / | 1.60 | filament | LE, VCR | 21 |
| CCl ₄ | W | 10 μ m | 4 mm | 2.2/190 μ s | +42.8 | / | 30.00 | tree | Schn, ICC | 8 |
| 2-methyl-pentane | W | 20 μ m | 4 mm | 2.3/1500 μ s | +45.1 | 9.33 / | 3.65 | tree | Schn, ICC | 9 |
| 2,3-dimethyl-butane | W | 20 μ m | 4 mm | 2.3/1500 μ s | +45.1 | 5.59 / | 4.14 | tree | Schn, ICC | 9 |
| benzene | W | 20 μ m | 4 mm | 2.3/1500 μ s | +45.1 | 1.68 / | 1.47 | radial | Schn, ICC | 2 |
| monochloro-benzene | W | 10 μ m | 4 mm | 2.2/190 μ s | +42.8 | / | 76.00 | tree | Schn, ICC | 9 |
| trichloro-benzene | W | 10 μ m | 4 mm | 2.2/190 μ s | +42.8 | / | 62.00 | tree | Schn, ICC | 8 |
| dodecyl-benzene | W | 10 μ m | 4 mm | 2.2/190 μ s | +42.8 | / | 2.30 | tree | Schn, ICC | 8 |
| iodo-benzene | W | 10 μ m | 4 mm | 2.2/190 μ s | +42.8 | / | 15.00 | tree | Schn, ICC | 8 |
| toluene (5.0 MPa) | Stl | 35 μ m | 2.5 mm | 4 / 3 / 4 μ s | +123 | / | >25.0 | tree | Schn, ICC | 13 |
| 1-hexene | W | 20 μ m | 4 mm | 2.3/1500 μ s | +45.1 | 4.51 / | 2.92 | tree | Schn, ICC | 2 |
| 1,5-hexadiene | W | 20 μ m | 4 mm | 2.3/1500 μ s | +45.1 | 15.21 / | 6.49 | tree | Schn, ICC | 9 |
| cyclo-hexene | W | 20 μ m | 4 mm | 2.3/1500 μ s | +45.1 | 8.81 / | 4.36 | tree | Schn, ICC | 9 |
| DOP | W | 1 μ m | 4 mm | 50ns/2 ms | +21.0 | / | 0.90 | filament | LE, SS | 21 |
| DOP (+2.84mol AN) | W | 1 μ m | 4 mm | 50ns/2 ms | +22.0 | / | 1.00 | filament | LE, SS | 21 |
| H ₂ O (2 · 20.2 M Ω .cm) | W | 20 μ m | 4 mm | 2.3/1500 μ s | +28.5 | 2.73 / 45.30 | 0.04 / 26.70 | bush tree | Schn, ICC | 9 |
| L-Helium | W | 20 μ m | 2.2 mm | 1/1600 μ s | +42.0 | 0.33 / | 0.02 | sphere | Schn, ICC | 9 |
| L-Nitrogen | W | 20 μ m | 4 mm | 1/1600 μ s | +39.6 | 0.31 / 29.60 | 0.12 / 18.70 | bush tree | Schn, ICC | 9 |
| L-Nitrogen (initiation) | W | 1 μ m | 5 mm | 0.2/540 μ s | +17.6 +17.6 | 0.18 / 1.34 | 0.05 / 0.13 | bush filament | SG, ICC | 14 |
| PFPE | Stl | 35 μ m | 5 mm | 4 / 3 / 4 μ s | +65.0 | / | 30.00 | tree | SG, ICC | 15 |
| PFPE (initiation) | W | 1 μ m | 5 mm | 0.2/540 μ s | +20.3 +24.7 | 0.37 / 8.21 | 0.18 / 1.46 | bush filament | SG, ICC | 16 |
| Si-Oil (100 cSt) | W | 10 μ m | 1.2 mm | 450ns pulse | +10.9 | / | 2.00 | tree | SG, SS | 17 |
| TFO | W | 20 μ m | 4 mm | 2.3/1500 μ s | +43.3 | 5.00 / | 2.50 | radial | Schn, ICC | 18 |
| TFO (naphthenic) | Cu | 0.6mm | 67 mm | 1/180 μ s | +327 | 17.80 / 210.00 | 4.96 / 65.00 | bush filament | LE, ICC | 19 |
| White-Oil (naphthenic) | Stl | 3 μ m | 25.4 mm | 1/2500 μ s | +63.0 | 1.80 / | 1.07 | tree | Schn, SS | 22 |

1MN:1-methylnaphthalene W:tungsten
 DMA:N,N'-dimethylaniline Stl:steel
 NB:nitrobenzene Cu:copper
 TCE:tetra-chloroethylene
 DOP:di-octylphthalate
 AN:acetonitril
 PFPE:perfluoro-polyether
 TFO:transformer oil

v_{max} :maximum velocity Schn:Schlieren
 v_{av} :mean velocity SG:shadowgraph
 LE:light emission
 SS:single shot
 ICC:Image Converter Camera
 VCR:video camera

fig 2.27 shape and breakdown characteristics in positive polarity for different liquids [Beroual].

2.3.4 An example: Positives modes reported in oil liquids

This classification is based on the discharge morphology and its propagation velocity. "Streamer" is here designating any filamentary discharge occurring in a liquid. This terminology is adopted in analogy with the filamentary discharges occurring in gases. However, it does not signify that we really have a real "streamer mechanism" with charge space separation, ionization

wave and photoionisation. In particular the secondary streamer in liquids does not refer to the return ionization wave when the gas streamer reaches the opposite electrode in a corona or the dielectric material in a DBD.

The term “**leader**” also appears in literature [Ushakov] for describing discharges inside liquids. See [Raizer] for a complete description of leader discharges in gases. Basically a leader discharge is quite thermal streamer channel supporting many branches. This discharge regime appears in particular in natural lightning or in streamers with very long interelectrode gap, long applied voltage pulse duration and heavy branching. In gases, there is a streamer to leader transition when a parent channel needs to support current of many children filaments at a branching node. Since discharges inside liquids convey one order of magnitude more current (or injected charge per filament) than in gases, the term “leader” can be appropriate.

The following classification is the recent result of a fair consensus among the liquid dielectric community and has been verified for a wide range of different dielectric liquids such as water, oils, esters and other organic liquids [Hebner][Lesaint] [Beroual][Brosseau] [Massala] [Tobazkon1994]:

- **primary streamer = or first mode = primary mode in this report**
- **Secondary streamer = second mode = secondary mode in this report**
- **tertiary streamer = tertiary mode**
- **fourth mode streamer = fourth mode**

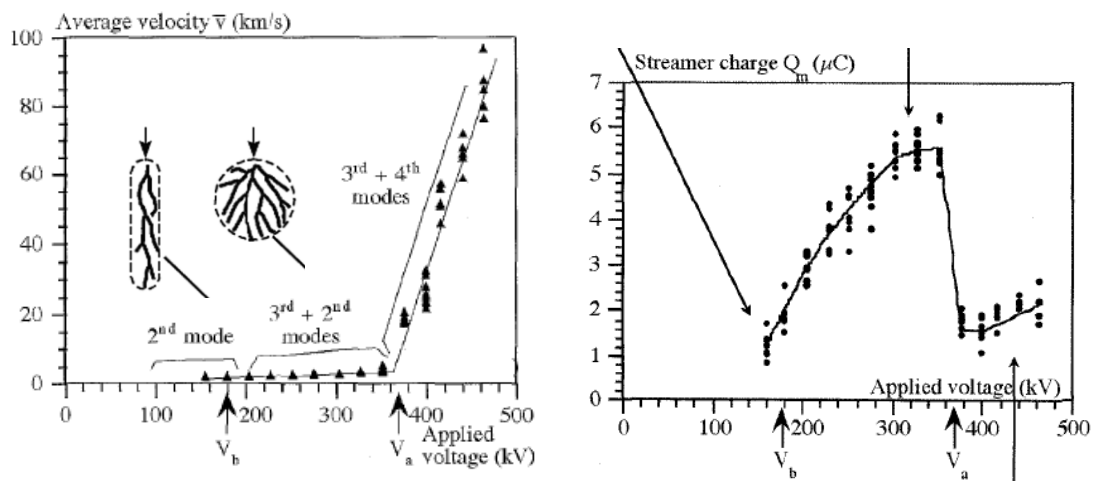


fig 2.28 propagation velocity of the positive plasma discharge in oil, 1st 2nd 3rd 4th plasma modes, classification based both on voltage transition and morphology, V_b is the breakdown voltage, V_a is the acceleration voltage. Charge injected into the discharge, there is a progressive increase from second to third mode and a clear decrease at the transition to the fourth mode, from [Lesaint1998].

- The **positive primary** streamer (PPS) is a slow positive streamer, it appears at moderate positive voltage and has bush-like shape with a lot of tiny branched filaments of low emission intensity and propagating with a hemispheric envelope. It propagates at velocity ranging from 100m/s to some km/s with voltage dependence. Usually this mode has a hemispherical shape, propagates at subsonic velocity and presents a low current (1e-4A in oil) [Lesaint].
- The **positive secondary** streamer (PSS) is more filamentary with less branching than the primary streamer. Basically the shape of the secondary streamer is very similar to the shape of the primary streamer but on a larger space scale. The emission intensity is more important and the propagation is very fast (30km/s for water in the present report) and has often a voltage independent velocity depending on the liquid nature. Usually the velocity stays constant across the gap in oil [Lesaint][Yamada].

- The **third mode** is essentially identical to the secondary streamer but with a voltage dependant velocity. The second mode can have a rather cylindrical envelope. With an increase of the voltage, more filaments propagate and this cylindrical envelope transforms into a spherical envelope [Ushakov]. This mode begins with a fast phase followed by a slow phase identical to the secondary mode. The velocity of this fast phase sometime called as “initiating streamer” is voltage dependant.
- The **fourth mode** can be described as an ultra fast mode and can be obtained at a voltage threshold identified as the “acceleration voltage”. The velocity of this mode increases with voltage. It is a fast filament emerging from the second or the third mode discharge and that bridges the remaining gap between the discharge and the opposite electrode.

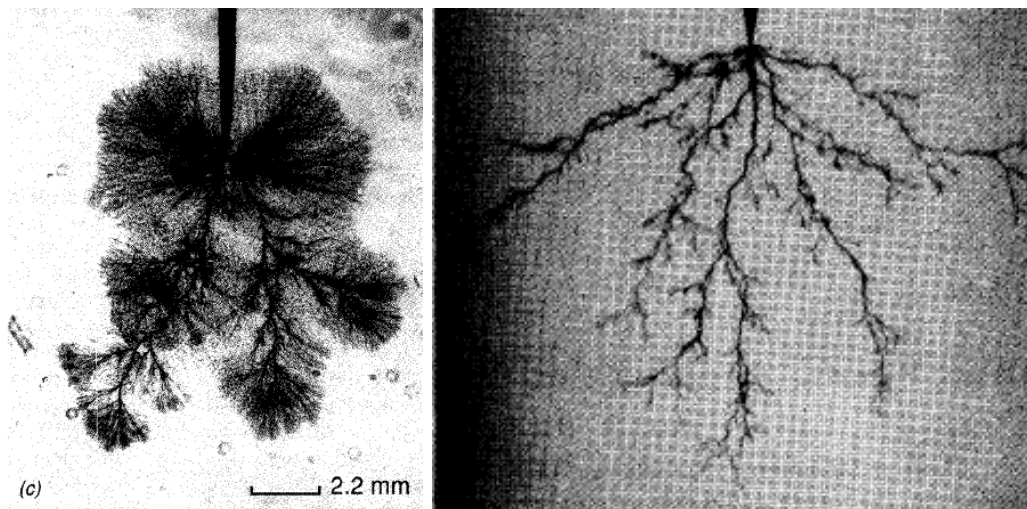


fig 2.29 propagation of fast positive streamer in transformer oil in a point to plane electrode configuration under $85\mu\text{s}$ applied voltage pulse with 178kV , gap is 27.5mm , pin radius is $30\mu\text{m}$, gate is 8ns , schlieren image [Beroual1998]. Positive streamer in nhexane 632ns delay, 3mm gap, 16kV , 390pC capacitor.

In this report we will use the general terms as “discharge” or “mode” instead of “streamer” or “leader”. We will try to keep this terminology in order to avoid any confusion.

The transition from one mode to another occurs when increasing the applied voltage as shown in **fig 2.28**. The threshold voltage for each transition can be designated as “acceleration voltage”.

| polarity | Propagation velocity | Classification 1 | Classification 2 | Classification 3 | description |
|----------|----------------------|------------------|------------------|-----------------------|---------------------------------|
| positive | slow | subsonic | bubbling | | |
| | fast | supersonic | primary | 1st | |
| | | | secondary | 2nd | Filamentary voltage independant |
| | | | tertiary | 3rd | Filamentary voltage dependant |
| | | | 4rth | Filamentary ultrafast | |
| negative | slow | | | | Bubbly shape |
| | fast | | | | filamentary |

This classification is quite universal and can be applied to several liquids even if the voltage thresholds and the exact characteristics of each mode are different from one liquid to another. Each mode is likely to be caused by a specific dedicated propagation mechanism. A better understanding of each mode and its underlying mechanism can be achieved by checking its dependence to relevant experimental parameters.

2.4 Influence of experimental parameters: parametric experimental studies performed in literature

Parametric studies has been performed in literature in order to determine the main processes explaining plasma discharge inside liquids.

2.4.1 Influence of applied voltage polarity

For a given voltage, the **polarity of the voltage** has a strong influence on the discharge shape as shown in **fig 2.25** and also in tables **fig 2.26** and **fig 2.27**. One of the reasons can be the sign of the divergence of electronic current. The other reason is that negative charges are either supplied or need to be extracted.

Indeed in a strongly **inhomogeneous electric field** such as in point to plane electrode configuration, the electrons are either repelled or on the contrary attracted toward the high field region. Such polarity effect is also observed in the gas phase discharge case and leads to a well known morphology difference between positive streamers and negative streamers [Kulikovsky]. In gases at positive polarity, electrons need to be created ahead of the filament tip by collisional ionization and also mainly by photoionization. At negative polarity electrons are directly available and are thus injected ahead of the plasma filament. In liquids, the propagation mechanism is likely to be completely different: in the negative case **electrons are impacting** on the **gas/liquid interface**, whereas in the positive case **electrons are extracted** from the gas/liquid interface. These opposite processes explain the morphology and propagation differences.

Regarding dielectric insulation, breakdown conditions are completely different between positive and negative high voltage. In early switch studies and breakdown tests, the typical procedure involves sphere to sphere electrode configuration. In this case the breakdown often occurs because of the easier propagation of the secondary positive mode. Strongly asymmetric electrode configuration such as point to plane is thus required to clearly dissociate positive discharges from negative discharges.

For slow mode that occurs mostly for **AC voltages** in HV transformers [Beroual], both negative and positive streamers can be observed successively during positive and negative half periods of the power supply. The filamentary channel show filamentary positive streamers during positive polarity and leaf-like negative streamers at negative half period polarity with a short time offset related to charge removal at the gas/liquid interface of the cavity (capacitive effects).

2.4.2 Influence of electric field/applied voltage level

The higher amount of **available power** is related to an increased **number of plasma filaments**: each filament is associated to an injected charge inside the dense medium and at higher voltage more charges are available and can be consumed by more filaments. This idea of a number of filaments associated with a **charge per filament** is quite common for gas phase

streamers. In gases this can be due to more eligible sites at the electrode or more charges available and split between more filaments.

In a general way, the electric field is a main parameter for plasma discharge because the ionization **source term has strong dependence on the electric field**. It is usually observed that the discharge initiates at an inception voltage, the transition from one mode to another is also driven by the voltage as discussed in the previous sections.

The applied voltage level is usually reported to **increase the propagation velocity** as shown in **fig 2.30** and in **fig 2.34**. However, some liquids or some modes are insensitive to the voltage level [Beroual][Lesaint]. An increase of the applied voltage also decreases the time lag to breakdown as shown in **fig 2.31**. Those two studies are of particular importance in the scope of the present thesis. In those studies performed in short gaps, it is not sure if the **propagation phase** is correctly decorrelated from the **initiation phase**.

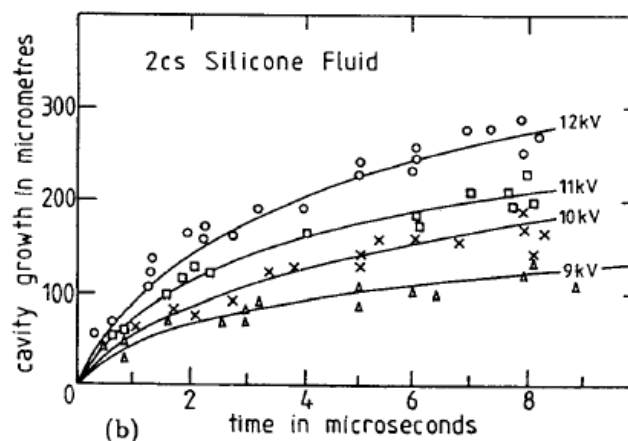


fig 2.30 influence of applied voltage on the discharge growth in 2Cs silicon fluid, in point to plane electrode configuration, with positive polarity, measured by observing the stopping length for different pulses duration, the applied voltage level is usually reported to increase the propagation velocity, from [Watson],.

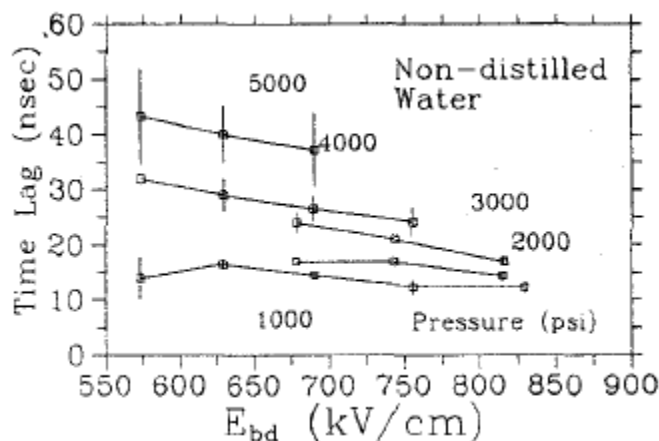


fig 2.31 influence of the electric field on the time lag to breakdown, for tap water in 100μm gap, for different applied pressure, time lag increases with applied pressure and decreases with higher electric field, from [Jones].

In fact, the **Laplacian electric field** is more relevant than the applied voltage. For example, in case of inhomogeneous electrode configuration, we use the voltage or even the electric field at the point electrode instead of the mean electric field across the gap. The mean electric field across the gap is not relevant for sharp pins and long gaps because the relevant electric field for the plasma initiation is **concentrated around the pin**.

The same field value can be obtained for different electrode curvature radi and voltage combinations. However, the divergence of the field is not be the same and the field decreases on different space scale. One needs to be careful when choosing the electrode radius and the applied voltage as shown in **fig 2.32**. The differences are that there can be a critical streamer radius or a critical region size required for the discharge initiation. For instance a very tiny electrode and a quite low voltage achieves a high electric field over a too short region and the plasma will not initiate even if we are well above the initiation field. Such **minimum electrode radius** for the discharge inception is reported by [Lesaint][Denat].

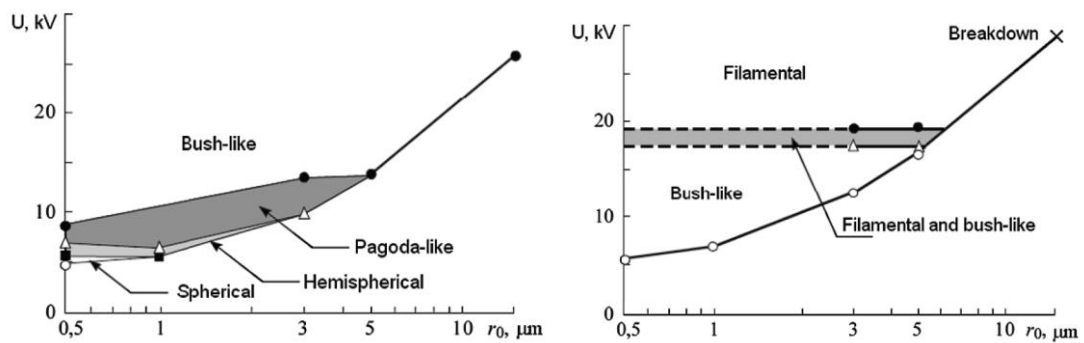


fig 2.32 influence of the point curvature radius in negative and positive polarity, 5mm gap, 560μs pulse with 0.2μs rise time, in cyclohexane, from [Ushakov].

If there is **space charge separation** somewhere in the plasma, the electric field relevant for the propagation is no longer the applied Laplacian electric field but the Coulomb electric field as in the streamer mechanism in gases.

2.4.3 Influence of the dielectric permittivity of the liquid

The relative dielectric permittivity of most liquids lies in the 2-5 range except for the specific case of water where the **permittivity arises from the highly polarisability of the molecule** and is equal to 80 over a wide range of frequencies up to the microwave region. In liquids the dielectric permittivity and the conductivity are uncorrelated parameters unlike plasmas. The permittivity arises from the polarisability of the liquid's molecules and the conductivity is dictated by the mobility of solvated ions impurities. The dielectric permittivity is linked to the polar nature of the liquid. A more polar liquid will deeply solvate the positive and negative ions into localised electronic states. It would thus be more difficult to promote an electron from this localised state to a delocalized state.

The permittivity has some importance to calculate the exact value of the electric field at the HV pin electrode, at the triple point with metal/dielectric contact, and above all the electric field inside the microbubbles. The electric **field inside a spherical microbubble** can be amplified depending on the bubble radius and depending on the dielectric permittivity difference between the liquid and the gas [Joshi]. For a same voltage and a same bubble radius, the permittivity difference thus dictates the ionization rate inside the bubble.

2.4.4 Influence of applied voltage pulse duration

The **voltage duration defines the final size of the discharge**. When the plasma filaments reach the opposite electrode, the reactor impedance is minimal and a large current can flow through the plasma filament, this current leads to plasma thermalization. This transition or **time lag to breakdown** depends on the time required to initiate the discharge after the beginning of the applied voltage pulse and also depends on the time required to propagate the plasma

filament across the gap as discussed in the initiation chapter of this report. Those two timescales depend on the streamer mode: nanosecond-microsecond breakdown for a fast mode (positive), microsecond-millisecond breakdown for a slow mode (negative). Thus, observation of the slow mode means long applied voltage duration, and observation of the fast mode require higher but shorter voltage pulses.

From the electrical insulation point of view, the relevant experimental data is the breakdown strength. The breakdown strength is the voltage that a switch can sustain without breakdown during a precise time. Those **breakdown strength** plots were early known and were used to investigate the influence of the liquid nature, the polarity, the impurities, the pressure, etc on the breakdown voltage of a switch. [Martin] performed measurements of breakdown strength for several liquids as shown in **fig 2.33**.

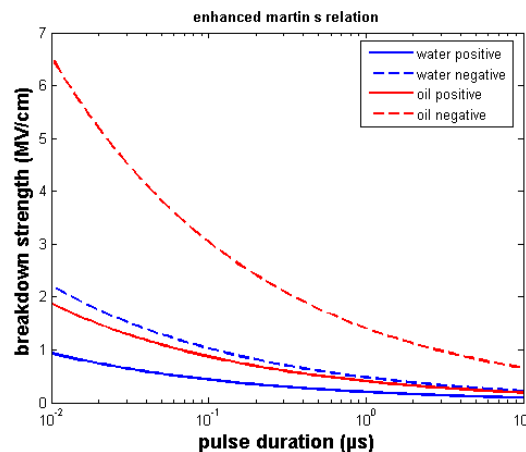


fig 2.33 dielectric strength for oil and water in positive and negative polarity for a gap of 1cm according to Martins's relation [Kolb].

The measurement procedure is performed in a sphere to sphere electrode geometry. The breakdown strength follows the experimental fit:

$$E_{breakdown} = \alpha K A^n \tau^{-1/3}$$

Where A stands for the electrode surface area, τ is the effective pulse duration, K depends on the liquid nature, and α is the non homogeneous electric field correction.

This breakdown strength combines several parameters as the gap, the initiation delay, and the propagation velocity. Those two parameters of the initiation delay and the propagation velocity are combined and need separated dedicated studies.

The voltage duration is often coupled to the voltage shape, if the voltage is square as those produced with cable generators discussed in the experimental setup section of this report then the pulse duration is obvious. On the contrary, if the pulse has a **capacitor decay shape**, the pulse duration needs to be defined as the **halfwidth**. This definition was made by people measuring the breakdown strength of dielectric liquids such as [Martin]. However this choice is quite arbitrary and should take into account the value of the initiation voltage and the value of the sustain voltage (or **stopping voltage**) for the considered discharge mode. The sustain voltage could indeed depend on the discharge length because of the voltage drop along the plasma filament and conversely the discharge length would depend on pulse duration.

2.4.5 Influence of the gap: reactor impedance

The interelectrode gap defines if the discharge is dominated by initiation or by propagation phase. The **reactor impedance** depends in a general way on the interelectrode capacitance, the interelectrode inductance and the gap resistivity. A larger gap usually means larger reactor

impedance and the reactor impedance defines the level of current flowing through the reactor during the discharge initiation phase. The **resistive** behaviour is dominant if the discharge operates by charge conduction. On the contrary the **capacitive** behaviour will be dominant if the discharge operates by charge injection and charge storage at some interface. The interface can be purely resistive or on the contrary **charges can be stored on the interface** depending on the **removal rate**, the interface capacitance, and plasma channel resistivity.

The discharge current level is not very high in the case of a non thermal discharge and the **inductance** due to the plasma filaments can be neglected. The inductance would induce some **LC ringing and overshoots** in the current/voltage waveforms. The interelectrode inductance can be neglected if the rise time of the applied voltage is below the time delay to initiation.

The value of the capacitance is dictated by the **plasma/liquid surface exchange** and should evolve with the propagation of the filaments, their thickness, the branching... The capacitance before the discharge is simply the interelectrode capacitance given by the electrode surfaces and the dielectric permittivity of the liquid.

Larger interelectrode gap induces larger discharge current according to [Lesaint] in positive polarity. This gives some insight on charge amplification across the gap as discussed in [Chadband] but in this case for negative discharge.

2.4.6 Influence of the conductivity of the liquid

The liquid bulk conductivity is driven by **the ionic mobility of the solvated ions**. This conductivity is caused by ionic solvated impurities in tap water and not by the **pH** dependant concentration of OH⁻ and H₃O⁺ ions. **Distilled water conductivity is below 10µS/cm, tap water is typically at 500µS/cm, an electrolyte or a saline is above 2mS/cm**. Unlike metal, in a dielectric liquid the **impurities** are responsible for the electrical conductivity of the liquid, not the free electrons. The ion impurities present in the liquid are solvated as a clusters of molecules with some limited drift velocity associated to a low ionic mobility because of drag force. The static ionic conductivity can be enhanced when applying an electric field by increasing the ionic mobility (field dependant mobility) or by multiplication of the charge carrier (avalanche). We can speak of **field enhanced conductivity**.

The conductivity has a strong influence on the **discharge shape**. A higher conductivity leads to **higher current** running through the reactor for the same applied voltage and the same gap. This means that more charges are available and could lead to **more plasma channels** simultaneously propagating or more **branching**, or **more power available for propagation**. In a general way one can expect the liquid ionic conductivity to have an influence on the plasma parameters and on the propagation velocity. On **fig 2.34** the average propagation velocity decreases at same applied voltage when increasing the water conductivity at positive voltage polarity. The opposite behaviour is observed at negative voltage polarity. The velocity slope as a function of the voltage slope does not change. It can be just variation of the initiation phase with conductivity and not a true dependence of the propagation with conductivity as discussed previously. This last interpretation is however contradictory with results presented in **fig 2.35**. At this stage one can easily realise that literature about discharge inside water is contradictory.

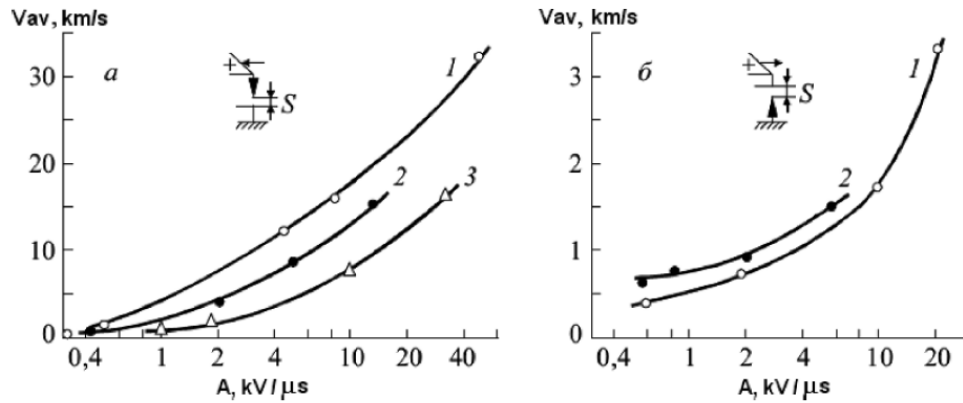


fig 2.34 dependent of the average discharge propagation velocity on the applied voltage slope for positive (a) and negative (b) point in distilled water with (1) $7\mu\text{S/cm}$, (2) NaCl solution at $100\mu\text{S/cm}$, (3) 1mS/cm , [Ushakov].

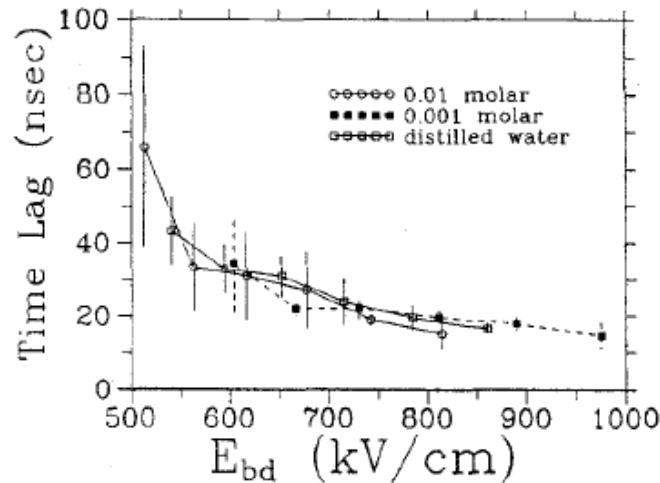


fig 2.35 influence of conductivity on discharge in tap water, time lag to breakdown is plotted as a function of the electric field, for different conductivities, $110\mu\text{m}$ gap, from [Jones], time lag to breakdown is insensitive to the water conductivity in short gap.

The water conductivity can also play a role of **charge removal at the gas/liquid interface**. If too many charges are stored on the gas/liquid interface, the electric field will be screened and the voltage along the gap is not sufficient to sustain the discharge. The discharge turns off or stops until the charges are evacuated and the propagation can continue [Suguiarto]. This mechanism is invoked for stepwise propagation or reilluminations. In this case, the removal rate or the channel conductivity regulates the steps or the reilluminations repetition frequency.

2.4.7 Influence of applied pressure

The **hydrostatic pressure** is of particular importance since the plasma discharge inside the liquid is likely to be gaseous. The applied pressure could thus influence the discharge morphology, the **discharge initiation**, the **discharge propagation**, the **discharge stopping**. According to [Jones][Ushakov], an increase of the pressure of the gas over the liquid free surface has an influence on the propagation velocity as shown in fig 2.37. It has an influence on the time to breakdown as shown in fig 2.31 and fig 2.36.

The pressure has also been reported to have some influence on the stopping length of the discharge [Ushakov]. The earlier stopping can thus be due to a smaller filament radius or a higher gas density inside the channel that leads to a higher plasma resistivity. The additional

pressure would thus increase the voltage drop along the plasma channel and make the discharge stops earlier.

In fact the decrease or the increase of the pressure also has an influence on the **gas content of the liquid**. More gas can be dissolved into the liquid when increasing the hydrostatic pressure and conversely an underpressure would help to remove the gas from the liquid. A complete removal of all **microbubbles** from the liquid to reach a high state of purity is almost impossible to achieve in water.

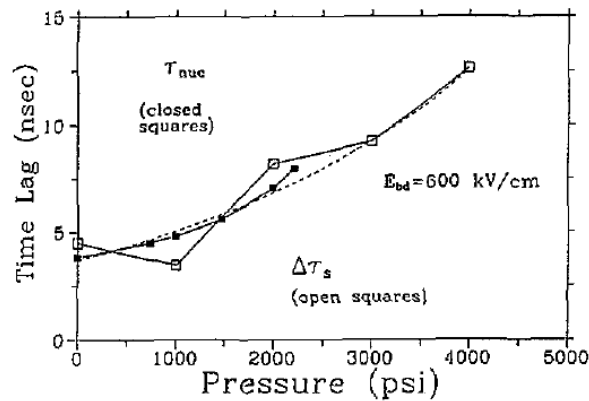


fig 2.36 influence of the pressure on discharges in distilled water, gap 110 μ m, 600kV/cm, the statistical time lag is well fitted by the theoretical bubble nucleation time, from [Jones].

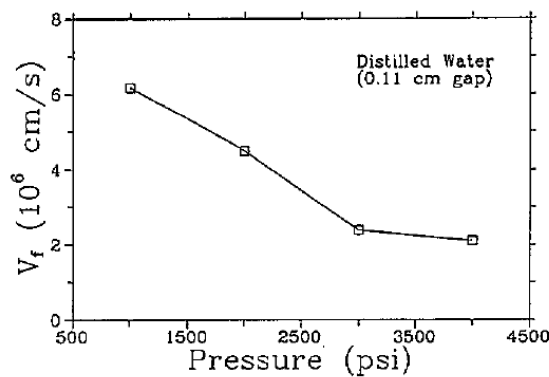


fig 2.37 propagation velocity of the ionizing front in distilled water as a function of pressure, 110 μ m gap, 600kV/cm, from [Jones].

2.4.8 Influence of the liquid viscosity

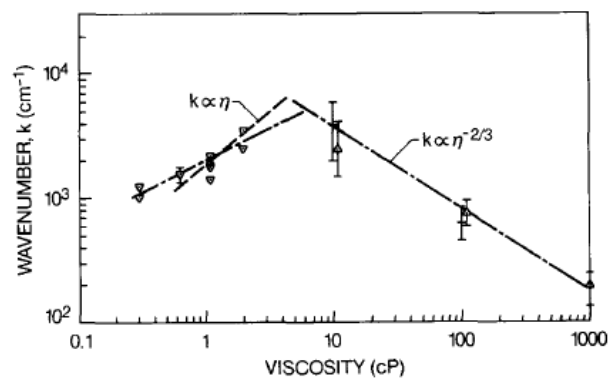


fig 2.38 wavenumber of the interfacial instability, points are from shadow measurements in organic liquids, lines are wavenumber in inertial limited or viscosity limited cavity expansion, the cavity expansion in negative polarity is assumed to be driven by a negatively charged interface repelled from the point by electrostatic pressure, from [Jones], the viscosity has an influence on both the growth rate and the morphology of the negative discharge.

Viscosity is reported to influence slow negative mode in organic liquids [Beroual] [Fofana][Jones] as shown in **fig 2.38**. The viscosity of the liquid is associated to the tangential friction of adjacent fluid layer (shear stress). The viscosity can create a **drag force** as the liquid is pushed aside by the propagating gas channel. This observation is very important for theories of streamer propagation based on equilibrium between a kinetic energy of the liquid displaced by the streamer and the drag force of the viscous liquid. The viscosity has almost no influence at all on the propagation velocity of positive streamers and a weak influence on the initiation of the positive discharge mode.

The viscosity has an obvious influence on the **postdischarge dynamics** of the gas channels and the **removal of the microbubbles leaved behind by the discharge**. Paradoxically the breakdown strength of a highly viscous liquid will be lower because of the problematic evacuation of the microbubbles left behind by the partial discharges. Those microbubbles can play the role of easily ionisable gas pockets.

2.4.9 Influence on the surface tension

Surface tension is one of the main liquid parameter (with viscosity) that could influence the **gas/liquid interface**. The surface tension is associated to the spring behaviour of an interface, this force arises from the asymmetric intermolecular bounding of the fluid molecules at the interface.

It is reported to have a weak influence on the initiation and no influence on the propagation. This parameter has a similar role as viscosity because it will try to limit the expansion of a gas cavity. It also intervenes in the interface instability growth rate and thus has an influence on the gas cavity shape and the post discharge gas channel fragmentation into a cloud of microbubbles.

The **pre-existing microbubbles** inside the liquid before the discharge initiation will have a **radius** dependent on the surface tension. The microbubble radius distribution is thus influenced by this experimental parameter and can influence the discharge initiation and the discharge propagation by changing the typical size of the available gas pockets inside the liquid.

Changing the surface tension by introducing some **surfactant** molecules will also modify the liquid ionic conductivity. Only high conductivity measurements will be possible.

2.4.10 Influence of liquid molecular structure

Different studies inside several oil liquids [Beroual] [Ushakov] have shown that the **liquid nature has a strong influence on discharge shape, initiation, threshold voltages and propagation velocity**.

However, changing the liquid changes almost **all experimental parameters at the same time** and thus it is difficult to correlate those phenomenons to the organic carbon chain length or other parameters such as the position of the organic functions or the carbon chain cycles.... Integrated parameters such as ionisation potential or electronic affinities discussed in the following section are much more relevant.

The longer the carbon chain, the larger the solvation energy of the localised electronic states (described in the following). It would be harder to promote (electrically or thermally) the localised electrons to the quasi-free state of the conduction band [Lewis]. Any double or triple C-C bond will increase the scattering rate of the electrons and thus decrease the electronic mobility [Date].

2.4.11 Influence of additives: electronic affinity and ionisation potential

Various additives have been tested in dielectrics liquid by the power HV transformer community [Beroual][Ingebrigtsen2007]. The main observation is that **additives with strong electronic affinity have no influence on positive streamers but increase negative streamer velocity** [Beroual] as shown on **fig 2.40**. On the contrary, low ionisation potential additives have no influence on the negative streamers but increase the positive streamer velocity [Beroual] as shown on **fig 2.39**.

| Additives | Concentration, M | Velocity $\bar{v}_d \cdot 10^{-5}$, cm/s |
|--|------------------|---|
| Pure | | 2.60 |
| DMA | 0.008 | 2.62 |
| | 0.016 | 2.63 |
| | 0.040 | 2.70 |
| | 0.079 | 2.78 |
| | 0.158 | 2.86 |
| | 0.395 | 2.78 |
| SH ₃ C ₁₀ H ₇ | 0.007 | 2.58 |
| | 0.072 | 2.96 |
| | 0.145 | 3.22 |
| | 0.362 | 3.19 |

fig 2.39 influence of additives on the propagation of the positive discharge in nhexane, from [Ushakov], point to plane configuration, 1cm gap, 45kV.

| Additives | Concentration, M | Velocity, $\bar{v}_d \cdot 10^{-4}$, cm/s |
|---|------------------|--|
| Pure | | 0.6~0.9(0.8) |
| CCl ₄ | 0.010 | 1.0~2.3(1.8) |
| | 0.052 | 1.9~4.3(2.9) |
| | 0.104 | 3.3~6.9(4.7) |
| | 0.208 | 3.3~7.5(4.8) |
| | 0.520 | 4.4~7.3(5.9) |
| CF ₃ (CF ₂)CF ₃ | 0.005 | 1.4~2.2(1.9) |
| | 0.050 | 1.8~2.8(2.3) |
| | 0.100 | 3.0~4.0(2.8) |
| | 0.250 | 3.2~6.2(4.1) |
| SH ₃ C ₁₀ H ₇ | 0.007 | 1.3~2.1(1.6) |
| | 0.072 | 1.9~2.2(2.1) |
| | 0.145 | 1.6~2.2(1.9) |
| | 0.362 | 1.7~2.2(2.0) |

fig 2.40 influence of additives on the propagation of the negative discharge in nhexane, from [Ushakov][Foster], point to plane configuration, 1cm gap, -45kV.

Ionisation potential will be relevant to for **field ionization** or **impact ionization** mechanism. Positive streamers are of course sensitive to the electron extraction from the liquid. The mechanisms able to supply electrons from the liquid at positive polarity are:

- vaporization followed by impact ionization in the gas phase [Joshi]
- Impact ionization in the liquid phase [Joshi] [Felici] [Atrazev]
- Field ionisation of the liquid molecules (autoionization) [Ushakov]
- Electron detachment from the negative ions

The **electron affinity** is associated to the energy level of the quasi-free electronic state, it is typically of the order of 1eV. The electron affinity can be positive or negative. A positive value will lead to a high probability to localise the electron into a negative ion state, on the contrary a

negative affinity means that the molecules are repelled from a solvated electron, the electron will have a surrounding shell. Such electron bubbles have been identified in liquid noble gases.

This study is of most importance for the propagation mechanism of streamer in liquids. Negative streamers propagation seems to be related to electron impact on the gas/liquid interface. The attachment rate dictates the recombination rate of electrons at the interface. Those electrons release their energy depending on the electronic affinity of the liquid molecule. This electronic affinity is related to the cross section associated with the several electron energy dissipation processes.

2.4.12 Brief summary on the influence of experimental parameters

| parameter | initiation | propagation | Stopping length | shape |
|----------------------|---|---|------------------------------------|--|
| Interelectrode gap | Influenced via the reactor impedance | Series resistance with the plasma | Series resistance with the plasma | |
| Voltage amplitude | Influence joule heating, charge injection, electrostatic stress | Influence charge injection and extraction, electrostatic stress, avalanches | | More branching, More filaments |
| Voltage duration | | | Stopping voltage | |
| Conductivity | Joule heating | Charge removal | Reilluminations, DBD-like behavior | |
| Hydrostatic pressure | Bubble pressure | | Channel pressure | |
| Surface tension | Bubble nucleation | | | Interface shape |
| viscosity | Bubble nucleation | Drag force | | Interface shape |
| additives | | Electron affinity influences negative discharge, low ionization potential influences positive discharge | | |
| Dielectric barrier | DBD versus current needed for plasma ignition | Discharge needs to go around the barrier | Avoid spark | Discharge can be attracted or repelled by the dielectric barrier |

2.5 Electrostatic considerations

The **tree-like** plasma structure can be considered as an **electrical network** and can be modelised as a **simple electrical circuit**. Such model is able to correlate the plasma structure shown in **fig 2.41** to the discharge current knowing the equivalent value of the plasma channel resistance and its capacitance in respect to the opposite electrode. It is a macroscopic predictive (once calibrated) model that does not require a detailed understanding of the microscopic processes.

The following electrical model can be found in [Beroual][Aka-Ngnui2001] At each time step, a plasma branch is created according to a probability law for the branch length and its direction. Then node law and branch law are applied to obtain a system of electrokinetic equations which will be solved by matrix iterative solver.

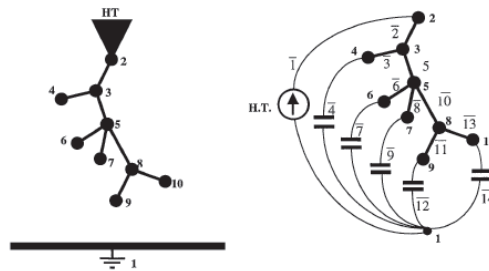
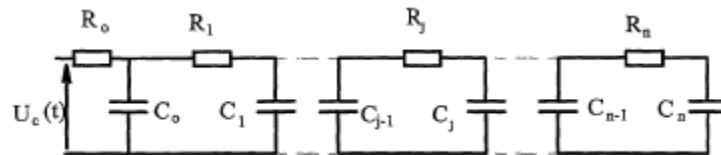
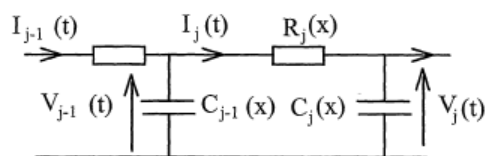


fig 2.41 plasma tree-like structure modeled as a network of resistive branches with capacitive coupling of the branch tips with the opposite grounded electrode [Beroual].

For a single filament, the inception of a new branch segment is associated to a new **RC cell**, one can thus make the following equivalent circuit:



With each new cell defined as:



Node law for current and cell law for voltage give:

$$i_j(t) = C_j(x) \frac{dV_j(t)}{dt}$$

$$i_j(t) = \frac{V_j(t) - V_{j-1}(t)}{R_j(x)}$$

$$C_{j-1}(x) \frac{dV_{j-1}(t)}{dt} = i_{j-1}(t) - i_j(t)$$

$$i_j(t) = \frac{U_c(t) - V_0(t)}{R_0}$$

Where $U_c(t)$ is the voltage waveform at the point electrode, V the voltage at the node, i the current at the node, R the resistance of the branch, C the capacitance of the branch.

- At the point electrode or at the tip of one filament the electric field can be determined by the relation in the case of a filamentary mode (secondary positive mode for instance):

$$E_p = \frac{2U_j}{R_p \ln 4 \left(\frac{D - Sz_j}{R_p} \right)}$$

- For and hemispheric shape of the plasma structure (primary positive mode or other slow modes in oils):

$$E_p = \frac{U_j}{D} \left[Sz_j D \left(1 - \frac{Sz_j}{D} \right) \right]$$

With the filament length, the gap distance and the counter electrode defined in:

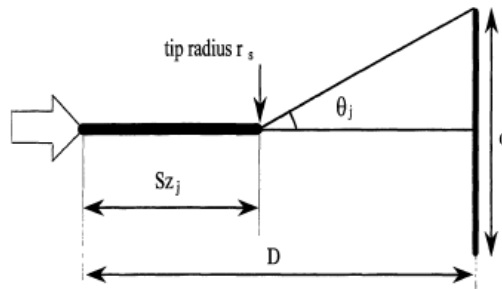


fig 2.42 resistive plasma branch j of length Sz_j , with remaining gap $D - Sz_j$ and collection angle θ_j with the opposite grounded electrode of diameter ϕ .

However, this electric field is not used to calculate the streamer **velocity**. It is used to check at each time step if its value is above the threshold field value for the propagation of the considered plasma mode. This criterion consists in checking if the electrostatic energy available is above the heat vaporisation of the liquid required to evaporate the new section of liquid. If this propagation criterion is met, a new section is generated with a random length and a random direction.

Here is the procedure to solve the electrical network. The discharge current is distributed among the several branches and is purely capacitive displacement current. The **occupied branch tip is a node**, the **free branch is linked capacitively to the ground plane electrode**.

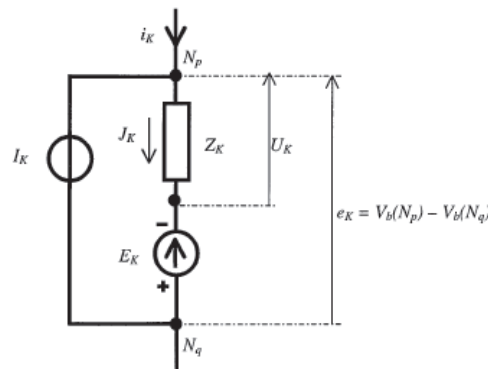


fig 2.43 each plasma branch between two branching nodes can be considered as a resistive component Z_k , a current source (displacement current) I_k , and voltage source E_k . With E the voltage source in the branch, e_k the voltage across the branch, i the current of the branch, J the current in the passive resistive element, I the current source (capacitive).

fig 2.44 presents the numbering of the cell and the nodes for the first step:

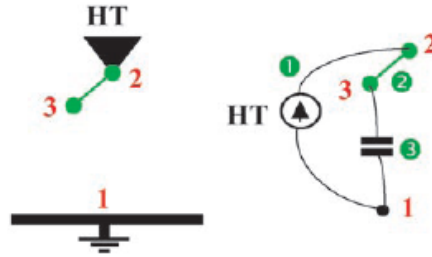


fig 2.44 branch and node numbering

Each connected node has a current source and voltage source. The plasma branch lineic resistance R is related to the channel radius r_0 and the plasma conductivity σ :

$$R = \frac{l}{\sigma \pi r_0^2}$$

The equivalent capacitance C_{capa} of a tip and the ground plane is obtained from:

$$C_{capa} = 2\pi \varepsilon_0 \varepsilon_r \alpha_c \left(1 + \frac{m_1}{1 - m_2}\right)$$

$$\text{With } \alpha_c = 1 - \left(1 + \left(\frac{\phi/2d}{1 - m_2}\right)^2\right)^{-1/2}$$

$$m_1 = r_0/d$$

$$m_2 = L_{axial}/d$$

ϕ and d are defined on fig 2.42.

See [Beroual 1998] and [Beroual 2000] for the nodal resolution using a voltage source matrix, current source matrix, node/branch matrix, and admittance matrix.

The **propagation velocity is used to calculate each branch length and is assumed to consume a percentage β of 10% of the injected electrostatic energy available**. The propagation velocity is assumed to have a pressure, density, and channel diameter dependence according to the **experimental fitting** in hydrocarbon liquids:

$$v = \left(\frac{2\beta P}{\rho \pi r_0^2}\right)^{1/3}$$

with P the pressure, and ρ the mass density.

This simple electrostatic model is based on several assumptions that can limit its relevance and its reliability. The assumed propagation velocity will only be valid for some specific plasma modes in oil. We also need to know precisely the channel diameter which is not obtained selfconsistently. The plasma conductivity (estimated at $5e-2\Omega/cm$) is also not a known parameter and precisely need to be determined from the channel diameter (estimated at $10\mu m$), the plasma whole structure and the measured discharge current, etc. The plasma **tree-like structure is assumed to be randomly generated** and does not emerge from an intrinsic instability mechanism of the plasma propagation itself. It is true that branching can be driven by an impurity mechanism such as randomly distributed bubbles, but in this case the random generation of the plasma structure should follow the microbubble distribution and not this arbitrary probabilistic distribution.

A more detailed understanding of the microscopic processes responsible for initiation and propagation is thus required.

2.6 The liquid state and its ability to withstand electron avalanches: from gases to liquids and vice versa

In this section we present the electronic state of liquids and its ability to endure an electron multiplication process leading to a plasma discharge.

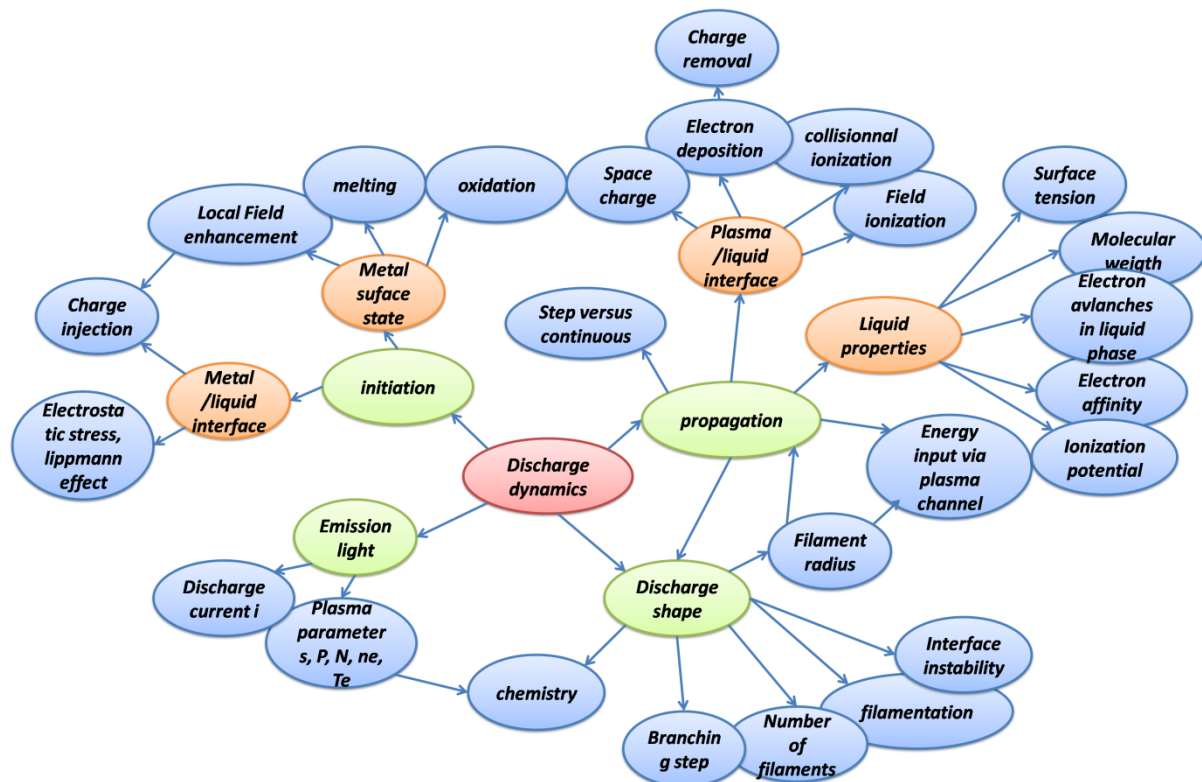


fig 2.45 schematic illustrating the concepts linked to plasma discharges inside liquids.

In a first step, we describe here the classical plasma discharge physics in the case of gases in order to have some background and to introduce in a second step the case of the plasma discharge in the liquids. Hence we start from well established mechanisms in gases and will intend to introduce the differences which are specific of the liquid state.

2.6.1 Plasma discharge in gases

Two main regimes can be distinguished in gases in pulsed or DC fields depending on the operating pressure (neutral density):

- Townsend discharge (steady state glow) at low pressure
- Streamer discharge (transient and filamentary) at high pressure, followed by spark or arc

2.6.1.1 The Townsend gas discharge theory

The gas discharge physics is very well known for decades and based on the Townsend discharge mechanism. The glow discharge is based on **electronic avalanches** and **secondary emission** at the cathode space charge layer. Here is some basic notion of the glow discharge physics according to [Raizer Gas discharge physics].

The basic equation of motion of an electron of mass m accelerated by an electric field E and subjected to collision at a frequency ν_m gives the asymptotic behaviour for electron velocity v_d :

$$v_d = -eE/mv_m$$

Thus one can define the **electron mobility** μ_e which is basically inversely proportional to the neutral particles density

$$\mu_e = e/mv_m$$

And the electron **drift velocity** in the electric field will thus be proportional to E:

$$v_d = \mu_e E$$

| Gas | $\mu_e p,$ $10^6 \frac{\text{cm}^2 \text{Torr}}{\text{V} \cdot \text{s}}$ | $\nu_m p,$ $10^9 \text{s}^{-1} \text{Torr}^{-1}$ | $\sigma p/n_e,$ $10^{-13} \frac{\text{Torr} \cdot \text{cm}^2}{\text{Ohm}}$ | range of $E/p,$ $\frac{\text{V}}{\text{cm} \cdot \text{Torr}}$ | $l_p,$ $10^{-2} \text{cm} \cdot \text{Torr}$ |
|-----------------|--|---|--|---|---|
| He | 0.86 | 2.0 | 1.4 | 0.6-10 | 6 |
| Ne | 1.5 | 1.2 | 2.4 | 0.4-2 | 12 |
| Ar | 0.33 | 5.3 | 0.53 | 1-13 | 3 |
| H ₂ | 0.37 | 4.8 | 0.58 | 4-30 | 2 |
| N ₂ | 0.42 | 4.2 | 0.67 | 2-50 | 3 |
| air | 0.45 | 3.9 | 0.72 | 4-50 | 3 |
| CO ₂ | 1.1 | 1.8 | 1.8 | 3-30 | 3 |
| CO | 0.31 | 5.7 | 0.5 | 5-50 | 2 |

[Mobilities were found by approximating the experimental curves $v_d(E/p)$ with the function $v_d = \mu_e E$; ν_m and σ were calculated using the value of μ_e . Mean free path lengths, $l = (N\sigma_e)^{-1}$, refer to electron energies of 1 to 10 eV, typical for the positive column of glow discharges.]

fig 2.46 transport parameters in the Townsend discharge for several gases [Raizer].

The electronic current density j flowing through the plasma will be:

$$j = -en_e v_d = en_e \mu_e E = \sigma E$$

With σ the electrical conductivity of the plasma, n_e is the electron density.

The electron will be accelerated and collide on the neutral molecules and thus drift according to their mobility but also the electron density gradient will induce some electron pressure and the electrons will diffuse and gives the flux Γ_{\pm} :

$$\Gamma_{\pm} = \pm n \mu E - D \nabla n$$

According to some **diffusion coefficient** D:

$$D = \langle v^2 / 3 \nu_m \rangle$$

According to Raizer this diffusion coefficient can be fitted:

$$D_{e,thermiq} = K \frac{1e5}{p[\text{torr}]} \text{cm}^2/\text{s}$$

With the coefficient K given by the following table:

| gas | He | Ne | Ar | H ₂ | N ₂ | O ₂ |
|-----|----|----|-----|----------------|----------------|----------------|
| K | 2 | 20 | 6.3 | 1.3 | 2.9 | 12 |

The species balance is thus described by:

$$\frac{\partial n}{\partial t} + \text{div } \Gamma = q = S - L$$

With S describing the source and L loss terms of charged particles, Γ the flux, n the density. Basically the production of electrons comes from ionization and detachment, the loss of electrons comes from recombination or attachment.

The electronic density diverges for some value of the applied voltage called the **breakdown voltage**. The Townsend discharge follows a scaling law called the **Pachen law**. The Townsend breakdown voltage only depends of a product of **pressure*gap** and the gas composition as shown in **fig 2.47**.

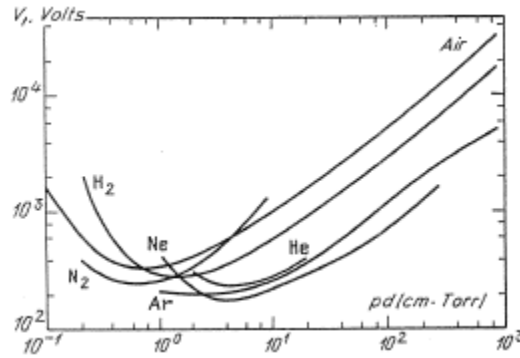


fig 2.47 Paschen curve , breakdown voltage V_1 as a function of the product pressure*gap.

and can be fitted by the following expression:

$$V_1 = \frac{B(pd)}{C + \ln(pd)}, \quad \frac{E_1}{p} = \frac{B}{C + \ln(pd)}, \quad C = \ln\left(\frac{B}{\ln(1/\gamma + 1)}\right)$$

$$(pd)_{min} = \frac{e}{A} \ln(1 + 1/\gamma), \quad (E/p)_{min} = B, \quad V_{min} = \frac{eB}{A} \ln(1 + 1/\gamma)$$

With A and B constants depending on the gas, γ is the secondary emission coefficient of the considered gas.

At steady state the electric field in the discharge is screened on a length called the **Debye length** and the electric field is in fact restructured and concentrated in non quasineutral regions at the boundary of the plasma. On the cathode side, the cathode layer is a region depleted of electrons and contains only drifting ions. This is a positive space charge region. The ions are accelerated in this space charge and impact on the cathode and cause the emission of secondary electrons. At steady state, the discharge current running through the discharge is only carried by those secondary electrons.

The Townsend discharge theory can be pushed much further to describe microplasmas, thermal constriction, dark discharge regime, instabilities and striations. Some discrepancies can be observed in some very specific discharge regime but the Townsend mechanism is quite universal. This mechanism holds for pd values under some threshold. Beyond that threshold, in particular near atmospheric pressure, another mechanism takes place: the streamer mechanism. Discharges in liquids present more similarities with streamer discharges than Townsend discharge because of they occur at high pressure and have a filamentary shape.

2.6.1.2 The gas streamer theory

For high pressure*distance value, the electron avalanches grow very quickly and the amount of heavy positive ions left behind constitutes a **space charge** that induces an electric field. The transition from Townsend mechanism to the streamer mechanism is reached when the space charge electric field cannot be neglected compared to the applied Laplacian electric field. This threshold is called the **Meek criterion** and can be associated to an absolute number of electrons in the avalanche of 10^8 cm^{-3} in air at atmospheric pressure at **30kV/cm**. The Meek criterion is equivalent to a threshold in the avalanche growth rate $\alpha d = 18-20$. At this point the plasma discharge transforms from diffuse to filamentary shape. This criterion is met for pd value above 200torr/cm. For streamer mechanism see [Raizer] [Meek1940] [Babaeva] [Bourdon] [Celestin] [Dyakonov] [Ebert] [Koslov] [Kulikovskiy] [Kogelschatz] [Pancheshny] [Serdyuk].

The space charge left by the primary electron avalanche generates a positive space charge electric field that attracts electrons as shown in **fig 2.48**. The **seed electrons** present in the medium ahead of this space charge converge toward this region and make secondary avalanches by collisional ionization. Those secondary avalanches sink into the positive head and neutralize it. They also leave behind heavy positive ions that constitute the new space charge region. It is

thus an **ionization wave**, one individual electron does not cross the entire gap, only the ionization front advances across the interelectrode gap. The streamer phenomenon can be described as an ionization front or an ionization wave advancing and leaving behind a weakly conductive plasma channel.

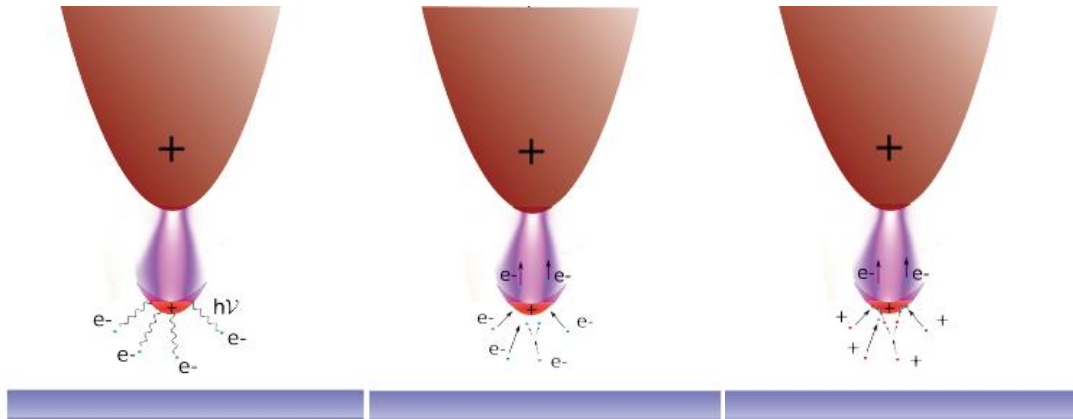


fig 2.48 positive streamer propagation in gases : photoionization of seed electrons ahead of the plasma filament tip, avalanche of electrons converging toward the filament tip, positive space charge left behind the avalanches [Celestin2008].

The streamer model follows the set of fluid equations in cylindrical coordinates (r,z) [Kulikovskiy1997]:

$$\begin{aligned} \frac{\partial n_e}{\partial t} + \frac{1}{r} \frac{\partial(rj_{er})}{\partial r} + \frac{\partial(rj_{ez})}{\partial z} &= S_{ph} + S_i - L_{att} - L_{ep} \\ \frac{\partial n_p}{\partial t} &= S_{ph} + S_i - L_{ep} - L_{pn} \\ \frac{\partial n_n}{\partial t} &= S_{att} - L_{pn} \\ \Delta V &= -\frac{e}{\epsilon_0} (n_p - n_e - n_n) \\ j_e &= -D_e \nabla n_e - \mu_e n_e E \end{aligned}$$

Only three families of species are considered: electrons with density n_e , heavy positive ions n_p , neutrals n_n , V is electric potential.

The transport equations of heavy ions and neutrals neglect the ion current: only the electron current $j_e = j_{er} + j_{ez}$ is taken into account on the time scale of the streamer propagation. The mobility difference of positive ions and electrons is quite convenient and allows to assume that ions are immobile. The electron current follows the drift-diffusion approximation with the electron mobility μ_e .

$$\mu_e = 2e6 (0.1E/N)^{0.8} cm^2/V/s$$

with N the neutral density.

Those equations are non **linearly coupled through the electric field**. The source terms depends strongly on the Townsend coefficient and thus on the electric field. The loss term depends on the chemistry of the gas mixing. In air the electron collision on the neutral molecules will lead to the production of chemical radicals as shown in **fig 2.49**.

ELECTRON-MOLECULE REACTIONS AND PARAMETERS OF THEIR RATE CONSTANTS
 $k = A \exp(-B/(E/N))$. B AND E/N ARE IN Td ($1 \text{ Td} \equiv 10^{-17} \text{ V} \cdot \text{cm}^2$)

| Reaction | A , cm^3/s | B , Td |
|---|--|---|
| $e + \text{O}_2 \rightarrow e + \text{O}_2(\text{a}^1\Delta)$ | $\begin{cases} 1.0 \times 10^{-9}, & E/N \leq 40 \\ 6.3 \times 10^{-11}, & E/N > 40 \end{cases}$ | $\begin{cases} 120, & E/N \leq 40 \\ 8.1, & E/N > 40 \end{cases}$ |
| $e + \text{O}_2 \rightarrow e + \text{O} + \text{O}$ | 1.3×10^{-8} | 309 |
| $e + \text{O}_2 \rightarrow e + \text{O}(\text{1D}) + \text{O}$ | 1.0×10^{-8} | 338 |
| $e + \text{N}_2 \rightarrow e + \text{N}_2(\text{A}^3\Sigma)$ | 1.0×10^{-8} | 336 |
| $e + \text{N}_2 \rightarrow e + \text{N} + \text{N}$ | 6.3×10^{-9} | 949 |
| $e + \text{H}_2\text{O} \rightarrow e + \text{OH} + \text{H}$ | 2.0×10^{-11} | 322 |
| $e + \text{N}_2 \rightarrow e + \text{N}_2(\text{C}^3\Pi)$ | 6.3×10^{-9} | 486 |

fig 2.49 collisional dissociation reactions in air by electron impact [kulikovsky].

S_{ph} is source term of electrons by photoionization, S_i is source term of electrons by collisional ionization, L_{att} is loss term of electrons by attachment on electronegative species, L_{ep} is electron/positive ions recombination, L_{pn} is positive ions/neutral recombination:

$$\begin{aligned}
 S_i &= \mu_e E \alpha n_e \\
 S_{att} &= \mu_e E (\eta_2 + \eta_3) n_e \\
 L_{ep} &= \beta_{ep} n_e n_p \\
 L_{pn} &= \beta_{pn} n_n n_p \\
 \alpha &= N 1.4e - 16 \exp\left(-\frac{600}{E/N}\right) \text{ cm}^{-1}
 \end{aligned}$$

The **stiff dependence to this electric field** leads to a precise threshold for the streamer initiation voltage. The electric field is the sum of the Laplacian electric field and the space charge electric field. The electric field is numerically solved by several overrelaxation methods SOR or UMPACK or PARDISO routines. A careful attention should be reserved to the electrode boundary discretisation and a ghost fluid method should be implemented to avoid any electric field oscillations at the metal electrode surface due to the stair case electrode boundary following the discrete mesh. This electric field oscillations has been observed to produce artificial streamer branching. The ghost fluid method defines image charge on the grid point inside the metal to obtain the exact value of the electric field on the exact position of the electrode boundary instead of defining the boundary as a stair [Celestin].

The streamer has a filamentary structure with a space charge separation around the whole filament that encloses a quasineutral weakly ionized plasma as shown in **fig 2.51**. This sheath and the quasineutral plasma filament are surrounded by the background neutral gas. The space charge amplitude is higher at the filament tip and thus this tip is the most active region. The streamer propagation is driven by this streamer head as shown in **fig 2.50**. The head is a space charge region with intense electric field that leads to intense excitation and light emission. The emission of the head will induce photoelectrons in front of the plasma filament tip in addition to the natural seed electrons as shown in **fig 2.48**. This **photoionization** is of most importance to explain the streamer propagation. Experiments have shown that streamer in air propagates at velocities of 10^8 cm/s well above the drift velocity according to electron mobility in a reasonable space charge electric field. Thus it is impossible to explain the propagation velocity of streamer without any non local ionization mechanism such as photoionization.

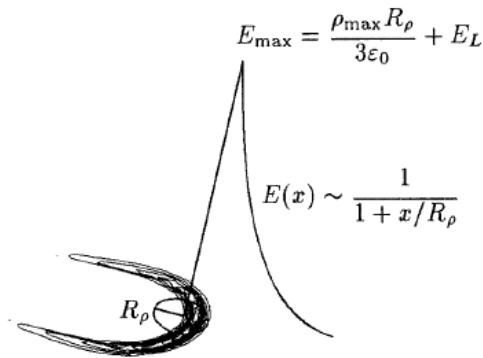


fig 2.50 space charge at the streamer head generates an intense electric field that superimposes with the applied Laplacian electric field E_L , R is the radius of the equivalent charged sphere producing the same electric field ahead of the streamer head, x is the distance from the streamer head [Kulikovskiy].

The numerical simulations such as **fig 2.51** and **fig 2.52** are most of the time initialized with a **Gaussian quasineutral plasma spot** $n_p(r, z)_{t=0}$ close to the high voltage electrode. They do not start from some isolated seed electrons and do not model the **avalanche to streamer transition**.

$$n_p(r, z)_{t=0} = n_e(r, z)|_{t=0} = n_0 \exp\left(-\left(\frac{r}{\sigma_r}\right)^2 - \left(\frac{z - z_0}{\sigma_z}\right)^2\right)$$

This numerical initialisation has an influence on the initiation time of the streamer discharge. The avalanche to streamer transition depends on this numerical initialisation. The initiation has only a little influence on the positive streamer but is critical in the case of the negative streamer [Kulikovskiy].

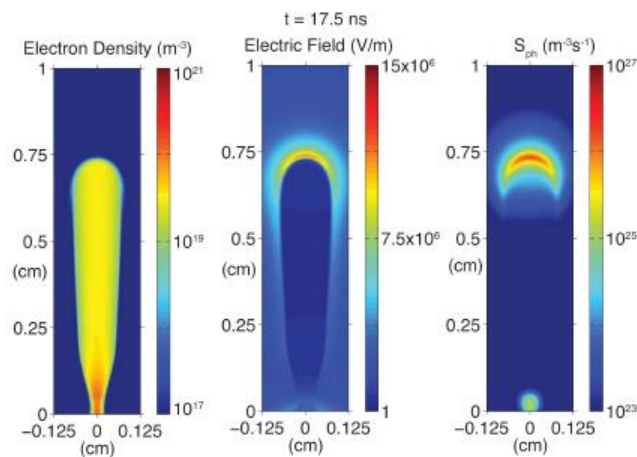


fig 2.51 structure of a streamer in air: electron density, space charge, photoionization source [Celestin]

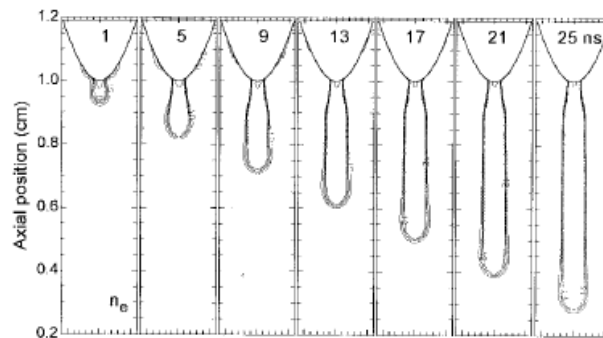


fig 2.52 propagation of the positive streamer [Kulikovskiy].

The plasma filament has an almost constant electron density of typically $1e14\text{cm}^{-3}$ at atmospheric pressure and the electric field along the filament is not very strong compared to the field around the streamer head as shown in **fig 2.53**. Those values and dependence of the electron velocity are just trends and may vary according to initial conditions of the simulation (preionization, plane to plane vs pin to plane geometry...).

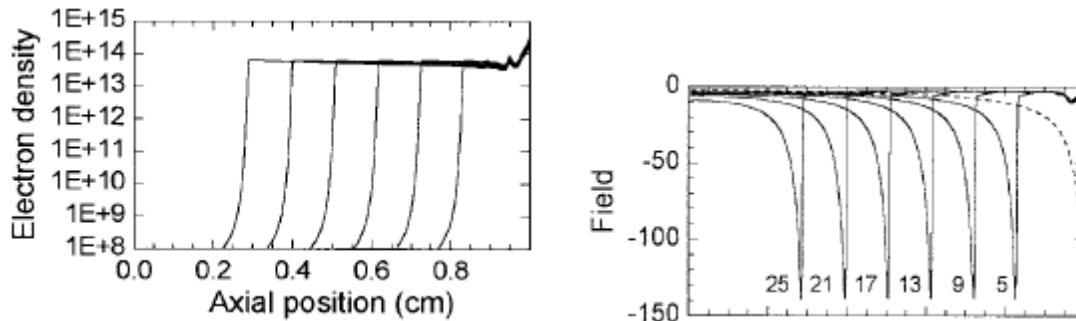


fig 2.53 electron density and electric field during the streamer propagation [Kulikovsky].

The propagation stops when the ionization rate equals the loss rate and the head neutralises and diffuses before vanishing.

In homogeneous fields the streamer radius and the **streamer propagation velocity** are reported to **increase exponentially** across the gap. On the contrary in a **strongly inhomogeneous** electrode configuration such as point to plane, the streamer propagation reaches a stationary regime quite soon and the radius and the propagation **velocity stays constant** [Kulikovski].

The streamer velocity is related to:

- the streamer head radius,
- the space charge separation magnitude
- the presence of seed electrons
- the photoionization rate and the typical absorption length of the photoionization photons in the medium
- the balance between the collisional ionization rate and the photoionization rate

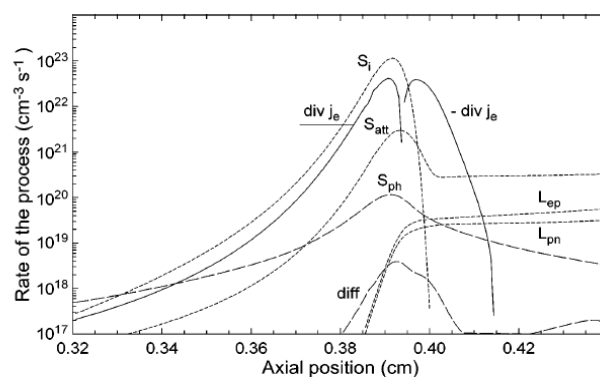


fig 2.54 rates of the different electron sources, S_{ph} photoionization, S_{att} electron attachment, diff diffusion, S_i collisional ionization, $div j_e$ divergence of the electronic current, L_{ep} recombination electron-proton, L_{pn} recombination proton-neutral [Celestin2009].

The relative importance of collisional ionization rate compared to the photoionization rate such as presented in **fig 2.54** strongly influences the propagation velocity. Close to the streamer head, the collisional ionization dominates. On the contrary, far ahead from the head the photoionization dominates and provides the seed electrons. The influence of the seed electrons is different from one author to another. The concentration of the seed electrons has been

proved to slow down the streamer and reduce the electric field in the head [Panchesni]. On the contrary according to [Starikovskiy] more **seed electrons** will lead to an acceleration of the propagation velocity and an increase in the streamer optical (apparent) radius and the streamer electrodynamic (true) radius. The discussion around the role of seed electrons is useful in the case of the repetitive discharges where the plasma occurs in a gas containing radicals and excited species that are more readily ionisable than the neutral gas.

The propagation velocity of the positive streamer obtained numerically are in good agreement with experimental results and the following fit depending only on the **streamer head diameter** d :

$$v = 0.5d^2[mm/ns]$$

The larger the streamer head, the larger the propagation velocity. For the negative streamer it is the opposite, a larger streamer head leads to a slower streamer in weak Laplacian electric field. The positive streamer is always faster than the negative streamer which is quite surprising because in the case of the negative streamer the seed electrons are already available and are immediately injected in the gas medium whereas in the case of the positive streamer, the electrons need to be produced by photoionization. In the case of negative streamer, the propagation velocity will always be at least equal to the electron drift velocity. The propagation depends mainly on the electric field generated by the streamer head, this field is amplified in the case of the **positive streamer** because of the $\text{div}(j_e)$ and will be smoothed in the negative streamer. This explains why the **negative streamer** is slower than the positive streamer in weak Laplacian electric field. At high Laplacian electric field, the difference between the positive and the negative streamer is less pronounced. This has been shown experimentally [Veldhuizen].

In the case of negative streamers, it is argued that photoionization is not required for the propagation since the electrons are injected into the medium and thus they would not need to be produced ahead of the filament.

The importance of $\text{div}(j_e)$ will influence the streamer radius. This factor explains most of the **morphological differences observed between the positive streamer and the negative streamer**. In the case of the negative streamer the electrons are injected into the neutral medium and in a divergent way that is to say escaping from the streamer head. It is always surprising that the negative streamer propagation velocity is always lower than the positive streamer. In fact the negative streamer **injects electrons into the medium** and does not require to **extract electrons** but the divergence of the electron injection plays against the propagation as it participates to spread the streamer head and reduces the magnitude of the space charge.

The **Townsend coefficient** has an influence on the propagation velocity. Decreasing the α/N coefficient leads to a strong decrease of the propagation velocity and an elongation of the streamer head from spherical to ellipsoidal. The Townsend coefficient will be particularly reduced in the case of a dense gas because of the reduced mobility of the charge carriers.

In liquids several differences from this gas streamer theory can be underlined:

- in positive polarity seed electrons are not necessarily produced by photoionization, they can come from microbubble impurities or field ionization.
- The electrical conductivity of the channel in the tail of the filament head can be more important in liquids where the electron density is likely to be one order of magnitude higher than in gases. Thus the point electrode voltage is better reproduced at the tip of the plasma filament and the space charge field will have less influence.
- Propagation timescale is also very slow compared to gases allowing for ion motion and the thermalisation of the channel (streamer to leader transition). Ion motion induces directed flux of particles able to etch interfaces. The leader transition implies a stepwise process.
- The density scaling between gas and liquids is important and thus electron transport parameters are quite different in liquids [Joshi][Atrazhev][Tobazeon].

2.6.2 Electron avalanches in liquid phase: the liquid state, ionization, recombination

The description of the electronic state of liquids is less understood compared to gases and solids. Liquids are an intermediate case between gases and solids: they have the solid density but they lack long range order.

There are two schools to describe the liquid state:

- Semiconductor analogy
- Dense gas approximation

Regarding plasma discharge, the main tricky question about the liquid state is to know if there are free electrons and if there can be 2 body collisional ionizations that would lead to electron avalanches.

2.6.2.1 Conduction in dielectric liquids according to semiconductor analogy: electronic state and mobility

According to the “**semiconductor approximation**” [Dyakonov1988] [Lewis], a liquid can be described as having a **valence band**, **conduction band** and **band gap**. In the plasma discharge scope we need to identify the solvated electronic states and the free electronic states. The mobility of solvated and free charges is indeed very different.

The electronic description of a liquid contains **localised (solvated)** and **delocalised (free) states**. The positive ions created from the dissociation of neutral molecules will have a localised state as a solvated positive ion and a delocalised state as holes. Conversely, the electrons are localised in solvated negative ions and delocalised as free charges. The liquid conductivity without free charges is based on heavy positive and negative ions dissociated from an ionic salt crystal and solvated by the liquid. The **typical mobility of a localised ion is of $1e-6m^2/V/s$** . The molecular dissociation into two ions depends on the energy levels of the positive and the negative ions and on the dielectric permittivity of the liquid. The dissociation is easier with high dielectric constant liquid such as water due to Coulomb force screening between the two ions. The thermal agitation would be able to easily dissociate the more weakly bounded molecule. The positive ion is situated at energy of I_g from the ground state and the negative ion is at A_g as shown in **fig 2.55** and will be quickly solvated by the liquid molecules electrostatic interaction with the newly formed ion. The molecules of the liquid will influence and polarise the atomic bonds inside the ion (**inner sphere influence**). This solvation will shift the negative and the positive ion levels by an energy P of typically 1eV for low permittivity dielectrics ($\epsilon = 2-3$) and several eV for liquid having a high dielectric permittivity. Those solvated ions are in a transient delocalised state $E(0)$ and will be quickly further solvated by a solvation shell (**outer sphere influence**): the surrounding molecules of the solvent align themselves with the solvated molecules. Because of this last contribution, the energy level will be further shifted by an energy amount of λ (of typically 1.7eV in the case of water) to a level $E(\infty)$. The λ shift is slower than the P shift, and thus two levels $E(0)$, and $E(\infty)$ can be distinguished.

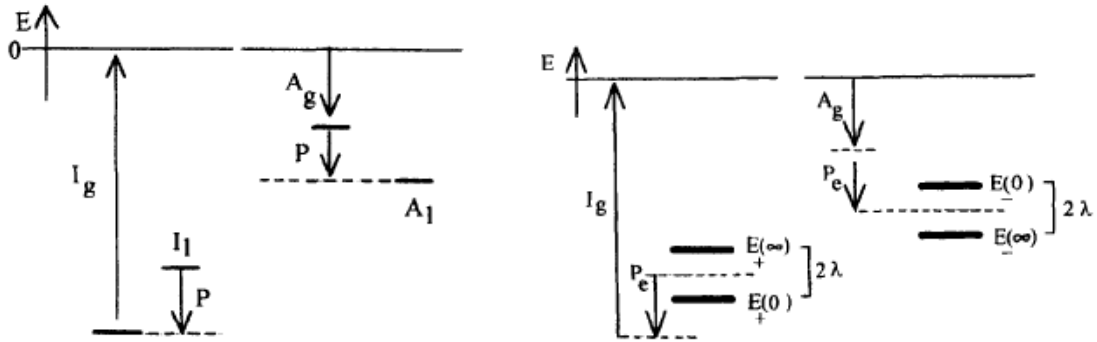


fig 2.55 electronic states in a liquid : polarization P due to inner shell influence results in delocalized electronic state $E(0)$, further slow polarization λ due to outer sphere influence results in fully localized electronic state $E(\infty)$ [Lewis1994].

Due to the thermal motion of the molecules those levels $E(0)$, and $E(\infty)$ are distributed into some valence and conduction bands. The **water band gap is 8.3eV**. Delocalised states have a much higher mobility and thus a higher drift velocity than localised states. Above $E_-(0)$ and below $E_+(0)$ are the conduction and the valence bands for quasifree electrons and holes. Localised state can be delocalised by applying an electric field.

The electrons and the holes can just **tunnel from one molecule to the next** as shown in fig 2.56. This hopping process is known to happen in solids. The hole conduction can occur in the liquid bulk or at the liquid-electrode interface or at the plasma filament head. The hopping happens across some barrier potential between the electron level and the empty hole level. The transition probability has an exponential dependence with intermolecular distance and the potential barrier amplitude. In a liquid the inter molecule distance is less rigid in the liquid than in a solid. It means that the tunnelling probability strongly fluctuates if the molecules get closer, thus the electron conduction by hopping process is quite likely. The potential barrier can be reduced by applied electric field, in particular at the metal/liquid interfaces near the electrode (charge injection).

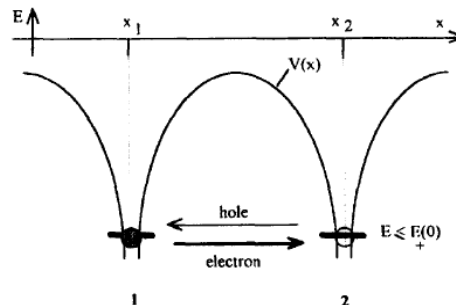


fig 2.56 electron/hole hopping through potential barrier $V(x)$ between two adjacent molecules separated by x_2-x_1 , between an hole in the conduction valence band and an electron at the same energy level, delocalized electronic state mobility [Lewis1994].

The electron tunneling through a potential barrier of $U - \chi$ from r_1 to r_2 is given by the **WKB formula** [Ushakov]:

$$D = \exp \left[-2(2m/\hbar)^{1/2} \int_{r_1}^{r_2} (U - \chi)^{1/2} dr \right]$$

With the potential of a molecule in a strong electric field E is given by:

$$U = - \left(\frac{e^2}{4\pi\epsilon\epsilon_0 r} \right) - eEr$$

The electron can be extracted from the molecule without collision but just by the electric field, this process is called **field ionization or autoionization**. This mechanism could explain how

electrons are extracted from the liquid in the case of the positive discharge mode. Autoionization is associated to zener tunnelling of an electron from its attached state to a free state.

In the case of a liquid where the electronic states can be described in terms of valence and conduction band with a valence band width τ of 3eV for water where have the autoionization transition probability D:

$$D = \exp \left[- \left(\frac{I}{Eed} \right) \left(\ln \left(\frac{2I}{\tau} \right) - 1 \right) \right]$$

and the current j:

$$j = \frac{N_e E e^2 d^2}{2\hbar \left(\ln \left(\frac{2I}{\tau} \right) - 1 \right)} D$$

with $I=8.76\text{eV}$ the ionization potential of water (12.6eV for vapour) (-1.3eV at the bottom of the conduction band of water), N_e is the electron density, d is the distance between two water molecules.

In the **delocalised free state, the electrons are slowed down by collisional elastic dissipation processes such as vibrational excitation, excitation, ionization**. The vibrational levels are a very important sink of energy in molecular liquids such as water, nitrogen, and hydrocarbon. This is not the case for liquid noble gases. Noble gases are also molecular liquids made of dimers, but each vibrational level will have a collision cross section maximum for some energy and thus the electrons will be able to accelerate almost freely between two cross section maxima. Thus the rovibrational excitation levels strongly influence the electronic mobility. See [Bonifaci1997] [Frayssines2003] for plasma discharges in noble gases.

The **electronic mobility** is calculated with the transition probability and the dissipation processes. For example the electronic mobility of an electron in water is $2e-7\text{m}^2/\text{V/s}$ with is below the mobility of a solvated ion which is of the order of $1e-6$. For comparison, in other liquids such as hydrocarbons the measured mobility is of the order of $1e-3\text{m}^2/\text{V/s}$, $1e-1$ for liquid xenon, $1e-8$ for ethanol.

2.6.2.2 The dense gas approximation: field ionization, collisional ionization, electron energy losses

Good physical considerations about plasma discharge in liquids assuming a dense gas approximation have been discussed in [Chadband][Athrazev][Felici].

Liquid density leads to collective interactions not from the electromagnetic point of view but because of **N body collisions**. The “**dense gas approximation**” assumes that two body collisions are still valid and that there is no fundamental difference between a liquid and a dense gas, the only parameter is the neutral particles density.

The transition probability of a field ionization can be calculated from the WKB formula as in the previous section and we obtain the transition probability D [Ushakov]:

$$D = \exp \left[- \left(6.8 \cdot 10^7 \frac{I^{3/2}}{E} \right) \theta(y) \right]$$

With I the ionization potential and y :

$$y = 7.6 \cdot 10^{-4} E^{1/2} / \epsilon^{1/2} I$$

And thus the current density j:

$$j = D e N \nu \frac{1}{6.8 \cdot 10^7} 2/3 \pi^{1/2}$$

with ν the attempt frequency to escape of the electron against the potential barrier, $\nu = 1e15/\text{s}$, and N is the density.

The dependence on the ionization potential of the molecule is of course quite violent as shown in **fig 2.57** and explains why adding an easily ionisable impurity inside the liquid has a strong influence on the positive mode.

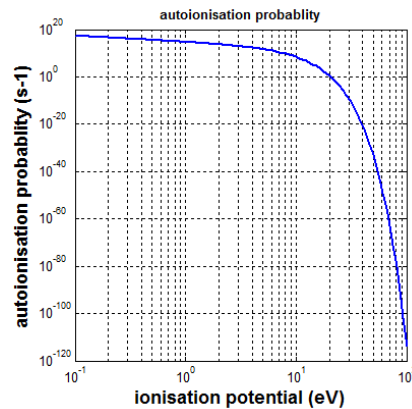


fig 2.57 field ionization rate dependence to the ionization potential of the molecule, Matlab plot using formula in [Ushakov], for 1.5 μ m channel radius, 5mm gap, 12.5kV .

The autoionization depends if the liquid is polar or not. The autoionization probability has also a very strong dependence with the electric field as shown in **fig 2.58**.

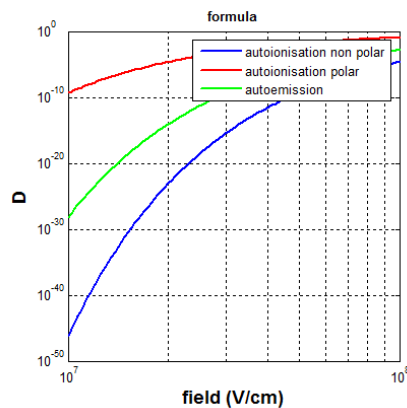


fig 2.58 field ionization for polar and non polar liquid at the anode (autoionization), and charge injection at the cathode (autoemission), D is the transition probability, replotted from [Ushakov], with same conditions as in .

The electron collisional data in liquids comes mainly from e-beam experiments and **radiolysis** or **radiochemistry** [Date][Champion][Munoz] [Jonah1976] [Joshi2007] [Laverne1993] [Thomas1964]. Those studies have shown that an **electron is solvated almost instantly** (fs) in the liquid and the hydrated electron state has a **ps lifetime** before recombination. Only a few analytical calculations in the case of liquid water have been made because it requires a complex interaction potential. The 2 body electron cross section with the water molecule is often a density extrapolation from gas phase cross section measurements. Because of the high density of the liquid compared to a gas, the collision angle coupled with the collision frequency will give a quick isotropisation of the avalanche. The classical two terms approximation in boltzmann equations solvers is no longer valid here. The electron avalanche has difficulties to move forward rather than radially except at very high electric fields.

From the **collisional data**, one can obtain the fluid **transport parameters** such as electron mobility and diffusion coefficient. Some Monte Carlo simulation has been performed by several authors [Joshi] that give the electron elastic collision, ionization and recombination rates show in **fig 2.59**. Those transport parameters in **fig 2.59** are required to determine the transport parameters in **fig 2.60** perform a **fluid modelling** of the discharge.

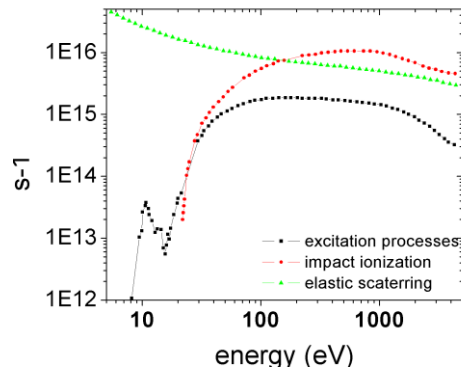


fig 2.59 rates of electronic dissipation processes in water : elastic scattering, inelastic collisions such as vibrational and excitation processes, ionization processes [Joshi].

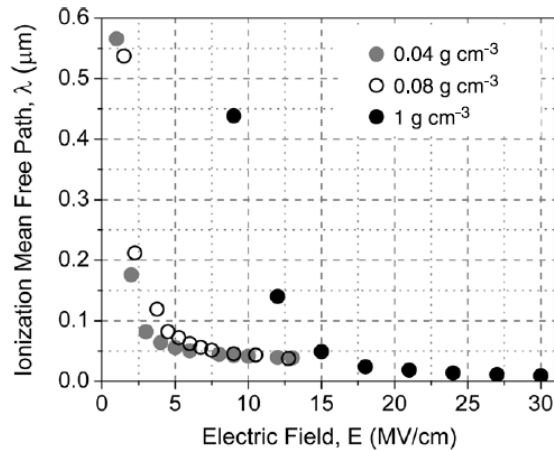


fig 2.60 Monte Carlo simulation of electron ionization mean free path as a function of the electric field for different water densities, dependence in $1/E$ [Kolb2008].

The charged particle balance depends on the ionization vs recombination frequencies in fig 2.59. This balance defines the discharge initiation threshold which can be defined as the moment where the charged particles number starts to diverge. The initiation electric field observed is much smaller than the predicted electric field for a pure liquid state. The simulation gives the correct electric field if there is a density lowering of the medium as shown in fig 2.61. It means that a pure liquid discharge is not possible but a full phase change to atmospheric pressure gas is not required either. A “**density lowering**” of the liquid is sufficient to reconcile this fluid model and the observed **discharge ignition threshold**.

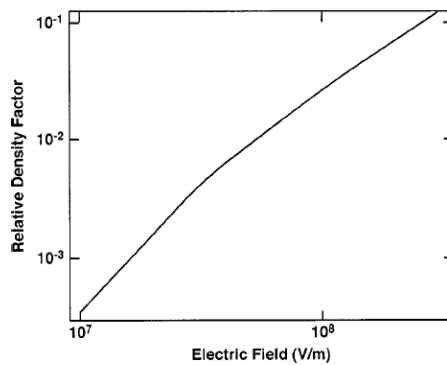


fig 2.61 water density versus electric field required for ionizing multiplication, density lowering of the liquid is required to reconcile the simulation and the experimental initiation voltage, Monte Carlo simulation [Joshi].

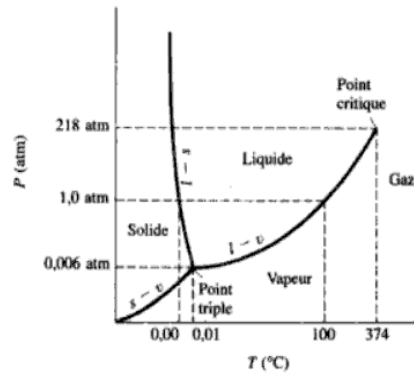


fig 2.62 phase diagram, the gas/liquid transition is smooth above the critical point at high pressure, above this point the dense gas approximation seems quite relevant.

This density lowering corresponds to a point in the **phase diagram** close to the **critical point** shown in **fig 2.62**. Hence the phase change can be quite smooth in term of density. It can be a phase change above the critical point at high pressure. Pressure measurements should be performed to test this assumption. This is why we tried to determine the **pressure in the nucleated gas phase** by measuring the **shock waves** emitted by the plasma discharge. Such pressure would be obtained for a fair amount of **superheating** of the liquid which means that the **energy deposition** (liquid heating) needs to be fast. A lower **heating rate** would lead to a gas change at lower pressure and lead a plasma discharge but probably a different mode since ionization would be much easier and thus the plasma parameters would be very different.

2.6.2.3 Gas content of the liquid, dissolved gas and microbubbles: impurities explain discharge propagation and morphology?

According to the electron transport parameters determined in the previous section, the **gas** content already dissolved into the liquid can thus be of primary importance. It would be an **impurity** driven mechanism.

The amount of gas dissolved inside the liquid and the radius of the microbubbles depends on:

- Surface tension
- Temperature
- pressure

Fluid simulations of a dense gas with lower density regions similar to microbubbles have been performed by [Joshi2004][Babaeva][Kushner2008]. In those recent simulations, the presence of bubble is simulated by **regions initialised with a lower density** (10 times typically) compared to the surrounding, the transport parameters are extrapolated from data obtain in gases or from Monte Carlo simulations presented in a previous section. They have shown that the bubble distribution (bubble radius and position) could explain at the same time the propagation and the morphology of the discharge as shown in **fig 2.63** and **fig 2.64**. The **gas bubble plays the role of a pocket of easily produced charges**.

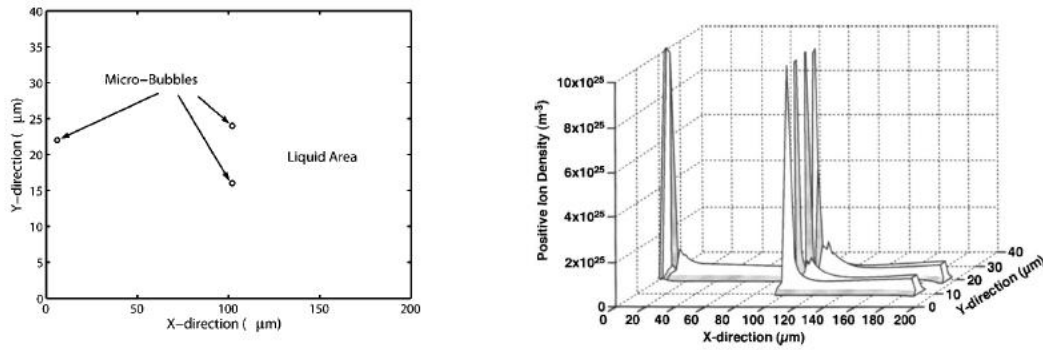


fig 2.63 microbubble inside the liquid are a supply of readily ionizable molecules and can favor the formation of plasma channels inside water, fluid simulation of plasma discharge in water [Joshi2005] using the transport parameters for electrons in a dense gas to extrapolate those parameters for density of liquid water.

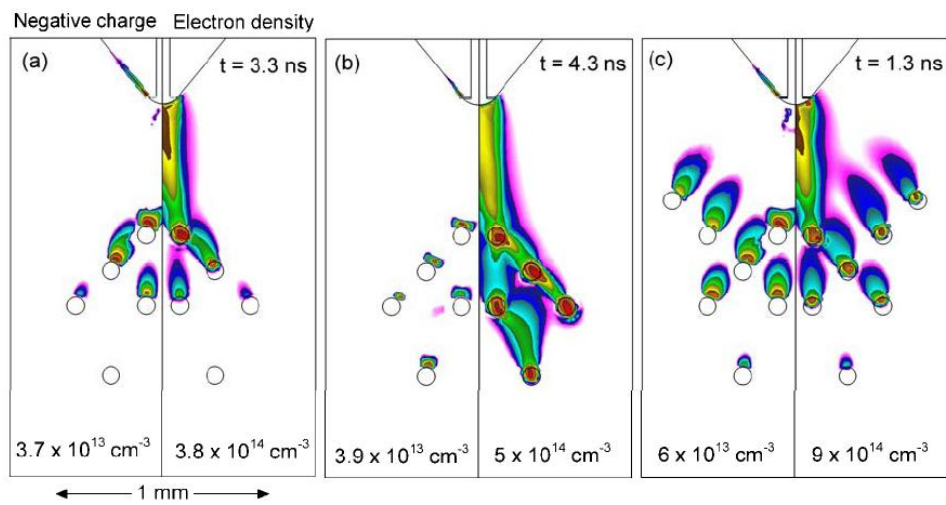


fig 2.64 simulation of a positive corona discharge in humid air with random bubble distribution in a 2atm gas with 0.2atm gas bubbles to simulate the presence of bubbles inside a liquid, left side is negative charge, right side is electron density, (max value indicated + 2decades in colorscale) [Kushner2008].

Bubble ignition is triggered by the advancing filament which brings a high electric field close to the microbubble as shown in fig 2.65. The microbubble then constitutes a new plasma filament branch that reconnects back to the main plasma structure. This **backward step propagation** is observed in simulations in positive polarity and should be easily observed in experiments provided the microbubbles are resolved by the optical setup.

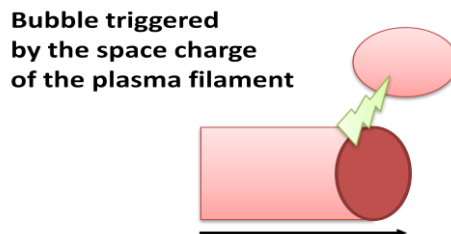


fig 2.65 the microbubble distribution inside the liquid can have a main role in the plasma filament propagation, the bubble would be triggered by the advancing filament and a positive and a negative streamer would start from the microbubble, then reconnect to the main plasma structure and advance in a new plasma branch.

The random behaviour of branching can thus be explained by the random distribution of the microbubbles inside the liquid. However there should be spots ahead of the plasma filament tip and there should be backward propagation of this spot that reconnects to the main plasma filament. The plasma discharge should also be strongly influenced by any change imposed on the microbubble distribution.

2.7 Bubble processes

The plasma state is an ionized gas phase, thus one could first suppose that plasmas in liquid are not a peculiar conductive state of the liquid but only a plasma inside a **gaseous cavity** inside a liquid. The propagation of a plasma into the liquid will then be the result of a **vaporization** stage followed by an ionization stage.

Bubble processes are likely to play a role for the discharge initiation or negative modes. Negative modes are often reported to be slow and bubbly shaped. **Gas/liquid motion** can then be a dominating mechanism in that case.

2.7.1 Bubble motion

2.7.1.1 Rayleigh motion: natural oscillation frequency

The plasma filament growth rate can be interpreted as a bubble elongation following the Rayleigh motion. The present section is based on papers from [Devin1959] [Howkins1965] [lightton2002] [Leroy2005] [Prosperetti1998] [Rath1980] [Strasberg1956] [Walton2005].

The Rayleigh motion mechanism is a **balance between the gas compressibility (spring) and the liquid inertia (mass)**. The gas bubble can be considered as an oscillator and thus have an oscillating response with some damping. The **damping** can be due to:

- viscous force during the dilatation and contraction of the interface,
- sound wave emission,
- thermal exchange

The **excitation term** can come from:

- external pressure excitation through the liquid
- gas source term by vaporisation
- gas thermal expansion
- cavity electrostatic expansion (because of a charged interface)

The response of this **bubble oscillator** can be linear with small deformation amplitude and non linear with large deformation amplitude. The basic **Rayleigh-Plesset** equation of motion is [prosperetti1998] [Leroy]:

$$R \frac{d^2 R}{dt^2} + \frac{3}{2} \left(\frac{dR}{dt} \right)^2 + \frac{4 \eta}{\rho R} \frac{dR}{dt} + \frac{2 \sigma}{\rho R} = \frac{1}{\rho} (P_{plasma} + P_{tension} - P_{hydrostatic})$$

with R the bubble radius, ρ the liquid density, η the dynamic viscosity, σ the surface tension, P_{plasma} the gas pressure inside the bubble due to the nucleation process and energy (thermal or electrostatic) release inside the bubble, $P_{tension}$ the pressure due to the surface tension, the $P_{hydrostatic}$ the applied hydrostatic pressure on the free surface of the liquid.

And easier approach is to use the **lagrangian equations**, the potential energy equal the work of the pressure along a displacement amplitude ξ [leroy2002]. For adiabatic compression

between initial pressure P_0 and volume V_0 and final pressure P'_2 , with interface velocity v , and the **adiabatic** constant γ [devin1959]

$$P'_2 - P_0 = -\left(\frac{\gamma P_0}{2V_0}\right)v$$

The potential energy PE is given by:

$$PE = -\int_0^v (P'_2 - P_0)dv = \left(\frac{\gamma P_0}{2V_0}\right)v^2$$

For an isolated spherical bubble, we have the velocity potential Ω (the potential is different in the case of a bubble attached to a wall, or a non spherical bubble):

$$\Omega = \frac{\dot{v}}{4\pi R}$$

With v the interface velocity and R the bubble radius.

And thus we can derive the velocity and the kinetic energy:

$$KE = \frac{\rho_2}{2} \int_{R_0}^{\infty} \dot{R}^2 (4\pi R^2) dR$$

With ρ_2 the liquid density

thus establish the lagrangian L from the kinetic and the potential energy:

$$L = \left(\frac{\rho_2}{8\pi R_0}\right)\dot{v}^2 - \left(\frac{\gamma P_0}{2V_0}\right)v^2$$

The equations of motion are given by the lagrangian equations. From Lagrange equation we deduce the **linear response** ω_0 of the system in the adiabatic approximation:

$$\omega_0 = \sqrt{\frac{K}{M}} = \frac{1}{R_0} \sqrt{\frac{3\gamma P_0}{\rho}}$$

With K the stiffness constant and M the equivalent mass. This is the **Minnaert frequency** or the breathing frequency of the bubble. Any bubble will respond to and impulse external stress with this frequency in the linear regime. In different geometries with non spherical bubble or close to a boundary the mechanism of oscillations remains the qualitatively the same but the expression of the breathing frequency would be different. This analysis comes from **sonoluminescence** studies where the bubble oscillator undergoes a resonance under some continuous external stress at the **breathing frequency**.

Here are the equation of motion with the displacement ξ , the breathing frequency ω_0 and the damping Γ in the free relaxation regime:

$$\ddot{\xi} + \Gamma \dot{\xi} + \omega_0^2 \xi = 0$$

With and external pressure stress we would have:

$$\ddot{\xi} + \Gamma \dot{\xi} + \omega_0^2 \xi = -\frac{4\pi R_0^2}{M} p_{ext}(t)$$

With R_0 the initial radius and $p_{ext}(t)$ the external pressure

During compression, the work done by the pressure is given by:

$$\frac{dW}{dt} = -(P'_2/v') \frac{\partial v'}{\partial t_1}$$

Which corresponds to an internal energy increase:

$$\frac{dU}{dt} = \rho_1 S_{v1} \frac{d\theta_1}{dt}$$

With S_{v1} the specific heat of the gas, and θ_1 is the temperature. The thermal energy q transferred by thermal conduction is given by:

$$\frac{\partial q}{\partial t} = K_1 \nabla^2 \theta_1$$

With K_1 the thermal conductivity. The heat dissipation by conduction will lead to damping and departure from the adiabatic assumption.

In case of **non spherical motion** but tubular motion the plasma bubble can be considered as a gas layer surrounded by two liquid masses as shown in **fig 2.66**. In this 1D geometry the Minnaert frequency is written [Prosperetti1998]:

$$\omega_a^2 = K/M_{eq}$$

With A the cross section of the tube, K is the equivalent spring constant of the bubble oscillator:

$$K = -A^2 \frac{dp_i}{dV}$$

And M_{eq} is the equivalent mass of the bubble oscillator taking into account the tube geometry:

$$M_{eq} = \rho A \left(\frac{1}{L_1} + \frac{1}{L_2} \right)^{-1}$$

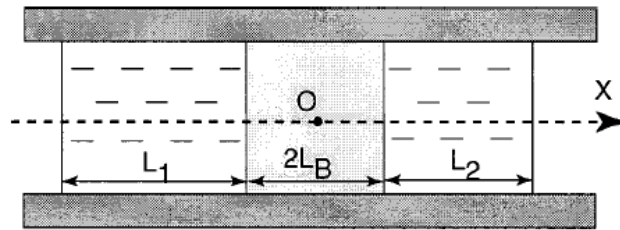


fig 2.66 oscillation of a gas layer between two water columns of length L_1 and L_2 in a capillary.

This bubble motion is well known in the sonoluminescence and soft matter communities. The growth rate from this mechanism can be an interpretation for the growth rate of the gas bubble at the early stage of the plasma generation inside a liquid [Chadband].

2.7.1.2 Inertia-limited bubble expansion

This bubble motion mechanism has been tested in particular for the high viscosity liquids such as oils or other organic liquids. In those insulating liquids spherical gaseous structure can be observed and constitute a slow prebreakdown phenomena or an early stage of the discharge. This structure does not present a filamentary aspect and is growing in a rather spherical symmetry. **The growth rate can be limited by the liquid inertia or by the liquid viscosity.** [Watson1991]

Here we consider that the **driving mechanism is the electrostatic pressure, not heating**. This assumption comes from a quick estimation of the pressure endured by a charged compared to the thermal pressure of temperature in the 1000K range. In **point to plane configuration** one can express analytically the **electric field** E with an hyperboloid to plane approximation,

$$E(R) \approx \frac{V}{R \ln(2(a/R)^{1/2})}$$

a is the distance between the center of the hyperboloid and the plane, R is the radius of the hyperboloid, V is the voltage. The plasma discharge cavity is considered as an expanding conductor of radius R. the **electrostatic pressure** is thus given by:

$$P_{electrostatic} = \frac{1}{2} \epsilon \epsilon_0 E^2(R) = \frac{1}{2} \epsilon \epsilon_0 \frac{V^2}{a^{1/2} R^{3/2}}$$

Integrating the pressure over the swept expanding discharge radius one obtains the **work done** by the driving electrostatic pressure:

$$W = \frac{4}{3} \pi \epsilon \epsilon_0 \frac{V^2 R^{3/2}}{a^{1/2}}$$

Equating this work to the **kinetic energy** of the repelled liquid with initial radius 0 we obtain the growth $R(t)$:

$$R(t) = \left[\frac{2\varepsilon\varepsilon_0 V^2 t^2}{a^{1/2} \rho} \right]^{2/7}$$

2.7.1.3 Viscosity-limited bubble expansion

In the case of a viscosity limited gas cavity growth driven by electrostatic pressure, the work done by electrostatic pressure is no longer equal to the kinetic energy of the liquid but is equal to the **dissipated energy by viscosity**. [Wtason][Jomni1997]. For incompressible flow around and expanding cavity at velocity U we have the fluid velocity:

$$v(r) = R^2 U / r^2$$

The energy dissipation due to the stress tensor can be expressed:

$$E = \frac{1}{2} \eta \int \left(\frac{\partial v_i}{\partial x_k} + \frac{\partial v_k}{\partial x_i} \right)^2 dV$$

With η the liquid dynamic viscosity, stress is radial.

$$\frac{\partial v}{\partial r} = 2R^2 U / r^3$$

and thus the dissipated energy due to the viscosity:

$$E_{diss} = (32/3) \pi \eta R U^2$$

Equating the dissipated energy to the work done by the driving electrostatic pressure over the expanding volume we obtain the growth [Watson1988]:

$$R(t) = \left[\frac{3\varepsilon\varepsilon_0 V^2 t}{10\eta a^{1/2}} \right]^{2/3}$$

A **transition** between those two growth rate has been observed in organic liquid and depends on the viscosity of the liquid. This transition dimensionless number is obtained by equating the viscous loss (obtained in the viscosity limited case) to the kinetic energy (obtained in the inertia limited case):

$$\frac{\rho R U}{\eta} = 16/3$$

2.7.2 Bubble nucleation: electrostatic crack mechanism

2.7.2.1 Electro-thermally induced “holes” in the liquid “lattice”

On short timescale (nanosecond) we can consider the liquid as a solid media and a **crack** can form under **electrostatic stress**. Such crack could explain the filamentary tortuous plasma and the branching. This theory is suggested by the morphological similarity between a classical crack network and the plasma discharge **branching**. The crack mechanism has two main steps: small molecular vacancy holes which are thermoelectrically induced, and a crack formation by electrostatic stress [Lewis].

The first assumption is that **defects (holes in the “mesh”)** can exist in a liquid on the molecular level. The liquid molecules are in a thermal continuous motion and establish bounds between each other. The intermolecular bounds are most of the time low energy long range interactions such as Van Der Walls bonds. The bound energy depends on the polar nature of the liquid: non polar liquids are more weakly bounded than polar liquid such as water. When a molecule is missing a cluster of molecules forms around with an **activation energy**. This “hole” in the liquid “lattice” is formed with a thermally activated mechanism limited by a mean activation energy U_g and is destroyed with a mean **recombination** energy U_c as shown in **fig 2.67**.

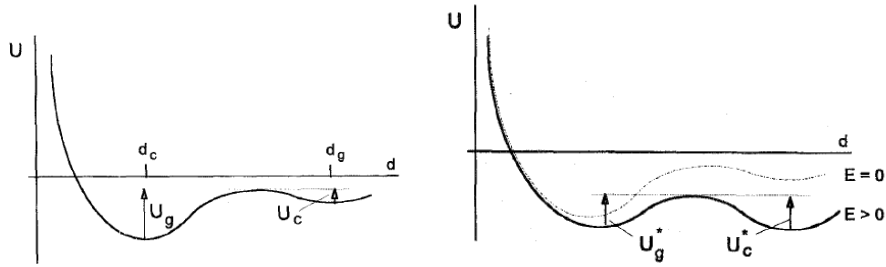


fig 2.67 d_c is the distance before a hole is generated, d_g is the distance after a hole formation in a liquid cluster, U_g is then the activation energy to create a hole (hole means cavity in this chapter, not positive charge) in the liquid, U_c is then energy required to collapse. The equilibrium concentration depends on $U_g - U_c$, this level difference can be modified in favor of hole formation with applied electric field.

Such holes are potentially responsible for:

- density lowering of the liquid
- charge localisation
- macro-crack propagation

Thus a **whole population of thermally activated holes can exist in a liquid**. The hole clusters are more **weakly bonded** than the bulk molecules of the liquid. Those evanescent holes have a population number strongly dependant on the temperature and on the pressure. The rate of formation of those holes under thermal or pressure stress is a nanosecond scale mechanism described by a formation rate K_b :

$$K_b = \omega \exp[-U_b/kT]$$

With ω the attempt frequency, U_b the activation energy and T the thermal agitation.

The rate of formation K_b of the holes is increased by the presence of an applied electric field and thus the equilibrium concentration is strongly dependant on this electric field.

$$K_b(E) = \omega \exp[-(U_b - \gamma_b \varepsilon E^2)/kT]$$

With ε the relative dielectric permittivity, γ_b the surface tension, and E the electric field, k is the Boltzmann constant, T is the temperature. The recombination rate K_r is given by:

$$K_r = \omega \exp[-(U_r + \gamma_b \varepsilon E^2)/kT]$$

And thus we have the hole particle balance equation:

$$\frac{dn}{dt} = K_b(N - n) - K_r n$$

With n the concentration of holes in the liquid "lattice" and N the concentration of liquid molecules. The solution is given in fig 2.68.

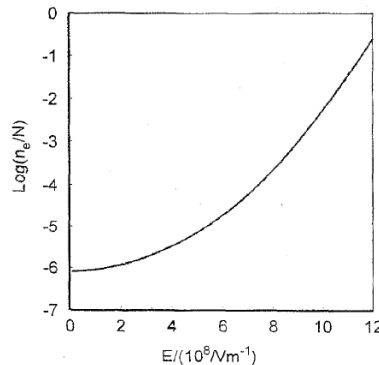


fig 2.68 equilibrium of the hole concentration as a function of the applied electric field in the case of n-hexane [Lewis].

2.7.2.2 Electrostatic stress and crack formation

The criterion for a **crack formation** can be lowered by this electrically enhanced hole population described in the previous section as illustrated on **fig 2.71**.

According to the **Lippman equation**, a **potential difference across an interface** (zeta potential of typically 1V over some nanometers for a double layer in a liquid) is balanced by a mechanical tension on the interface. This **superficial tension** depends on the electric field stress and a radial force can thus occur. This radial force works against the cohesive forces of the molecules bounds at the interface as shown in **fig 2.72**.

$$\Delta\gamma = -q\Delta V$$

with γ the surface tension, and V the voltage across the interface

$$\Delta\gamma = - \int_0^\delta \varepsilon E^2 dz$$

with γ the surface tension, ε the relative dielectric permittivity, E the electric field and δ the double layer thickness. This theory can be applied on a cavity inside a liquid. An electrical field will have a radial stress on a cavity as shown in **fig 2.69** helping the growth of macro-cracks in **fig 2.70**.

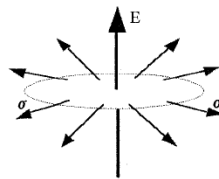


fig 2.69 tensile stress σ orthogonal to the electric field

$$F = \rho E - 1/2 E^2 \nabla \varepsilon + 1/2 \nabla (E^2 \rho_m \frac{d\varepsilon}{d\rho_m})$$

With F the radial volumic force on the crack, ρ_m the material density, E the electric field, and ε the relative dielectric constant.

The criterion for crack propagation can be taken from the well known **Griffith criterion** illustrated in **fig 2.70** which has been elaborated for solids mechanical ageing.

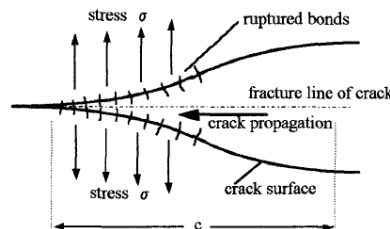


fig 2.70 Griffith criterion for crack formation : the energy of the newly formed crack length c needs to be lower than the stress energy that was stored in the medium.

The holes in the liquid lattice and the crack are two distinct ideas. Even if the crack mechanism is not valid, electrothermally enhanced holes in the liquid can still exist and need to be taken into account.

A crack development is very similar to a zip fastening, intermolecular bounds must be destroyed along a crack line and the local energy stored in the stressed medium must be above the energy of the new created interface. The branching or the tortuous morphology of a crack network is related to the statistical nature of the hole generation in the liquid. A defect is likely to appear with some distance from the crack line and a bifurcation will occur and can be identified as branching in filamentary plasmas. According to this crack theory there should be a strong effect of temperature, pressure, applied voltage amplitude, and applied voltage polarity. The effect of pressure, temperature, voltage originates from the activation energy modification for a hole formation.

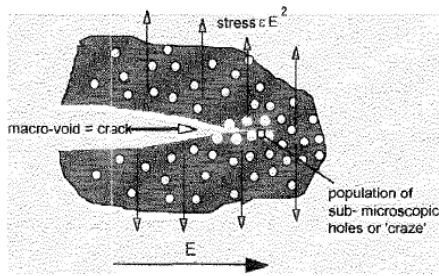


fig 2.71 hole formation by electrostatic stress can favor the opening of a macro crack in the liquid.

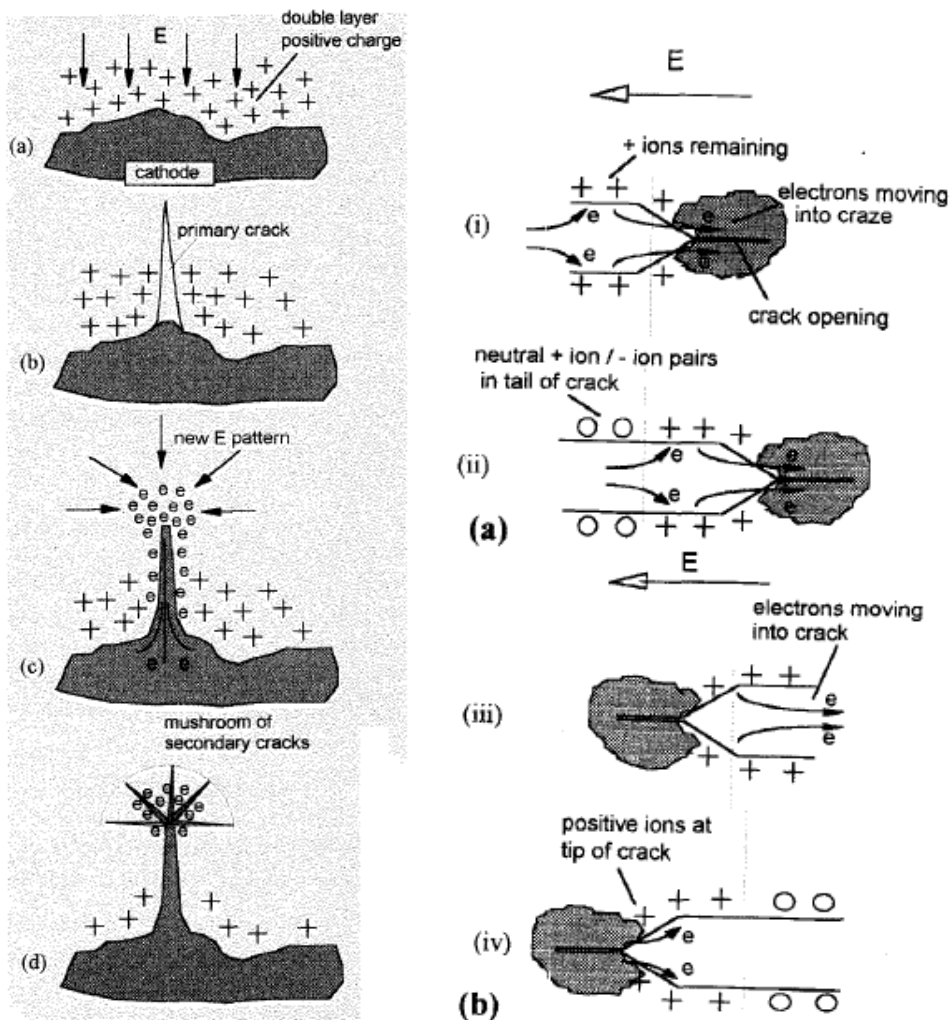


fig 2.72 the double layer at the electrode/liquid interface create MV/cm field on some nm layer, this field can induce a crack that will be ionized and report the electrode potential fruther on inside the liquid., the hole population electrostatically induced at the tip of the plasma filament will create new electronic states at the tip and allow electron injection (at negative polarity) or conversely electron extraction (field ionization at positive polarity).

The polarity effect originates in the fact that in the case of positive discharges electrons are extracted from the liquid microcavities whereas in negative polarity electrons are injected inside those microcavities as shown in fig 2.72. Basically the cavity is a void and can be filled with gas at the saturation pressure. Electron avalanches can occur in this low density medium and plasma will fill the cavity reporting the electrode potential at the cavity tip. The presence of those cavities in the liquid introduces new available electronic state (as in semiconductor doping) and

the injected or extracted electrons do not need to come from solvate localised or delocalised states. Consequently, electrons can be extracted from this liquid with lowered density at positive polarity and electrons can be injected and stabilised with better energy dissipation into those microcavities at negative polarity.

2.7.2.3 Bubble elongation by electrostatic pressure

Once bubble is formatted, its growth can be driven by vaporisation, thermal pressure or electrostatic pressure as mentioned previously. The electrostatic pressure mentioned previously was due to a charged interface repelled by the applied field. Here we present a last **electrostatic effect of an inhomogenous electric field on a bubble**.

In a general way, the pressure on a gas bubble is the sum of several contributions [Ushakov]:

- the surface tension of the gas bubble interface: P_σ
- viscosity: P_η
- the electrostatic pressure on the bubble: ΔP_E
- the electrostriction pressure [Ushakov]: ΔP_{str}

$$P_\sigma = \frac{2\sigma R}{r_0^2}$$

$$P_\eta = \frac{4\eta\mu E}{R}$$

$$\Delta P_E = \frac{3\varepsilon_0(\varepsilon - 1)\varepsilon E^2}{2(2\varepsilon + 1)}$$

$$\Delta P_{str} = \varepsilon_0\rho \frac{\partial \varepsilon E^2}{\partial \rho} \frac{1}{2}$$

With σ the surface tension, R the final radius, r_0 the initial radius, η the viscosity, E the electric field, ε the relative dielectric permittivity, ρ the density .

The electrostatic pressure arises from electric field energy integrated over the bubble volume. The minimisation of electrostatic energy causes a bubble elongation along the field gradient. The electrostriction pressure arises from the difference of dielectric permittivity between the liquid and the gas bubble. For instance, this latter pressure exerts a force f deriving from a pressure P_0 :

$$f = -\nabla P_0 = -\nabla(P - \varepsilon_0\rho \frac{\partial \varepsilon E^2}{\partial \rho} \frac{1}{2})$$

The value of the electrostriction would be completely non significant if we did not take into account the dipole saturation of the water molecule. At high electric field, the dipoles of the water molecule will no longer have a random direction and will have a promoted axis along the electric field lines. This will induce a permittivity change that can be described by the empirical formula for the differential permittivity $\frac{dD}{dE}$:

$$\frac{dD}{dE} = \varepsilon_0 \frac{\varepsilon(0) - n_0^2}{1 + bE^2}$$

Where $\varepsilon(0)$ is the permittivity of water at zero field, $n_0 = 1.78$, $b = 1.2 \times 10^{-13} \text{m}^2 \text{V}^{-2}$, this give the relative electric permittivity ε as a function of the electric field E.

$$\varepsilon(E) = \frac{\varepsilon - n_0^2}{bE^2} \text{arccot}(bE^2) + n_0^2$$

Thus the **dipole saturation** leads to an even higher electric field at the electrode surface. And thus the electrostatic pressure can no longer be neglected. For example, the value of the electrostriction pressure is of the order of 3.5MPa at 1MV/cm and 2.2GPa at 20MV/cm. Those values are very high and can be sufficient to induce electrostatic cavitations of a microbubble.

According to electrostatic pressure mechanism the velocity should then depend on the applied voltage, polarity effect should also not occur, and the existence of fast and slow modes remains unexplained. This mechanism is only suitable to describe initiation stage of the discharge.

2.7.3 Bubble nucleation: Local joule heating and the microexplosive nucleation

The other mechanism for producing bubbles is **joule heating** jE . This **vaporization** is induced by **local energy deposition** (because of **local electric field amplification** at the plasma filament tip or at the tip electrode) and not global energy deposition (the whole reactor is not boiling).

Usually, the total energy available from applied voltage pulse is well below the amount of energy required to heat all the volume of liquid inside the reactor. One of the best candidates for the local heating is the joule heating by ionic conduction inside the liquid. The other possibility is the flux of charged particles impacting on the gas/liquid interface (heating, not etching). A small current can be conducted through the medium before the plasma initiation. This current will lead to local heating especially in high Laplacian electric field region close to the low curvature radius electrodes or around constricted current path. This local heating can be sufficient to locally vaporize the liquid and create a gas bubble.

The **nucleation rate** of a gas phase by liquid heating can be described by the expression [joshi2004]:

$$S = N \exp\left(\frac{-\lambda}{kT}\right) \left(\frac{2\sigma}{\pi m}\right)^{-1/2} \exp\left(\frac{-16\pi\sigma^3}{3kT(P_v - P)^2}\right)$$

with λ the vaporisation heat per molecule, N the liquid molecule density, σ the surface tension, P_v the saturation vapour pressure for the considered temperature. The heat source is just:

$$P = \sigma E^2$$

with σ the ionic conductivity of water and E the local electric field (Laplacian+coulomb)

Regarding the propagation dependence to experimental parameters, a vaporization mechanism by joule heating would be sensitive to parameters such as the liquid ionic conductivity and the applied voltage. There can also be some regulating mechanisms such as:

- the radius to the streamer tips,
- the number of filaments,
- the voltage drop along the filament.

More heating would lead to larger filament thickness but at the same time the larger tip would realize less efficient superheating of the surrounding liquid. More vaporization can mean more simultaneous filaments that would split evenly the energy between the several branches. If there is faster vaporization at the tip, energy will need to be supplied faster, but it would be regulated by the longer filament with a higher voltage drop. Those three self limiting mechanisms can be invoked on a more general basis for other driving discharge mechanisms.

One needs to explain the **filamentary shape** of the plasma filaments. The heating need to be higher at the tip compared to the sides of the plasma filament. The electric field will indeed be higher at the tip and thus the nucleation rate would be faster. The filamentation process is thus quite understandable in the scope of a local heating and not a global heating, and arises from an instability of the heating front.

Regarding the initiation, the typical nucleation time τ_{nuc} of a gaseous bubble of radius r_t can be defined as:

$$Sr_t^3 \tau_{nuc} = 1$$

The heat source is joule heating by the current j under the local field E_{loc} :

$$j(t)E_{loc}(t)dt = C_{p,liq}\rho(T)dT$$

with $C_{p,liq}$ the thermal capacitance of the liquid, ρ the density, T the temperature.

And thus the time required to the microbubble nucleation is given by:

$$\tau_{nuc} = \frac{C_{p,liq}}{jE} \left(\int_{T_0}^{T_{sat}} \rho_{liq} + \int_{T_{sat}}^{T_{nuc}} \rho_{gas} \right) dT$$

with $j.E$ the joule heating term, ρ the density of the liquid, T_{nuc} is the temperature at which the phase change occurs, and T_{sat} the saturation temperature.

The main uncertainty is the **pressure** inside the bubble that depends on the timescale of the heating process that leads to the phase change. A slow heating will lead to pressure equal to the atmospheric pressure in our case, on the contrary a very violent heating will lead to **superheating** and high pressure in the nucleated gas bubble. The pressure inside the gas cavity is given by the Clausius-Clapeyron formula and depends on the amount of superheating:

$$P_v(nuc) = P + (T_{nuc} - T_{sat}) \frac{\rho_v h_{fg}}{T_{sat}}$$

These thermodynamics considerations are useful to describe the time delay to the discharge initiation. This delay can be identified as the sum of several contributions:

- time required for superheating the liquid
- time required to nucleate and expand the gas cavity to a sufficiently low pressure to allow the electron avalanches
- electron avalanche growth

The microbubble size and pressure may need some time to expand and decrease the pressure in order to meet the Townsend or the streamer αd criterion.

Nucleation of bubbles can play a role for initiation processes. A detailed understanding of the metal/liquid interface is required to determine the real driving process leading to a bubble nucleation.

2.8 Interface processes

Interface processes are particularly relevant for initiation stage of the discharge.

2.8.1 Double layers : what happens at the interfaces according to electrochemistry

At the electrode there is a structure region separating the metal electrode from the **bulk** of the liquid called a **double layer**.

The structure of the double layer is presented in **fig 2.73**. Electron cloud around the ion matrix of the metal is the support for physisorption and chemisorptions of the liquid molecules. Impurities of the liquid adsorb in a **compact layer** at the metal interface, then several layers can be distinguished from the metal to the bulk of the liquid. Those layers are well known from the electrochemistry community [Adamson]. The charges adsorbed at the interface and the subsequent **charge image** in the metal forms a double layer. This non neutral region is present in all insulating liquids even without any applied potential. Those ions are positive or negative depending on the level difference between the **Fermi level** of the metal and the energy level of solvated ions. For usual metal and water these adsorbed ions are negative. If the ions are

polarisable, this compact layer can present a dielectric permittivity quite different compared to the bulk of the liquid. Then a little bit further from the interface, the solvated ions begin to have a full **solvation shell**. Next comes the diffuse layer which compensates for the space charge induced by the double layer. This double layer arises from the necessity to make a transition between the Fermi level and the liquid electronic states in order to have zero current through the interface at steady state conditions and without external electric field. A double layer potential as high as 1V over several nanometers can exist which gives very high electric field boundary condition. The thickness of this layer is very low on the nanometer scale for an electrolyte and can be of 0.1 μm for insulating liquids.

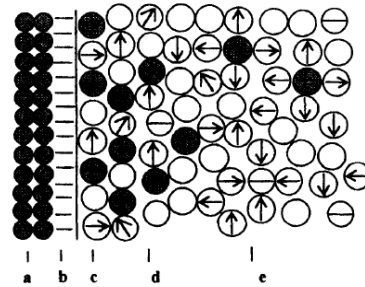


fig 2.73 double layer structure at the metal/liquid interface: metal ions, electron cloud, compact monolayer of adsorbed ions (inner Helmholtz layer), progressive solvation of the ions (outer Helmholtz layer), diffuse layer (Gouy-Chapman layer) transition from the double layer to the bulk of the liquid. [Lewis2003].

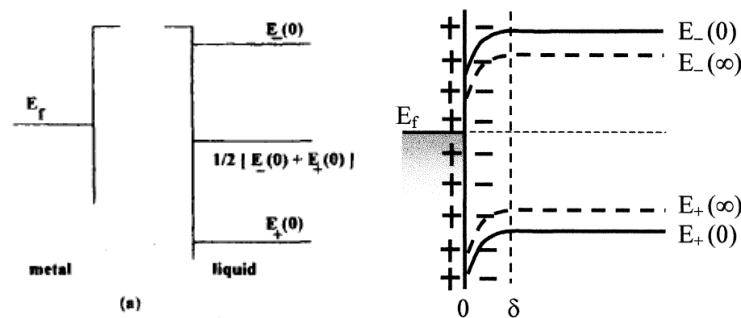


fig 2.74 metal fermi level E_f in regard with positive and negative solvated ions levels $E_+(0)$ and $E_-(0)$ of the bulk of the liquid before any formation of an interface double layer (a), after formation of a double layer, the negative ions adsorbed in the double layer in the case of water will induce an image charge on the metal side. The double layer is thus like a charged capacitor with charge separation over a typical thickness δ , the potential across the double layer adjust itself to bridge the Fermi level of the metal and the redox level $\frac{1}{2}(E_+(0)+E_-(0))$ of the liquid.

This **double layer** reacts as a sheath in DC or RF plasmas and the potential drop across the sheath can be enhanced by the external applied potential as shown in fig 2.75. Very high field will then exist at the vicinity of the metallic electrode and give birth to local field injection currents or **Lippmann effects (electrostatic stress)** as discussed in a previous section. With some applied voltage, the double layer barrier can be lowered until direct charge injection from the metal into the liquid begins possible (charge injection discussed in a next section). A homocharge (positive or negative net charge) can be injected inside a liquid and stored in the double layer region.

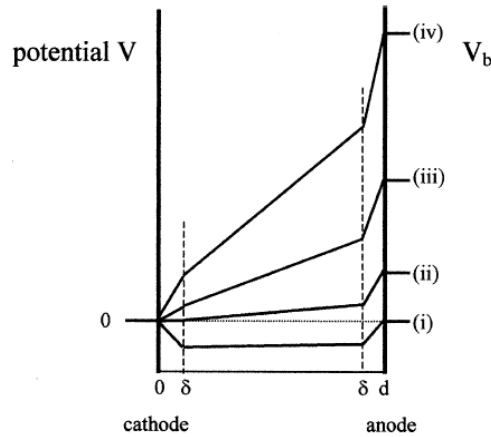


fig 2.75 at zero voltage there is a net negative charge on the liquid side, when applying a positive voltage, the cathode double layer electric field is reversed by on the anode side it is further increased. Thus a double layer will induce even higher electric field conditions close to the metal and thus can cause electrostatic stress with crack formation or cavitation by lowering the interfacial tension.

2.8.2 Charge injection from the metal electrode into the liquid

Understanding the metal/liquid charge exchange or charge generation is of particular importance for the discharge initiation. The very high applied electric field present at this interface induces charge (electrons or holes) injection.

2.8.2.1 Cathode electronic processes

At the cathode side, negative charges are injected into the medium. Electrons must flow from the lattice of the metal into the **liquid electronic states**. In the metal the electrons are at the Fermi level and can be extracted with an energy called the **work function** (typically 4eV) as illustrated by fig 2.76. The first way to increase extraction of electrons is then by thermoemission, the second way is to lower this work function by an applied electric field. The linear slope of the applied electric potential is superposed to the potential energy barrier, the maximum of the barrier is thus lowered and reach the **Fermi level** at high electric fields as shown in fig 2.77.

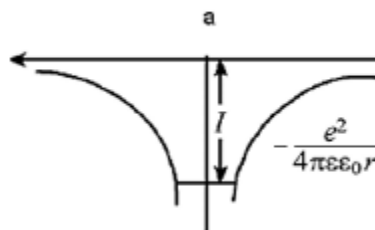


fig 2.76 single isolated molecule potential with ionization energy I, and with applied electric field E.

I is the Ionization potential of an isolated molecule, r is the distance from the molecule position. barrier potential V along axis x in strong electric field E:

$$V(x) = -\left(\frac{e^2}{4\pi\epsilon\epsilon_0x}\right) - eEx$$

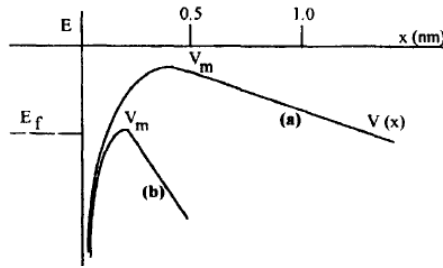


fig 2.77 potential barrier lowering due to the applied potential $V(x)$ until the Fermi level E_f of the metal is reached (b).

In the case of a transition from the molecule to the metal with a work function π , we have the **transition probability** D as a function of the electric field E :

$$D = \exp\left(-6.8e7 \left[I^{\frac{3}{2}} \theta(y - \pi^{3/2}) \right] / E\right)$$

with:

$$y = 3.8e - 4 E^{1/2} / \epsilon^{1/2} \pi$$

On the cathode side we have the **injection current** density j :

$$j = 1.5e - 6 (E^2 / \pi) \exp\left(- (6.8e7 \pi^{\frac{3}{2}} / E) \theta(y)\right)$$

Then, the electrons must enter the liquid either in a **stabilised state** or in a **free state** as discussed in a previous section. There are several paths for charge injection as shown on **fig 2.78**:

- neutralisation of a positive ion
- 1-2 auger processes
- 3-4 thermoemission
- 5 tunnelling of cold electrons from the Fermi level into the conduction band

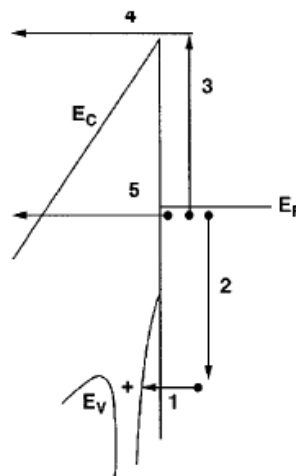


fig 2.78 electron injection mechanisms at the cathode [Joshi].

In the **Auger recombination** an electron from the metal Fermi level can **tunnel** and stabilise itself into an unoccupied liquid electronic state. There need to be a synchronous transition of an electron from a low metal level (2) and promotion of a high energy electron (3) as shown on **fig 2.79**. This process is usually much less important compared to the other processes [Lewis]. Tunnelling of a cold electron is unlikely if the potential barrier is not lowered, the **thermoemission** is not likely if there is not strong local heating of the metal. The usually most intense process is the direct neutralisation of an electron (1).

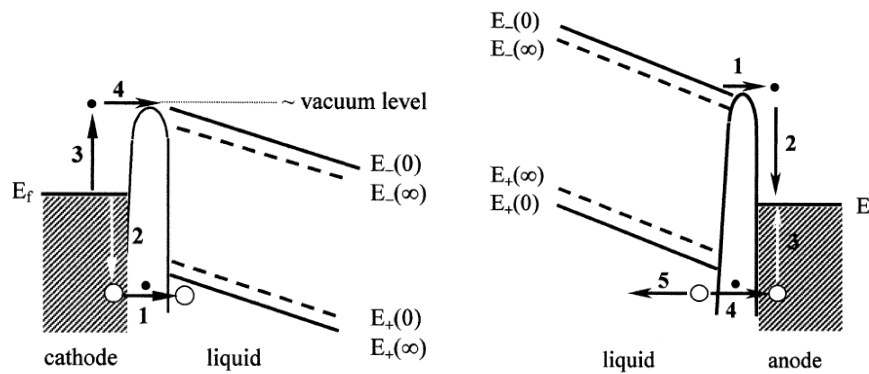


fig 2.79 Auger processes at the cathode and at the anode, at the cathode the hole or an ion is neutralized (1) with leads to the release of energy (2) allowing for and electron emission (3-4), conversely at the anode a negative ion or an electron is neutralized an allow the emission of a hole. [Lewis].

2.8.2.2 Anode electronic processes

At the anode the electrons can be detached from negative ions localised in the valence band as shown on fig 2.80. It is equivalent to a hole tunnelling from near the valence band of the liquid into the Fermi level of the metal. The negative ion can be OH^- or Cl^- . In the case of OH^- which is 0.7eV above the valence band level, the ion will be at the Fermi level at some distance from the metal electrode according to the linear potential slope in the gap. The transition will be stronger if the potential slope is stronger and the ion at Fermi level closer to the electrode. The transition depends on the overlap of the wave function of the ion and the electron.

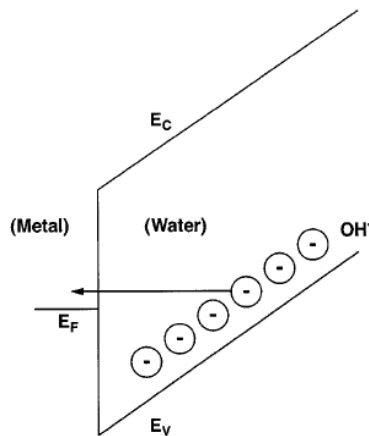


fig 2.80 ion tunnelling at the anode, the solvated ion level will be at the Fermi level of the metal at some distance from the metal/liquid interface depending on the applied electric field. [Lewis]

The second process that can occur at the anode side is the **electron extraction from a water molecule by field ionization** described in a previous section as shown in fig 2.81.

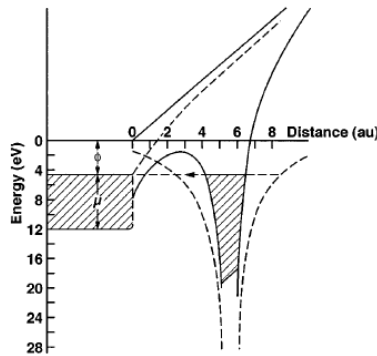


fig 2.81 electron extraction from a water molecule by field ionization, with a intermolecular distance of 0.21nm, ϕ is the work function of the metal. [Ushakov]

2.8.3 Surface state: field injection, electrode melting, microdischarge, oxide layer breakdown and formation of a plasma spot close to the metal electrode

A **plasma spot** is required to initiate streamer propagation in gas streamer simulations as discussed in a previous section. In those simulations it is not precised where this spot comes from. This plasma spot could be created by a microdischarge at an electrode asperity or oxide layer.

An **electrode asperity** would have very **high electric field** due to its reduced radius of curvature and thus the injection current described in previous sections would be very intense. The electrode can thus endure **local melting** and forms a plasma spot as in vacuum breakdown mechanism where the plasma is mainly created from the metal electrode vapour resulting from local melting under local intense current at asperities [Raizer][Korolev]. The surface stated of the electrode is also likely to present some oxide layer and can locally breakdown due to high electric field across this layer. This assumption comes from the known fact that discharges in high pressure gases depends more and more from the electrode surface state as the working pressure increases [Atrazhev].

Thus for liquids in the high pressure gas approximation, the surface state can be important for the discharge initiation criterion. An important clue is when the area of the electrode influences the breakdown voltage [Martin]. The metal will always presents some **defects** and some oxide layer, those defects can melt or breakdown under the high electric field stress and thus produce a plasma spot from witch the plasma filament will propagate.

2.9 Summary on the mechanisms for initiation and propagation

First of all, it is not sure if the initiation mechanism is identical to the propagation mechanism. The initiation can be associated to some processes required before steady state propagation. It is possible that the propagation does not start readily from the metal electrode. The metal/liquid interface is indeed quite different from the plasma/liquid interface. Only electron/hole injection into liquid electronic states need to be considered in the case of a metal/liquid interface, whereas for the plasma/liquid interface there can be ion flux impacting on the interface, field ionization, or interface charging.

2.9.1 Initiation mechanisms

Initiation can be due to:

- the electron avalanches in the liquid phase

- solvated ion conduction and local heat conduction followed by a microbubble nucleation
- charge injection followed by a microbubble nucleation
- electrostatic stress and crack formation
- formation of plasma spot at the electrode due to local melting or oxide layer breakdown

Basically there can be charge transfer mechanism across the interface from the electronic state of the metal to the electronic state of the liquid or/and there can be a bubble mechanism with nucleation of a gas cavity. It is possible that the microbubble needs to expand prior to the beginning of the plasma discharge propagation.

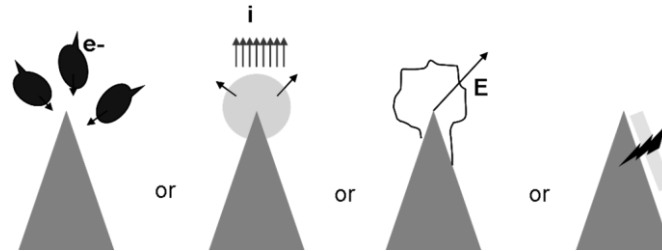


fig 2.82 possible initiation mechanisms at the metal/liquid interface : avalanches in the liquid phase, ion conduction and nucleation by joule heating, cavity or crack created by electrostatic pressure, breakdown of an oxide layer or local electrode melting and plasma spot formation.

Those processes need to establish a volume with suitable conditions for the propagation of a plasma cavity or a plasma filament.

2.9.2 Propagation mechanism

This chapter has shown that numerous physical processes can be invoked to explain the plasma discharge propagation inside the liquid:

- Interface charging and repulsion
- Interface instability
- Interface etching by ion bombardment, sheath at the filament head
- Density lowering, avalanches, filamentation
- Electrostatic crack

A unique mechanism is not an obligation: several processes can occur simultaneously and converge toward the propagation of a plasma cavity. However, each mode reported is likely to have a dominant process that explains its characteristics and its experimental behaviour.

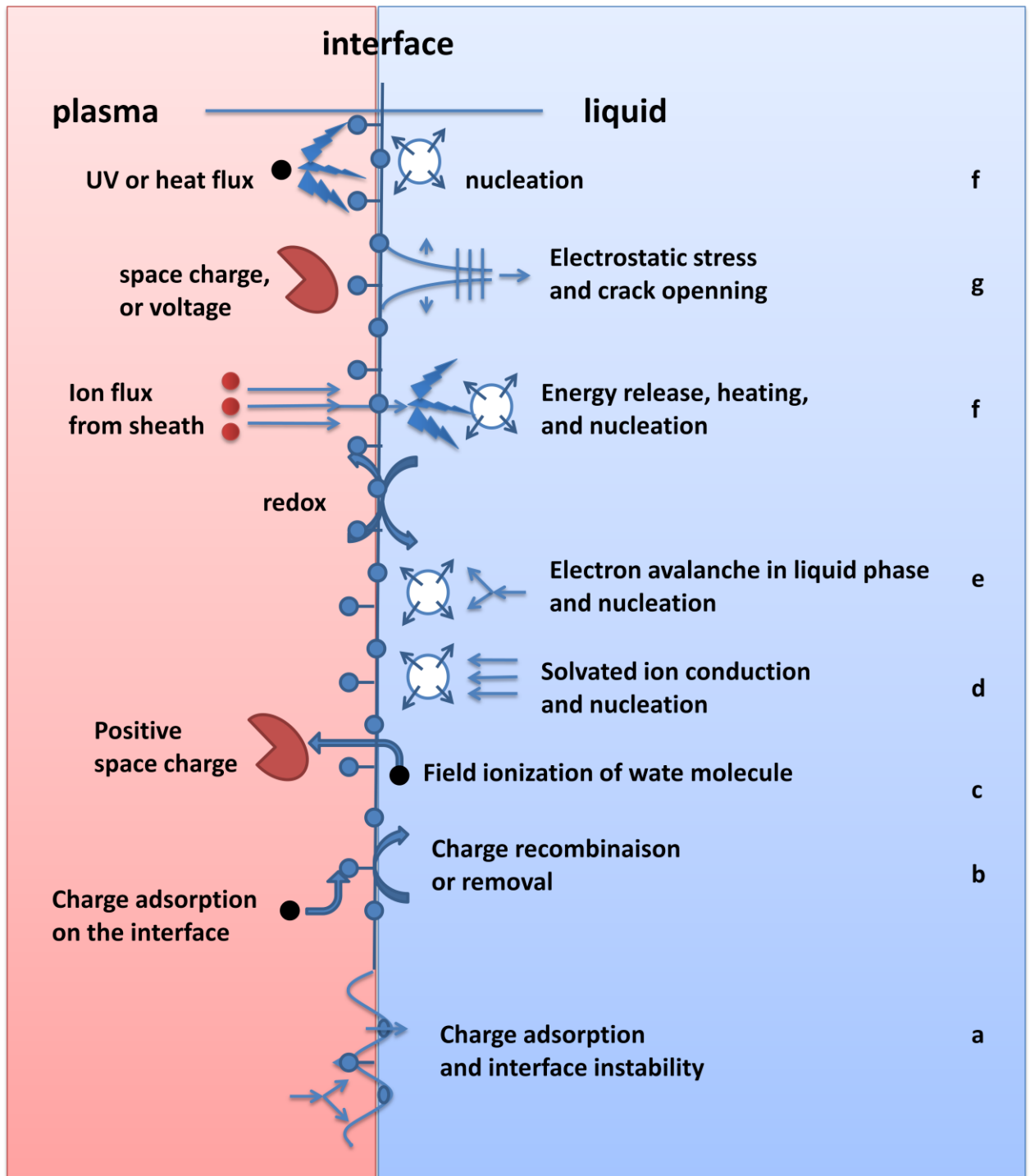


fig 2.83 summary of the physical processes at the plasma/liquid interface, (a) charge deposition and interface instability, (b) charge deposition and removal, (c) space charge separation and electron extraction, (d) solvated ion conduction and nucleation, (e) electron avalanches in liquid and nucleation, (f) electron exchange redox, (g) ion impact on the interface and nucleation, (e) electrostatic crack, (i) UV or thermal flux.

2.10 Purpose of this work: a fine time resolved study of the case of water

The purpose of this study is to perform a complete and **precise physical study** of the discharge inside one particular liquid such as water. This original **experimental study has been designed with the constant objective to better understand the initiation and propagation mechanisms of each mode of plasma inside liquids**. The **influence of several experimental parameters** will be explored in the same conditions in order to discriminate if there are clues in favour of the mechanisms described above.

Given the wide phenomenology and the wide number of parameters already explored by many authors during several decades there is not a complete theory of plasma discharges in liquids. The literature often presents some contradictory or inconclusive experimental results in particular about the influence of the liquid ionic conductivity. In the present study we want to investigate in particular the **influence of the liquid conductivity** since it is a parameter that has a very important influence on the discharge growth, on the plasma parameters, and thus on the chemical yield.

| | | |
|---------|--|-----|
| 3 | experimental setup and experimental procedures | |
| 3.1 | Reactors..... | 82 |
| 3.1.1 | Capillary discharge reactor for Rayleigh motions study of a bubble..... | 82 |
| 3.1.2 | Point to plane high voltage water discharge reactor | 83 |
| 3.1.3 | Corona in water with bubbling through the needle electrode | 86 |
| 3.1.4 | An intermediate case at low voltage point to plane water discharge: the QUB medical plasma discharge | 86 |
| 3.2 | Electrical | 88 |
| 3.2.1 | HV pulsed power supply for the point to plane setup..... | 88 |
| 3.2.2 | Electrical diagnostics | 92 |
| 3.3 | Emission imaging..... | 93 |
| 3.3.1 | Time resolved imaging with 1 iCCD: one gate per shot..... | 93 |
| 3.3.2 | Time resolved imaging with 2 iCCDs: two gates per shot | 95 |
| 3.3.3 | Streak imaging: time resolved 1D..... | 97 |
| 3.4 | Transmission imaging..... | 98 |
| 3.4.1 | Schlieren imaging | 98 |
| 3.4.2 | Shadow imaging..... | 100 |
| 3.5 | Spectroscopy | 103 |
| 3.5.1 | Temperature measurements | 103 |
| 3.5.2 | Time resolved line broadening..... | 103 |
| 3.5.2.1 | Doppler broadening | 103 |
| 3.5.2.2 | Resonance broadening | 103 |
| 3.5.2.3 | Van Der Waals broadening | 104 |
| 3.5.2.4 | Stark broadening | 104 |
| 3.5.3 | Space resolved line emission intensity | 105 |

3 experimental setup and experimental procedures

In this section we present the several water discharge reactors and their associated experimental setup implemented during this thesis. The electrical, spectroscopic, and imaging diagnostic are presented.

3.1 Reactors

Several reactors were used during this thesis:

- A water filled capillary with confined bubble
- Point to plane high voltage discharge (main subject investigated)
- Point to plane high voltage discharge with bubble injection
- Point to plane low voltage discharge

3.1.1 Capillary discharge reactor for Rayleigh motions study of a bubble

The purpose of such a setup is to have a **1D problem** with a **controlled bubble** in which the plasma discharge will occur. The purpose was to better control the experimental parameters compared to a classical HV point to plane discharge in liquid where multiple filaments are emitted in radial direction from the point electrode.

The reactor is made of two 100mL glass vessels linked with a 10cm long capillary as shown **fig 3.1**. The inner diameter of the capillary is 600 μ m and the outer diameter is 6mm. this capillary is curved to help the bubble localization at a fixed position for easier imaging. The reactor is filled with distilled water after a proper ultrasonic and chemical cleaning procedure. Water initial conductivity is adjusted in the 100 μ S/cm to 5mS/cm range with NaCl or H₃PO₄ addition.

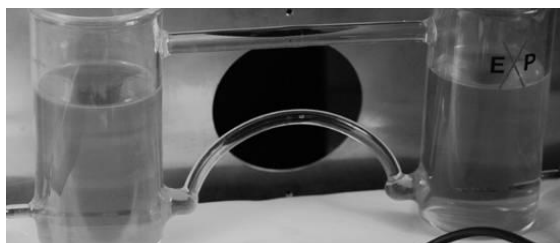


fig 3.1 water-filled capillary glass reactor, the discharge is produced in an atmospheric air bubble confined in a curved capillary of 600 μ m inner diameter.

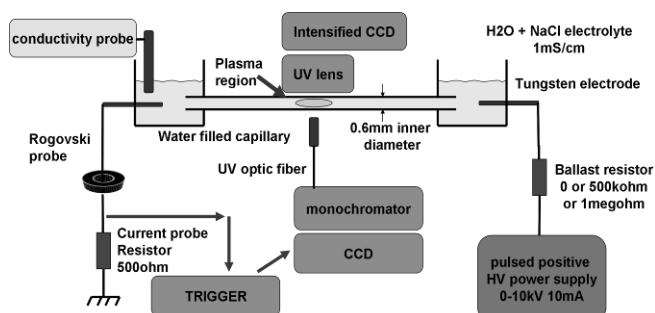


fig 3.2 experimental setup of the water filled capillary discharge, pulsed DC ballasted microplasma.

A schematic of the experimental setup is presented in **fig 3.2**. An air bubble of controlled volume is introduced in the capillary before the discharge. The bubble initial composition is then air with water at the saturation pressure for the initial room temperature. The plasma discharge will occur in this bubble. Tungsten electrodes are immersed in each vessel along the capillary. This discharge is thus an electrodeless configuration or a water electrode configuration: the plasma is in contact with 2 water meniscus and not the metal electrode. An additional resistor of typically 500 ohm can be added in series with the capillary to vary the predischage and the discharge current resistor is put in series for discharge current measurement.

A triggered **solid state power supply** gives square voltage pulses of **0 to 10kV** amplitude and variable duration from **0.5ms to 500ms** in this study, the repetition frequency is set at 1Hz. Rise time is of 1μs.

The imaging diagnostic and spectroscopic diagnostic are described in a following section.

This setup was though to be a simplified version of the more widely spread point to plane discharge in a liquid where the plasma is though to ignite in a vaporized region. However we will see that in fact this setup is very peculiar and cannot be used as a simplification for the “true” plasma discharge in the liquid.

3.1.2 Point to plane high voltage water discharge reactor

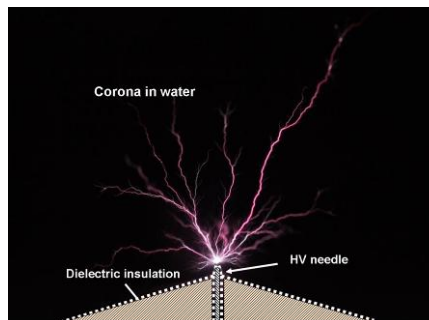


fig 3.3 picture of underwater plasma discharge, fast positive mode, the insulated point is the anode, both electrodes are underwater, special care need to be taken for the dielectric insulation at the base of the point electrode.

A **point to plane electrode configuration** is used to obtain enough **electric field amplification** to initiate the plasma discharge in the **40kV** range. The typical shape of the plasma discharge is presented in **fig 3.3**. The point to plane geometry allows to obtain an **non homogeneous electric field** and an electric field amplification. This electric field amplification is higher for sharp electrodes with low radius of curvature. The following analytical development is taken from [Celestin2008]. The needle can be approximated by a hemispheric volume or a paraboloid with the following equation in cylindrical coordinates.

$$\frac{x^2}{a^2} - \frac{r^2}{b^2} = 1$$

For a parabolic point, the equipotential lines are the confocal paraboloids. One can express the hyperbolic coordinates as a function of the cylindrical coordinates:

$$\begin{aligned} x &= \alpha\xi(1 + \eta^2)^{1/2} \\ r &= \alpha\xi(1 - \xi^2)^{1/2} \end{aligned}$$

The potential in hyperbolic coordinates is given by [Durand][Eyring1928]:

$$V(\xi) = A/2 \log((1 + \xi)/(1 - \xi)) + B$$

$$\text{with } A = \frac{V_a - V_c}{\log\left(\frac{1 + \xi_0}{1 - \xi_0}\right)} \text{ and } B = \frac{V_a + V_c}{2}$$

and the coordinate $\xi^2(x, r) = \frac{\alpha^2 + x^2 + r^2 - ((\alpha^2 + x^2 + r^2)^2 - 4\alpha^2 x^2)^{\frac{1}{2}}}{2\alpha^2}$

here is the amplitude of the electric field in the whole domain as presented in **fig 3.4**

$$|E(x, r)| = \frac{1}{\Xi(x, r)} \frac{A}{1 - \xi^2(x, r)}$$

$$\Xi(x, r) = \alpha \left(\frac{\eta^2 - \xi^2 + 1}{1 - \xi^2} \right)^{1/2}$$

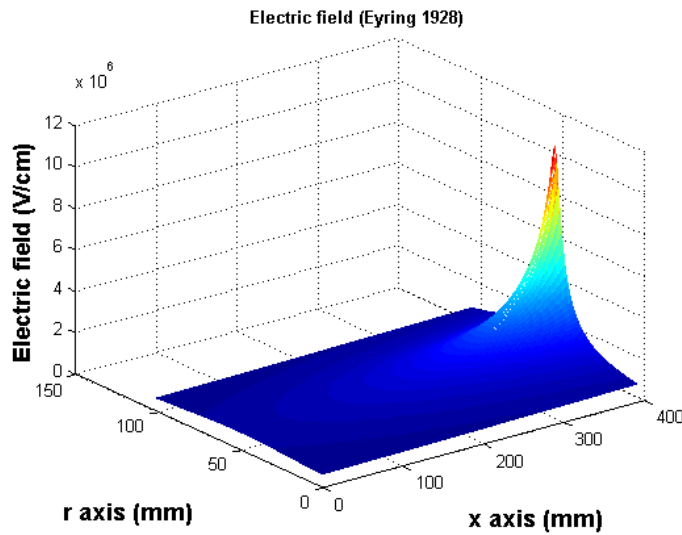


fig 3.4 matlab plot of the norm of the electric field in a point to plane configuration according to [Eyring1928], for 4cm gap, 180 μ m curvature radius of the point electrode, applied voltage is here 13kV.

The **Laplacian electric field** in our conditions can also readily be calculated by the Poisson solver of comsol multiphysics as presented in **fig 3.5**:

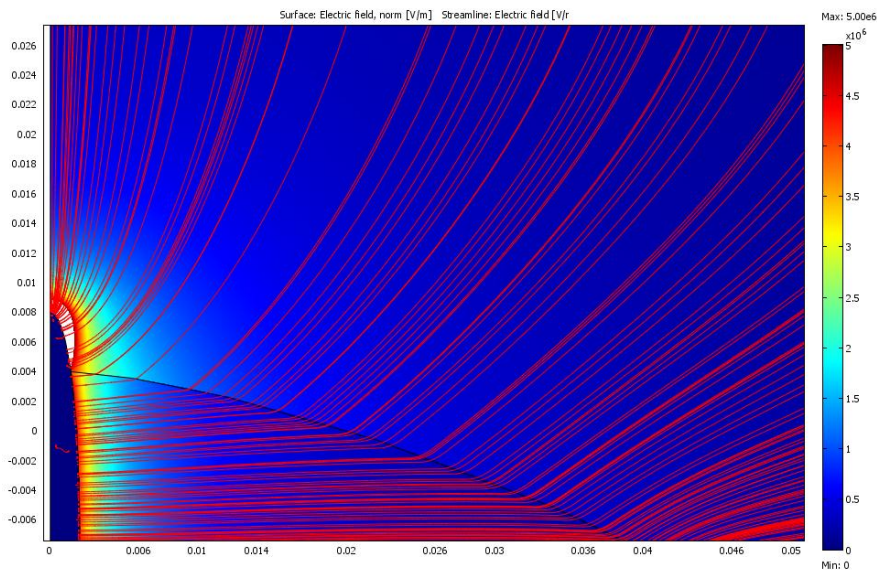


fig 3.5 calculated applied electric field in point to plane configuration for the first reactor implemented during this thesis, point radius is 300 μ m here, 2D axisymmetric simulation with poisson solver in Comsol multiphysics3.3, 4cm gap, 35kV, the norm of the electric field is in colorscale (max of 5e6V), electric field lines are mapped.

The interelectrode gap is varied from 5mm to 6cm. Shorter gaps are not a suitable solution to obtain higher electric field because the electric field value depends mostly on the curvature radius of the pin electrode and much more weakly on the interelectrode gap as shown previously. In addition a smaller gap will not leave enough length for the discharge to develop entirely. The reactor volume is 1L. The reactor shown in **fig 3.6** and **fig 3.7** is made in polymer inert for corrosive solutions and with low water absorption properties.

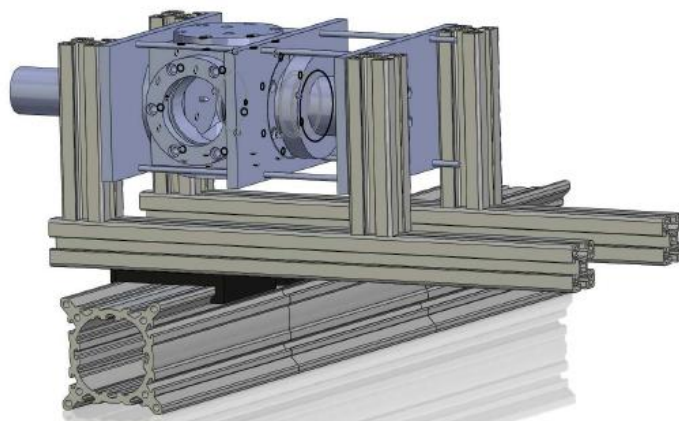


fig 3.6 point to plane reactor and its positioning on the optical rail, solidworks2006assembly.

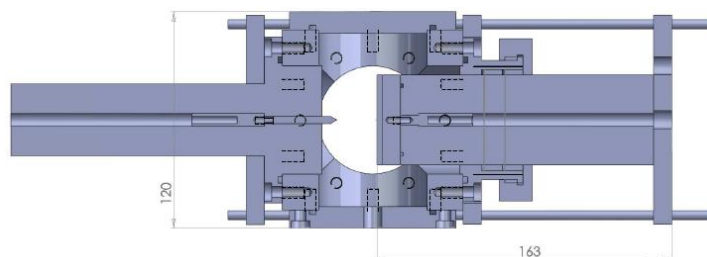


fig 3.7 cross section view of the point to plane reactor realized in the laboratory, notice the HV cable feeds.

The **liquid conductivity** is adjusted over 2 decades from $10\mu\text{S}/\text{cm}$ to $1\text{mS}/\text{cm}$ by adding phosphate or sodium salt to distilled water. The conductivity was measured by a classical conductivity probe. The liquid was prepared and renewed after a few hours of operation. Typically 1h was left before operation to obtain ungasping and equilibrium with the surrounding room air. No conductivity drift or “ageing” of the liquid inside the reactor was observed during several hours of discharge operation at 1Hz. The electrode erosion is not a problem over one week of operation.

The **high voltage point or needle** is insulated till 1mm from the pin with epoxy resin or torseal: the discharge initiation voltage is very sensitive to this insulation. The electrode must have a reduced surface contact with the liquid to concentrate the current. And additional effect is the dielectric permittivity of the insulating material used. The electric field lines are concentrated and the electric field value at the pin is increased. Thanks to this dielectric insulation of the point electrode, less energy is dissipated in the liquid and thus lower storage capacitance can be used in the power supply.

A **dielectric plate** was coated on the plane electrode in order to avoid sparking. This sparking occurs when the plasma filaments reach the opposite electrode. It can damage the point by melting, the power supply by too much current drain, and the iCCD. The plane electrode was not insulated completely in order to allow resistive current to flow through the reactor. It is not a DBD setup.

The pulsed power supply, imaging, and spectroscopic diagnostics are described in detail in following sections.

This point to plane discharge is a “true” plasma discharge inside water unlike the capillary setup. This point to plane discharge constitutes the main focus of the present thesis.

3.1.3 Corona in water with bubbling through the needle electrode

This setup is usually used by **chemist** because plasma ignition is **easier** to achieve at lower voltage. The purpose here is to study this configuration from the physical point of view. The present setup is a point to plane electrode configuration with gas injection through the point electrode as shown in **fig 3.8**. The **injected gas phase** is thus controlled and the plasma is able to initiate inside this controlled gas cavity.

The air flow fragments itself into a stream of bubble that rises from the high voltage electrode toward the ground plane electrode. The size of the bubble depends mainly on the nozzle size. The bubble size is a difficult parameter to control: it depends weakly on the injected air pressure or flow. An increase of the input gas flow just increases the bubble emission repetition rate. At usual flow of a few SCCM, 2atm and submm nozzle 3 or 4 bubbles are present at the same time in the gap. As the bubbles are rising through the liquid toward the ground plane, they oscillate at their breathing frequency and if the bubbles are large enough higher modes of oscillation can occur (not 1D anymore) as shown in **fig 3.8**.

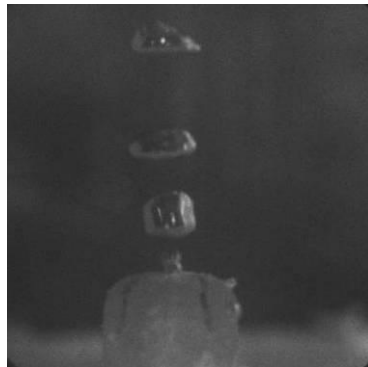


fig 3.8 point to plane electrode configuration with bubbling trough the HV needle, 10 μ s gate.

An inox **syringe** was used as high voltage electrode. The radius of curvature of this syringe is of the order of 50 μ m. We used 5cm gap and low conductive water under 10 μ S/cm. The applied voltage is a 1ms 10kV square pulse supplied by a solid state switch. Air at 1SCCM is bubbled through the needle.

The iCCD is triggered on the voltage waveform. The imaging diagnostic is described in detail in a following section.

3.1.4 An intermediate case at low voltage point to plane water discharge: the QUB medical plasma discharge

Plasma inside saline solution for medical applications are most of the time low voltage **pulsed repetitive discharges that progressively nucleate a gas layer around a set of pin electrodes**. The plasma is ignited inside this gas layer.

The actual device used in hospital and the experimental setup associated with this device is presented in **fig 3.9**. A commercial pulse generator is powering the device.

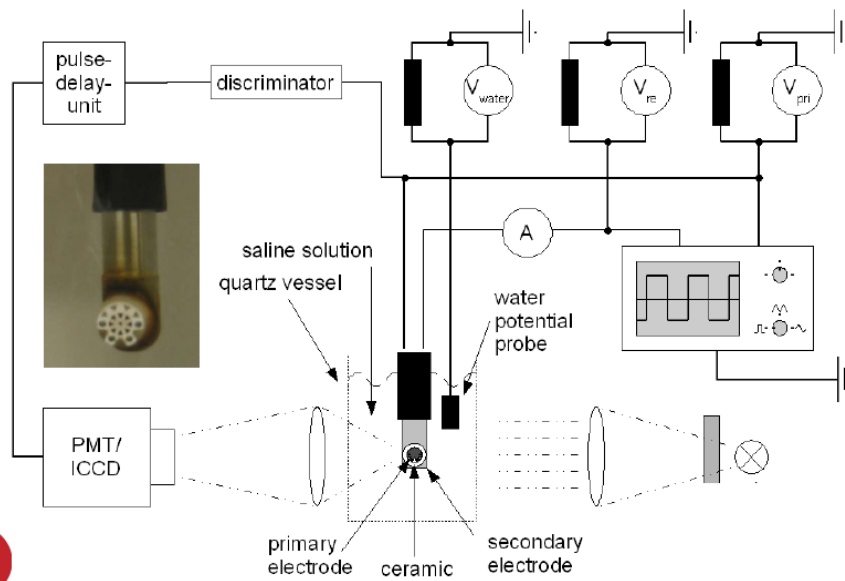


fig 3.9 experimental setup of the Queen's university medical plasma device, Arthrocare.

From the experimental point of view it is more relevant to perform a **single pulse discharge on a well defined test electrode** as shown in fig 3.10.

A **glass or quartz vessel** of typically 200mL is glued with epoxy or UV glass glue. The reactor is filled with **saline solution with 10mS/cm by using NaCl salt**. The ground electrode is immersed underwater at some corner of the vessel. The HV pin electrode is embedded in a glass capillary in order to minimise the surface of electrode in contact of the liquid. The **electrode is tungsten rod of 500µm diameter**. The pin is 500µm above the glass capillary top. The capillary has a round termination and the shape of the capillary top has an influence on the discharge growth.

The operation voltage is 300V at 40°C and 600V at 25°C the HV DC power supply is switched with a **Belhke module** (6kV, 1kA, variable on time) and allow precise voltage duration and triggering with flat pulse and controlled rise time. The discharge is typically operated in single shot mode or at 1Hz with is different from the commercial operation mode of this kind of microplasma devices in saline solution. The pulse duration is adjusted to obtain the complete nucleation and collapse of the vapour layer around the electrode. This duration is then changed when changing the applied voltage level or the liquid ionic conductivity.

A **photomultiplier** is put in front of a quartz window on the side of the reactor to observe the time resolved emission of the plasma. Given the submillimeter scale of the discharge, the optical emission is spatially integrated. The PM is triggered with the voltage and current sensor measurement. The voltage probe is a commercial capacitive divider probe. The current sensor is an inductive probe put on the discharge current return path or direct measurement on small resistor in series with the reactor.

Precise description of the shadow imaging a spectroscopic measurements are presented in a following section.

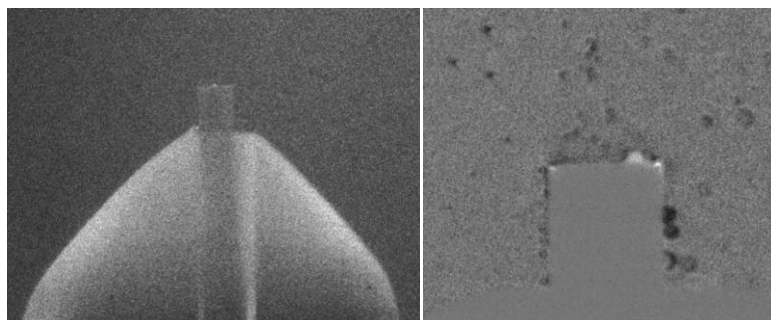


fig 3.10 close view on the tungsten electrode and the glass capillary dielectric insulation, diameter of the electrode is 500 μ m.

This configuration operates at lower voltage and larger water conductivity. It is complementary to the high voltage point to plane experiment. This setup is also particularly relevant to study the nucleation of a gas layer prior to the plasma discharge ignition.

3.2 Electrical

3.2.1 HV pulsed power supply for the point to plane setup

In this section we present the several pulsed voltage supply used to perform discharges inside water:

- Marx generator and pulse forming network using discrete capacitive storage
- Cable generators

The first requirement for plasma discharge inside water is to have a **pulsed voltage source** in order to remove voltage before the partial discharge can bridge the interelectrode gap and before **breakdown** of the interelectrode gap can occur. There are many ways to produce high voltage pulses. Most of the HV techniques use storage of electric energy in a capacitive way or an inductive way followed by fast switching: opening switch when the energy is stored magnetically or closing switch if the energy is stored capacitively. This switching can be performed with a solid state module or by a classical and more robust spark gap. Several pulsed power supplies were made and used in the present work. The most basic and versatile is a **simple HV ceramic capacitor DC charged and discharged by a self triggered pressurised spark gap**.

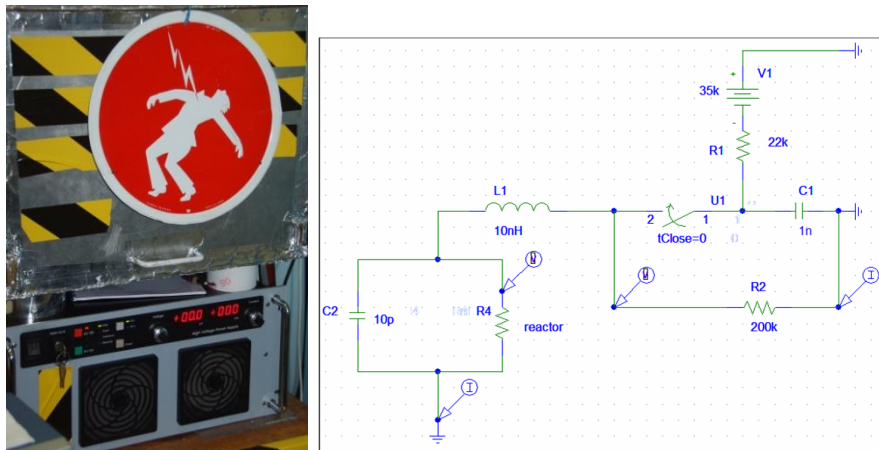


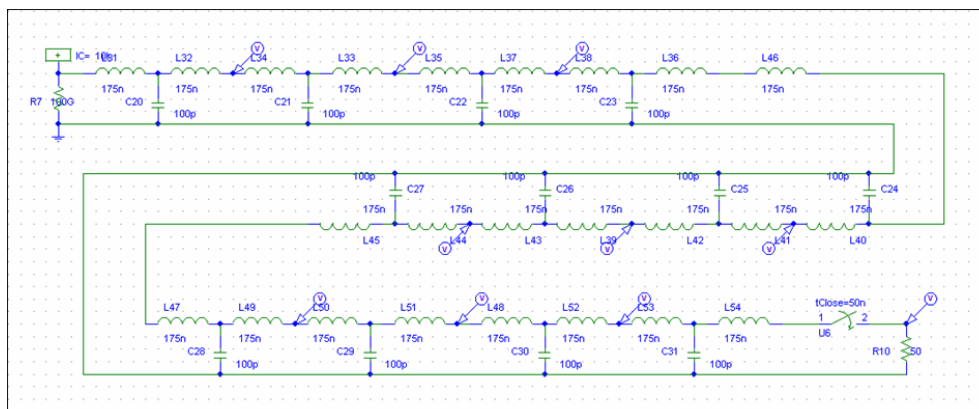
fig 3.11 picture of the home made power supply, Technix 50KV+ 1KJ/s capacitor charging power supply on the bottom, marx stage and its faraday box above, typical equivalent circuit of a marx generator (capacitor + switch) discharging into a plasma reactor (resistive + stray capacitance).

The pulsed power supply is made of a current limited capacitor charging power supply, a storage capacitance bank using individual ceramic capacitors of 0.5-2nF and a pressurized self triggered spark gap. A **PSpice schematics** is shown in **fig 3.11**. The pressure of the spark gap is varied to adjust the applied voltage maximum. We could also have changed the interelectrode gap distance in the spark gap at a constant pressure. However, the inductance of the spark gap arc is a function of the gap distance and we should reduce the gap distance to obtain better rise time. In such simple capacitor discharge setup, the applied voltage rise time is limited by the stray inductance of the circuit. In reality in our conditions the plasma discharge has typically a

microsecond scale initiation delay. Thus the 25ns **rise time** of our spark gap is of no use here and is the source of undesired electromagnetic noise that disturbs the operation of the iCCDs and gas flowmeters. A tail resistor is put in parallel with the reactor to adjust the **pulse length** and ensure voltage removal for security reasons. In fact we changed the storage capacitor value to adjust the voltage pulse duration. The applied voltage waveform is thus a classical RC decay with the capacitance constituted by the whole Marx generator capacitance and the resistance is the equivalent tail resistor consisting of the reactor and the resistance of the marx in parallel with the reactor. The typical operating **repetition frequency** is 1Hz at minimum charging current of the DC power supply. For a physical study, a higher frequency would just heat the high voltage electrode and increase its melting and its erosion. The bubbles leaved behind in the interelectrode gap by the plasma discharge would remain in the liquid and have no time to rise and evacuate outside the discharge region. In most of this thesis work we used this classical Marx generator with only one stage.

To increase the voltage a Marx generator setup was used. This generator is made of several stages charged in parallel and discharged in series thus performing a **voltage multiplication**. Each stage is made of a HV capacitor, the closing switch and a charging resistor. The problem is the simultaneous switching of the several stages that control a correct voltage rise: the first stage must fire first and the other stages must follow the first one. The firing usually depends on the stray capacitance between the stages or the generator surrounding. The firing of the first stage can be self triggered or remotely triggered. The second stage should be overvolted to fire correctly. This overvoltage depends on stray capacitance of the stages [Jérôme BAC Ph.D. Thesis].

The pulse shape of a marx generator is a capacitor decay. Such decreasing voltage can have some influence on the plasma propagation. To obtain a flat pulse one can use a cable generator or a pulse forming network setup. The problem of the **cable generator** is that many cables need to be used in parallel to sustain the discharge current in water that is in the 10A range. The **pulse forming network (PFN)** [Rim2003] is based on successive discharge of several capacitors to approximate a flat pulse with minimal ripple. The rise time depends on the decay of the first capacitor, the ripple of the flat depends on the number of stages and the value of the components. Some judicious combination values exist and can be found in the [NRL pulse power formulary] and is illustrated by the PSpice simulation in **fig 3.12**.



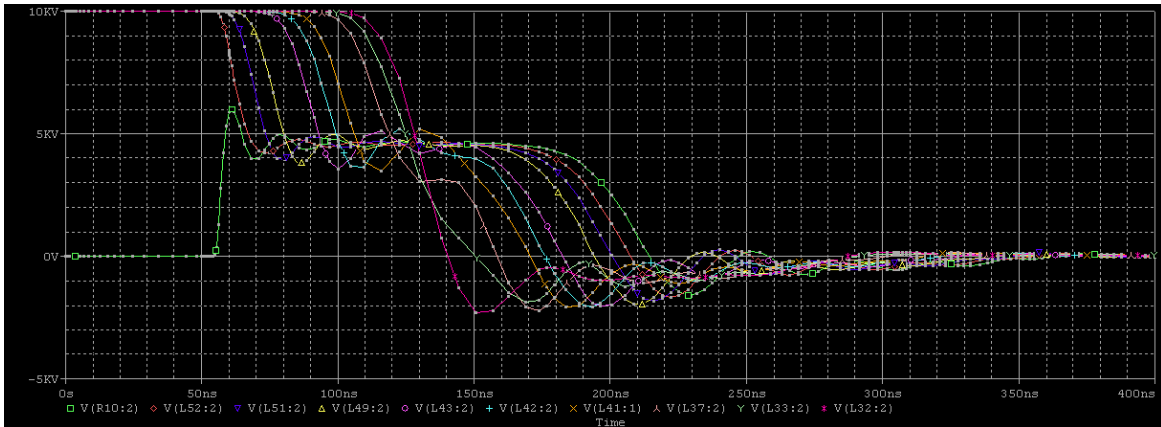
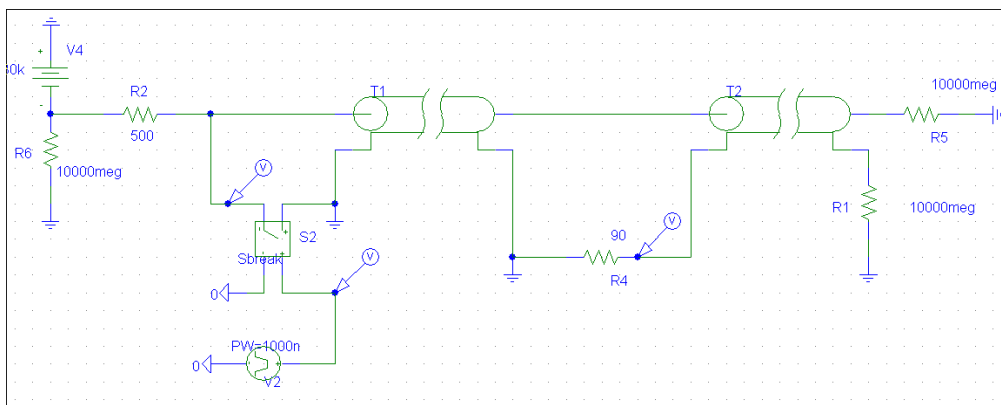


fig 3.12 Pspice simulation of a pulse forming network to obtain flat output pulse, values from the pulse power formulary [Glasoe Lebacz].

The **cable generator** is very similar to the Marx generator but is based on distributed cable capacitance instead of discrete capacitance storage [Rossi] [Verma] [McGregor] [Davanloo] [Pecastaing] [Sevick]. The cable is charged through a current limiting resistor and discharge when a switch closes. The typical linear capacitance of RG HV cable is 100pF/m. With one cable the voltage at the reactor is half the charging voltage value. The pulse duration is fixed by the cable length and this type of generator is thus used for pulses in ns to 1 μ s range. The switch can be between the cable and the load or between the cable and the ground. The switch should be closed during all the pulse time. A trick is to use the **blumlein setup** to have a pulse amplitude equal to the charging voltage amplitude as shown in PSpice simulation in fig 3.13 When the switch closes, a voltage wave propagate through the cable, half of the wave is reflected back because of the impedance mismatch between the cable and the load. The half wave transmitted goes through the second section of the cable and is reflected at its termination. Those cable generator need to have a precise load impedance with is not the case in partial discharge reactor. However, the reactor impedance is in the 10-200kohm range, so a resistance in parallel with the reactor can be used for impedance adaptation. The problem is the power that can be supplied by the cable while discharging is insufficient for discharges inside water.



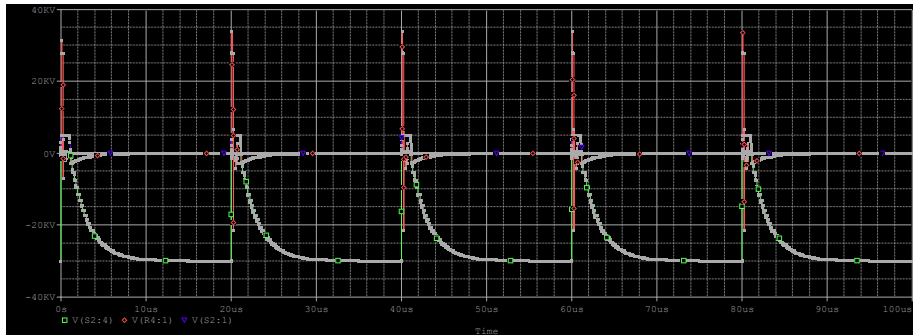


fig 3.13 Pspice simulation of a cable generator in blumline configuration with repetitive operation, the load is placed between two cables and should have twice the cable impedance.

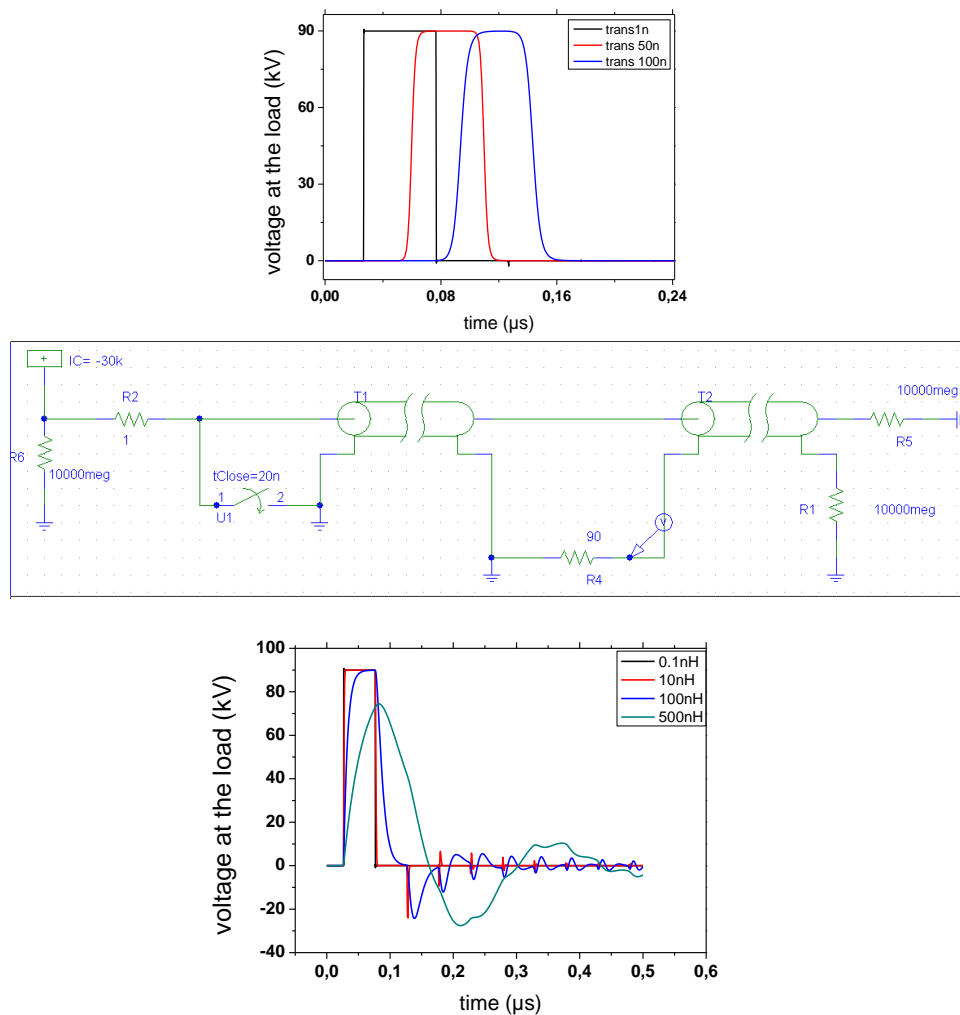


fig 3.14 Pspice simulation of a cable generator in blumline configuration, pulse response for several load inductances.

The rise time is driven by the switch inductance as in Marx generators. If there is **impedance mismatch** there will be **reflection** after the main pulse as shown by the PSpice simulation in **fig 3.15**. The reflection amplitude depends on the mismatch degree. The polarity of the pulses depends if there is underload or overload.

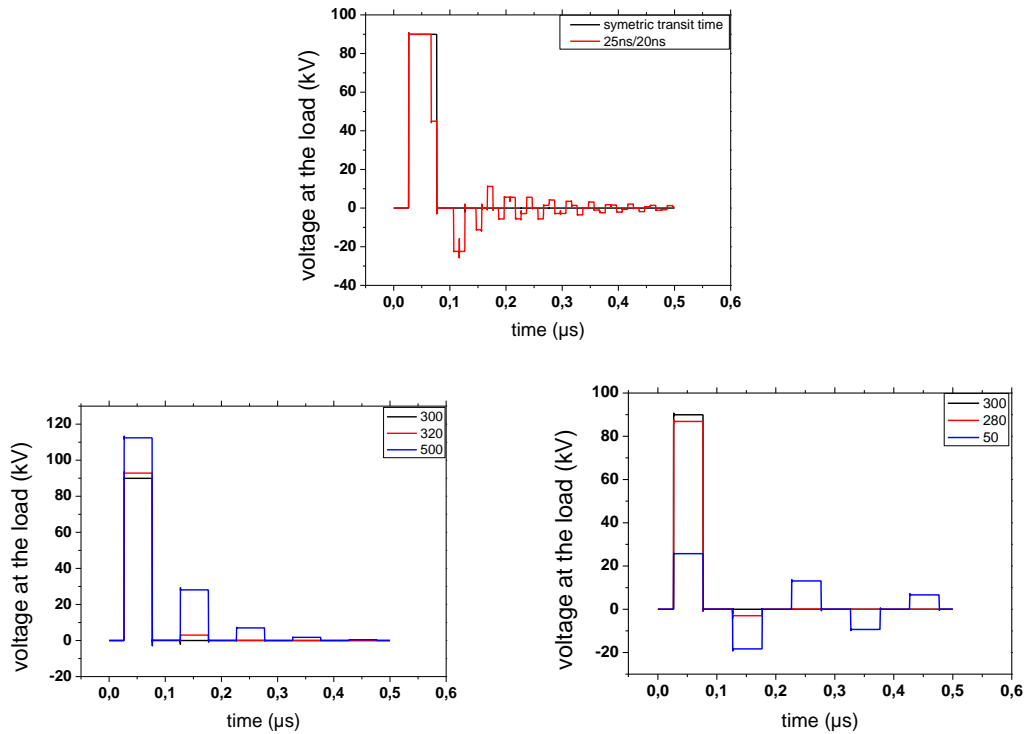


fig 3.15 Pspice simulation of a cable generator under impedance load mismatch conditions.

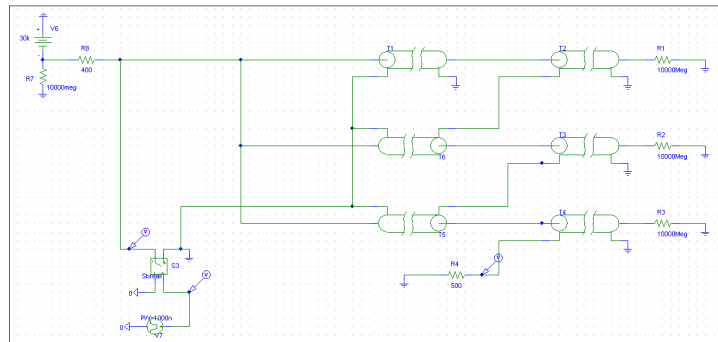


fig 3.16 stacking of cables stages to perform voltage multiplication.

The cable generator can be staked in several stages to operate voltage multiplication as in Marx generator as illustrated in the schematics fig 3.16. In this case it is a cable transformer [Rossi].

3.2.2 Electrical diagnostics

A 1GHz rogovsky probe (Pearson 6585) is put after the ground plane to measure the discharge current on the return path to the ground. This probe works as a **wide band current transformer** when connected into 50Ω scope. A factor 2 should be used in the factory calibration coefficient which is usually given for 1MΩ termination.

A differential technique is sometimes used for current measurement in rare gas liquids or organic liquids in order to separate the conduction current from the displacement current [Lesaint]. The displacement current is due to the polarisation of the reactor cell event without any plasma discharge inception. The conduction current is due to the charge injection in the liquid and is often very weak for highly insulating liquids. In water the current is mainly conductive and consequently such a technique is not really needed.

The **capacitive divider probe** (PPE20kV Lecroy) performs a voltage division from the HV measurement point to a voltage measurable at the scope. The division ratio depends on the

ratio of impedances, the bandwidth of the probe also depends on this ratio as shown in the PSpice simulation in **fig 3.17**. This kind of voltage probe only works for short pulse duration. For longer pulses the tail will not be correctly detected and compensation will be needed.

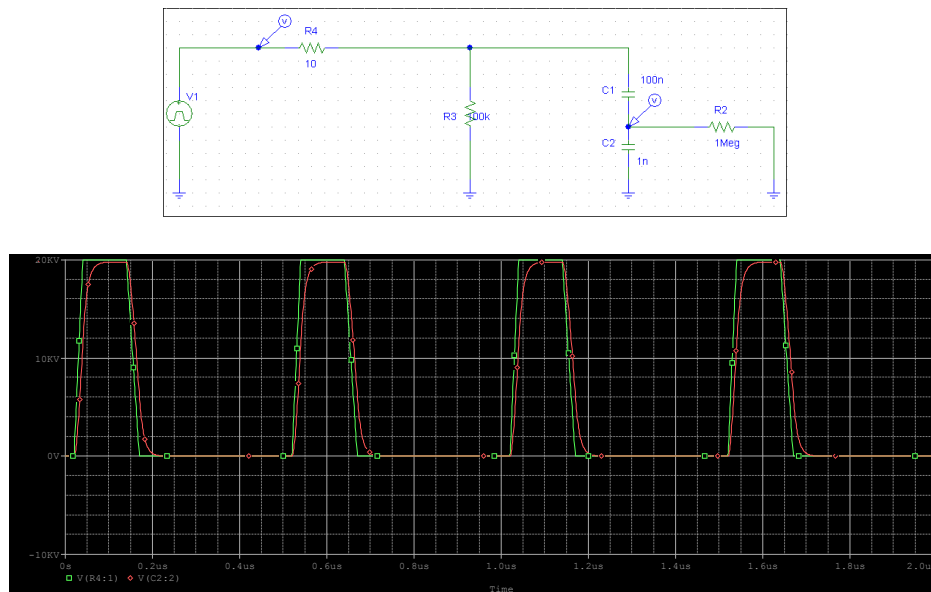


fig 3.17 PSpice simulation of the response of a capacitive probe (red) to an impulse excitation (green).

Because of the voltage level used in the present study and the operating voltage of the commercial probe, the possibility to implement a **home made capacitive probe** was investigated. A home made capacitive divider probe consists just in a metal surface forming a head capacitor in capacitive coupling with the high voltage point to measure. A larger capacitor is put between this surface and a high voltage cable lead. Given the voltage rise time and the values of the capacitances, such probe is purely derivative in our conditions and measures the displacement current due to charging of this probe capacitor. Integration is thus needed with baseline subtraction to obtain the current signal.

3.3 Emission imaging

In this section we present the principle of operation of intensified cameras, triggering and gating, and the implementation of a shadow diagnostic.

3.3.1 Time resolved imaging with 1 iCCD: one gate per shot

The DH734 iStar Andor is a 1024*1024 pixel CCD detector combined with an intensifier tube as shown in **fig 3.18**. The first phosphor layer receives incoming photons and translates them into electrons with some quantum yield of typically 90%. Then those electrons are accelerated by a high voltage grid and multiplied by electron avalanches inside the **intensifier tube**. The electrons are converted back into photons through the phosphor layer and the photons impact on the **CCD array**. The photocathode layer accumulates those photons energy and gives an electrical signal when the pixel is charged. UV photons can however be converted even in CW off mode of the CCD and this can be a problem in the case of a streamer to spark transition where the UV emission is very intense. The intensifier tube is electrically controlled and can thus be opened and closed very fast. This is the reason why intensified CCD allows very short gate in the nanosecond range. The **readout time** of each CCD pixel is about 1 μ s and defines the repetition

rate of the CCD in the Hz range when using the whole detector surface. This kind of iCCD can open **only one gate during a plasma pulse**, it cannot operate as a fast repetition rate camera.

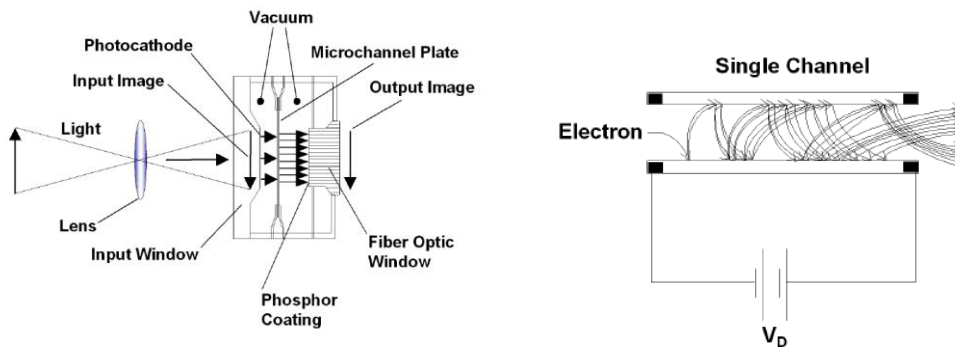


fig 3.18 schematic of the iCCD and the microchannel plate (intensifier).

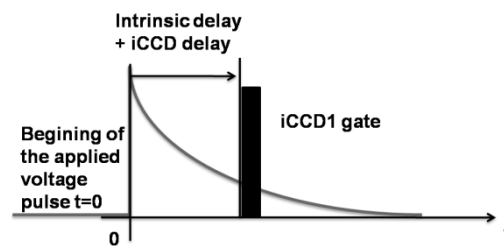


fig 3.19 iCCD triggering schematic.

The camera can be externally triggered with TTL level. **Delay** and **gate** are defined by fig 3.19. The power supply is self triggered and thus we use the discharge current detected by the inductive current probe to obtain time $t=0$. From this value $t=0$, the digital delay generator integrated in the camera can be defined in the software at some precise position of the plasma growth. Unfortunately the oscilloscope can only give 0.1V trigger level that need to be translated into TTL level. The camera has an intrinsic delay of 50ns and the translation from 0.1 to 5V takes 170ns, there is an overall **intrinsic delay** of 220ns in our conditions from the beginning of the pulse to the first gate that can be opened with the camera. This intrinsic delay induces some limitations.

On **time integrated measurements**, the maximal length is taken and can be clearly distinguished from the background illumination level. No arbitrary intensity level is required to mark the end of the plasma discharge.

Only **one gate per plasma shot** as in fig 3.19 can be not sufficient to really understand what is going on in the discharge. The discharge is filamentary and thus is quite **chaotic**. The time resolved discharge length can be measured and the propagation velocity of the discharge can then be determined from the discharge radius and the time delay to initiation of the discharge. This time delay to initiation is associated to a big discharge current jump and is clearly seen on the discharge current waveform. The fact that a “**discharge radius**” can be defined is only possible because the plasma filaments grow simultaneously and at the same velocity as shown in fig 3.20 witch is the case in the primary positive mode and the secondary positive mode but witch is not the case for the negative mode as shown in fig 3.21. One should keep in mind that the discharge is also **3D** and the filaments are projected along a plane and thus their length can be underestimated. Not stereoscopic view of the discharge was performed in the scope of this study.

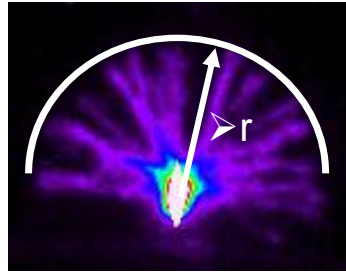


fig 3.20 measurement of the positive discharge radius, simultaneous propagation of a several plasma filaments of typically 50 μ m diameter, point 100 μ m, 40kV, 100 μ S/cm, delay 40ns, gate 2ns.

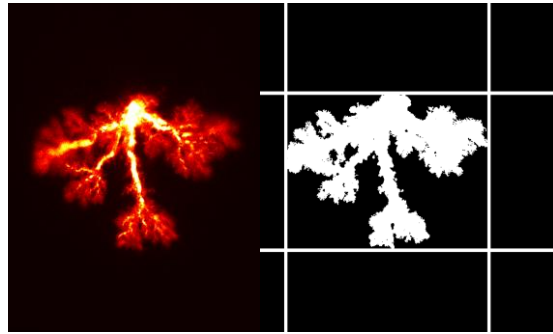
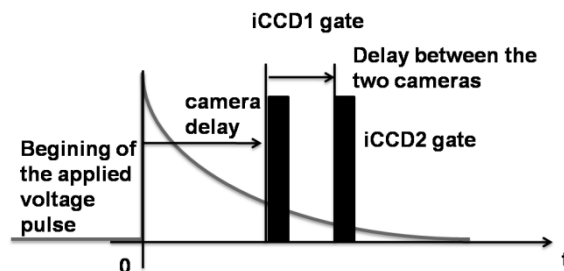


fig 3.21 slow negative mode filament maximal length, Matlab script for automatic image treatment and boundary detection. point 100 μ m, 40kV, 10 μ S/cm, delay 15 μ s, gate 1 μ s.

A first each images was exported manually with an suitable colorscale into bmp files and exploited with a Inkscape vectorial drawing freeware to analyse the size of the discharge in pixel. An Andor basic script was developed to make this colorscalling and bitmap export automatically. Then a **Matlab script** using the Matlab image toolbox script was implemented in order to transform the RGB bitmap into a greyscale image with auto histogram. The greyscale image is then converted into a binary image to perform automatic morphology and boundary recognition analysis.

3.3.2 Time resolved imaging with 2 iCCDs: two gates per shot

The propagation velocity of the discharge calculated with only one iCCD and accumulated images can be misleading because of the huge **jitter** of the initiation delay of the discharge. To avoid such problems, an experimental setup with 2 simultaneous iCCDs was implemented to perform direct measurement of propagation velocity during the same single shot. **2 successive iCCD gates** are opened with a precise time delay between the two gates as indicated in fig 3.22. iCCD offers very precised triggering and short gate capabilities but unfortunately they cannot be used as fast repetition rate cameras on the nanosecond or microsecond time scale. Specific (and expensive) iCCD design may allow opening 2 or 3 gates which is not the case of the Andor iCCD. Thus we must use 2 iCCDs at the same time and triggered on the same delay generator.



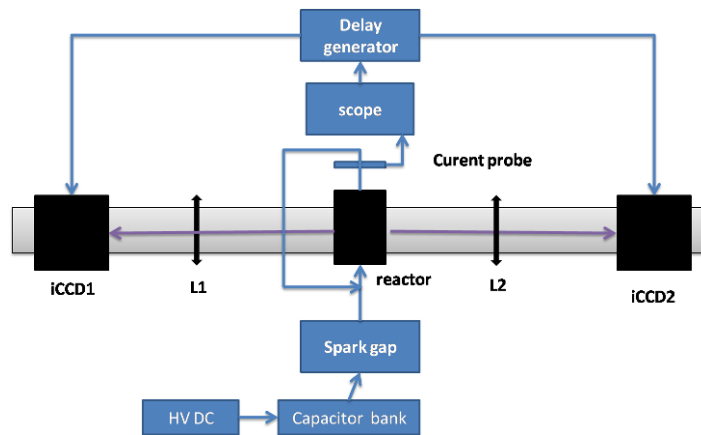


fig 3.22 two iCCD emission imaging, iCCDs on each side of the reactor along an optical rail, the gates are triggered successively allowing for 2 images per plasma shot, each iCCD has its own imaging lens.

An alternative solution is to split the collected light and make time delay by playing with the optical path length and focus those beams on different area of the iCCD array to obtain successive images on the same chip. The time delay of typically a few nanoseconds could be obtained by some tens of centimeters of additional optical path [Baumung]. The limitations of those optical paths give the maximum delay between two successive images. Two or 3 images can be made on a same captor. In our conditions we are interested by longer delays in the tens of nanoseconds or microseconds.

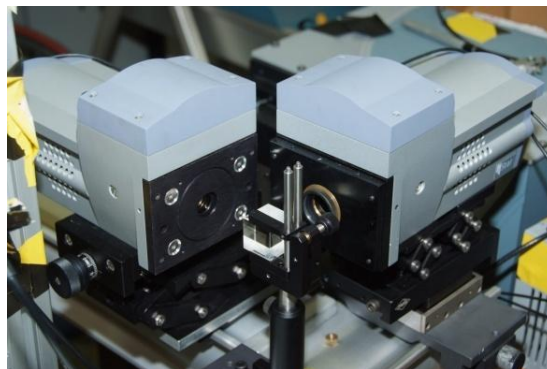
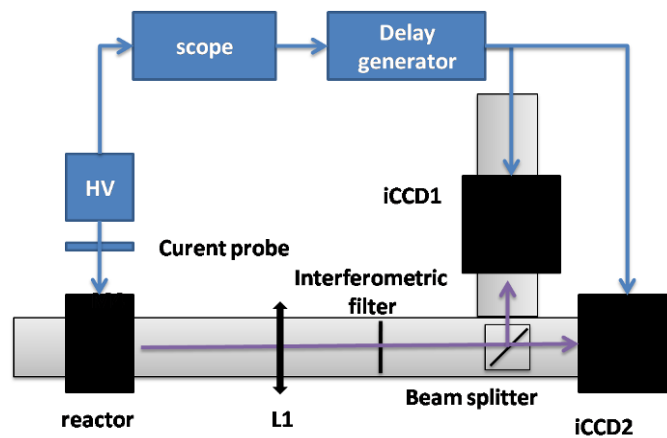


fig 3.23 two iCCD imaging, the beam splitter allows more precision compared to the previous setup.

At first the two iCCD were used on each side of the reactor, each camera having a different zoom objective lens as shown in **fig 3.22**. Most of the time a simple focusing and size tunings are performed for imaging because we just wanted to observe the global shape of the discharge and the maximum position of the filaments. The imprecision of the measurement was due to 3D effects. This setup was enhanced by using single imaging **achromatic doublet** lens follow by a **beam splitter** cube as shown in **fig 3.23**.

3.3.3 Streak imaging: time resolved 1D

The streak camera allows to observe the complete **time developpement** of the discharge with high time resolution but only along 1D. The image of the discharge is focused on the entrance slit of the streak tube, the slit image is converted into a beam of electron by the photocathode, and then this beam is amplified in the **amplifier tube** and deflected electrostatically to realize a **time sweep** as show in **fig 3.24**. The range of this time sweep defines the intrinsic time delay of the streak camera with is typically 1.5 times the range. This intrinsic delay again induces some limitations. The thickness of the entrance slit defines the time resolution. The electron beam is focused on a phosphor cathode and converted back into photons and impact on a CCD array.

The streak is triggered with a delay generator with some delay from the beginning of the applied voltage pulse and is synchronized with a iCCD to have a 2D image at the same time in the same principle shown in **fig 3.22**. This additional iCCD in **fig 3.25** was used to check if the plasma filaments are in front of the entrance slit and to select the valid acquisitions as shown on **fig 3.26**. The discharge image could be compressed along one direction by using a cylindrical lens and thus collect all the plasma emission and focus it on the entrance slit of the streak camera to avoid the problem of the alignment of the entrance slit with some plasma filament.

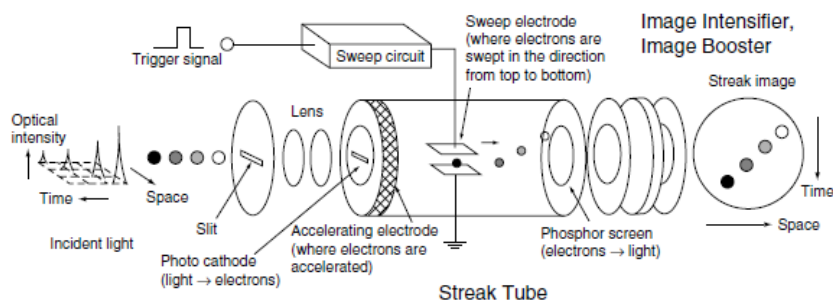


fig 3.24 schematics of a the intensifier tube of a streak camera, the time resolution is obtain by electrostatically deflecting an electron beam

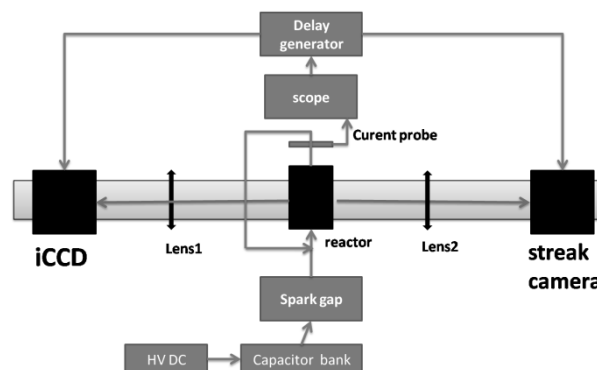


fig 3.25 streak camera and iCCD setup

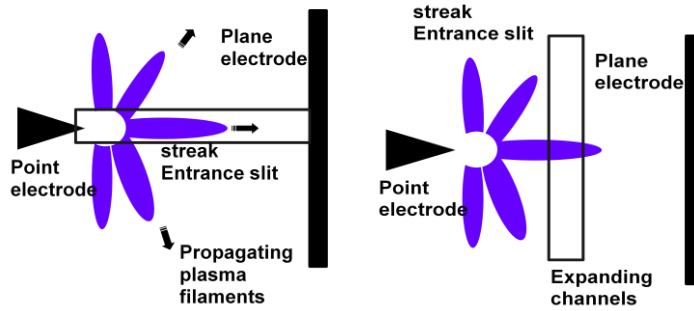


fig 3.26 entrance slit along the interelectrode axis to observe the propagation of the channel head or perpendicular to a channel to observe the channel radial expansion.

3.4 Transmission imaging

Transmission imaging uses **back light source** instead of light produced by the plasma itself.

3.4.1 Schlieren imaging

The plasma filaments are regions of **gradient density** or **gas-liquid interface** which can be considered as infinite gradient, the schlieren method is an imaging technique that allows observing those gradient densities [schlieren techniques Springer][Klimkin] [Larsson2001], this technique is quite ancient [Kao1958].

This technique uses a **back-light source** that is deviated by density gradient in the reactor. The output light is then concentrated with a convergent lens or a parabolic mirror and spatially filtered. The filtered light is then focused on the CCD and a negative image of very high contrast can be obtained.

In a general way, an incoming **parallel beam will be slightly deviated by the filaments** according to the refraction law:

$$\frac{d}{ds} \langle u \rangle = \nabla n$$

where s is the curve optical path, u is the tangent vector on the optical path, n is the optical index which depends on the medium density according to the **Gladstone-Dale relation** :

$$n - 1 = K(\lambda)\rho$$

with K the Gladstone-Dale constant that depends on the wavelength and the material.

When the **parallel beam is focused on a point the deviated light is focused aside this point and can be spatially filtered**. The filtered image will provide a high contrast image with bright field illumination if the main focus dot is conserved, and a dark field illumination if the refracted contribution is conserved.

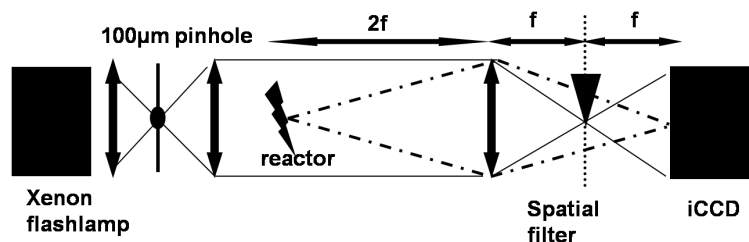


fig 3.27 principle of the schlieren transmission imaging technique, the refracting object is illuminated by a parallel beam and the output light is focused and spatially filtered to obtain a high contrast image of the optical index gradients.

The source is focused on a **pinhole** or a slit by a condenser. The slit is at the focus point of the first field lens that produces a parallel beam. The second lens is the imaging lens that focuses the source on a spatial filter. Then the object is imaged on the screen after filtering. The source and the spatial filter on one hand, and the object and the screen on the other hand, are optical conjugate planes. The resolution of such a system depends on the focus length of the second lens and on the amount of cut-off.

The **density gradient range is mapped on a grey scale and its range depends on the amount of cut-off**. The **contrast and the range are thus in competition**. In a general way, one must be careful about not to separate too much the non refracted spot and the refracted light. If it happens, the contrast would be maximised but the range is zero. Thus the image will no longer be encoded in greyscale but will be binary and no quantitative data analysis would be possible: only edge detection would be possible. In our case edge detection is suitable.

The beam should be monochromatic to avoid **chromatic aberrations** from the lens, However colour schlieren can be performed with a white source and a special colour filter. The colour will encode the direction of the optical density gradient or the optical density gradient value encoded in hue with is much easier to measure than a grey scale intensity value. In particular, colour schlieren is less sensitive to the non uniformity of the background illumination of the detector.

The **field of depth** depends on the size of the light source and on the focal length of the first lens that is used to make a parallel beam.

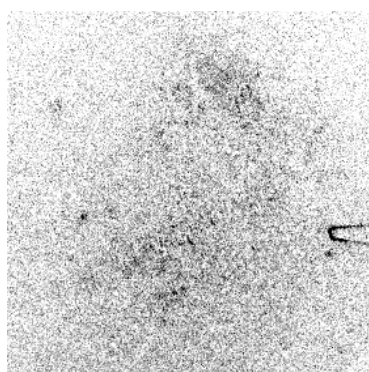


fig 3.28 typical image of the point to plane reactor without plasma discharge, the signal results mainly from diffusion of the HeNe laser on the sharp surfaces such as the reactor windows defects, the stray microbubbles of the liquid, and the HV pin, the pin is 400 μ m radius of curvature

In our case, a 1mW HeNe at 682.8nm was used as shown in **fig 3.29**. The 800 μ m output beam of the laser was expanded in a 1cm beam by an home made **beam expander**. The quality of this beam was not very good but it played its role as a very intense light source. Spatial care was made not to introduce any spherical aberration that would compromise the uniformity of the background illumination of the detector. The interference fringes were not a problem but the diffraction at the sharp edges was quite important. The diffraction overlap and even dominates the schlieren signal in our case, this diffraction was in fact quite useful at first for a pure edged detection diagnostic. The schlieren image of the point without plasma is shown in **fig 3.28**. A **laser** source should be avoided since any defect from the lenses will lead to interferences.

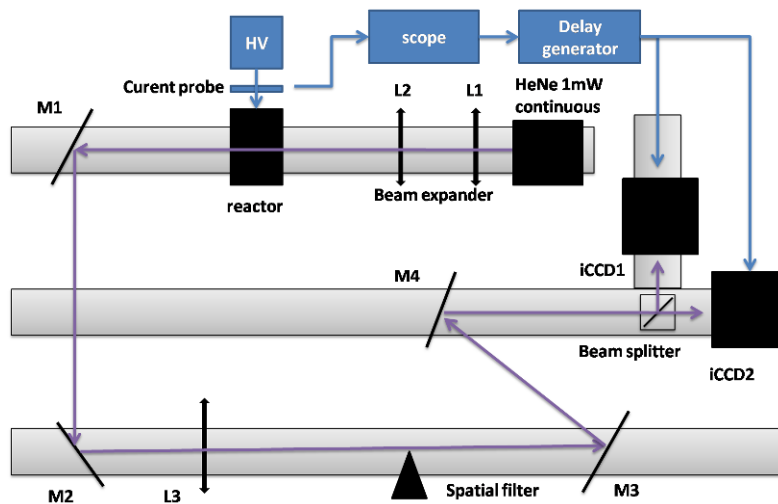


fig 3.29 schlieren imaging with two iCCD and an 1mW continuous HeNe laser.

If a **continuous light source** is used, only the **schlieren** image technique would be possible because a continuous illumination of the iCCD is dangerous. With continuous light source and schlieren setup, light will come on the iCCD only when density gradients are present in the test region that is to say when the plasma is turned on. On the contrary with a **shadow** setup the light source must be pulsed to avoid continuous illumination of the iCCD photocathode.

3.4.2 Shadow imaging



fig 3.30 picture of the Perkin xenon flashlamp and the parallel beam output.

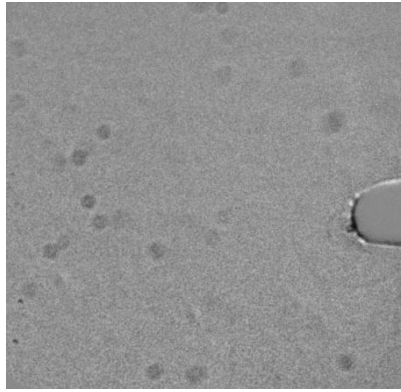


fig 3.31 typical image of the point with shadow diagnostic and background subtraction.

The shadow imaging also uses an external light source but the source must be pulsed when using an iCCD with high intensification in order to avoid captor damage. The xenon **flash lamp** of 10W (continuous power not peak power) is show in **fig 3.30** delivers triggered pulses of typically 10 μ s duration at maximum 10Hz.

A complete explanation of **triggering** and discharge timings is presented in **fig 3.33**. The flashlamp is triggered with some delay from the beginning of the applied voltage pulse. The iCCD is triggered and opens a gate at the maximum emission of the flashlamp. The emission begins only 2 μ s after the flashlamp triggering because of intrinsic delay and the maximum emission of the flashlamp is reached at 2.5 μ s. The power supply is selftriggered and thus the delay generator is triggered from the beginning of the applied voltage pulse detected by the inductive current probe.

The **intrinsic delay** of the flashlamp and the self triggered power supply induces some limitations when one need to see some early events in the plasma discharge growth. The initiation delay jitter can be used and the observation of late plasma ignition is thus still possible. Another limitation is when one want to use 2 iCCDs with shadowgraphy, the first iCCD must be triggered at the beginning of the flashlamp pulse and the second iCCD must be triggered before the end of the flashlamp pulse. Maximum delay difference between the two iCCDs cannot exceed a few microseconds as shown in **fig 3.32** even when using maximum intensification or larger gates for the second iCCD.

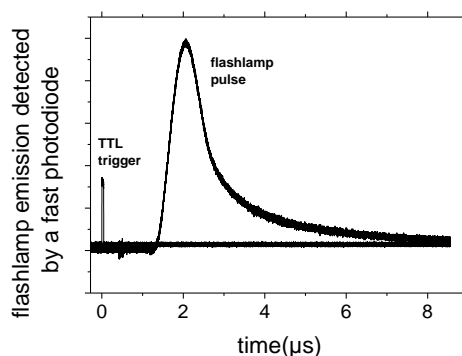


fig 3.32 flashlamp pulse duration and intrinsic delay detected by a photodiode.

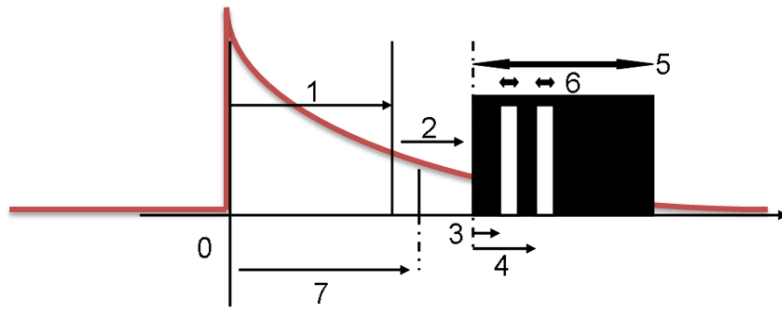


fig 3.33 timings description: 0 start time = beginning of the applied voltage pulse detected by the inductive current probe, 1 delay generator to trigger the flashlamp, 2 intrinsic delay of the flashlamp, 3 first iCCD gate delay, 4 second iCCD gate delay, 5 flashlamp pulse duration, 6 iCCD gate duration, 7 delay to plasma initiation

The 2 iCCD setup coupled with shadow imaging uses a beam splitter cube as shown in fig 3.23 just in front of the two iCCD which proved to be a very efficient technique in this study.

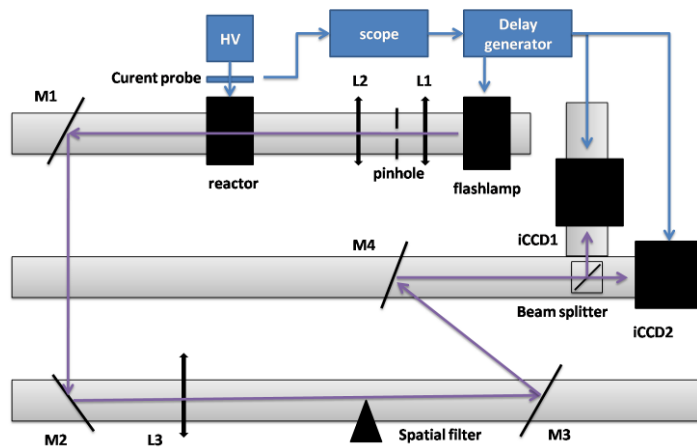


fig 3.34 shadow imaging with two iCCDs and a triggered xenon flashlamp

At first a 75cm focus length achromatic doublet was used to obtain 1:1 magnification and see the whole discharge as show in fig 3.34. The doublet lens minimises the unfocusing effect of the shadow image due to the broadband light source. A 50cm doublet was used for 5:1 magnification. A 7cm quartz lens was used for 10:1 magnification as shown in fig 3.35.

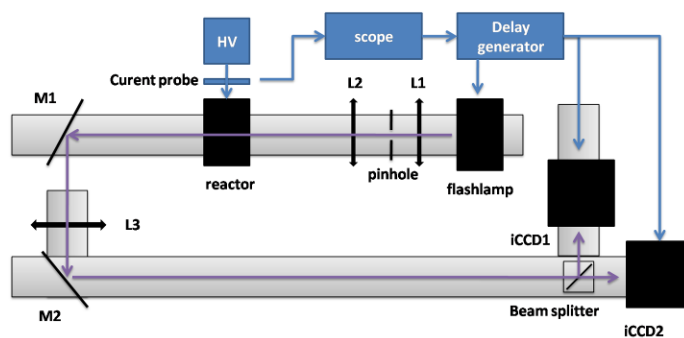


fig 3.35 the imaging lens is used to perform magnification from 1 : 1 ratio until 10 : 1 ratio

3.5 Spectroscopy

3.5.1 Temperature measurements

In a general way, hot electrons collide with the molecule in the liquid or in the plasma filaments and lead to continuum or line emission according to a collisional radiative scheme. The line emission comes from the electron dissociation products and recombination. In water one could expect H α , H β , and O lines. OH band should also be present and N₂ band from dissolved N₂ may be observed.

The discharge emission is focused on an UV grade optical **fiber** and a **monochromator of 30cm** focal length with **40 μ m entrance slit** aperture and **2400l/mm grating**. The monochromator was wavelength calibrated with a mercury lamp and the apparatus broadening was measured to be **0.07nm**. The apparatus broadening was observed to be almost constant below 40 μ m, between 40 μ m and 20 μ m only the collected intensity changed as shown in **fig 3.36**. The monochromator aberration leading to non symmetrical line shape seen in **fig 3.36** was minimised by taking into account only the central region (100 lines) of the iCCD chip in the vertical binning. A shamrock monochromator coupled with the Andor iCCD were used to obtain time resolved spectra of the discharge. Even with maximum intensification the collected light intensity is not enough to resolve the line shape on single shots. Accumulation over tens of shots is needed to observe clean band shape or line broadening.

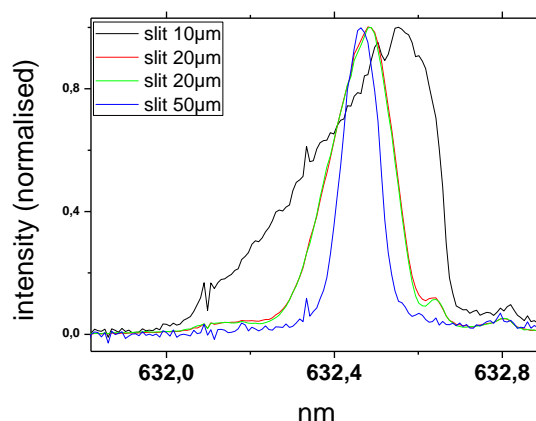


fig 3.36 apparatus broadening for 2400l/mm grating as a function of the entrance slit aperture

3.5.2 Time resolved line broadening

The following broadenings are taken from [A physicist desk reference 1989].

3.5.2.1 Doppler broadening

Doppler broadening is due to **motion of emitting atoms**. Emitters weight M is in atomic mass unit, wavelength λ in angstrom. Broadening is Gaussian for a maxwellian thermal motion at temperature T, and gives the full half width at maximum:

$$\Delta\lambda_{1/2}^D = 3.58e^{-7} \cdot \lambda \cdot (T/M)^{1/2}$$

3.5.2.2 Resonance broadening

Concerns only the line with a initial or final level combined to ground level by a **dipole transition**.

$$\Delta\lambda_{1/2}^R = 4.3e^{-30} \cdot (g_i/g_k)^{1/2} \lambda^2 \lambda_r f_r N_i^{1/2}$$

N_i is the ground level density, λ_r is the wavelength of the dipole resonant line, f_r is the oscillator strength of the transition, g are the statistical weights of the upper and the lower level of the transition.

3.5.2.3 Van Der Waals broadening

The dipole interaction of an excited atom and a polarized ground state atom leads the relevant **pressure broadening** term in our conditions.

$$\Delta\lambda_{1/2}^W = 1.5e^{-16} \cdot \lambda^2 C_6^{2/5} (T/\mu)^{3/10} N$$

N is the concentration of collider atoms. $C_6 = C_h - C_l$ and C_i are the Van der Waals coefficients defined by $C_i = 9.83e^{-10} \cdot \alpha_p R_i^2$ with α_p the polarisability of the neutral molecule considered. In our case we consider the water molecule as the collider of reduced mass $\mu = (18 \cdot 1)/(18+1) = 0.95$ atomic units. The water molecule polarisability in liquid state is $\alpha_p = 6.7e^{-25} \cdot (3I_H/4E^*)$, I_H is the hydrogen ionization potential and E^* is the first level of collider. $\alpha_p = 9.78 \text{ au} = 9.78 \cdot 0.53 \text{ angstrom}$ according to [Millot2008], we will take $\alpha_p = 1.56e^{-24} \text{ cm}^3$. $R_i^2 = 2.5 \cdot (I_H/(I - E_i))^2$, I is the emitter ionization potential (hydrogen in our case), E_i are the level of the upper and the lower state of the considered transition.

We consider the H α transition, the (H α is at 656.3nm)

$$R_u^2 = 2.5 \left(\frac{109678}{109678-97492} \right)^2 = 202.52 \text{ for } n=3 \text{ upper level}$$

$$R_l^2 = 2.5 \left(\frac{109678}{109678-82259} \right)^2 = 40 \text{ for } n=2 \text{ lower level}$$

$$\text{thus } C_6 = 9.83e^{-10} 1.56e^{-24} (202.5 - 40) = 2.48e^{-31}$$

$$\text{and finely } \Delta\lambda_{1/2}^W = 1.5e^{-15} \cdot 656.3^2 2.48e^{-31 \frac{2}{5}} (T/0.95)^{3/10} N \text{ nm}$$

$$\frac{\Delta\lambda_{1/2}^W}{N} = 3.25e^{-22} T^{0.3}$$

N is given by $N = P \cdot 2.687e19 \cdot (298/T) \text{ cm}^{-3}$ according to perfect gas law

$$\text{And thus } \Delta\lambda_{1/2}^W = 3p/T^{0.7} \text{ nm}$$

We need to know the gas pressure and temperature. For example the halfwidth at maximum of H α line broadened by water vapor at 2400K and 400bar is 5.16nm.

3.5.2.4 Stark broadening

This broadening is due to **charged perturbators**.

$$\Delta\lambda_{1/2}^S = 1.25e^{-9} \cdot \alpha_{1/2} N_e^{2/3}$$

with N_e the electron density and $\alpha_{1/2}$ the half width parameter. This parameter is tabulated for different gas temperatures and electron densities. For example a classical tabulation on H β if given by:

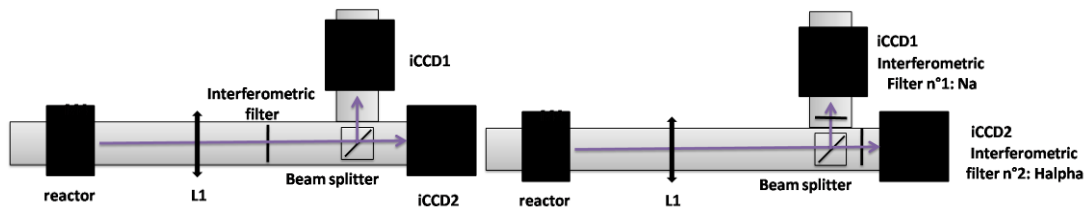


fig 3.38 a single interferometric filter can be put before the two iCCDs to obtain two 2D line intensity mapping at different times, when different filters are put on each iCCD we can observe the 2D intensity mapping at the same time for different lines.

| | | |
|---------|--|-----|
| 4 | The positive polarity | |
| 4.1 | General description of the positive mode: primary mode, secondary mode, reillumination, post discharge | 108 |
| 4.2 | Electrical characterization, discharge current | 111 |
| 4.3 | Initiation of the discharge for positive polarity..... | 115 |
| 4.3.1 | General description of the time delay to initiation of the plasma | 115 |
| 4.3.2 | Statistical nature of the time delay of the plasma initiation : formative time lag and initiation time lag | 116 |
| 4.3.3 | Influence of the applied voltage..... | 118 |
| 4.3.4 | Influence of the liquid ionic conductivity | 119 |
| 4.3.5 | Discussions and conclusions on the discharge initiation | 120 |
| 4.4 | Propagation of the positive mode | 122 |
| 4.4.1 | The primary mode in positive polarity..... | 122 |
| 4.4.2 | Transition from the primary to the secondary positive mode | 125 |
| 4.4.3 | The fast secondary mode in positive polarity | 127 |
| 4.4.3.1 | Discharge morphology: branching, conductivity influence, dielectric obstacle influence..... | 127 |
| 4.4.3.2 | Propagation velocity measurements | 133 |
| 4.4.3.3 | Influence of applied voltage on the propagation velocity..... | 135 |
| 4.4.3.4 | Influence of liquid ionic conductivity on the propagation velocity..... | 135 |
| 4.4.3.5 | Influence of the gap on the propagation velocity..... | 136 |
| 4.4.3.6 | Influence of additives on the propagation velocity..... | 137 |
| 4.4.3.7 | Stopping length of the discharge..... | 138 |
| 4.4.4 | Shock wave emission and “continuous propagation” | 139 |
| 4.4.5 | Reillumination and step propagation | 145 |
| 4.4.6 | Gas channel expansion in post-discharge | 148 |
| 4.4.7 | Time resolved emission spectroscopy on H_{α} and OH(A-X): plasma parameters | 151 |
| 4.5 | Discussion and conclusions on the positive mode..... | 153 |



4 The positive polarity

4.1 General description of the positive mode: primary mode, secondary mode, reillumination, post discharge

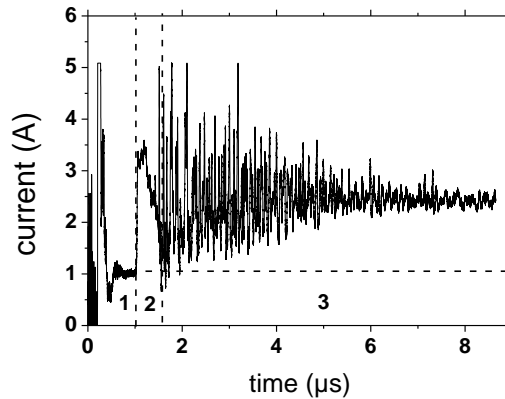


fig 4.1 Current for medium conductivity ($100\mu\text{S}/\text{cm}$), (1) preinitiation current (displacement charging of the pin to plane electrode geometry and then conduction through resistive water), (2) discharge propagation, (3) reilluminations spikes are superimposed to a baseline resistive conduction current, (1cm gap, 30kV, voltage halfwidth is $10\mu\text{s}$ here)

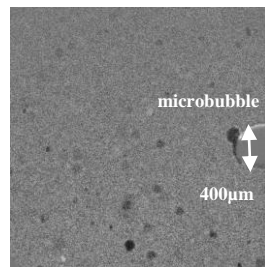


fig 4.2 shadow image of the microbubble nucleation, the HV pin is $400\mu\text{m}$ diameter, ($100\mu\text{S}/\text{cm}$, 30kV, 30ns gate, 5μs delay)

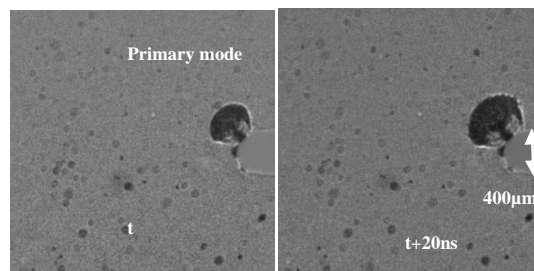


fig 4.3 successive shadow images of the primary mode taken on the same shot with 200ns delay between the two images. The primary mode is a tree like filamentary structure starting from the top of the nucleated microbubble on the metal surface and growing in the wake of a spherical shock wave, (1cm gap, 30kV, 20ns gate)

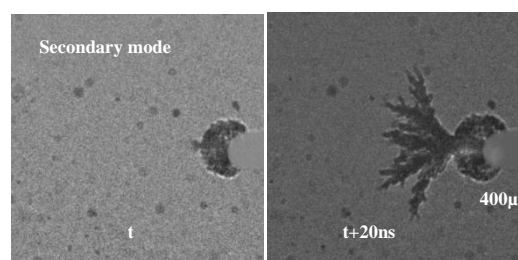


fig 4.4 successive shadow images of the secondary mode taken on the same shot with 30ns delay between the two images. (50 μ S/cm, 30kV, 20ns gate)

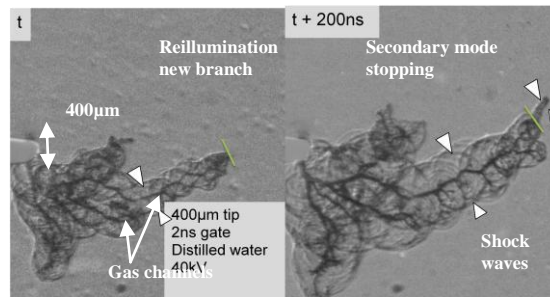


fig 4.5 shock wave pattern emitted by the secondary positive mode and a new created segment by reillumination, (50 μ S/cm, 30kV, 20ns gate)

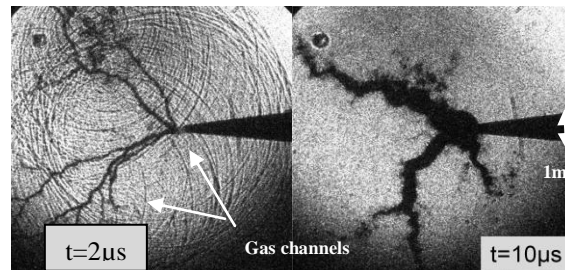


fig 4.6 shadow image of the postdischarge gas channel expansion and fragmentation at 2 and 10 μ s first image shows the late stage of shock wave propagation, (50 μ S/cm, 30kV, 20ns gate)

Here is brief description of the growth of the positive discharge in water:

- there is some **delay** from the beginning of the applied voltage pulse to the first observable phenomena , stage (1) on **fig 4.1**, typically 1 μ s.
- A **small dark spherical region** can be observed on the surface of the HV electrode with shadow diagnostics in **fig 4.2**.
- This **microbubble** evolves after some time into a **tree-like structure** with many filaments and perfect hemispherical shape as in **fig 4.3**. This spherical structure is the “**primary mode**” it is mostly observed at low conductivity and low voltage. It propagates quite slowly and is weakly luminous. Stage (2) in **fig 4.1**
- Then a new structure appears to emerge from the surface of this primary mode and also presents a tree like structure and branching but on larger scale compared to the primary mode. This **secondary mode** is much more luminous and much faster as can be seen on **fig 4.4**. stage (2) in **fig 4.1**
- Then this discharge **stops** to propagate and can **reinitiate** after some variable delay. Depending on the experimental conditions, this **reillumination** can be a full discharge restart or a different mode of plasma discharge occurring in some of the gas channel leaved behind by the secondary mode. A pair of shadow images before and after a reillumination is shown in **fig 4.5**, stage (3) in **fig 4.1**
- When the secondary mode or the reillumination reach the opposite electrode a spark (transient arc, see **fig 4.9**) will occur and there will be thermalization of the plasma channels. If the interelectrode gap is sufficient or the applied or the applied voltage pulse short enough the **spark** will not occur.
- In the **post discharge**, the **shock waves** emitted by the plasma propagate and the gas **channels expand and fragment** into a **cloud of microbubble** as shown in **fig 4.6**.

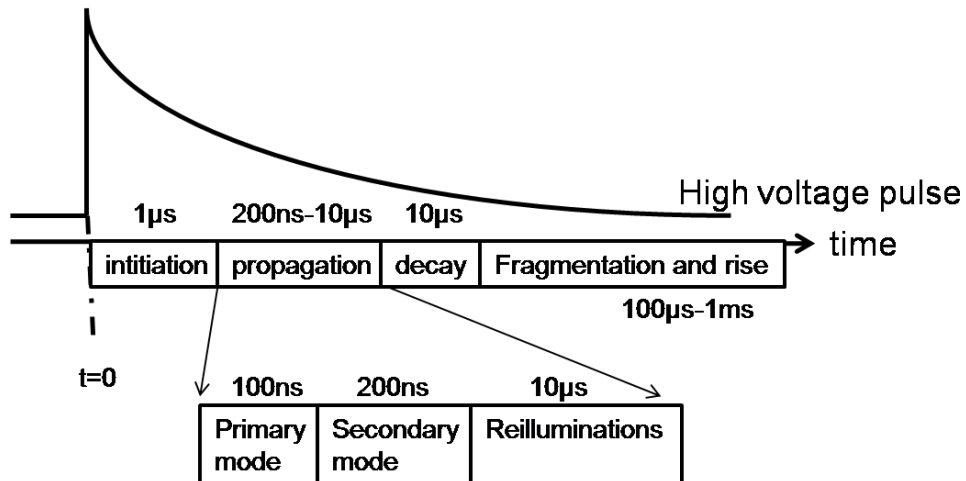


fig 4.7 shadow schematic of the different stages of the discharge during the applied voltage pulse and the associated time scales

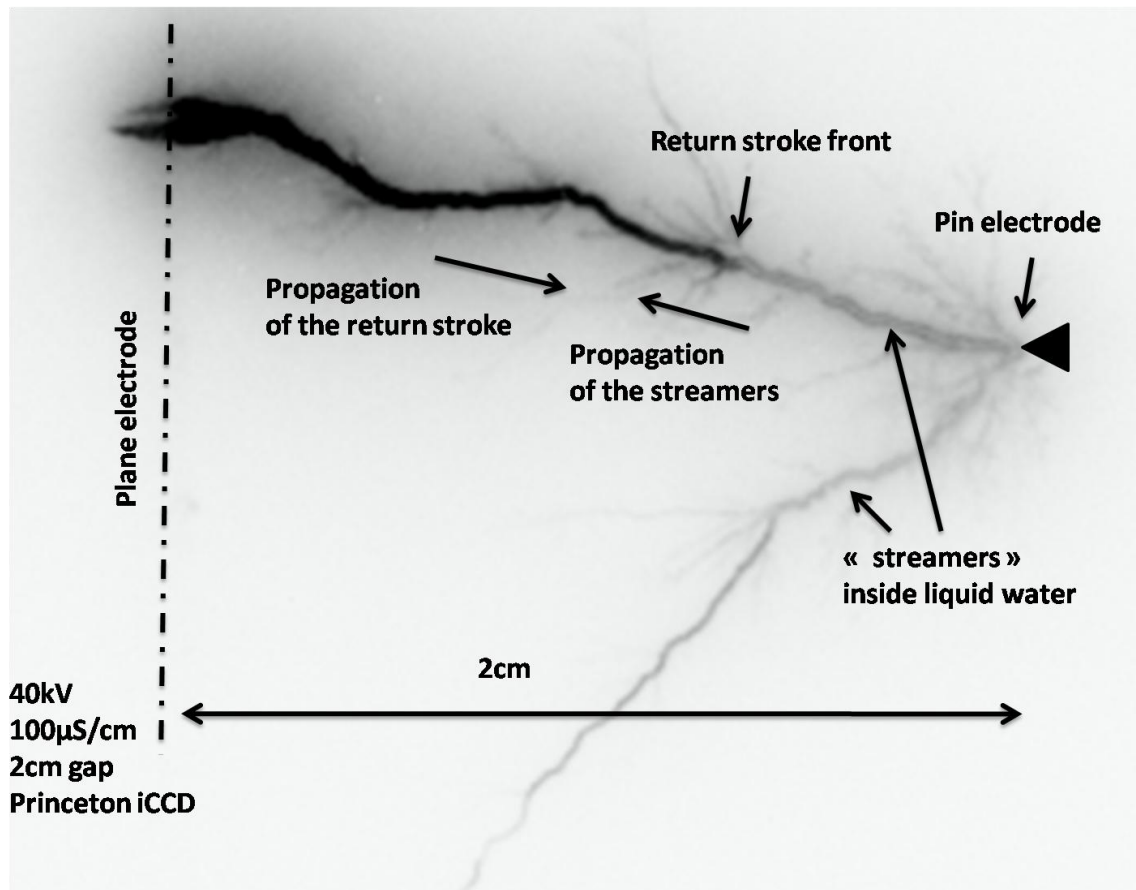


fig 4.8 emission image of the transition to spark if the applied voltage is too long, the streamer filaments are propagating through the water from the pin electrode toward the plane and the thermalisation return stroke propagates from the plane to the pin, (40kV, 100μS/cm, 2cm gap, 2ns gate).

4.2 Electrical characterization, discharge current

The current electrical waveform has the following pattern (see fig 4.1, fig 4.10, fig 4.11, fig 4.12, and fig 4.13):

- **displacement current** due to the charging of the **interelectrode capacitance** of the reactor (0) in fig 4.12.
- **conduction current (or initiation current) before plasma ignition** (1) in fig 4.12.
- the **primary mode** current that is a **ramp** lasting less than 100ns and of **mA** amplitude as shown in fig 4.30.
- step increase due to the **secondary mode** current in the **Amp** range as shown in (2) in fig 4.12 and in fig 4.13.
- huge increase of the current in the **kA** range is observed and correspond to a **spark** regime when the plasma filaments reach the opposite electrode as shown in fig 4.9.

The **displacement** observed after the beginning of the applied voltage pulse is a **stray** current. The ringing lasts hundreds of nanoseconds. This current **ringing** was an important **obstacle** for identifying the exact beginning of the plasma discharge. This problem implied to use indirect techniques such as Laue-plots to detect the plasma initiation. The ionic conduction current is followed by a step increase when the plasma filaments begin to propagate. This current increase is correlated to the first light emission nearby the high voltage electrode. The current increase can be used as a criterion for the discharge beginning. Unfortunately this current increase happens most of the time during the capacitive current ringing. Later on, a resistance was successfully added in series with the reactor in order to **damp** this electrical resonance.

The **primary mode** when it exists has a very weak current contribution and can barely be seen without zooming in because its **amplitude is very small** compared to the conduction current or the secondary mode current. Some **oscillations** can be seen on the primary mode current but it is not sure if they are physical or if it is due to the current measurement ringing. Those small peaks have not been correlated to any obvious event on the iCCD images.

The **secondary mode** current has a **typical amplitude of several Amps and increases during the propagation**. However, at low conductivity, the current increases at first but quickly starts to decrease during the propagation.

The **arc current is limited** by the energy stored in the high voltage **power supply**, the arc resistance, the external circuit resistance, the rise time of the spark current and its oscillating behaviour depends on the **inductance of the circuit**.

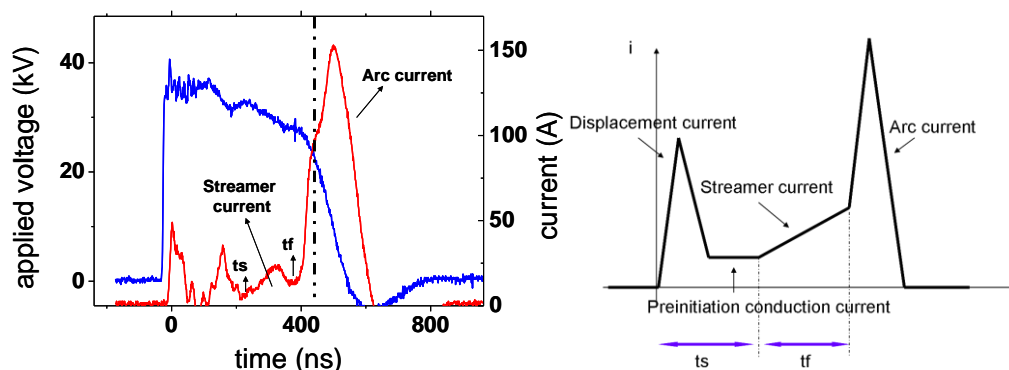


fig 4.9 typical voltage and current waveforms, displacement current, initiation current, discharge current (primary and then secondary), spark current

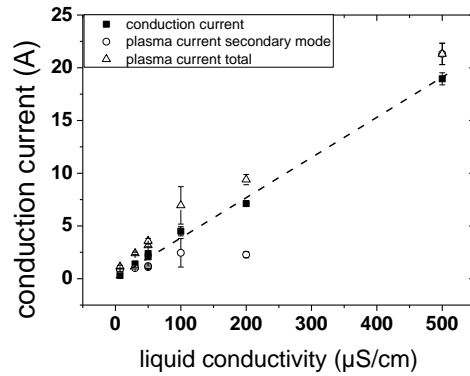


fig 4.10 pre-initiation (or initiation) current running through the reactor before plasma initiation, secondary mode peak current with baseline subtraction, total peak current, (30kV, 1cm gap).

The total current increases proportionally with conductivity as shown on fig 4.10 and with applied voltage level. There seem to be a correlation between the current due to the plasma and the propagation velocity. The primary mode is slow and its current is weak, the secondary mode is fast and its current is high. Such a behaviour is consistent with a pure **capacitive current** associated with the displacement of a charge along the interelectrode gap. The charge can be located in the filament head. The plasma filament would be a charge or a space charge that propagates across the gap and produces a **larger displacement current as it moves faster through the gap**. The other possibility is that the discharge behaviour is on the contrary **purely resistive** and the plasma filaments of the secondary mode have a larger **surface of contact with the liquid** or a larger filament conductivity. One can say that the plasma filaments multiply the **contact area** of the pin electrode and the liquid according to the number of filaments, their diameter, their length, and their conductivity. A large discharge volume leads to high current. The **discharge current value is thus related to the discharge number of filaments and the filaments length or ramified pattern**. Those two parameters drive the surface of plasma in contact with the liquid. The conductivity of the plasma filaments could be estimated if one knows all the parameters mentioned previously.

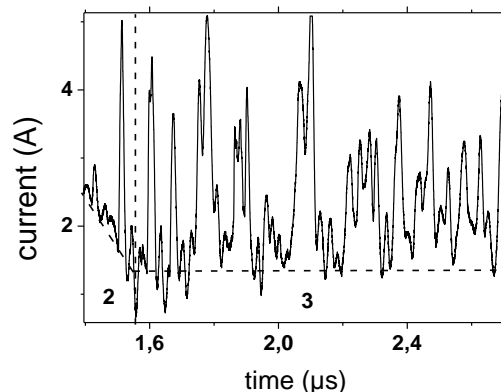


fig 4.11 preinitiation zoom on the reillumination current spikes (3), (2) end of the propagation of the secondary positive mode, (30kV voltage has decreased by typically 25% at this stage, 50μS/cm)

The shape of the current is quite smooth at high liquid conductivity on fig 4.13 whereas at low ionic conductivity the discharge current is a pulse and is followed by current spikes on fig 4.12. Those current spikes (3) on fig 4.11 are associated to **reillumination** and will be further discussed in the following. At low conductivity, the secondary mode current decreases at the end of the propagation and **falls down again to the conduction current level** as shown in fig 4.11. The **filaments are not conductive between two reilluminations, that is to say between two current spikes**. On the contrary, at high conductivity on fig 4.13, the current follows the

applied voltage RC decay, it means that the plasma filament remains conductive in the post-discharge.

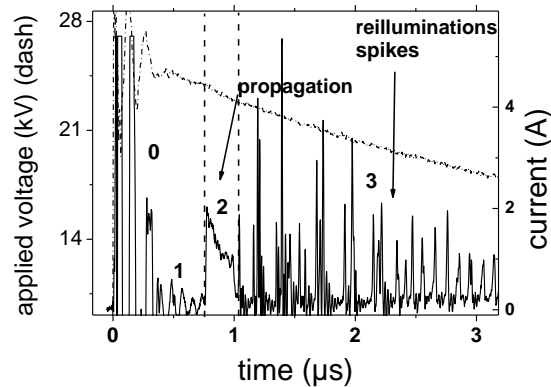


fig 4.12 current waveform in distilled water, (0) stray displacement current, (1) preinitiation current due to water conductivity, (2) large pulse of the secondary positive mode followed by (3) reillumination spikes with decaying amplitude, (4cm gap, 40kV)

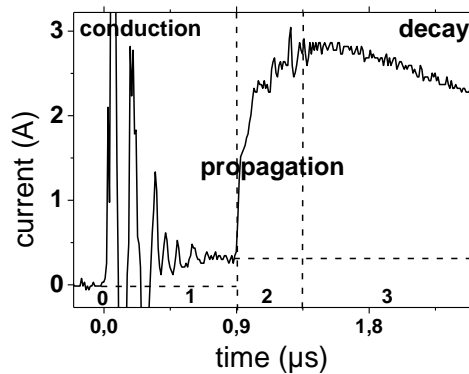


fig 4.13 no reillumination spikes at large water conductivity ($800\mu\text{S}/\text{cm}$ here, threshold is not clear and disappearance of reillumination is progressive), large current even when the discharge has stopped to propagate and just decay according to the voltage pulse decay, (4cm gap, 40kV)

A **capacitor can be put in series with the reactor** to check the injected charge. The injected charge slope increases when the plasma discharge begins and is associated to the increase of the current trough the reactor when the discharge begins as shown in **fig 4.14**. The charged transferred is typically of the order of **μC per filaments** in our conditions for a point to plane electrode configuration. This value is much higher than the conventional value of 1nC per filament observed for plasma in gases and is an indication of the power required to propagate the plasma filaments through a dense medium. The injected charges in water are also several orders of magnitudes higher than in insulating liquids. The **case of discharge in water is thus special and may not be representative of discharges in liquids in general**. At first, a 2nF capacitor was put in series with the reactor for security and avoid spark, in fact in order to avoid long spark a small value of capacitor must be chosen but given the injected charge required for the plasma propagation, the voltage drop would be too important and the discharge would stop almost immediately. It means that a DBD water discharge is not possible because the reactor capacitance required would be too important.

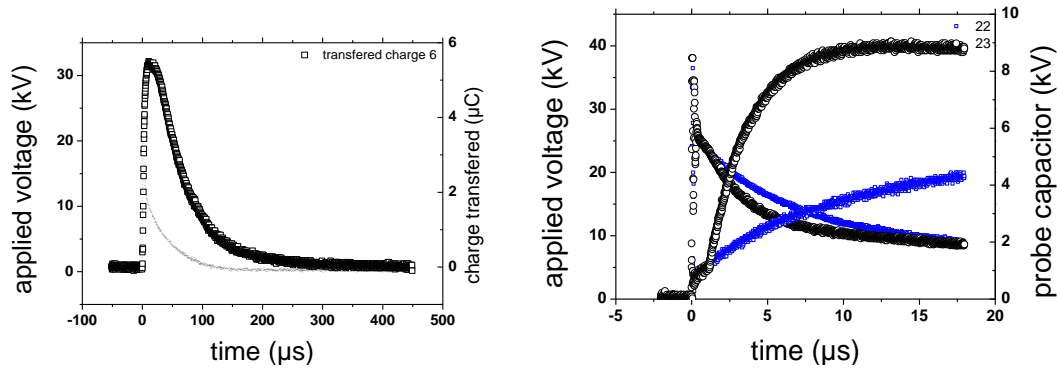


fig 4.14 voltage on a 2nF capacitor put in series with the reactor, charging due to resistive conduction through the water and then faster charging due to plasma discharge

The **pulse duration is increased by changing the RC decay time**. A longer pulse leads to more injected charges. The **discharge current level has the same growth rate but the peak value reached is higher since there is more time for the discharge to grow** as shown on fig 4.15. On the contrary, the **current growth rate increases when the applied voltage is increased** as shown in fig 4.16. The current slope (di/dt) increases with the applied voltage and this can be easily explained by the **increased number of simultaneous propagating filaments**: large number of charged tips or larger number of plasma/liquid surface. The gap dependence is weak: the current decreases by 20% when doubling the gap. The **thickness of water remaining** between the plasma filament tips and the opposite electrode is equivalent to a **series resistor**.

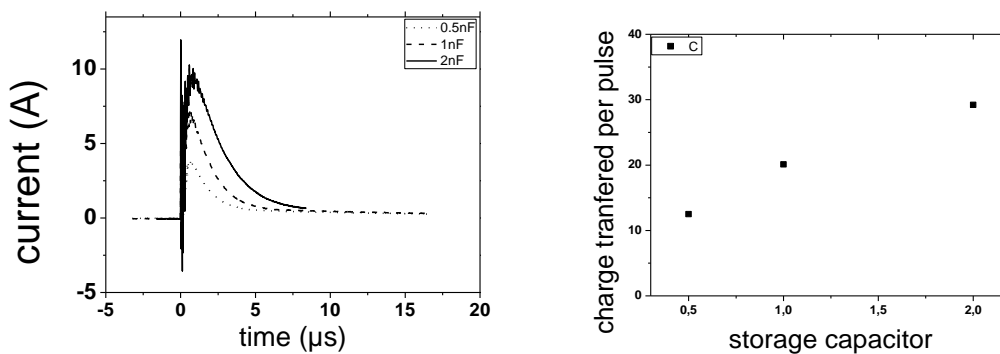


fig 4.15 increasing the storage capacitor of the power supply do not change the plasma current slope but only change the current pulse duration

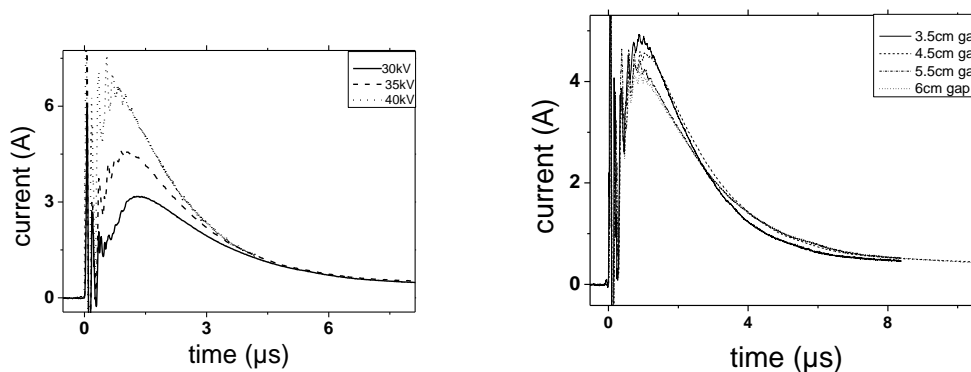


fig 4.16 current waveform for different voltages and different gaps

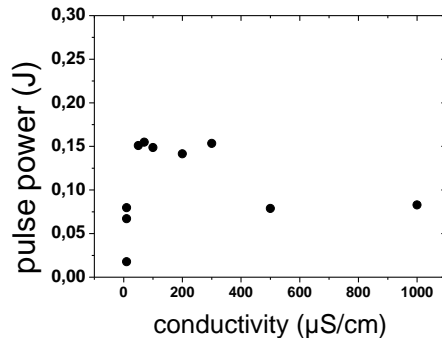


fig 4.17 $P=UI$ pulse energy as a function of the water conductivity.

4.3 Initiation of the discharge for positive polarity

The **behaviour of the delay to initiation with several experimental parameters** has been tested in the present study. This behaviour will give us **insight in the initiation mechanism** of the discharge inside water. If the experimental behaviour of the delay to initiation is different compared to the plasma propagation it would mean that the initiation follows a different mechanism and cannot be reduced to some unified mechanism. We observed that the plasma does not readily start to propagate, there must be some **criterion built up or reached prior to initiation**.

4.3.1 General description of the time delay to initiation of the plasma

The first obvious statement about the plasma ignition inside water is that it happens after some **time delay from the beginning of the applied voltage pulse at $t=0$** as shown on **fig 4.1**, **fig 4.9**, **fig 4.12**, and **fig 4.13**. The applied voltage pulse rise time is of the order of 20ns and the plasma initiation **delay is typically of some hundreds of nanoseconds**. As a consequence, the plasma ignition does not happen while the applied voltage is still rising at the electrodes but on the contrary while the voltage has already decreased due to its RC decay shape. The rise time of the applied voltage is not relevant in the present study.

The time delay to plasma initiation is very unstable and presents a **jitter** of typically several times its mean value as shown on **fig 4.19**! To give an idea, the initiation delay is typically 1μs with 10μs jitter and the main phase of the propagation only lasts for a few hundred of nanoseconds in distilled water.

With emission imaging one can observe that the discharge initiates from a **bright spot** at the pin electrode. Then tens of low intensity filaments start to propagate simultaneously from the positive needle toward the ground plane.

To observe non luminous events prior to the discharge ignition, the shadow diagnostic is more appropriate. The preinitiation phenomena can indeed be of **gaseous nature and not self luminous**. With shadowgraph images we observed that a spherical bubble is nucleated at the high voltage electrode pin as shown on **fig 4.18**.

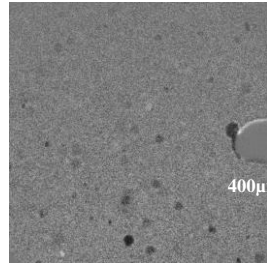


fig 4.18 gas bubble nucleation at the HV needle without plasma discharge after a delay of 5μs after the beginning of the applied voltage pulse

This gaseous cavity appears also after some delay from the applied voltage, its **nucleation does not seem to be a progressive process from the beginning of the applied voltage pulse**. This is because of the time needed to heat up the liquid to the vaporisation temperature and also because of superheating. This microbubble nucleation is thus responsible for the plasma initiation jitter.

The **microbubble appearance is not immediately followed by the discharge initiation**. The expansion rate of this gaseous cavity is quite slow, and in any case slower than the following propagation of the plasma. It means that the appearance of the gas bubble is a necessary requirement but it not sufficient. Due to the **microbubble size and the pressure** inside this gas cavity the criterion for electron avalanches can only be reached after some pressure drop. This would explain why the plasma does not start as soon as some gas phase is nucleated. The jitter would then be sum of two contributions: the formation of the microbubble, and the expansion time until a critical radius*pressure value is reached.

4.3.2 Statistical nature of the time delay of the plasma initiation : formative time lag and initiation time lag

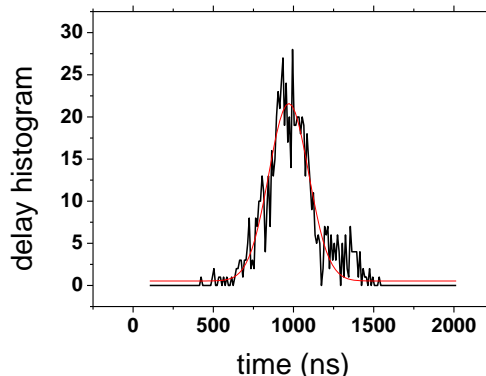


fig 4.19 delay to breakdown statistical distribution (delay between starting of the voltage pulse and complete electrical breakdown of the water gap), histogram established for 200 shots, 40kV, gap 5mm, 100μS/cm

A **direct measurement of the initiation delay directly from the discharge current waveform** is not very easy because the plasma current is often of the same order of magnitude than the stray capacitive current. This is why it is difficult to distinguish the time at which the discharge begins. A photodiode can be used to monitor the plasma emission with a 10ns time resolution, however the electromagnetic noise around the reactor make this measurement impossible and we observed that the photodiode only pickups the surrounding noise. The capacitive current can

be neglected compared to the plasma current at high liquid conductivity (above 100μS/cm) but is a real issue at low conductivity (10μS/cm).

Another approach is to measure the time delay to breakdown. The breakdown current can easily be seen on the current waveform and is one order of magnitude higher than the plasma current. This breakdown time delay t_{lag} contains information about the initiation and the propagation of the plasma. The time delay to breakdown is the sum of two typical times: the time **delay to initiation (statistical time lag t_{st})** and the **propagation time (formative time lag t_f)**. Each one has a statistical distribution $f(t_f)$ and $f(t_{st})$. The mean value \bar{t}_{st} and \bar{t}_f of those distributions and their halfwidth σ are useful to analyse the breakdown mechanism. One can consider that the formative time lag has a **normal distribution** and the statistical time lag has a **binomial distribution**.

$$f(t_f) = (1/\sigma\sqrt{2\pi})exp[-(t_f - \bar{t}_f)/2\sigma^2]$$

$$f(t_{st}) = (\mu exp(-\mu t_{st}))$$

Indeed, if the probability to initiate is proportional to the time inside each time interval, then the probability to initiate the discharge at time t gives a binomial distribution law.

$$p = \mu\Delta t$$

$$P(t) = Np(1 - p)^{N-1}$$

$$f(t) = \mu exp(-\mu t)$$

$$\bar{t}_{st} = 1/\mu$$

$$\sigma^2 = \bar{t}_{st}^2$$

$$t_{lag} = t_{st} + t_f$$

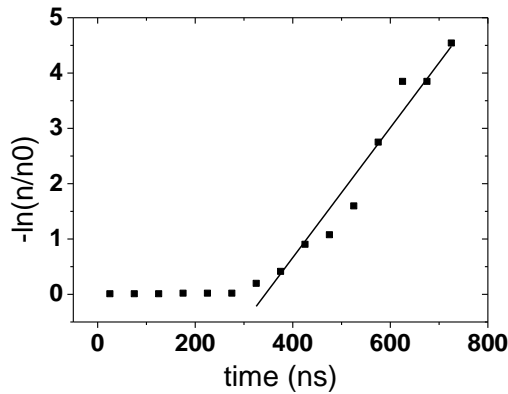


fig 4.20 Laue-plot, statistical study of the delay to breakdown. Cumulative histogram of the number N of breakdowns above a time t among N0 shots, obtained from fig 4.19.

N is the number of breakdown occurring below some precise time and N0 is the number of breakdowns. Usually a number of 30 breakdowns is sufficient to plot a clean curve. The linear part of the ln(n/n0) plot gives the mean formative time lag and the non linear part is due to the binomial distribution component.

If the mean statistical time lag has a value close to the mean formative time lag, there will be a superposition of the two distributions. Otherwise, the total distribution will be either dominated by the normal distribution or the exponential distribution.

We performed the **measurements with short gap of 5mm**. this value of the gap is large compared to traditional discharge in “short gap” in the 200μm range and sufficiently small to obtain breakdown in 90% of shots with the available pulse duration of our power supply. This larger gap allows to obtain a full discharge growth with initiation and propagation processed and thus avoid any artefact due to pure initiation processes without plasma ignition (cavity without

plasma). Thus in **fig 4.21** the delay to breakdown is not simply dominated by initiation processes as in [Jones].

The distribution of the propagation time is most of the time due to the **3D effects**. Knowing the propagation velocity of the discharge established in following chapters we can deduce trends of the initiation behaviour from delay to breakdown plots.

4.3.3 Influence of the applied voltage

For the positive polarity, the **mean delay to initiation decreases with an increase of the applied voltage** as shown on **fig 4.22** and **fig 4.23**. The decrease is quite linear. The dependence has been tested with accumulation measurements on 100 shots for each voltage. Single shot measurements have also been performed on **fig 4.23** to test the validity of the Laue-plot on **fig 4.21**. On the velocity/growth curve presented in **fig 4.46**, the initiation delay does not vary much but this variation is above the error bar.

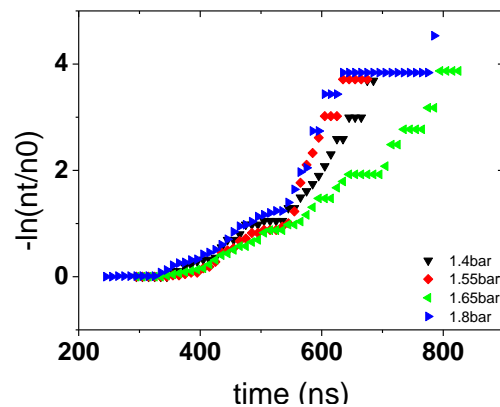


fig 4.21 laue plot a function of the applied voltage, pressure is the pressure inside the spark gap, the larger the pressure the larger the applied voltage value (25-45kV)

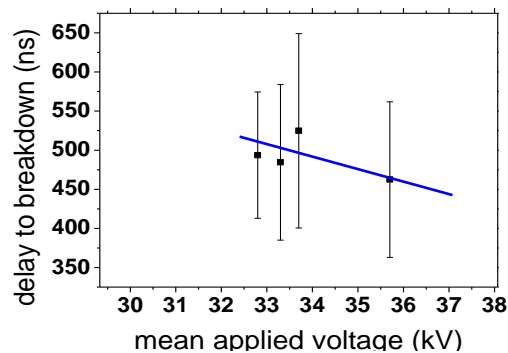


fig 4.22 delay to breakdown as a function of the applied voltage obtained from Laue plot , mean values, the “error bars” are in fact the jitter halfwidth

The **influence of the applied voltage level is significant** and has even been the reason why we were able to perform some shadow measurement of early stages of the discharge only at low voltage (30kV) due to the large intrinsic delay of the flashlamp.

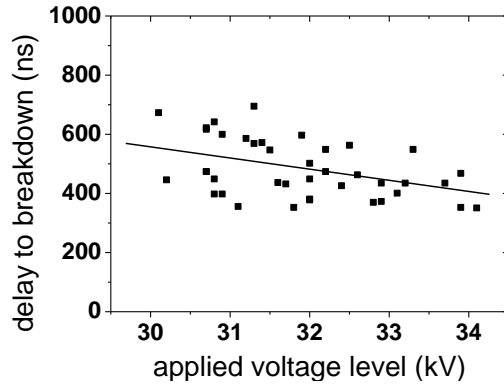


fig 4.23 plasma discharge initiation delay decreases when increasing the applied voltage, 5mm gap, 100 μ S/cm, single shots

4.3.4 Influence of the liquid ionic conductivity

The initiation delay decreases with an increase of the liquid ionic conductivity as shown on fig 4.25. This decrease is quite linear.

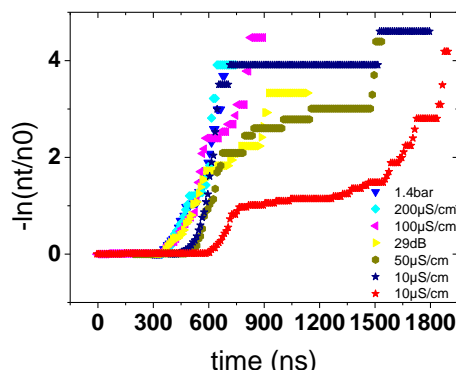


fig 4.24 Laue-plot of the timed delay to breakdown as a function of water conductivity

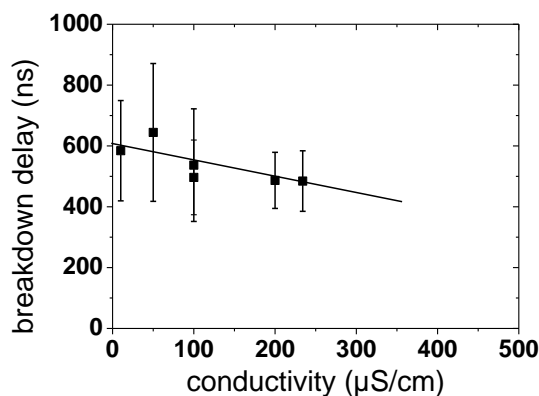


fig 4.25 plasma discharge initiation delay decreases when increasing the liquid conductivity. The error bar indicates jitter and not uncertainty, 5mm gap, 40kV

The statistical time lag decreases at high conductivity, the formative time lag is almost the same between the high and the low conductivity. The error bar is consistent with a weak decrease of the propagation velocity (measured and discussed further) of the discharge inside tap water. The saturation of the curve in fig 4.24 on the distilled water is likely to be due to

reillumination processes that happen at low conductivity. This reillumination will be discussed further.

The dependence of the initiation delay on the liquid conductivity is less clear since a first set of experiments gave a decrease of the initiation delay with an increase of the liquid ionic conductivity but later experiments in another reactor gave the opposite result. The reason is that the applied voltage decreases faster at higher conductivity and thus both conductivity and voltage effects are superimposed.

4.3.5 Discussions and conclusions on the discharge initiation

This observed decrease of the time delay to initiation with conductivity and voltage is unfortunately **consistent with many initiation mechanisms**. The microbubble joule nucleation will be influenced by applied voltage but the crack mechanism or charge injection would also be influenced. The influence of the conductivity is a strong hint in favour of joule heating.

The **influence of pressure is a main parameter that could have an effect on the discharge initiation** but would also influence both the crack mechanism and the bubble mechanism but would not influence a liquid avalanche process. Due to our reactor mechanical limitations the pressure increase or decrease was not implemented.

Since a density lowering is required prior to the plasma ignition, a gas **bubble was manually injected to test** if the plasma starts readily without any initiation delay. In fact the only delay expected is the electron avalanche amplification. The bubble introduced was at **atmospheric pressure** with a **millimetre size**. We observed that the plasma mode obtained with manual gas injection near the point electrode is very different from the plasma obtained with no gas injection. The **plasma filaments crawl along the bubble on tens of microsecond time scale**. **They are not able to penetrate inside the liquid and are confined inside the gas cavity** as shown on **fig 4.26**.

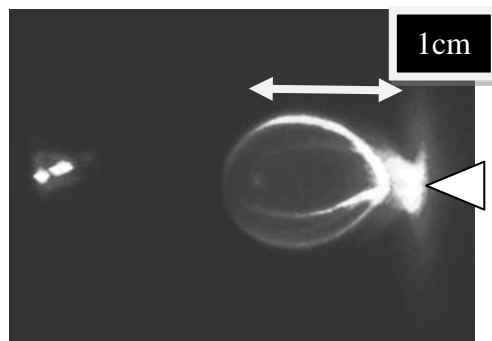
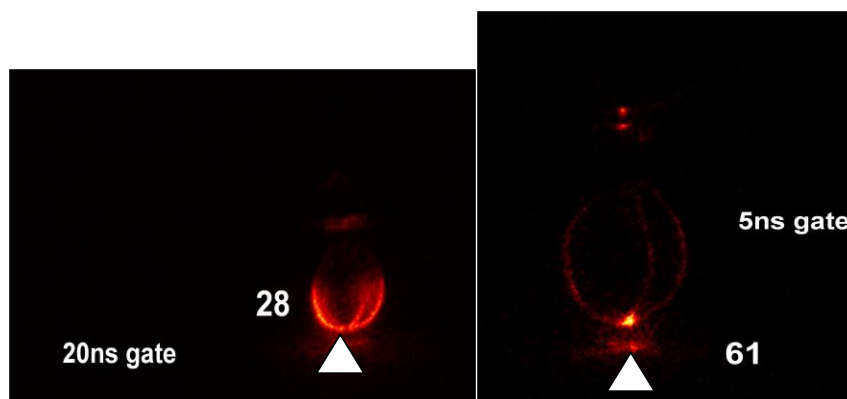


fig 4.26 plasma filaments stay confined inside the injected gas bubble, air bubble at atmospheric pressure is injected through the high voltage needle electrode, the size and/or the pressure of this bubble induce a plasma confinement and the plasma is not able to propagate inside the liquid, (4cm gap, 10kV, 100 μ S/cm, 1 μ s delay, 100ns gate)



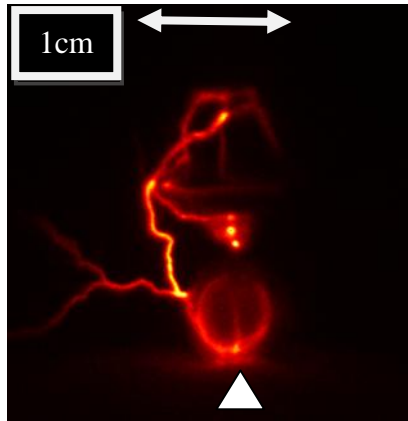


fig 4.27 initial stage of the plasma filaments inside the millimeter scale bubble, during some shot we can observe a mode transition from slow to fast filamentary mode. (Point to plane configuration, air bubbling through the point at atmospheric pressure, positive applied voltage pulse $2\mu\text{s}$ duration 40kV , 4cm gap).

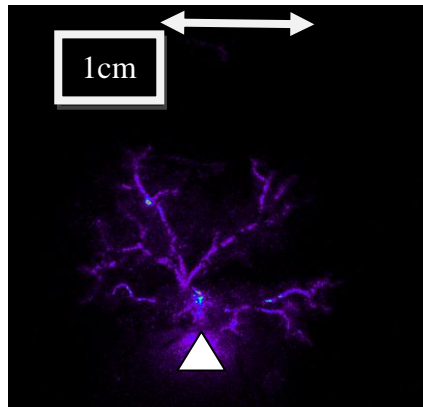


fig 4.28 tree-like structure of the slow positive mode. $1\mu\text{s}$ gate, $1500\mu\text{s}$ delay, (point to plane configuration, air bubbling through the point at atmospheric pressure, positive applied voltage square pulse 1ms duration 10kV , 4cm gap).

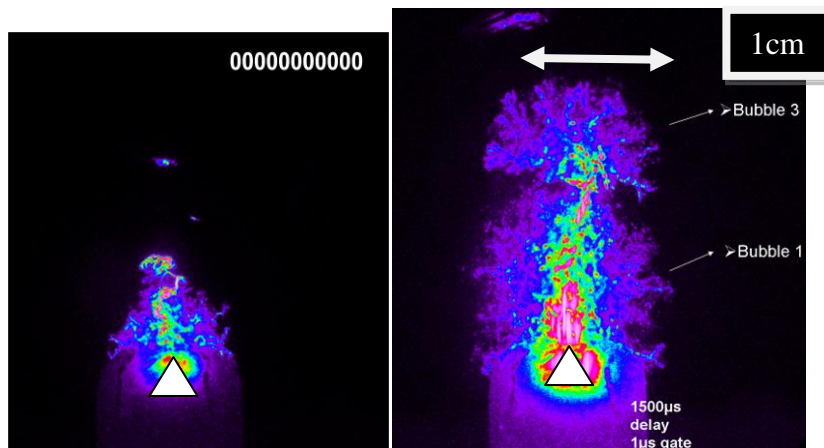


fig 4.29 the discharge can reach a second millimeter size bubble above the point, and even a third for very long pulse duration (2ms), (point to plane configuration, air bubbling through the point at atmospheric pressure, positive applied voltage square pulse 10kV , 4cm gap)

The plasma follows the motion of the gas interface on the hundred of microsecond timescale (1ms voltage pulse duration). The shape of the discharge at the end of the pulse is a tree-like structure that follows the tortuous gas cavity as shown in fig 4.28 and fig 4.29. This mode is very similar to the negative mode in terms of morphology. We can identify this mode to the “slow positive mode” or “subsonic mode” reported in [Touya2006].

This **slow positive mode** (different from **primary mode** and **secondary modes that can be qualified as supersonic modes or fast modes**) was obtained for a **low voltage** (10kV, not 40kV). The question is do we obtain a slow mode with same high voltage if we inject a gas bubble. It would mean that the pressure of the bubble is the main cause for a fast or a slow propagation. The fast mode is thus a high pressure mode, and the slow mode is a low pressure mode. Thus the injection of large bubble (millimetre) at atmospheric pressure instead of some tens of nanometer bubble at higher pressure (because of heating rate and superheating) dictates the plasma mode obtained. Thus the initial cavity size and pressure is of particular importance for the following plasma propagation.

Remark: The joule mechanism supported by the present study is likely to change with very high overvoltage of the water gap. At very high voltage, electrostatic processes presented in the state of art chapter can dominate over microbubble nucleation. The electrostatic pressure or crack formation can become the main driving force for the microcavity nucleation responsible for the plasma discharge initiation.

It does not seem relevant to use short nanosecond very high voltage pulses here, the pulse duration is of no importance, only the voltage level would drive the transition from a joule heating mechanism with superheating to an electrostatic mechanism.

4.4 Propagation of the positive mode

In this section we present the **time resolved propagation** of the **primary mode** and the **secondary mode**. We also present the **post-discharge phenomena** such as **shock wave propagation** and the **gas channel expansion**. The influence of many experimental parameters has been tested: voltage level, voltage halfwidth, voltage decay slope, interelectrode gap, water conductivity.

The **propagation velocity of the plasma discharge through the medium** is one of the main parameter that allows to distinguish between the several plasma modes inside a liquid and to discuss about the propagation mechanisms.

4.4.1 The primary mode in positive polarity

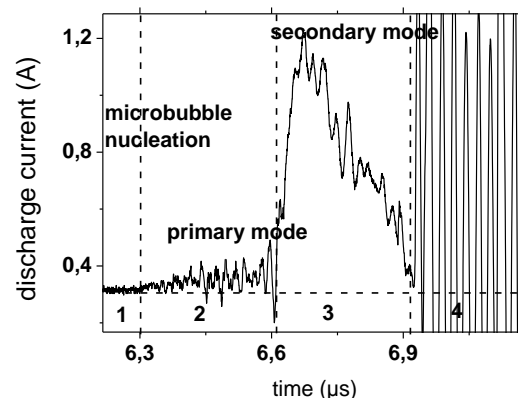


fig 4.30 current waveform, (1) preinitiation current due to conductivity of water 300mA, (2) current ramp of the plasma primary positive mode 20mA, (3) current increase of the secondary positive mode 1Amp, (4) reilluminations. (7µS/cm, 40kV)

The microbubble nucleation at the pin HV electrode is followed by the growth of a tree like structure of plasma filaments. The boundary of this structure is spherical. Since the plasma emission is not very luminous the best way to observe the primary mode is to use shadow imaging.

Two primary modes can propagate simultaneously. The root of the primary mode is not necessarily along the interelectrode axis. The primary mode begins at the top of the nucleated bubble.

The primary mode structure has a very **well defined spherical envelope**. It is not very clear if the primary mode is filamentary at the very beginning of its propagation. The filamentary structure of this primary mode is quite clear after 20ns. Many filaments can be observed. A shock wave is observed at the envelope of the primary mode discharge. The primary mode propagates at velocity close to **3km/s** and is thus supersonic. On **fig 4.32** It is not sure if the plasma filaments are in the wake of this spherical shock wave or if the shock wave is continuously emitted by the numerous filaments. In fact, **fig 4.34** shows that the observed shock wave results from the **superimpositions of the shock wave emitted by the individual channels**.

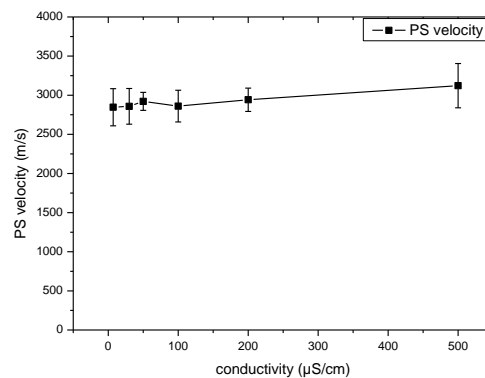


fig 4.31 velocity of the primary positive mode for different water conductivity. (1cm gap, 30kV)

The propagation of this mode is supersonic. It cannot be identified to the subsonic positive mode even if it is slower than the secondary positive mode (=supersonic mode [Touya2006]) described in the following section.

This mode is not observed for a too sharp point electrode (50μm) or at too high applied voltage (40kV). We observed it for a 400μm point electrode diameter and 30kV.

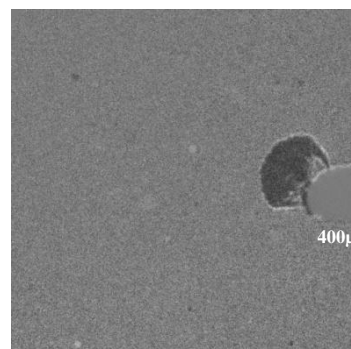


fig 4.32 typical shape of the primary mode, spherical shock wave, umbrella structure with poor resolution with filaments that can be distinguished at high resolution.

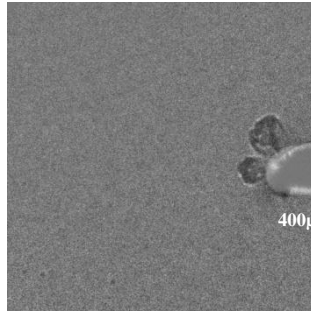


fig 4.33 possibility of two simultaneous growing primary modes at 500 μ S/cm.

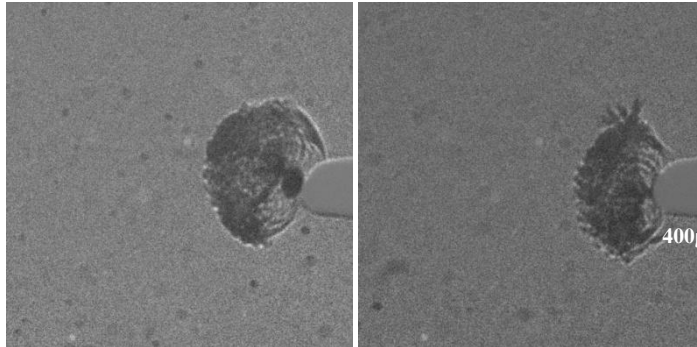


fig 4.34 filaments can be distinguished in the wake of a spherical shock wave, the filaments extremity coincide with the radius of the shock wave.

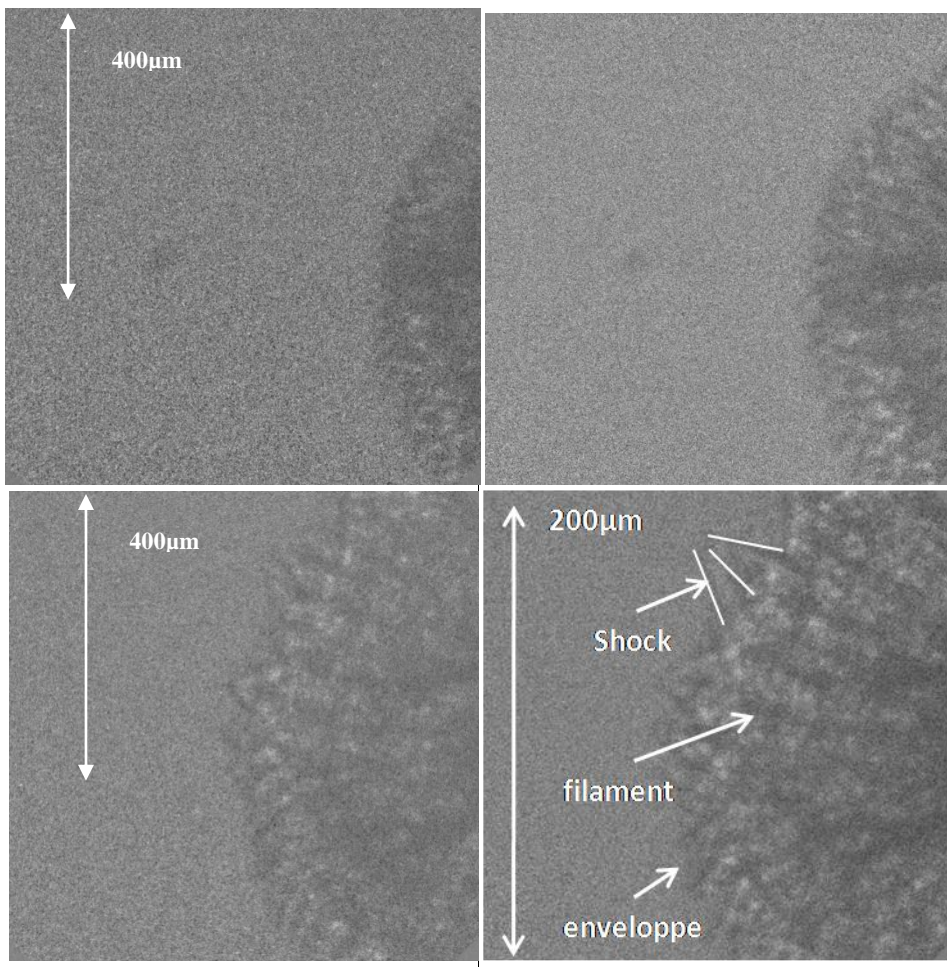
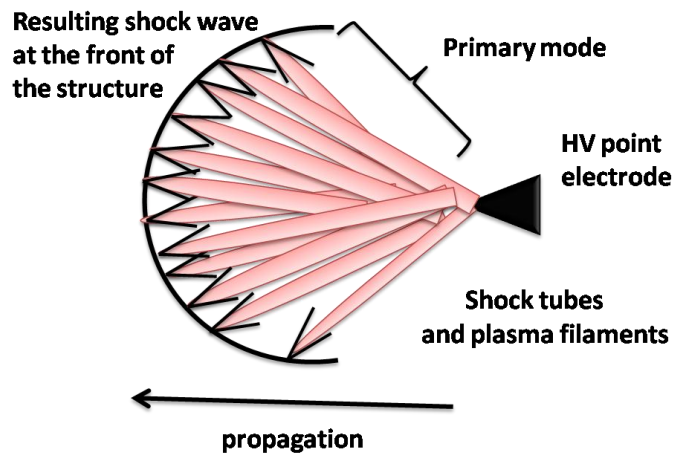


fig 4.35 pair of shadow images, primary mode at t and $t+30\text{ns}$, large magnification, the numerous dark filaments can be distinguished, each filament creates shock waves, the envelope of these shock waves is spherical.



4.4.2 Transition from the primary to the secondary positive mode

There is a **transition from the primary mode to the secondary mode** and this transition is characterized by the following features:

- one of first mode filament transforms into the **root of the new secondary mode** tree structure and have a very high emission intensity
- the secondary mode emerges from only one point of the surface of the primary mode hemispheric envelope.
- **stopping of the propagation of the first mode,**
- the shock wave from the first mode continues to propagate,
- The secondary mode produces its own shock wave tubes around the filaments as it begins to propagate

The primary mode gives birth to the secondary mode after some time or some distance from the HV pin electrode. The question is why a slow mode gives birth to a fast mode whereas the Laplacian electric field is lower far from the pin. The **transition between the two modes is not progressive**, it is a sudden event. The **criterion for this primary to secondary mode transition** can be caused by:

- Perhaps the filament must have a **sufficient electrical conductivity** which requires some time as the electron density builds up or the channel expands. When the channel becomes more conductive, the field ionization (autoionization) of the liquid becomes sufficient. When this criterion is met the secondary mode can start.
- or the **head of the filament becomes narrower** as it propagates which increases the field enhancement.
- or there is **more spacing between two filaments tips** and the electric field between two filaments is less screened.
- Or the primary mode **encounters a gas microbubble** impurity during its propagation and this gas bubble would induce a propagation mode change as it supplies instantly a big amount of readily ionisable species.

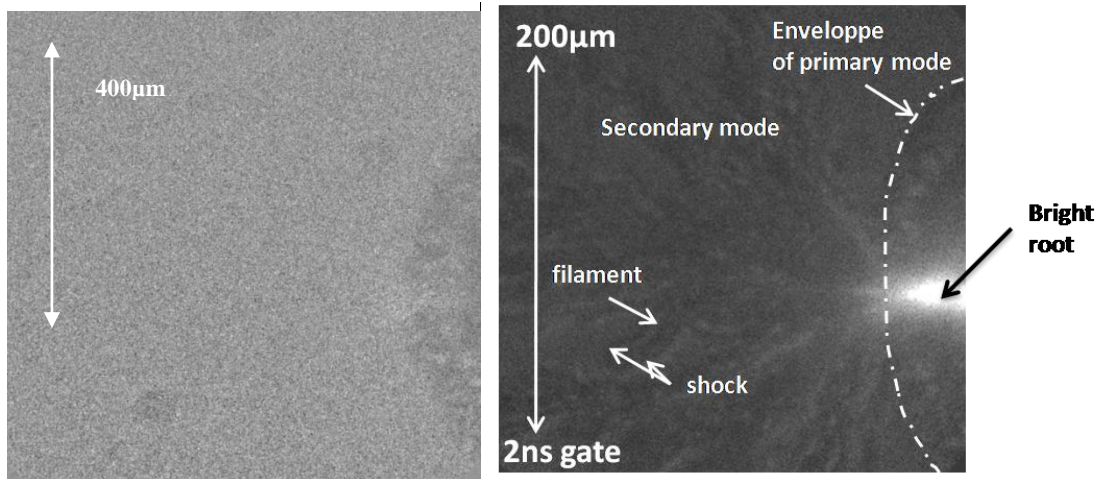


fig 4.36 pair of shadow images, primary mode at t and $t+30\text{ns}$, large magnification, transition from the primary mode to the secondary mode, emission from the plasma can be observed especially at the root of secondary mode structure.

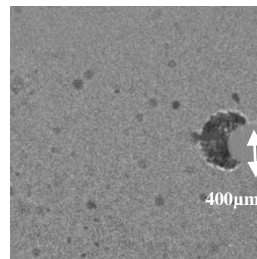


fig 4.37 transition from the primary to the secondary mode.

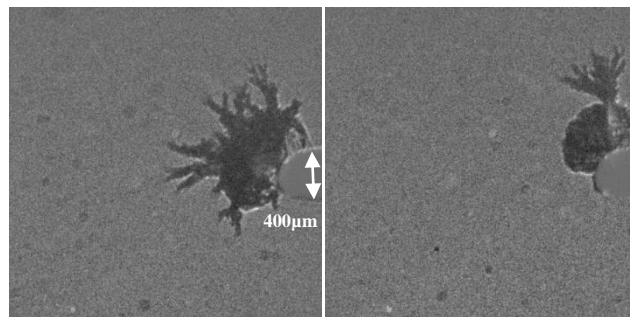


fig 4.38 the transition from primary to secondary mode does not necessarily happens along the interelectrode axis.

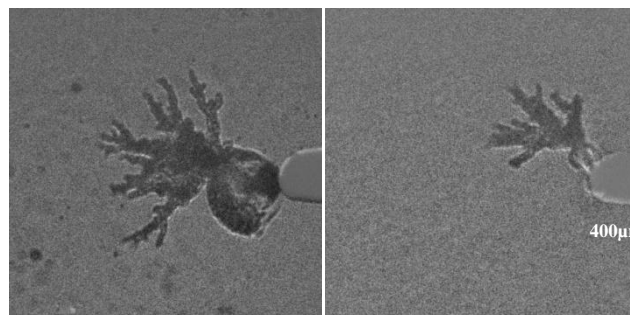


fig 4.39 a bright filament can be seen at the root of the secondary mode tree-like structure. The final radius of the primary mode structure is not the same on those two shots performed with same experimental conditions.

4.4.3 The fast secondary mode in positive polarity

4.4.3.1 Discharge morphology: branching, conductivity influence, dielectric obstacle influence

After some time or after some distance the **filament can split into several filaments**: this is called **branching**. A typical branching event can be seen on **fig 4.40**. The branching is one of the most striking characteristics of the filamentary plasmas. When branching occurs, the parent plasma channels stay in place and the new children filaments grow in a hemispheric shape as the main filaments and lead to an obvious fractal pattern. A dedicated study of the branching would be a nice idea at first [Kebbabi2006] but a closer look on the non reproducibility of the discharge over hundreds of shots (in the same experimental conditions) is sufficient to conclude that there is no obvious law followed by the branching. The branching seems to be quite chaotic. It is not sure if the branching comes from some **intrinsic mechanism or from the impurities** that are almost impossible to eliminate from the experimental point of view. The question is if branching is a phenomenon driven by the impurities or intrinsic instability, or regulating the propagation. This **random nature of the branching** suggest that it is highly non linear or driven by impurities. Impurities like dust or microbubbles are almost impossible to remove from the liquid even with careful filtering or intensive degassing by reducing the hydrostatic pressure.

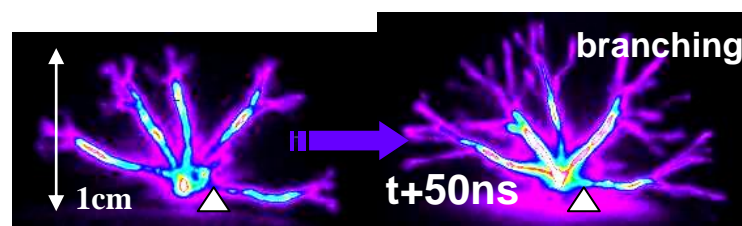
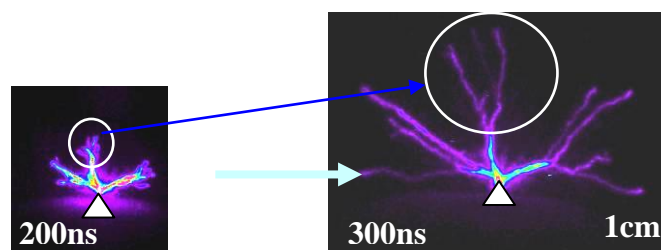


fig 4.40 2iCCDs emission imaging with same intensity colorscale, branching, pair of images taken on the same single shot (during the same voltage pulse), (2ns gate, 100 μ S/cm, 40kV)

Branching occurs most of the time and there is almost never a single filament without ramification or without tree-like structure. The tip of the filament is most of the time a hemispheric termination even at short gate in the nanosecond range. Some images show more structure termination of the filaments tips as shown in **fig 4.41**. This observation is quite interesting because the filament tip is though to be the active region responsible for the propagation, thus any substructure of this region would give an insight on the propagation mechanism. Indeed in the case of leader and lightning studies [Raizer], the main filament present a brush structure at its tip which are seed streamers converging toward the leader tip. A similar observation could be interesting to determine if the plasma channels inside the liquid is based on a streamer or a leader mechanism. With 2 iCCDs a more detailed approach is possible and after many acquisitions it turned out that in fact those brush just happens when the filament begins to split at a branching event.



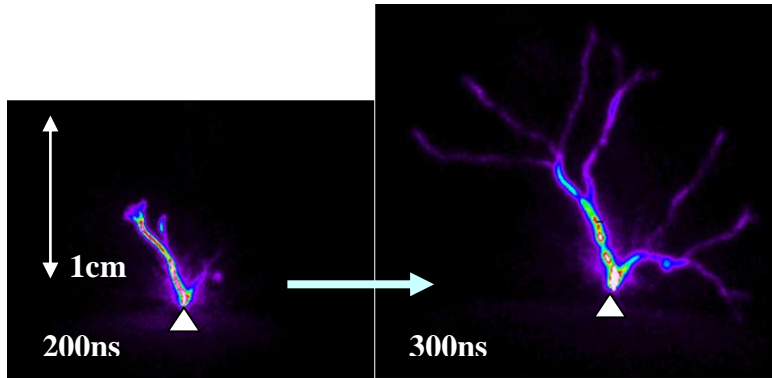
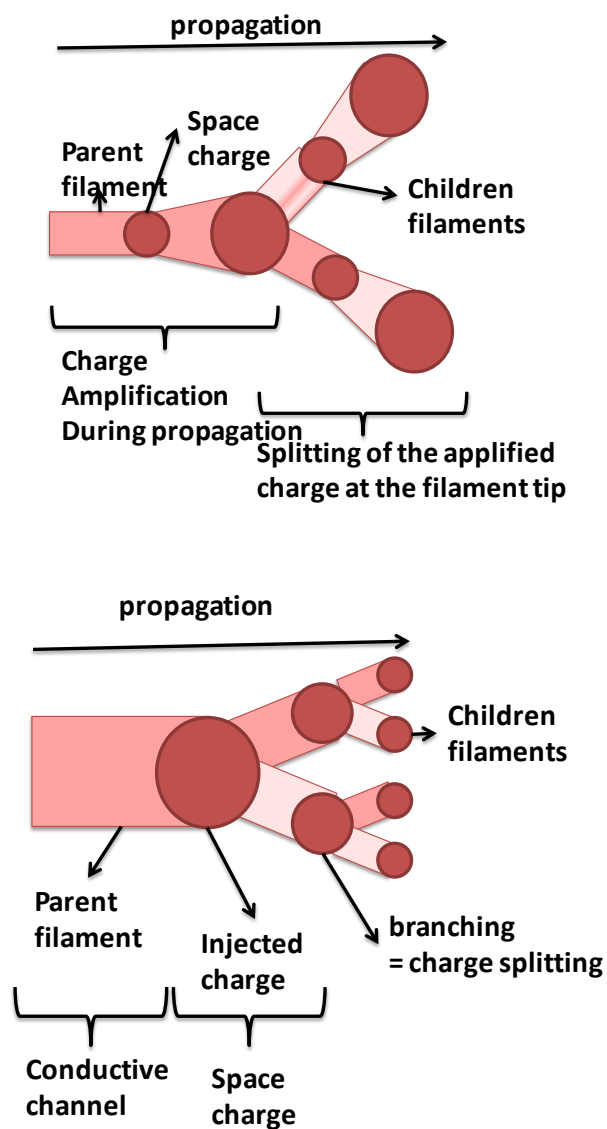
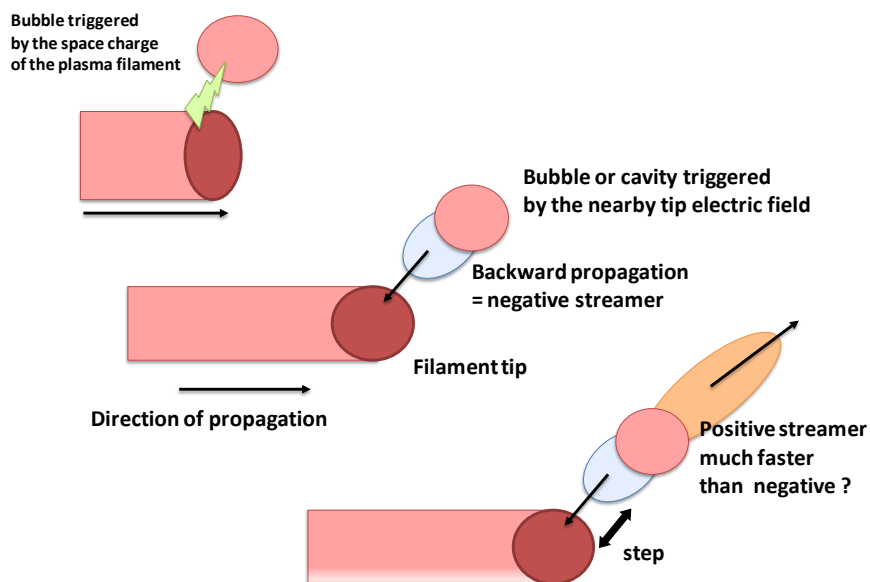
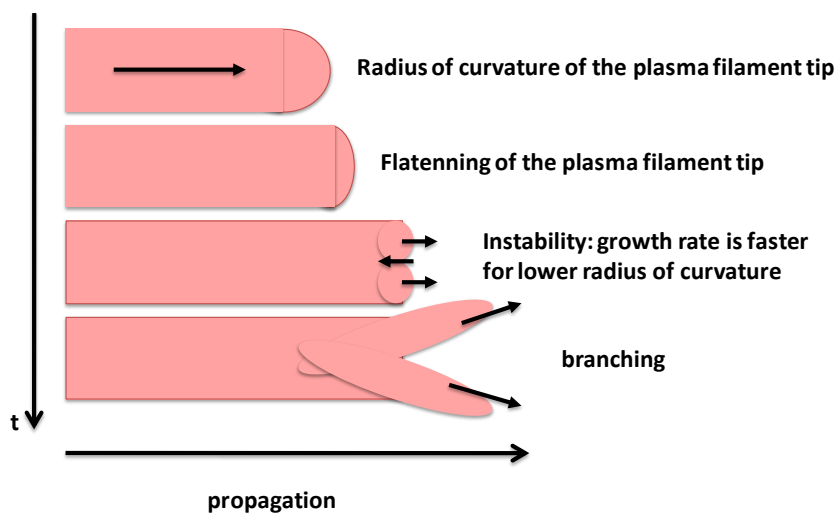
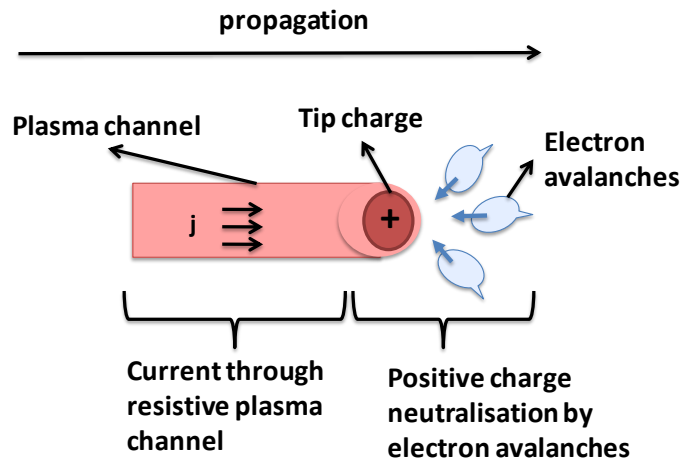


fig 4.41 two iCCDs emission imaging, pairs of images taken on the same shot, branching of the discharge, 200ns and 300ns delay, (35kV applied voltage, 4.5cm gap 100 μ S/cm, 2ns gate).





The **propagation velocity does not change before or after branching**, the branching does not seem to be associated to a slowing down or step propagation. However, to resolve any slowing down or any propagation step associated with branching, a very fine delay difference of

the order of 5ns between the two iCCDs is required. This refined study was not made as it is quite time consuming because one acquisition over 100000 shots (at 0.5Hz) would fall in the intended time range due to the initiation delay jitter.

An intensity calibration has been made between the two iCCDs and allowed to observe that any **branching event is followed by an emission intensity jump in the parent filaments** as shown in fig 4.42. **The children filaments have the same emission intensity as the parent filaments before branching.** It can be due to:

- transition from streamer to leader
- higher electron density
- higher electron temperature,
- higher current level in the parent filament.

With an additional level of branching, the intensity rises again in the root and rises also in the former children filament that becomes parent filament. Those higher intensity segments can thus be considered to have a step propagation as the intensity jump happens at each branching event. However the true propagation remains continuous at the tip of the plasma filaments. At our resolution (>30ns for the two iCCD setup on each side of the reactor, >5ns for the two iCCD setup with a beam splitter) the main propagation phase of the secondary mode is continuous and the step propagation denomination can only be applied to the reillumination as will be described further in a dedicated chapter. A step propagation could result from the misinterpretation of those intensity jumps in fig 4.42 occurring at each parent section during a branching event.

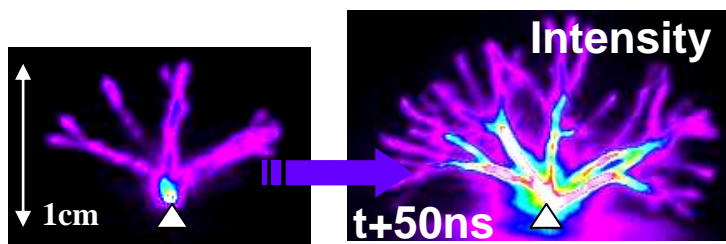
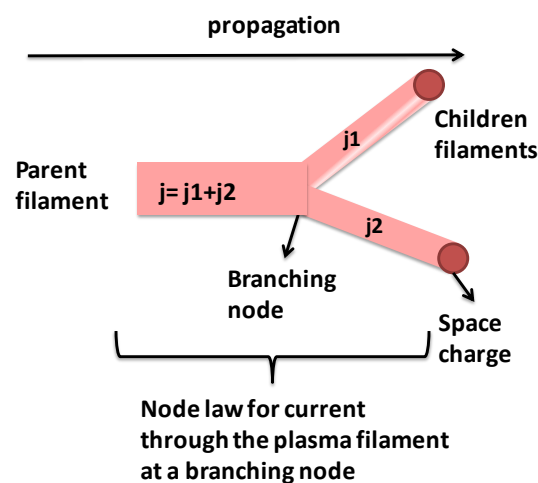


fig 4.42 2iCCDs emission imaging with same intensity colorscale, the branching induces an intensity jump on the parent filaments, the children filaments have the same emission intensity that the previous parent filament before branching.



Assuming that the **light emission intensity is related to the current flowing through the channel**, it means that more current is required to supply several children filaments and thus a higher current flows through the plasma channels. **Each node would split the current** flowing

through the plasma channels. The higher current level supplied in the parent channels are consistent with a **pure resistive behaviour of the plasma channel** but also with a capacitive behaviour with some displacement current flowing through the channel and associated with the tip charge motion across the interelectrode gap. At each node the tip charge can be replicated or split. If it is split, it would be depleted after some branching and would no longer be sufficient to ensure the plasma propagation. The splitting would also not require the current jump that we observed. On the other hand a duplication of the tip charge at each node would imply some progressive charge amplification process during the propagation or a brutal charge amplification at a node. The brutal change could be due to a gas microbubble in the scope of an impurity driven branching. The microbubble would supply some amount of readily ionisable molecules. This microbubble can be triggered and breakdown when the tip of the plasma filament arrives close by. The charge amplification/attenuation is explained by the divergence and the efficiency of the current flow in front of tip. The tip charge could accumulate charges faster than they are removed or neutralised and thus the tip charge can increase over time. When the charge amount required for the propagation of an additional filament is reached, the filament would split. An interesting observation is that usually more than two children filaments are observed at each node.

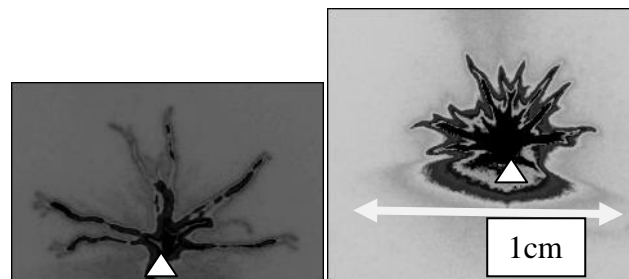


fig 4.43 morphology difference due to the higher liquid conductivity, filaments are brighter and more triangular shaped at high conductivity, 200 μ S/cm and 1mS/cm, influence to the liquid conductivity on the filament shape and the emission intensity. Emission intensity is much higher at large water conductivity. The filaments become triangular shaped, [40kV, 4cm gap]

The **morphology of the discharge is modified by changing the water conductivity** as shown in **fig 4.43**. There is not real change when using different ion species because the ionic mobility of most of dissolved ions is within one decade ($10\text{m}^2/\text{V}/\text{s}$ typically). We tested sodium salt and phosphate salt for any obvious morphology or plasma parameter change. The only change is of course the emission line of the salt we used. At higher conductivity, the propagation velocity remains the same as shown in a following section, and the **number of filaments does not change much** as shown on **fig 4.43**. Counting the number of filaments is quite tricky since it is linked to branching. If the discharge is longer the filaments has time or room enough to branch. Thus at high conductivity there seem to be less filaments on still images (integrated during the whole propagation or taken at the end of the propagation) because of the shorter applied voltage duration. However the plasma current due to the propagation of the secondary mode is higher at higher conductivity as shown on **fig 4.10** because of higher losses at the plasma/liquid interface. It means that the increased current at a parent filament is not associated to higher current needed for the propagation but is just a consequence of an increase of the plasma/liquid interface area. The level of the discharge current should also be related to the number of the propagating plasma filaments since most of the current will flow from the plasma to the liquid at the tip of the plasma filaments and weakly from the lateral sides of the filament due to larger distance from the ground electrode and lower electric field at the sides walls compared to the plasma filaments tips. The emission intensity of the discharge is also increased at higher liquid conductivity. There is more current per filament at high water conductivity. Given this resistive behavior, it is however surprising that the plasma propagation is not influenced by the liquid

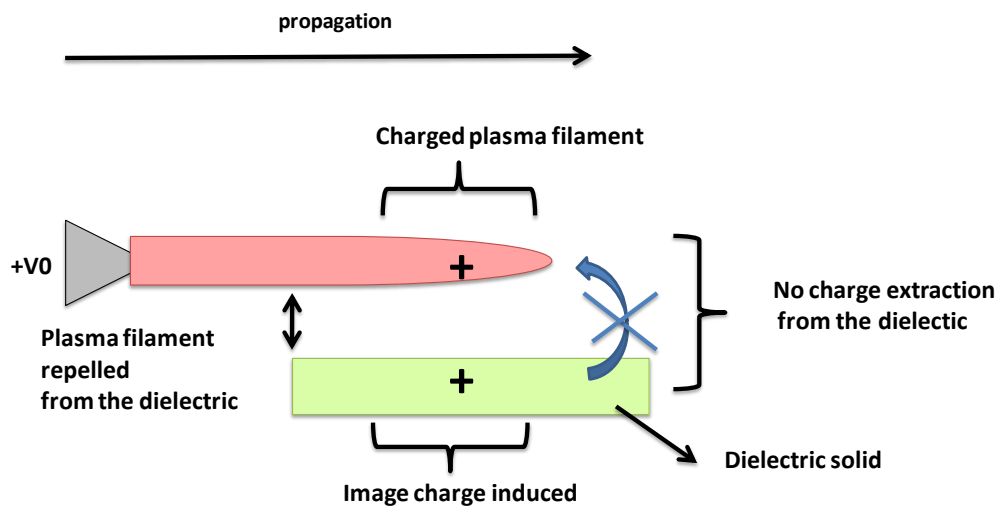
conductivity. If the deposition of energy is controlled by the gas side of the channel/liquid interface, an increased current should imply a higher propagation velocity which is not the case. And conversely, if the energy deposition is controlled by the liquid side, an increase in conductivity should have also some influence.

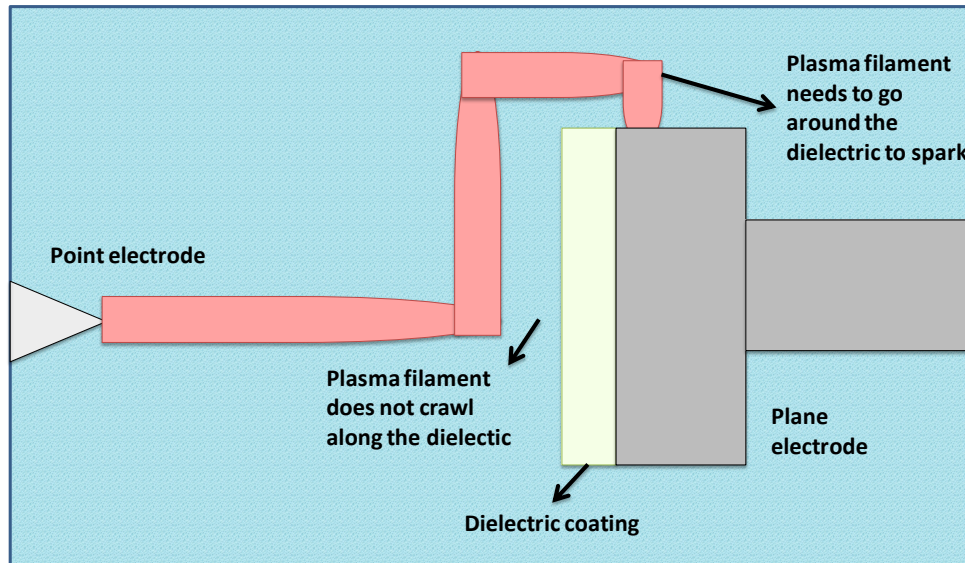
When a solid is put at the contact with the high voltage electrode, there is no discharge. When a solid plate is put on the path of the discharge, the **plasma filaments go around the dielectric plate and do not crawl on the plate surface** (no surface discharge or flashover). When a solid glass tube is put around the discharge the filaments develop along the axis of the tube and do not crawl along the tube. Those facts can be interpreted from two points of view:

- **induced image charge repulsion**
- **current lines**

The induced image of the charged tip into the solid creates an attraction or a repulsion depending on the electrical permittivity ratio between the liquid and the solid. In the case of glass and water this force is repulsive and explains why the plasma filaments in water are repelled from the glass surfaces on their path. The fact that the plasma filament is repelled from the solid surface is quite counterintuitive as in most of filamentary plasma discharge the surface discharge inception electric field is usually lower compared to gap discharges. It seems here that in the case of water the flashover is harder than the gap discharge.

Another interpretation could be that the **plasma filaments do not follow the Laplacian electric field lines but in fact follow the current lines** (water would behave as a resistive medium and not a dielectric). The heating of the liquid and its vaporization at the filament tip can be influenced by the current that can flow ahead of the plasma filament and the plasma would choose the lower resistivity path. This current in front of the tip is necessary to propagate.





4.4.3.2 Propagation velocity measurements

The filaments of the secondary mode initiate from the boundary of the primary mode hemisphere, they are **initiated at the same time and propagate simultaneously at the same velocity**. The **radius of the discharge can thus be defined as the hemispherical envelope** of the filaments tips. All the filaments have thus the same ability to propagate, there are not advantaged filaments. The filaments should then have the same physical plasma parameters or self regulate each other. The shape of the discharge is also globally hemispherical as in the case of the primary mode but it is less pronounced. The filaments follow the electric field lines of the Laplacian field. This will be discussed further with a dielectric barrier.

With only one iCCD, the position of the discharge is measured as a function of the delay to give **fig 4.44**. The crossing of the time axis corresponds to the mean time delay to the discharge initiation. The slope of the discharger growth is the propagation velocity, the saturation of the discharge growth is the stopping length. This experimental procedure is valid because of the reduced delay jitter at high voltage (45kV). At lower voltage of 30kV the jitter is much too important and the velocity-growth plot with accumulated images would just be a convolution of the true velocity and the jitter. On the velocity-growth curve, the data point error comes from the jitter of the initiation delay and the fact that the discharge is 3D phenomena and is observed projected on the 2D plane.

To verify those single iCCD measurements, additional experiments were performed as shown on **fig 4.44**. With two iCCDs operating on the same single shot event the propagation velocity can be measured without accumulating images over different shots and thus avoid the jitter problem. Due to 3D projection, the value of the propagation velocity has a big scattering if plotted for single shot events. The velocity can be thus underestimated and the maximal value or the upper envelope of the cloud of experimental data points should be taken

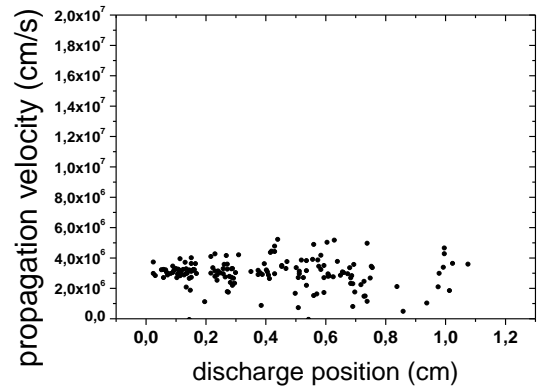
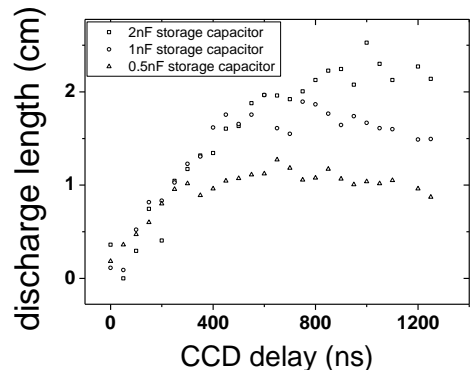


fig 4.44 velocity-growth plot on accumulated images with single iCCD: velocity of $3e6\text{cm/s}$ is obtained by derivating this plot, influence of the storage capacitor: a longer pulse duration leads to a same propagation velocity (no influence of the voltage decrease rate) but longer stopping length, confirmation of the propagation velocity measured with 2iCCD setup, 30km/s propagation velocity stays constant across the gap, (4cm gap, 40kV, distilled water)

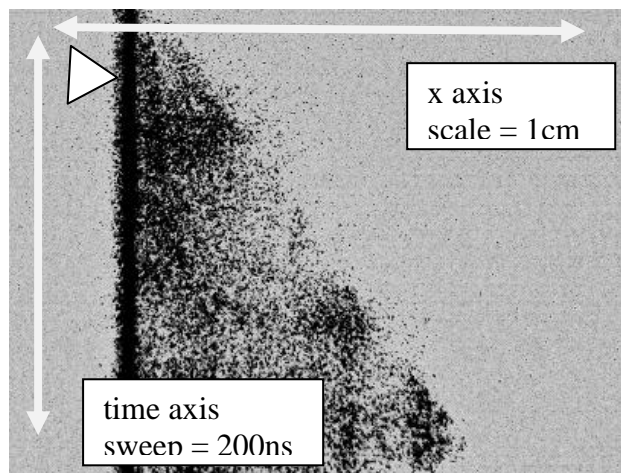


fig 4.45 streak image of the secondary mode propagation, the triangular shape clearly demonstrate constant propagation., $1\mu\text{s}$ time sweep (vertical axis), 1cm horizontal axis, the point electrode is on the left side (40KV, distilled water, 4cm gap).

To further investigate and confirm those velocity measurements, a **streak imaging** was implemented. This allows to check if the propagation velocity is decreasing or increasing along the gap. An increasing velocity would be associated to an exponential shape of the streak image, on the contrary a decreasing velocity would be associated to a log like shape. Here a very clear triangular shaped pattern can be observed on **fig 4.45**. This confirms the value of the propagation velocity and the fact that it remains constant.

4.4.3.3 Influence of applied voltage on the propagation velocity

The first surprise was to observe that the **propagation velocity is constant during the propagation along the gap** as shown on **fig 4.44**.

- A longer channel is more resistive. Thus the resistivity of the plasma channel does not influence the propagation velocity.
- Because of this plasma channel resistivity (estimating the resistivity requires access to the plasma filament radius), there is a voltage drop and the voltage at the tip is lower as the filament gets longer.

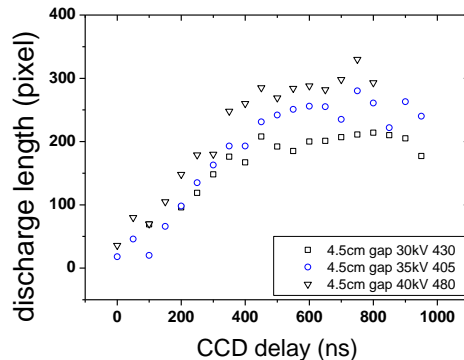


fig 4.46 influence of the applied voltage on the current and the velocity -growth

In **fig 4.46** the **propagation velocity does not change with applied voltage level at t=0**. One should keep in mind that due to the home made power supply the voltage range is not spread on several decades. Consequently, a weak variation of the propagation velocity with the applied voltage is still compatible with this experimental result. This introduces a strong constraint on the propagation mechanism. Either the mechanism does not involve an electric field dependence, or there is compensation or a limiting mechanism. However the phenomenology of filamentary plasma discharge inside a liquid has many similarities from one liquid to another. Thus there must be some universal propagation mechanism that explains the plasma discharge in all insulating liquids. The case of water seems to be a little bit special: according to numerous authors most of the dielectric liquid has a discharge propagation velocity sensitive to the applied voltage. The propagation velocity of oil discharges is reported to follow the Laplacian electric field. The discharge is first slowing down in the decreasing Laplacian field of the point to plane, then it accelerates again close to the opposite electrode because of the image charge induced in the metal. The difference of sensitivity of the propagation velocity on the electric field between several liquids is quite interesting. There can be an overlap of several mechanisms and the relative contribution can change from one liquid to another. It is remarkable that in the case of water there is a perfect balance leading to constant velocity. Another possibility is that the velocity measurements of the plasma discharge of other authors do not follow the same precision as the present study.

4.4.3.4 Influence of liquid ionic conductivity on the propagation velocity

The ionic conductivity is also one of the most relevant parameter in the case of water. The **propagation velocity does not change much with the ionic conductivity on 2 decades** from $10\mu\text{S}/\text{cm}$ to $1\text{mS}/\text{cm}$ as shown on **fig 4.47** and **fig 4.48**. There is even a little decrease at high conductivity. However this slight decrease is close to the measurement error bar on the velocity growth curve. Again the propagation velocity measurement was checked with the 2 iCCDs setup.

This fact is very important for the discharge mechanism. The first idea is that it is curious that the propagation velocity remains constant even with higher energy dissipation.

At higher conductivity, there would be several factors to be taken into account:

- More current flowing through the filaments
- More charge removal at the plasma/liquid boundaries
- More joule heating and energy dissipation at the head of the filament on the liquid side
- More screening of the charge inside the head of the filament, the tip electric field screened on a shorter space scale by solvated ions in the liquid

With more ion concentration inside the liquid ahead of the plasma channel tip one would expect that those ions would be accelerated and participate to local joule heating and thus originate a phase change or density lowering just ahead of the plasma tip. The negative ions can also be a source of detached seed electrons that undergo electron avalanches ahead of the plasma tip as in the gas phase streamer mechanism.

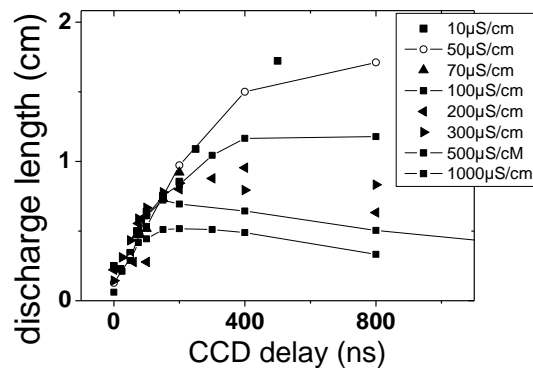


fig 4.47 velocity-growth plot as a function of the liquid conductivity, the propagation velocity stays almost the same and perhaps decreases weakly when increasing the conductivity.

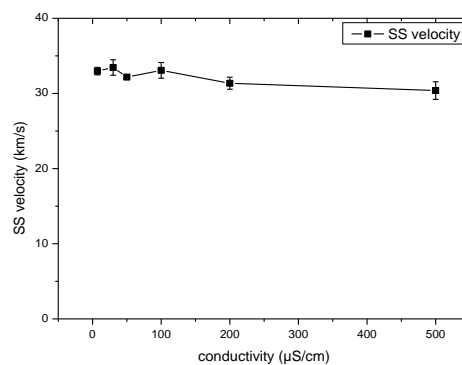


fig 4.48 propagation velocity as a function of the water conductivity, 2 iCCDs shadow setup using pairs of images taken on the same single shot (during the same applied voltage pulse), mean value obtained from typically 20 pairs of images.

4.4.3.5 Influence of the gap on the propagation velocity

changing the gap could have multiple effects :

- decreasing the electric field as same applied voltage, this effect can be neglected since the electric field at the tip is weakly influenced by the interelectrode gap but mostly by the curvature radius of the pin HV electrode.

- increasing of the reactor resistivity, there will be a different ballast resistor in series with the plasma filaments

Surprisingly the velocity growth plot shows **almost no change for the several gap values** investigated in

fig 4.49. The discharge current is also very weakly dependant on the gap over one decade on long gaps of centimeter scale as mentioned in a previous section in **fig 4.16**. The two iCCDs setup also do not show any influence of the gap in **fig 4.50**. Perhaps the range of gaps investigated was not sufficient. It was limited on the lower part by the minimal duration of the pulsed power supply and the necessity to avoid spark, and on the longer part by the size of the reactor.

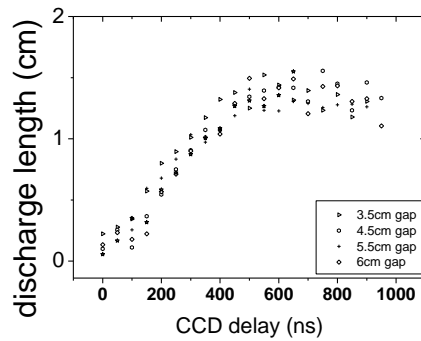


fig 4.49 velocity-growth for different gaps

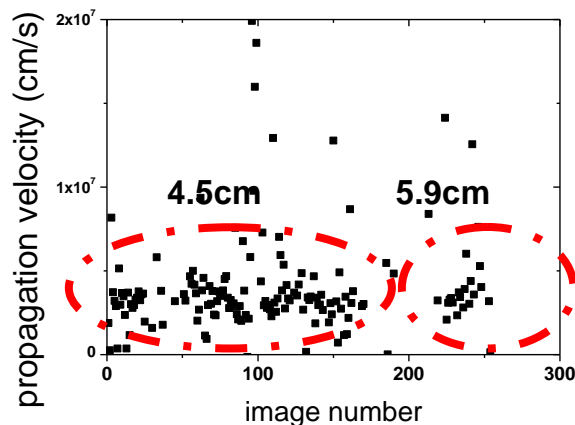


fig 4.50 propagation velocity measured with two iCCDs setup for different gaps

The minor influence of the interelectrode gap is an indication that the water layer between the plasma filament head and the opposite plane electrode does not play the role of a ballast resistor and is not relevant for the discharge propagation.

4.4.3.6 Influence of additives on the propagation velocity

Addition of ethanol was investigated. The water alcohol mixture has a similar behaviour as the discharge in pure water or in pure alcohol.

In pure alcohol, the discharge emission spectrum is not the same as in water. With the naked eye the discharge appears to be white instead of pink. The discharge current in pure alcohol is several order of magnitude lower than in distilled water due to the poor ionic conductivity of alcohol. The discharge current and thus the emission intensity of the discharge can be modified by increasing the water content or adding some salt. The bubble cloud formed after the discharge turns off is of smaller size in alcohol than in water due to the surface tension.

Adding some impurities inside the liquid changes a lot of physical properties at the same time: ionization potential, electron solvation time, viscosity, surface tension, molecular weight, vaporization temperature. Surprisingly, the initiation and the propagation are not drastically influenced by the alcohol content. The propagation velocity remains close to the 30km/s value.

4.4.3.7 Stopping length of the discharge

On **fig 4.46**, the saturation of the discharge growth can be associated to a “**stopping length**”. In **fig 4.46** this length changes because the voltage stays above a “**stopping voltage**” for a longer time with a larger storage capacitor in the power supply. The stopping length gives some insight on the **propagation threshold criterion**.

On **fig 4.47**, the stopping length is shorter at high liquid conductivity because the reactor equivalent resistance is shorter and the decay time of the power supply is shorter. One need to compensate by changing the storage capacitance value in order to compare the discharge at low conductivity and at high conductivity but with the same applied voltage half width.

The discharge stops to propagate because the applied voltage at the point electrode is not sufficient to sustain the propagation of the filament. This stopping voltage gives some criterion about the **propagation sustainment** as shown on **fig 4.51**. The stopping length is associated to a stopping voltage. It is not clear if this stopping criterion is the voltage at the plasma filament head taking into account the voltage drop along the filament that become insufficient for the filament propagation. The other possibility is that the field in the filament tail becomes insufficient to ensure conduction of charges through the filament. When increasing the liquid conductivity, the pulse duration also changes because of lower reactor impedance. Similar pulse duration for different liquid conductivities can be obtained by changing the storage capacitor value to obtain the same pulse duration. One can observe that the stopping voltage is higher at lower liquid conductivity. It can mean that the plasma filament is more resistive at lower conductivity or that charges are more difficult to extract from a low conductivity liquid at the filament head. In either case one can wonder why the propagation velocity would stay the same whereas the stopping voltage would be different. A more resistive filament can be due to smaller filament diameter, or lower electronic density. It is difficult to distinguish any change in the filament radius based on emission imaging in **fig 4.43**, shadow imaging would be more appropriate here. The emission intensity is however much brighter at higher liquid conductivity as shown in **fig 4.43** which could indicate a higher electronic density. Spectroscopic measurements are required to verify this assumption on electronic density.

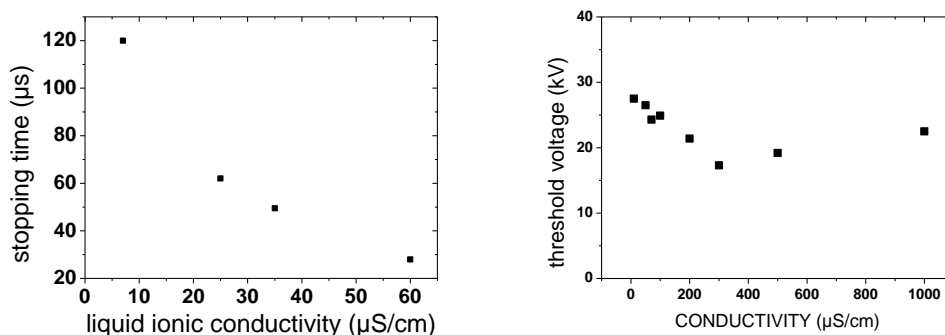


fig 4.51 the stopping length is linked to a threshold voltage required to sustain the plasma discharge propagation, this stopping voltage is reached earlier at higher conductivity due to higher applied voltage decay rate when the reactor is more conductive

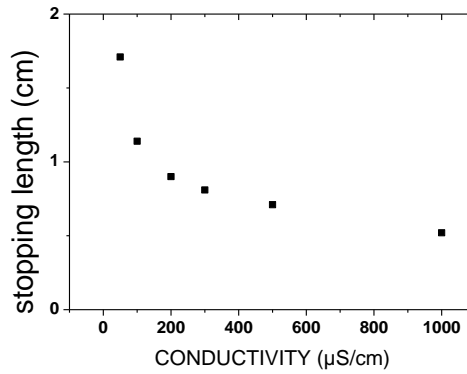


fig 4.52 stopping length voltage as a function of the liquid conductivity, sustainment criterion for the discharge propagation, obtained from fig 4.47 and fig 4.51.

4.4.4 Shock wave emission and “continuous propagation”

In this section we intent to identify:

- the shock wave pattern,
- the propagation velocity of the waves,
- their emission site
- and the reason why they are emitted.

Shock waves can studies can be found in [ridah] [Sunka2002] [Sunka2004] [Zhang2005] [Ann2007] [Ushakov] [Sayapin2006][zeldovich] [Katsuki2006] [Hemmert2003].

On shadow images, shock **waves can clearly be distinguished from the gas channels** as they appear with a different greyscale, this is of particular importance **at the early stage of propagation of the shock wave since the shock tube an the gas channel almost coincide and make the determination of the filament diameter quite hard to determine at the very early stages of the discharge.**

The **shock wave velocity ranges from 4km/s close to their source to 1.5km/s far from the source.** The velocity of a shock wave is related to the magnitude of the piston. The shock wave velocity is related to the pressure of the gas pusher trough the **Hugoniot relations:**

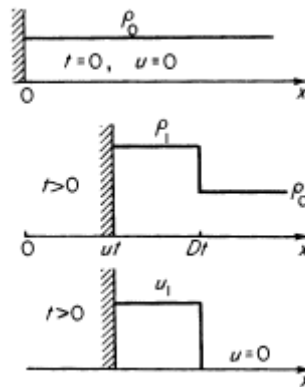


fig 4.53 schematics of a shock wave front.

The undisturbed fluid is referenced by the subscript 0 and the fluid behind the compression wave has the subscript 1. The **mass conservation**, the **momentum conservation**, and the **energy conservation** through the shock wave **discontinuity** gives the relations:

$$\begin{aligned}\rho_1(D - u)t &= \rho_0Dt \\ \rho_0Dut &= (p_1 - p_0)t \\ \rho_0Dt(\varepsilon_1 - \varepsilon_0 + u^2/2) &= p_1ut\end{aligned}$$

With u the **piston velocity**, D the **shock velocity**, ρ_0 and p_0 the **density and the pressure of the undisturbed medium ahead of the wave**, ρ_1 and p_1 the **density and the pressure of compressed medium**

The **expansion velocity of the gas channel of typically 30m/s**, the shock wave velocity of typically 2km/s, and the liquid density gives piston pressure of typically hundreds of bars (10-1000MPa)

The propagation velocity of the shock wave decreases because the energy is dissipated along a tube or a sphere. The velocity close to the source is quite difficult to measure with good accuracy close to the gas filament with only one gate per shot. A combined diagnostic of shadow and streak imaging have been used to obtain the time resolve dilatation of the filament and the time resolve propagation of the shock wave.

One of the first striking observation is that the shock waves always have a **circular pattern instead of some mach cone structure. Those circles origin from the gas filaments and form some tubes of shock waves around them.**

The shock waves can be emitted:

- 1/ during the propagation
- 2/ during branching
- 3/ during reilluminations

The **reillumination** does not occur at high conductivity as shown in **fig 4.12** and **fig 4.13** meanwhile shock waves are emitted at high liquid conductivity as shown in **fig 4.56**. Furthermore the shock waves are present even during the continuous propagation phase of the secondary mode. This means that the shock waves are caused by the plasma channel propagation or the branching or the energy deposition inside the channel and not energy deposition in the channel by reilluminations as shown by **fig 4.55**, **fig 4.59**, and **fig 4.63**

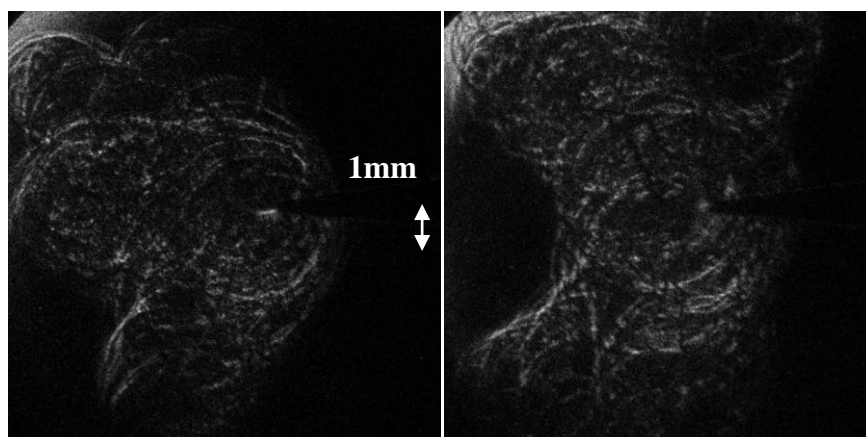


fig 4.54 schlieren imaging of the shock waves emitted by the discharge with 100ns gate.

Another possibility is that the shock waves can be due to pressure release in the gas channel at the moment of **branching**. The center of the wave cycles seems to be always centred on some branching node. The fact that the shock waves are centred on branching node is not trivial. During a branching event, we observed that the emission intensity of the father filament increases, this could mean that the father filament thermalizes as it need to supply more current

for the children filaments. This can be associated with a pressure jump, but it should be along a filament and not centred on a node. The circular pattern is observed quite early in the propagation of the shock waves and thus the circular shape cannot be associated with a large distance of the wave front from its emission source. It is difficult to imagine why the splitting of a filament should lead to a shock wave at the node. An interesting result is that at the initiation of the primary mode we have seen that the nucleation of a microbubble at the HV pin electrode surface do not lead to a shock wave, but the first shock wave is emitted when the primary mode starts to propagate from the microbubble. If the branching is due to microbubble impurities then the shock would be emitted similarly when the children filaments start to propagate away from the node. The emission of shock wave at branching node is not correct: there are more shock circles than nodes.

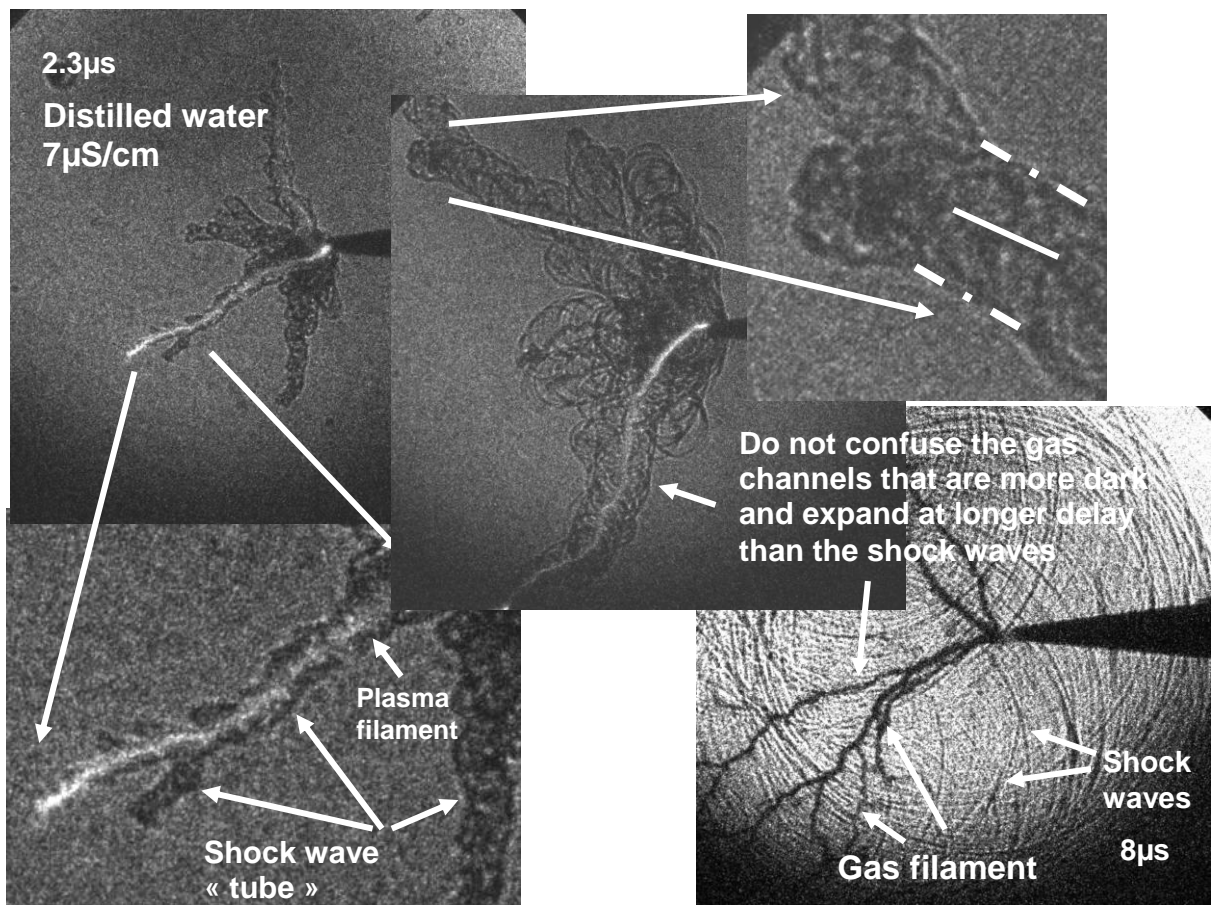
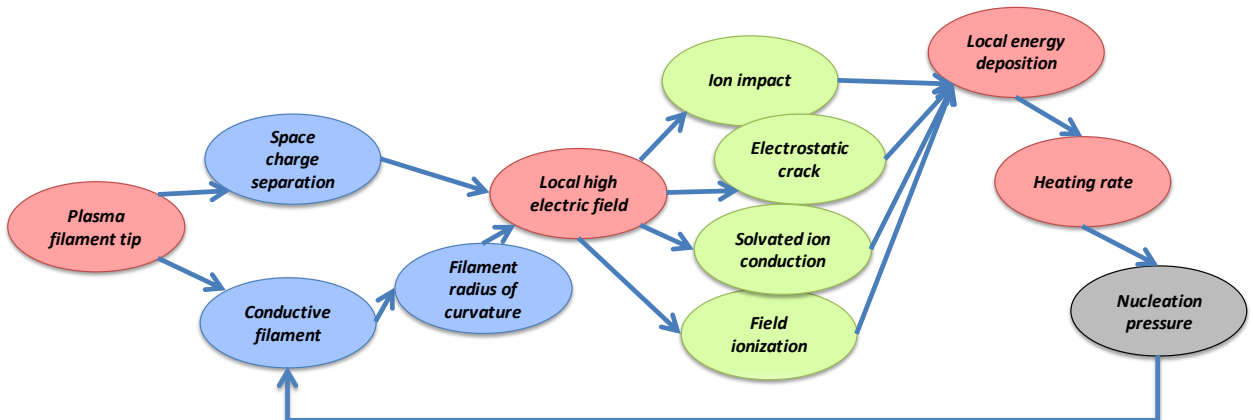
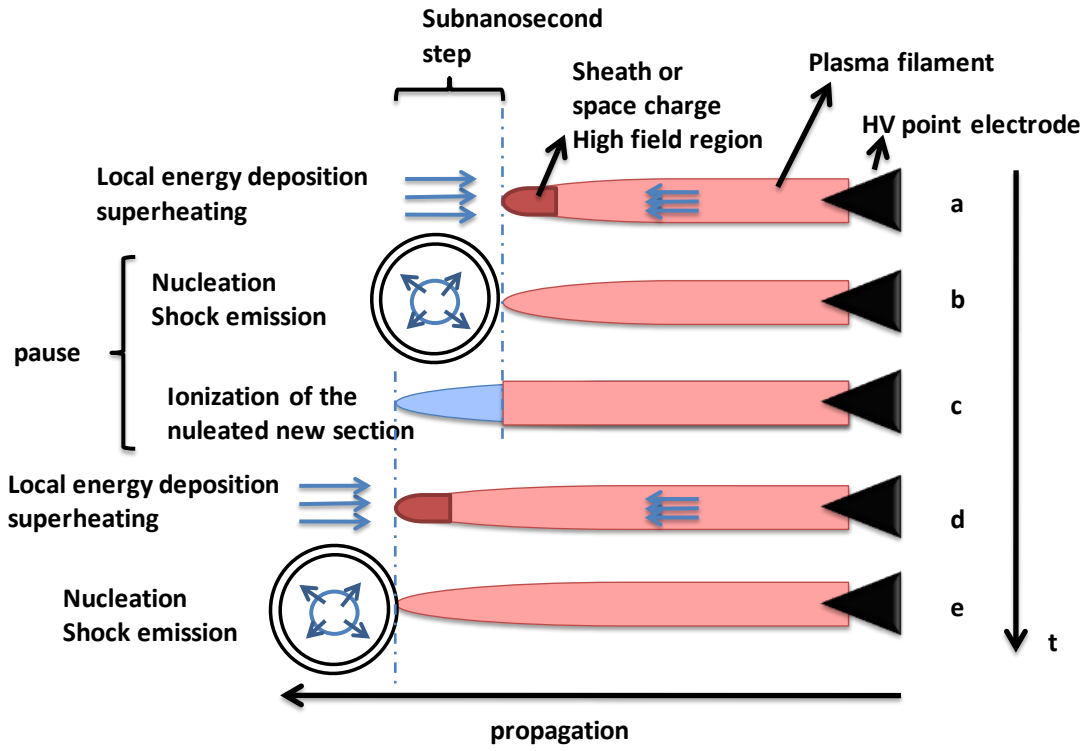
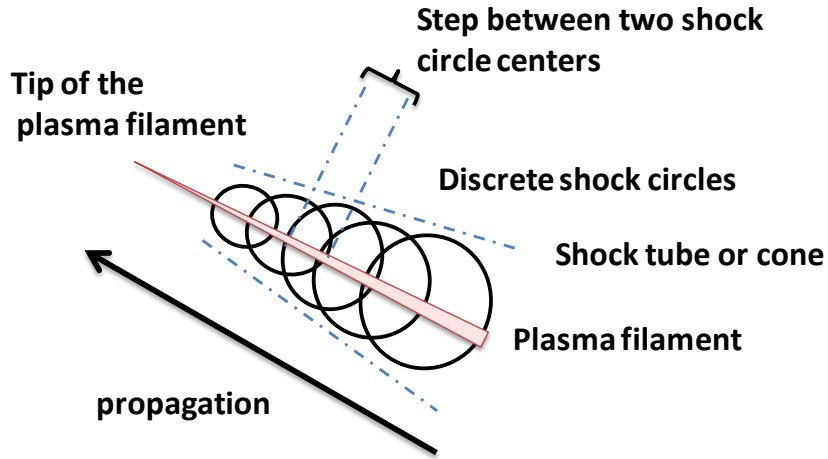


fig 4.55 shock wave tube at different stages of the propagation, in distilled water, shocks during propagation of the secondary mode, during reilluminations and in post discharge, the with filament is a reillumination a little bit out of focus because the focus is made on the shadow of the discharge.



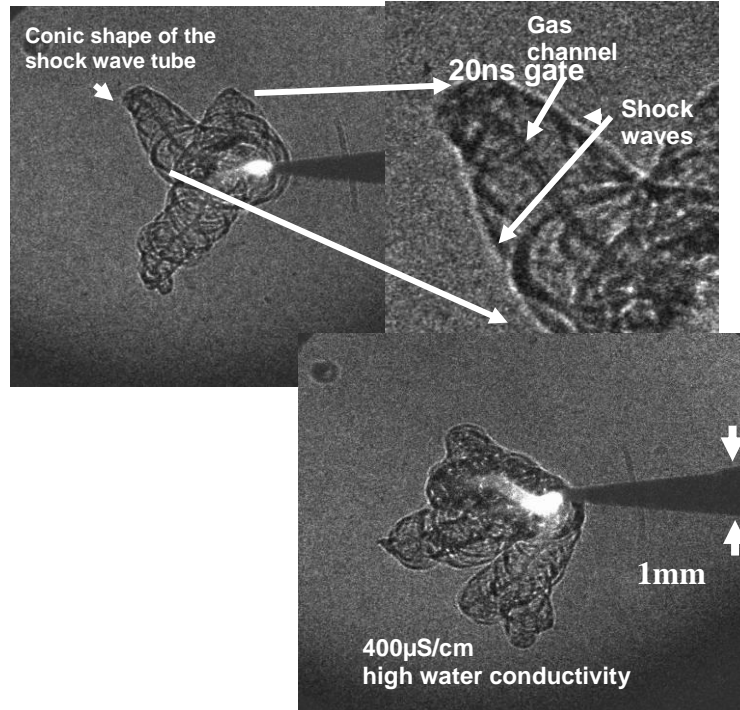


fig 4.56 shock wave tube emitted by the discharge at high liquid conductivity of $400\mu\text{S}/\text{cm}$, the gaseous filaments appears in dark and surrounded by a shock wave tube or cylinder, the bright white is plasma emission during plasma decay.

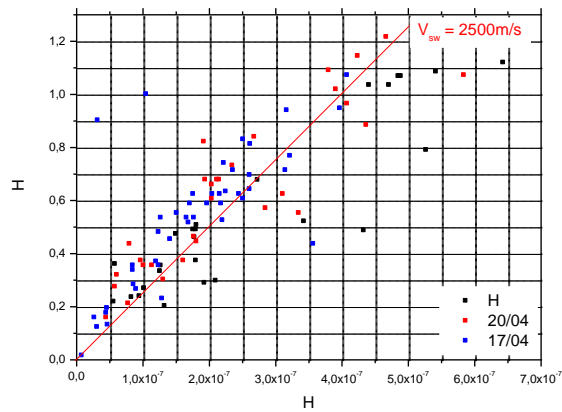


fig 4.57 position reached by the shock wave emitted by the primary mode as a function of the time of flight from the point electrode, obtained with single iCCD in shadow mode, a constant velocity and be determined from linear fit.

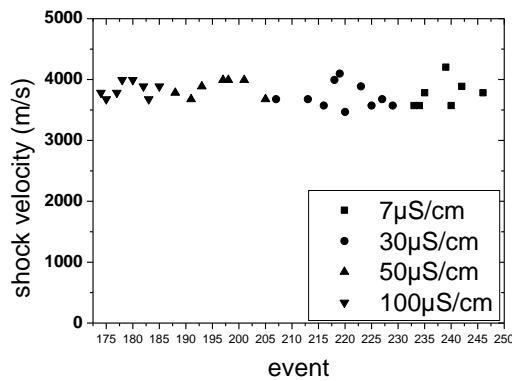


fig 4.58 shock wave velocity obtained with 2iCCDs shadow setup, measured on several images for different conductivities, measured typically 20 μ m away from their emission site, (1cm gap, 40kV).

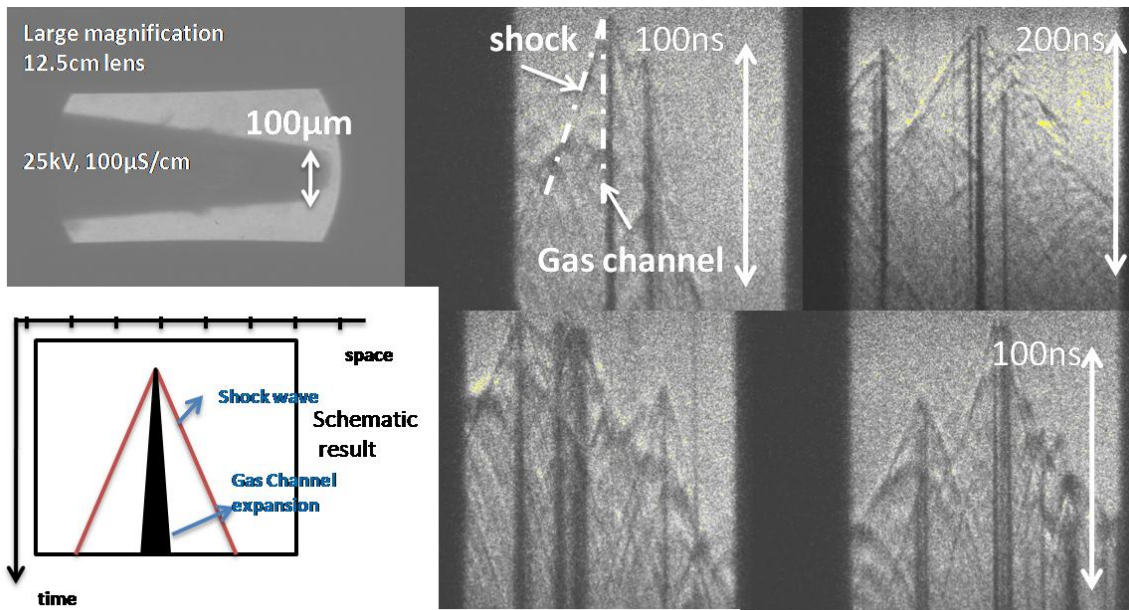


fig 4.59 shock waves and gas channel expansion observed with shadow and streak diagnostic, the entrance slit of the streak camera is perpendicular to a plasma filament, when the propagation plasma filament cross the entrance slit a vertical dark gas channel can be observed with an oblique shock wave, multiple channels are crossing the entrance slit on those images, the shock velocity is between 1.5-2km/s, the quick slowing down (from 4km/s) during the first ns is not resolved by the optical setup, (2cm gap, 30kV).

The propagation of the plasma channel is **supersonic**, thus the shock wave emission can be quite trivial and can be assumed to come from the supersonic tip of the plasma filament. The problem with this interpretation is that we have observed a **“continuous” propagation at 30km/s** and the shock waves are a **succession of circles**. The **discrete circles** are a quite obvious **clues in favour of a step propagation**. The distance between two circles is of tens of μ m which corresponds to a time resolution of some nanoseconds which is a little bit too short for our experimental setup with two iCCDs. It is possible the 300 μ m step (30km/s) associated with this 2iCCD setup is not sufficient compared to the steps of typically 200 μ m suggested by the shock wave pattern. And thus the propagation velocity observed previously with the iCCD is a **mean propagation velocity that is the result of the fast propagation steps and the pause phases**. At this stage we cannot conclude about those supposed steps at such time resolution during what we call the “continuous phase” of the propagation (or secondary mode) before the reilluminations. An even more refined imaging is required. A higher spatial resolution is needed on the 2 iCCD experimental setup to distinguish between a continuous propagation or a step propagation of the plasma discharge. The positioning of the two iCCD apart from the reactor and with standard imaging objective was not sufficient, a beam splitter is required to perform a better positioning and obtain higher spatial resolution or the two iCCD experiment.

This **shock wave velocity stays constant with the liquid ionic conductivity** which indicates that the **piston pressure does not come from the current flowing through the filaments but from the propagation itself as further suggested by the reilluminations**. The step would thus be associated with energy deposition (not by ionic conduction) with superheating and nucleation of a high pressure cavity in front of the filament head. The pause phase can be associated to the time required to ionize this new section of the filament or the time required to deposit a new amount of energy to nucleate a new section.

The **interaction of the propagating shock wave with the plasma channel** can be interesting as a shock is known to produce some space charge separation inside the plasma due to local overpressure that enhance recombination and quenching processes, and under pressure that enhance ionization processes. Some double layer can thus appear at the shock wave front in the plasma. In our case, the shock wave crossing the plasma filament can have an effect on the plasma itself or on the gas/liquid interface. The section of the channel could locally change at the crossing of the filament and the shock wave. The double layer in the filament could reduce the plasma column conductivity.

4.4.5 Reillumination and step propagation

After the propagation of the primary positive mode and the secondary positive mode, the discharge stops to propagate at a stopping length and restarts again with **successive reilluminations of extinguished filaments** as can clearly be seen on the streak emission imaging. In the case of positive polarity, only one filament at a time is reilluminated. This DBD-like behavior can be observed only at low water conductivity. At large conductivity, there cannot be charge deposition/electric field screening/ charge removal/reillumination processes, but only a smooth decay of the plasma channel. Between each reillumination, the channels are not conductive, the measured current falls to the conduction level, whereas at large conductivity, the plasma filament has stopped to propagate but decay on some μs with a smooth decrease of the current according the applied voltage decaying shape. This can be used to estimate the filament conductivity and thus the electron density during the decaying phase knowing the filament section and the discharge surface area.

With the shadow diagnostic we were able to observe that those **reilluminations propagate a little bit further and this step propagation induces the emission of shock waves only on the new created segment and not on the whole reilluminated channel**. We just observe the shock tube emitted during the propagation, there is no second shock tube emitted along the gas channel under the reilluminating section, a shock tube is created in the path of the newly created reilluminating section. This further proves that shock emission is linked to propagation and not energy deposition by current conduction through the filament.

The streak imaging setup allowed recording this reillumination. Discharge current peaks are not all correlated to a luminous event recorded by the streak camera. In order to understand what happened, an iCCD was triggered at the same time as the streak to obtain a 2D image and check if the streak entrance slit is well in front of the discharge event. It turned out that the reillumination in the positive discharge is constituted of just a few filaments. **Only one filament at a time reilluminates, not the whole tree structure** as shown in **fig 4.60**. This filament is not recorded by the streak camera in **fig 4.62** when it happens off axis but it is correctly recorded at the iCCD. Thus in fact every current event is correlated to a plasma event.

3 shapes of reillumination have been observed:

- A full restart of the discharge from the pin HV electrode
- A single plasma channel that takes all the gas channel length and with an intense luminous spot at the head
- A single plasma segment with a luminous filament at a medium position in the gas channel

The 2 iCCDs setup has shown that the reillumination is taking place inside a gaseous filament produced during the main continuous phase of the secondary mode. The question is, first, why the plasma propagation stops at a stopping voltage while at the same time it is able to reinitiate

after some μs even if the applied voltage has further decreased during those μs of pause. And second, why does only one filament reinitiates and not several filaments at the same time.

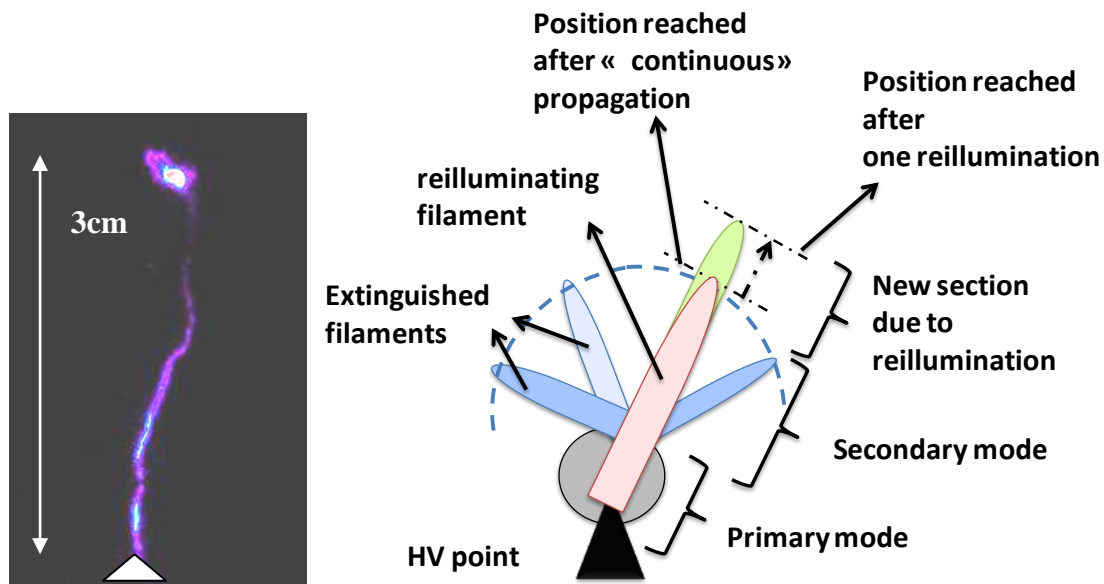


fig 4.60 emission imaging of a reillumination, a weak emission of the filament can be recorded usually a bright spot or a bright segment at the extremity, this reillumination takes place at low conductivity in one of the extinguished branches leaved behind by the main phase (continuous) of the secondary mode propagation, (4cm gap, distilled water, 40kV, 2ns gate, 3 μs delay).

The fact that this **reillumination happens only at low ionic conductivity of the liquid** and not at high conductivity indicates that some charge deposition, **electric field screening, and charge removal processes** should be the relevant mechanism explaining the reillumination phenomena. This reillumination would then be very similar to a DBD. The **pause period between two reillumination** can be associated to some **charged species deposition on the inner gas/liquid interface or charged species injected and accumulated locally**. According to this assumption, the frequency of the reilluminations would be related to the ability of the liquid to **remove/neutralize or diffuse** those charges and the ability of the plasma to supply charges by conduction through the plasma filament.

This step propagation at the end of the applied voltage pulse is correlated to current spikes with **Amp amplitude** (same level as the continuous phase of the secondary mode) and some **tens of nanosecond duration consistent with the length of the new formed segment at the tip of the reilluminated filament**. The propagation of the reilluminating section is identical to the propagation of the secondary positive mode in terms of propagation velocity and shock wave pattern. It is not a back discharge due to adsorbed charges as can be observed in monopolar DBDs. It is neither a gas phase glow discharge happening inside the gas channel.

Only one filament at a time reilluminates and that a reillumination does not last long. It means that the amount of charges deposited on the gas/liquid interface (on the gas side or at the liquid side) or that the rate of charge removal is different from one filament to its neighbors. This is because of the particular morphology of each filament even if the filaments have almost the same length due to simultaneous initiation and propagation. The **stopping of a reillumination** means that a new amount of charges is deposited on the gas/liquid interface.

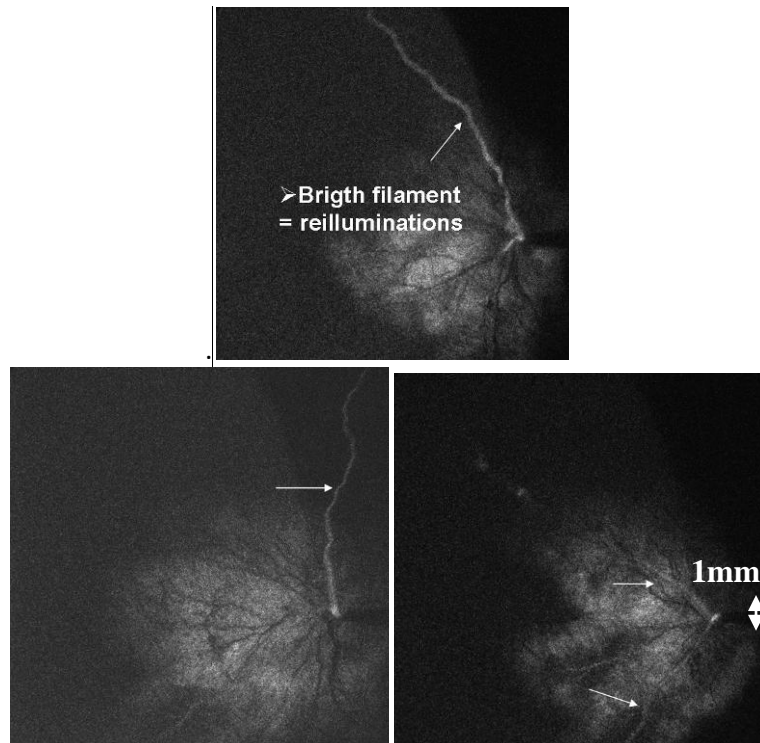


fig 4.61 schlieren imaging of a reillumination, the extinguished dark filaments appear in deep dark and the reillumination are the white filaments, the white blur is the shock wave tube not resolved because or too long iCCD gate (100ns gate, 2cm gap, distilled water, 40kV, 3 μ s delay).

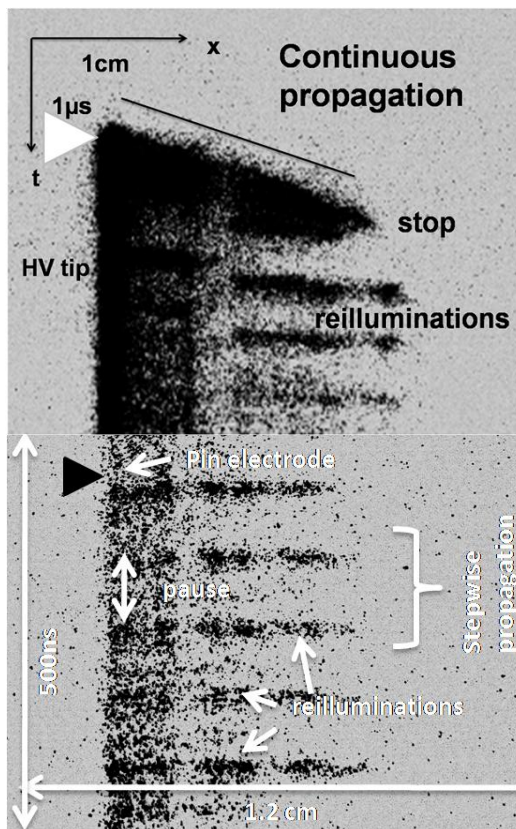


fig 4.62 streak images with the entrance slit of the streak is along the interelectrode axis, observation of the plasma emission, the propagation of the secondary mode is clearly visible with a triangular pattern followed by the reilluminations, the plasma turns on and off according to the current spikes, only one filament at a time reilluminates, here only reilluminating filaments along the entrance slit can be observed, (3cm gap, distilled water, 40kV).

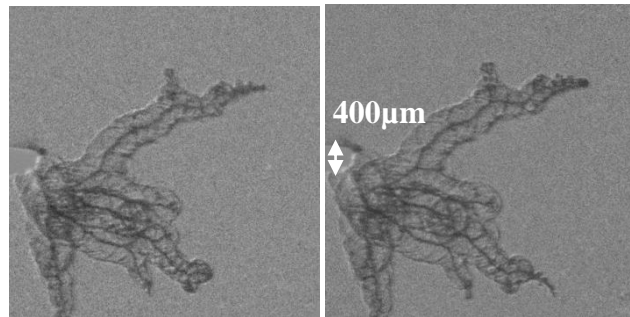
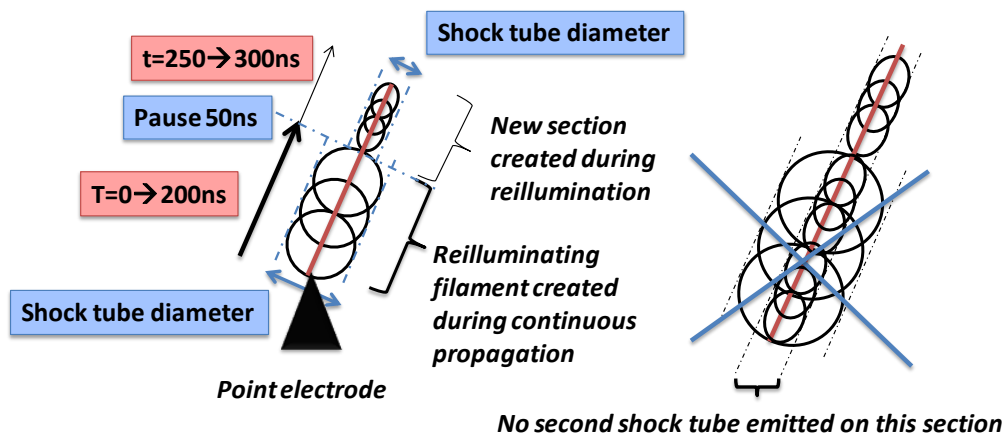


fig 4.63 shock wave pattern emitted by the secondary positive mode and a new created segment by reillumination, the reillumination propagates further, each reillumination is associated to a current spike, the succession of reilluminations can be qualified as a stepwise propagation. The reillumination also emit shock waves but only on the new segment, there is no second shock wave tube emitted in the previously existing section of the reilluminating channel, pair of shadow images obtained on the same shot with the two iCCD setup, ($50\mu\text{S}/\text{cm}$, 30kV, 20ns gate).



4.4.6 Gas channel expansion in post-discharge

The first difficulty is that the emission intensity of the plasma filaments in the positive mode is very bright compared to the schlieren signal. Large focus length of the imaging lens is not sufficient to decrease the amount of light collected. Some filtering was required to bandpass the laser wavelength and remove the plasma emission from the shadowgraph image.

However, the **simultaneous observation of the emission from the plasma and the schlieren signal can be useful**. During the main continuous propagation phase, there is an exact correlation between the number of plasma filaments and the number of gas channels. At low conductivity we can observe that the reillumination occurs in a gas channel leaved behind by the main phase of the plasma propagation. At high conductivity the plasma filament emission decays on microsecond time scale occurs at the same time as the gas filament is expanding. The plasma filament appears to be centred along the axis of the gas tube. The plasma does not seem to fill the entire gas channel section as the channel expands.

This long decay of the plasma intensity is due to the fact that the plasma remains conductive and current flow because the voltage pulse is not finished yet.

The **gas filaments do not move during their expansion and fragmentation wich is trivial because the rise time due to Archimedes force happens on a much larger timescale and the liquid bulk is at rest without any flow**. reilluminations occur during the beginning of the dilation of the gas channel. It is possible that the plasma reillumination process is related to a pressure decrease instead of adsorbed charges removal. The decreasing pressure would make

ionization of the channel easier and the conduction of the plasma channel can thus be re-established.

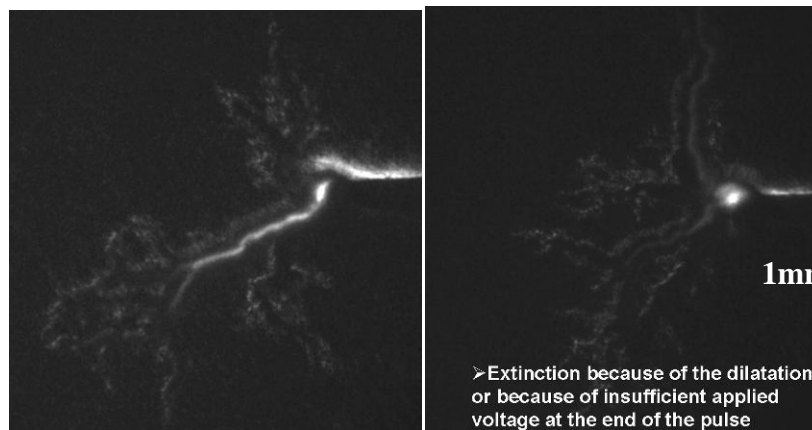


fig 4.64 schlieren imaging of gas filament expanding after the extinction of the discharge.

The **gaseous nature of the filaments is quite certain** as they appear with the same contrast and the same greyscale as gas bubbles that can be observed very late during the fragmentation process and the rise of the cloud of microbubbles in schlieren images such as in **fig 4.64**. The **gas channels appear as deep dark filaments** in shadow images such as in **fig 4.66** and **fig 4.67** and can be surrounded by some **diffuse white halo** in **fig 4.61**. We verified that this halo is not due to the laser beam diameter, it follows the discharge pattern as a diffuse contour. In fact this halo is only due to shock waves taken with a too long CCD gate of typically $1\mu\text{s}$. Short gates of typically 20ns are suitable to observe some shock waves. However, the resolution is quite poor with schlieren setup and we quickly moved on to the shadowgraph setup for this shock wave study. With the shadow diagnostic, we used $1\mu\text{s}$ gate to see the gas channels and 20ns gate to see the shock wave. As a general rule, we observed that the schlieren diagnostic is less interesting than the focused shadowgraph diagnostic in our conditions.

The filaments are clearly seen in the post discharge phase and their dynamics can be observed. They **expand in a timescale of hundreds of microseconds and fragment into a cloud of bubbles**. The dilatation rate of the filaments in **fig 4.65** depends on the water conductivity. At higher conductivity, more energy is deposited. More current flows trough each channel and the gas channel dilatation is thus faster.

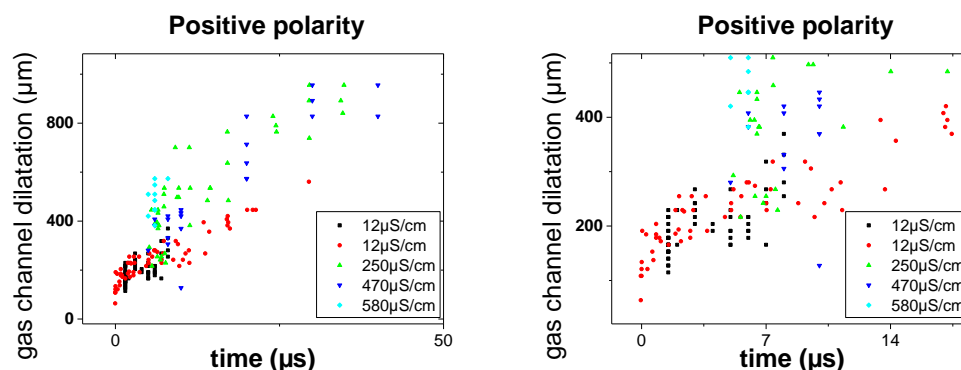


fig 4.65 gas channel expansion in the post discharge, the final expansion rate is of tens of m/s

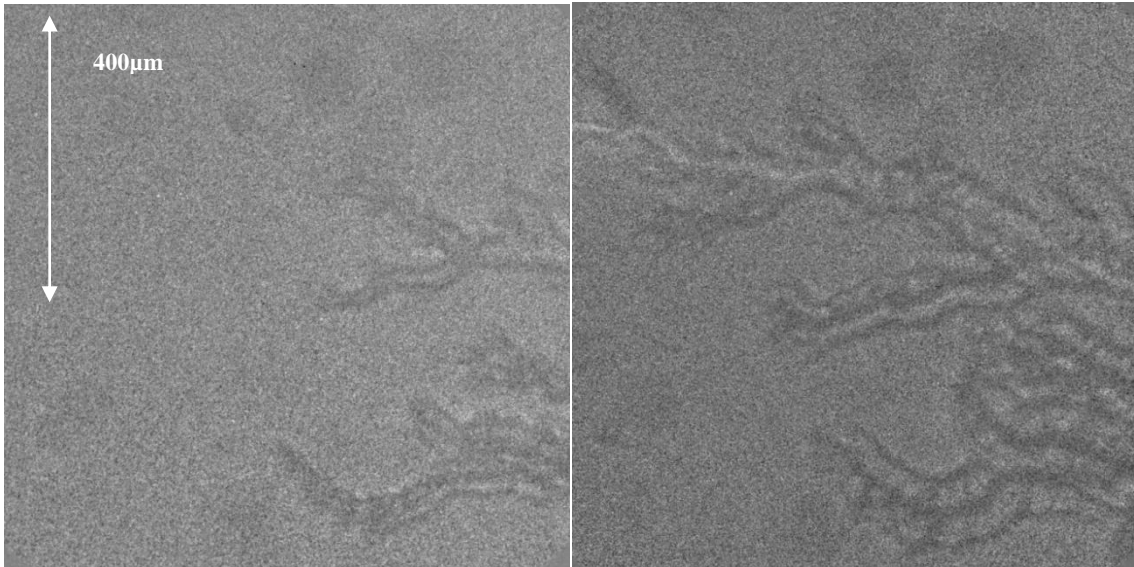


fig 4.66 pair of shadow images, primary mode at t and $t+30\text{ns}$, large magnification, the plasma channel diameter is not easy to distinguish at very early time after its creation, some tens of nanoseconds later the diameter of the channel is of the order of some tens of nanometer.

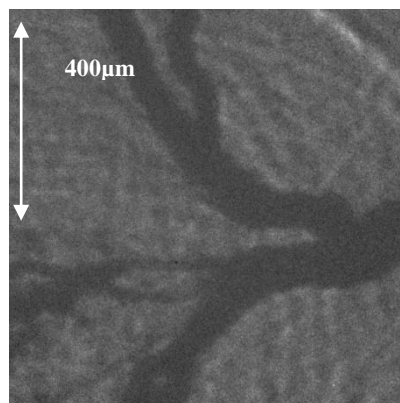
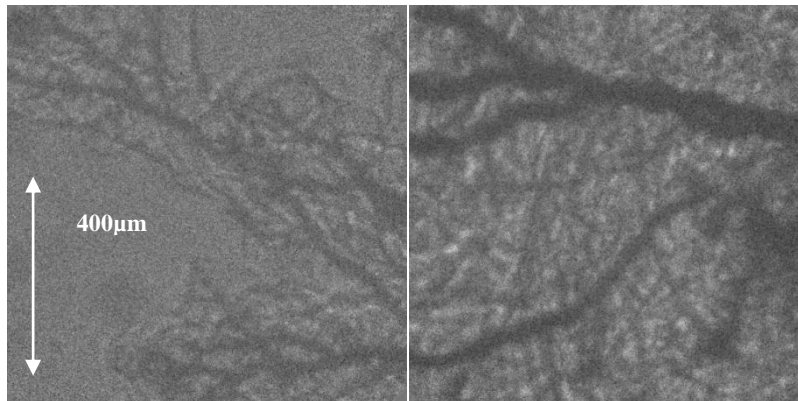


fig 4.67 shadow images, primary mode at different delay, large magnification, the plasma channel expansion is very clear some hundreds of nanoseconds after the channel creation.

The **expansion is always larger at the base of the channels** and is linked to the number of branches supported by the channel. Thus the diameter of the channel could depend on the energy deposition by conduction through the plasma filament. It is not due to the earlier creation of the base before the extremity which is not compatible with the observed post discharge expansion velocity of the channels. More children branches means more current flowing through the parent filament according to node law for current and as suggested by the

two ICCDs emission imaging setup. However, the pressure should be the same in the whole gas cavity and thus it is difficult to explain the larger base.

The **gas channels fragments first at their extremity**, the base of the filament is the latest to fragment. The **fragmentation occurs due to the gas/liquid interface instability**, the growth rate of this instability should depend on the gas channel radius and the surface tension. The smaller diameter filaments are the first to disappear due to this sausage instability.

The **formation of a spherical bubble attached to the metal electrode** can suggest that the whole gaseous cavity is sucked back to form this mm size bubble and this could explain the observed larger base.

4.4.7 Time resolved emission spectroscopy on H_{α} and OH(A-X): plasma parameters

The **gas temperature** could be measured with **nitrogen band**. We looked for that nitrogen emission by it turned out that the nitrogen dissolved emission was much too weak for our experimental setup. Nitrogen bubbling and saturation of the liquid were not implemented.

The **temperature measured on OH** is in general quite tricky to interpret and may not be in equilibrium with the nitrogen emission. The OH can result from several production paths: dissociative excitation of water molecule under electronic collisions or dissociative recombination of water ions. The rovibrational bolzmann plot is thus basically a two temperature distribution. The OH emission is sufficiently intense to perform some time resolved measurements on a reasonable number of accumulations. The accumulation process was triggered from the plasma beginning and thus missed the first 220ns due to the intrinsic delay of the optical setup. The ends of the continuous propagation and the reilluminations (or filament decay at high conductivity) were investigated. An approximate rotational temperature of **2400K** can be estimated from time integrated measurement accumulated over several shots in **fig 4.68**

The fact that emission is time integrated over a period including the post discharge can mean that we measure the temperature (if there was time to reach thermodynamic equilibrium with temperature of neutrals) near the end of the expansion of the gaseous channels when the quenching by neutrals has decreased.

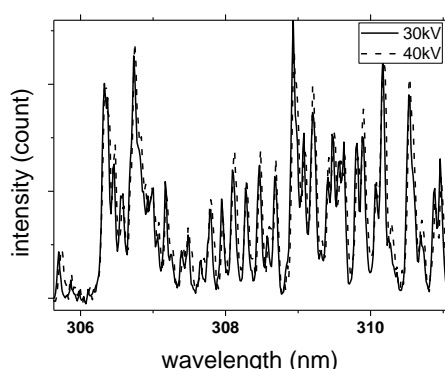


fig 4.68 OH emission band time integrated and accumulated over 200 shots, integrating during $1\mu s$, much less intense than H_{α}

H_{α} emission is also very strong and is readily observable. We performed H_{α} broadening measurements as a function of the liquid ionic conductivity. The H_{α} emission integrated over the whole discharge duration (primary mode, secondary mode, reilluminations) show that the broadening is higher for lower conductivity. On some acquisitions the line shape looked quite curious and seemed to be the superposition of two distinct lines shapes. We thus made time

resolved measurement and it turned out that the line broadening (half width maximum) is very large at the beginning of the discharge and decays as a function of time as shown in **fig 4.69** and **fig 4.70**. Thus the post discharge phase is shorter at high liquid ionic conductivity due to shorter applied voltage pulse, and conversely the post discharge reilluminations is quite long for distilled water. Consequently the time integrated measurement showed different line broadening because of different duration of the superposed components. In fact the broadening of the H α line is very large during the plasma propagation. A more detailed study of the time resolved H α line broadening during propagation and for several water conductivities would be interesting. Preliminary results obtained during this thesis have shown that the broadening during plasma propagation is quite similar as function of the water conductivity as shown in **fig 4.71**.

The H α broadening is the superposition of the temperature broadening, the pressure broadening, and the electronic density broadening. Thus to obtain the electronic density one must first know the pressure history of the channels and the gas temperature. This is why we performed shock waves velocity measurement and OH emission temperature measurement.

One needs to subtract the contribution of pressure which is very large in order to obtain Ne. **It is not sure if the halfwidth decay is a density decay or just a pressure decay.** The main difficulty is to have an estimation of the gas pressure inside the gas channel. The study of the shock wave velocity was performed to estimate the pressure during the discharge propagation phase, a more refined study of the pressure inside the channels is thus required to deduce the exact value of the electron density during discharge propagation.

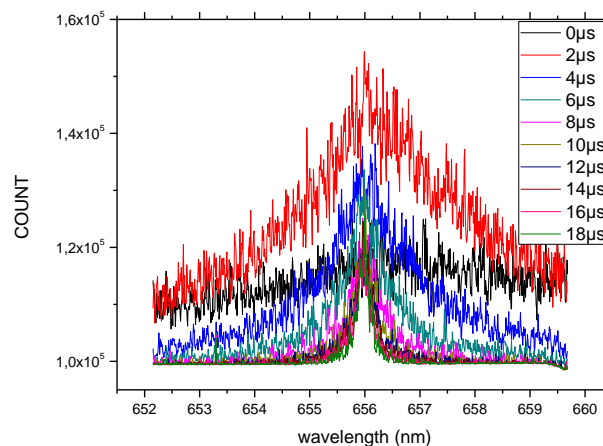


fig 4.69 time resolved H α emission line at 50 μ S/cm liquid conductivity, accumulated on typically 20 shotsn, space integrated.

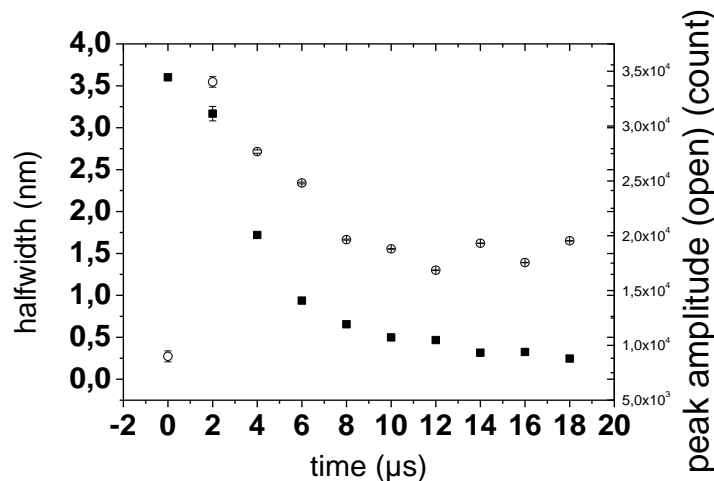


fig 4.70 H α line broadening and line intensity (Lorentz fit with background subtraction) time resolved for 50 μ S/cm water conductivity, (40kV, 1cm gap)

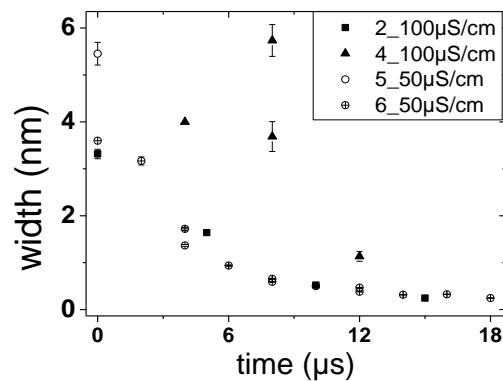


fig 4.71 H α line broadening time resolved for 100 μ S/cm and 50 μ S/cm water conductivity, (40kV, 1cm gap), the first point occurs during the discharge propagation, the decay happens in post discharge and result from: Ne decay, P decay and Tg decay contributions.

The decay shape of H α line in fig 4.70 and fig 4.71 should not be overinterpreted since only the first data point on the above figures occurs during the plasma propagation. The other data points combine the gas pressure/electron density/gas temperature decays with the discharge jitter statistics since the measurements is accumulated over 20 shots (realized at 40kV to minimize this jitter).

4.5 Discussion and conclusions on the positive mode

At least, this increased power dissipation through the filament in the wake of the propagating tip should have some influence on the plasma parameters (Ne, Te) and the gas pressure or temperature and thus modify strongly the induced chemistry [Lukes] even if the propagation velocity stays the same.

In a general way, charged particle generation and motion is likely to be strongly influenced by the applied electric field according to the classical gas discharge theory. Basically, the voltage is required at the tip of the filament to extract the electrons from the liquid, and to ensure the conduction of current trough the filaments in order to compensate for the losses and supply power to the propagating plasma filament tip. The applied electric field is superimposed to the space charge electric field at plasma/liquid interface. The lack of influence of the applied voltage - once the inception voltage is reached - can indicate that the propagation is ensured mainly by the space charge electric field at the tip of the plasma filament as in the case of gas phase streamers. A sufficient voltage would then be required to launch the filaments but after that, the filament is self sustained and any further increase of the voltage is not used for propagation but is likely used to form a larger number of plasma filaments that is to say branching. However, it is difficult to study branching in order to verify this last assumption. Branching pattern changes dramatically from one shot to another and no clear law can be deduced from experiments. In particular, the individual segment length between two nodes or the number of individual filaments at each time has more variability between several shots in same conditions compared with changing the water conductivity or the applied voltage.

The reported constant velocity across the gap and as a function of applied voltage and conductivity must be caused by a limiting or a self regulating mechanism: the phase change or branching. Limitation can be caused by the electron extraction process form the liquid or the vaporization process. Autoregulation can be explained by branching or by the filament resistivity. The branching can play an autoregulation feedback by splitting the space charge into constant tip charges along the gap or by screening the electric field from one filament to another adjacent filament. The plasma channel resistivity can also play a regulation role. The channel

resistivity will increase as the filament propagates and the space charge amplification across the gap could be balanced. On one hand, any acceleration will be associated to a longer filament and thus a larger series resistance. On the other hand, the space charge will have difficulties to maintain its value because less power will be available through the longer resistive filament. Thus the space charge electric field will decrease and the propagation will slow down.

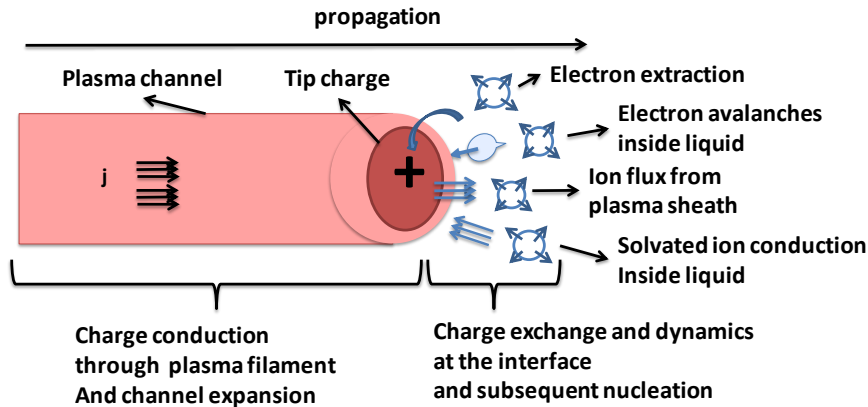


fig 4.72 guessed mechanisms that can occur at the filament tip and explain the plasma propagation.

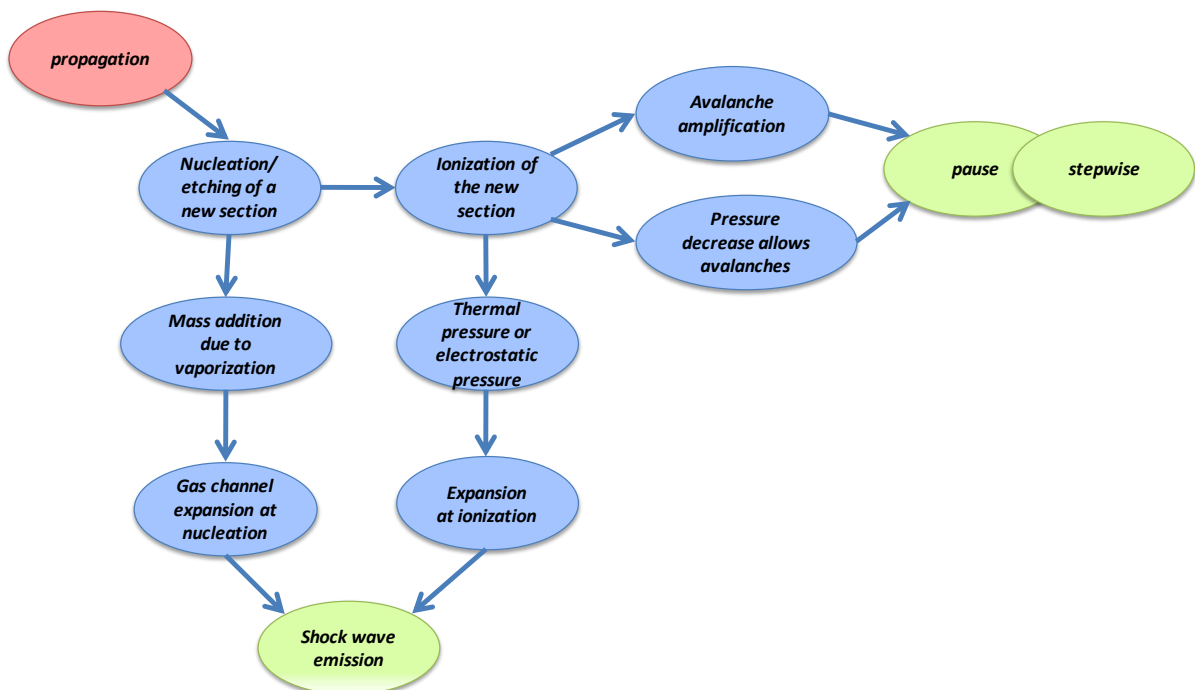


fig 4.73 summary of causes for a stepwise propagation and shock wave emission during the secondary positive mode.

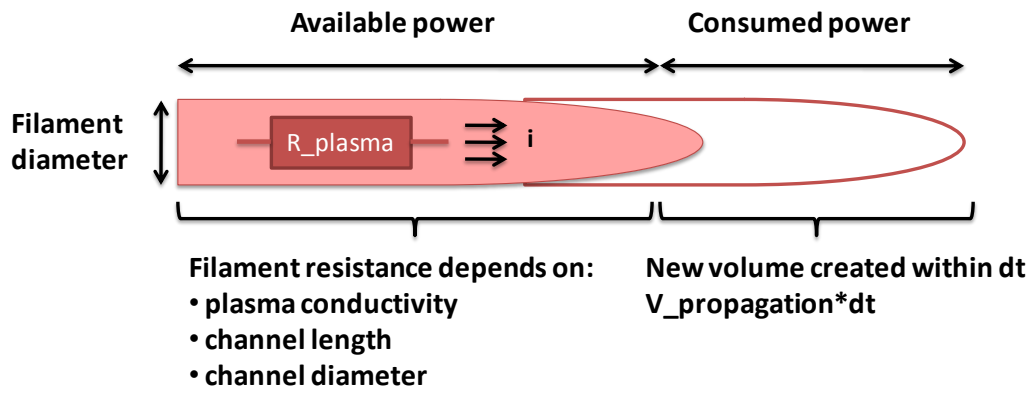


fig 4.74 regulation of the propagation velocity by the energy feed through the plasma filament from the point electrode to the tip of the filament.

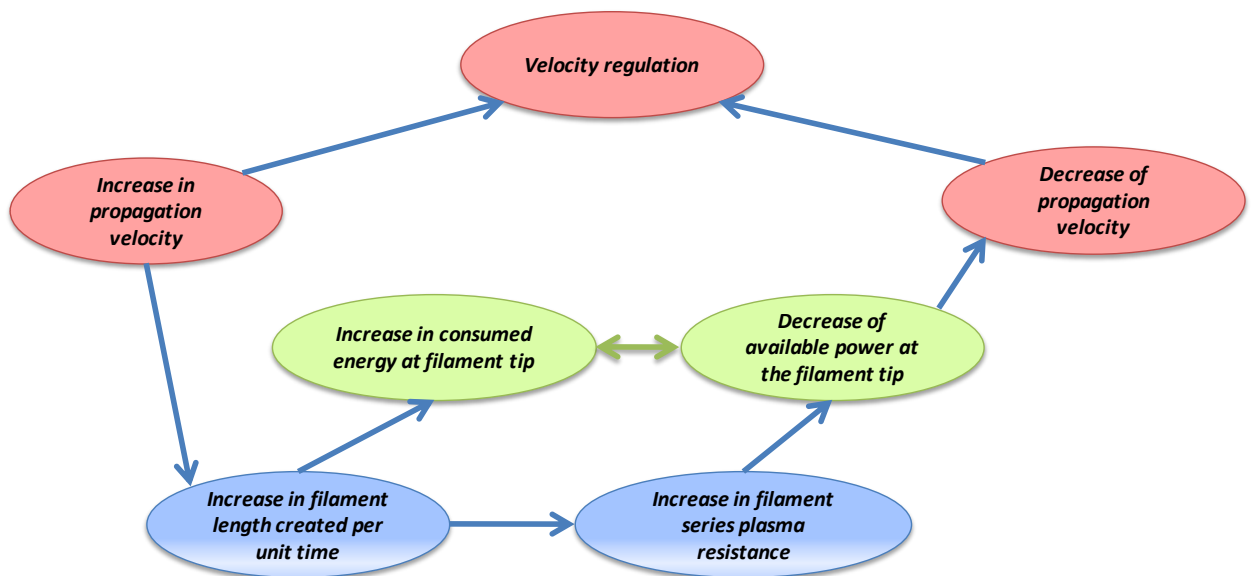
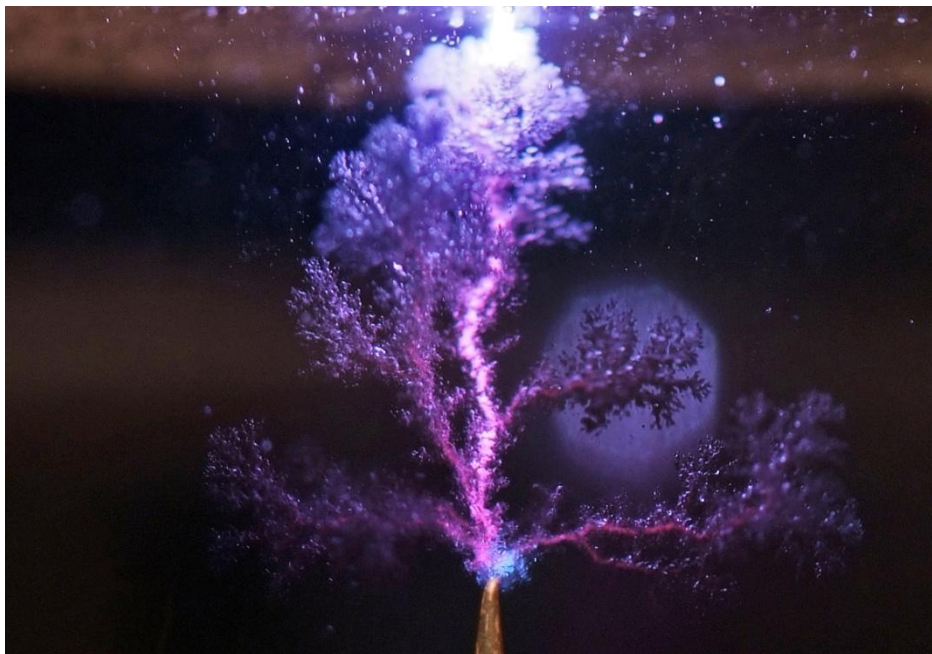


fig 4.75 regulation of the propagation velocity by the energy feed through the plasma filament.

| | | |
|---------|--|-----|
| 5 | The slow negative mode | |
| 5.1 | The QUB low voltage discharge..... | 157 |
| 5.1.1 | Nucleation of a gas layer, influence of applied voltage, temperature and conductivity..... | 157 |
| 5.1.2 | Plasma ignition, low voltage vs medium voltage | 159 |
| 5.1.3 | Time resolved emission spectroscopy on H α , H β , Na, OH | 162 |
| 5.1.4 | Gas layer collapse and shock waves emission | 162 |
| 5.1.5 | Conclusions on the QUB low voltage saline discharge | 163 |
| 5.2 | The HV point to plane negative mode | 163 |
| 5.2.1 | Morphology..... | 163 |
| 5.2.2 | Initiation..... | 167 |
| 5.2.3 | Imaging the propagation of the negative discharge | 168 |
| 5.2.3.1 | Time resolved emission/schlieren/shadow | 168 |
| 5.2.3.2 | Influence of the applied voltage on the propagation velocity..... | 171 |
| 5.2.3.3 | Influence of ionic conductivity on the stopping length and the propagation velocity..... | 172 |
| 5.2.4 | Discharge current and reilluminations in the negative mode..... | 176 |
| 5.2.5 | Shock wave emission..... | 179 |
| 5.3 | Conclusions on the negative polarity modes | 180 |
| 5.3.1 | On the low voltage saline discharge (QUB) | 180 |
| 5.3.2 | On the point to plane HV discharge (Palaiseau)..... | 181 |



5 The slow negative mode

In this section we present the plasma modes observed at negative polarity. First we present a low voltage negative discharge where the plasma is initiated after the nucleation and the expansion of a gas layer around the electrode. Then we present a high voltage discharge inside water at negative voltage.

5.1 The QUB low voltage discharge

5.1.1 Nucleation of a gas layer, influence of applied voltage, temperature and conductivity

The “low voltage” plasma discharge of the IRCEP laboratory at Queen’s University occurs in **highly conductive saline water solution** (some mS/cm). The first stage is the nucleation of a gas layer around the electrode. This nucleation is favoured by a higher applied voltage, a larger liquid conductivity, and a larger liquid initial temperature.

In the **commercial version** shown in **fig 5.6** with pulsed **repetitive power supply**, the **vapour layer** is progressively nucleated on a millisecond timescale. The junction of the metal electrode and its dielectric mount is a **triple point** and thus a high electric field region. The local joule heating would be higher at this position. It explains why the layer first grows from the side instead of the curved top of the electrode as illustrated by **fig 5.1**.

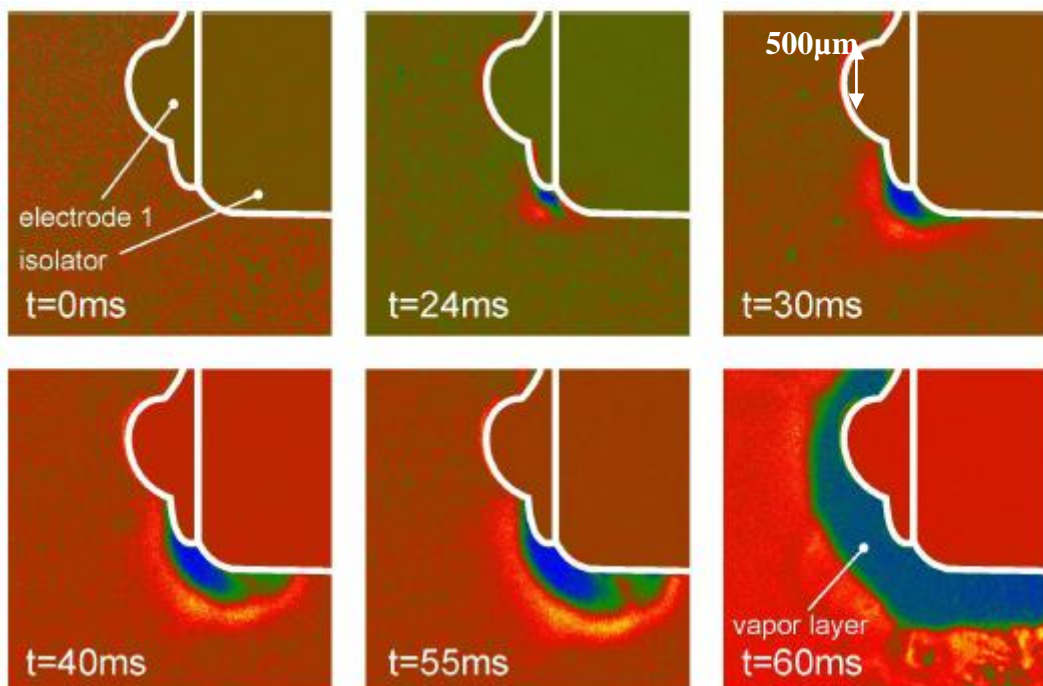


fig 5.1 vapor layer growth from the dielectric/metal triple point in the medical plasma setup [Shaper]

In the case of the **academic version** with a single shot long low voltage pulse, the vapour layer is first nucleated on the sharp edges of the electrode where the Laplacian electric field is higher as shown in **fig 5.2**. We observed that the **growth rate of the layer depends on the voltage level, on the liquid ambient temperature, and the liquid ionic conductivity** as shown in **fig 5.3**. A joule mechanism is obviously the cause of the nucleation. This vapour nucleation

happens with or without plasma. With plasma the nucleation is always faster: the plasma provides an additional heat source inside the layer.

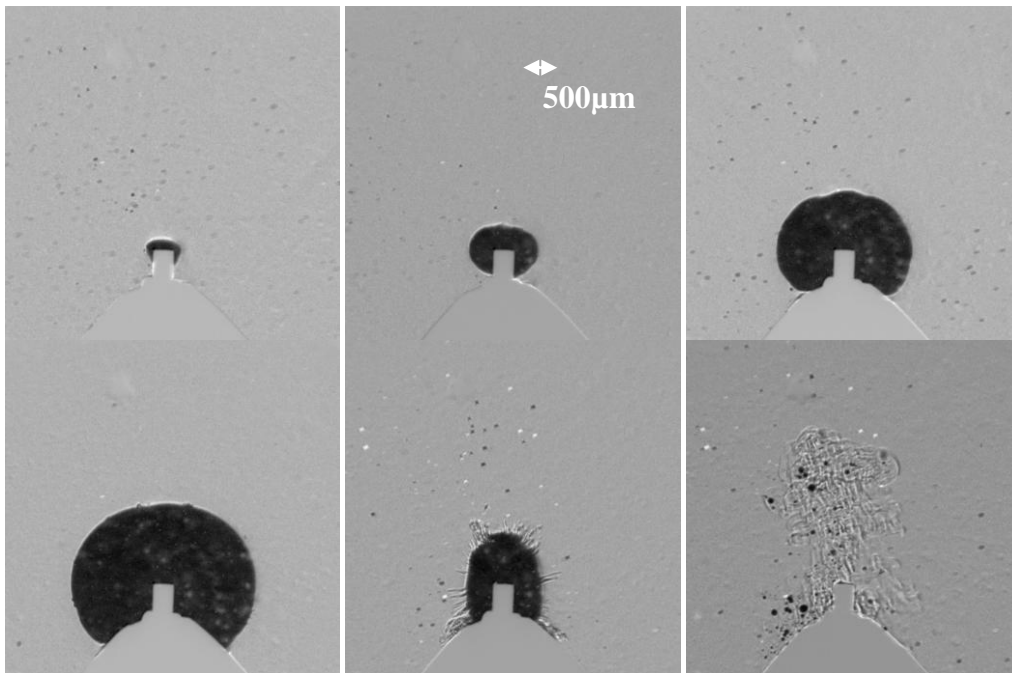


fig 5.2 vapor layer growth rate for long pulse duration and 600V at room temperature, pin is 500 μ m diameter, 20 μ s step between each images.

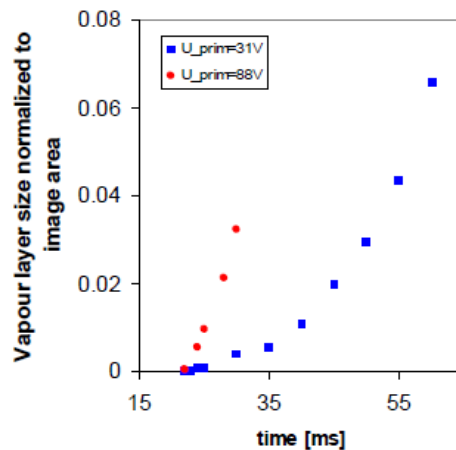


fig 5.3 vapor layer growth rate for different applied voltages at 40°C [Shaper]

The timescale of the vapor layer nucleation can be of the same order of the **hydrodynamic** motion of the fluid especially at low voltage and low conductivity where the growth rate is quite slow. In this case the vapor layer boundary is less regular and presents a **bubbly shape with instability** and **convection patterns** as shown in fig 5.4 and fig 5.5.

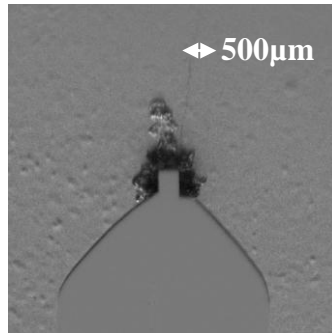


fig 5.4 vapor layer growth at low voltage 300V at room temperature, the cavity growth is slow and the cavity has time to begin to fragment.

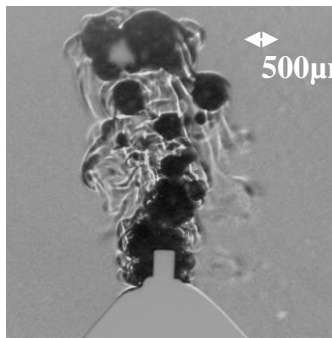


fig 5.5 successive growth and collapses for very long applied voltage pulse.

For unknown reasons, the vapour layer growth is slower at positive applied voltage in exactly the same experimental conditions and with correction for the electrode asymmetry. This means that the layer nucleation is not strictly due to joule heating since joule heating does not depend on voltage polarity and the solvated positive and negative ions have almost the same mobility.

5.1.2 Plasma ignition, low voltage vs medium voltage

On time integrated images, the position of the plasma is not reproducible at all, much less reproducible than the vapour layer nucleation. The plasma discharge occurs inside the gas layer and bridges the electrode and the water interface across the vapour gap as shown in fig 5.9.

The **plasma initiates only close to the maximum expansion time of the layer**. It does not start at the beginning of the layer nucleation. fig 5.10 shows that the nucleation of the gas layer is associated to a progressive decrease of the current.

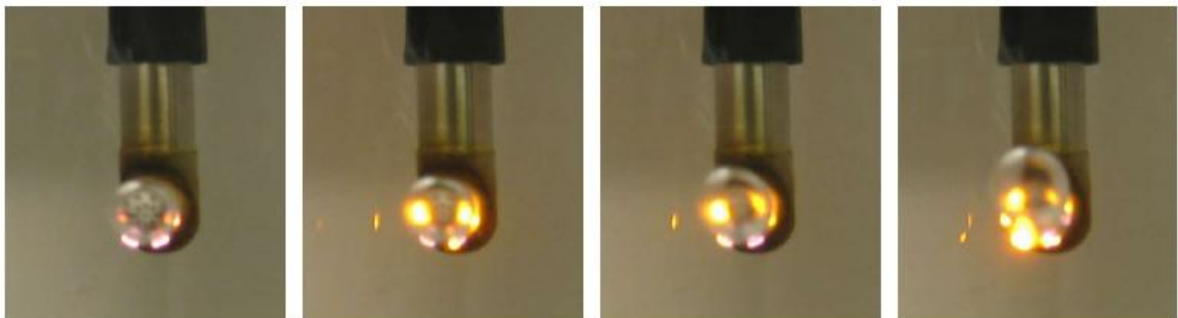


fig 5.6 medical plasma device, the yellow color of the plasma spots results from sodium emission

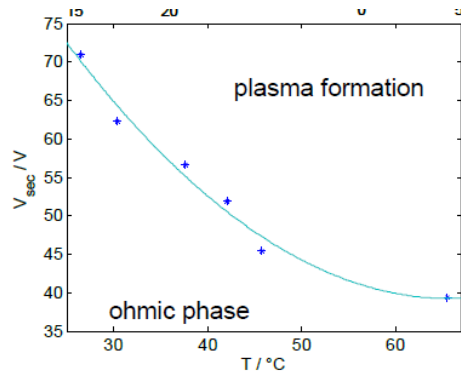


fig 5.7 plasma initiation criterion [Shaper]

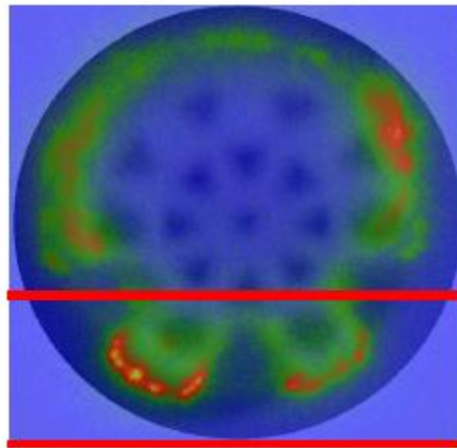


fig 5.8 top view of the sodium emission of the discharge [Shaper]

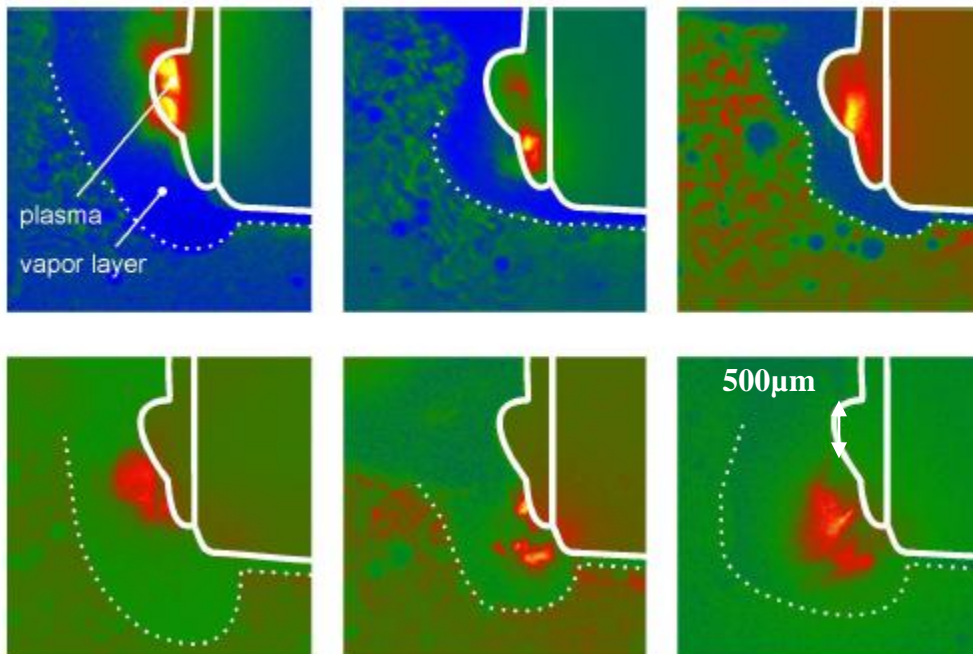


fig 5.9 side view of the sodium emission of the discharge [Shaper]

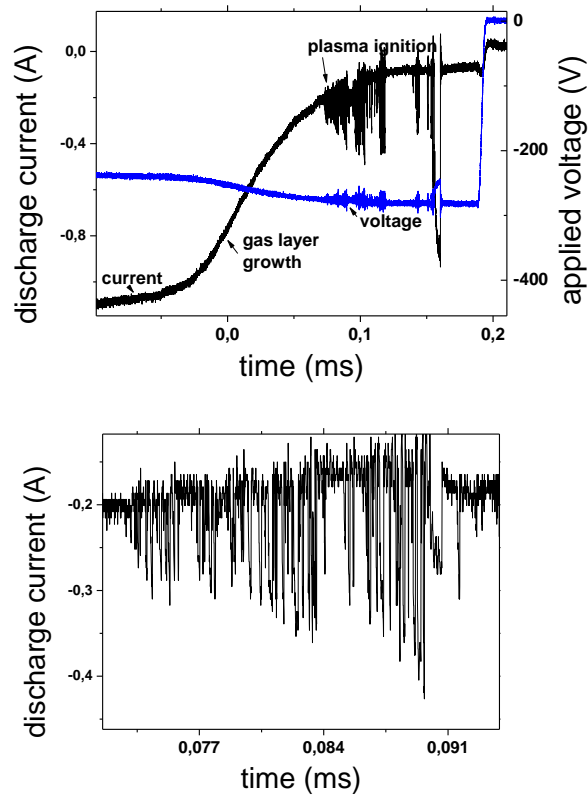


fig 5.10 current and voltage waveform at 300V, the gas layer growth is associated to a progressive decrease of the current, current spikes appear near maximum extension of the layer, the current spikes are associated to plasma ignition, zoom on the plasma current spikes.

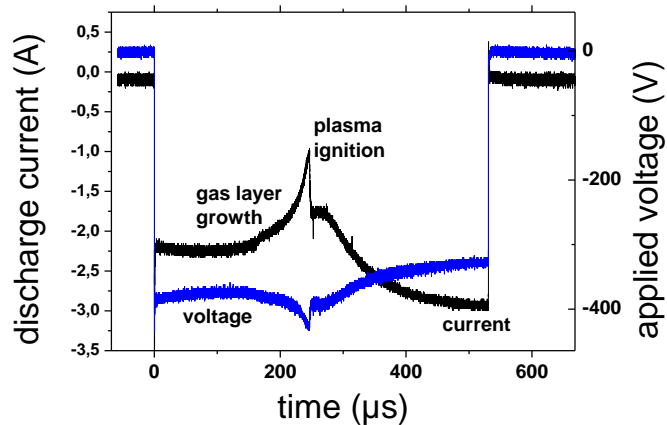


fig 5.11 current and voltage waveform at 400V, the gas layer growth is associated to a progressive decrease of the current, plasma current is now continuous

The plasma ignition is associated to current spikes on the current waveform in fig 5.10. Since the plasma is not present from the beginning of the applied voltage pulse but systematically starts at the maximum expansion of the gas layer, one can expect that **plasma ignition is triggered by a pressure decrease in the gas cavity**. The initiation delay of the discharge is not due to an applied voltage too close to inception voltage but to the high gas density.

At low voltage typically **300V**, the discharge current is a succession of short microsecond scale impulsions, those currents peaks in fig 5.10 transforms into a long continuous discharge current at higher voltage of **400V** in fig 5.11 or **600V**.

5.1.3 Time resolved emission spectroscopy on H α , H β , Na, OH

We observed with a photomultiplier that the **emission intensity of OH and H α lines follows the discharge current**. On the contrary the **sodium emission is much stronger and quite independent** and can vary strongly (100%) during the current pulse.

With an interferometric filter in front of the iCCDs we checked if the sodium emission was more localized close to the electrode and the simultaneous observation of 2D mapping of two different emission lines on the same single shot. We observed some glow emission, spots and some lines which are more likely deformation of the plasma emission through the deformed interface of the vapour layer.

5.1.4 Gas layer collapse and shock waves emission

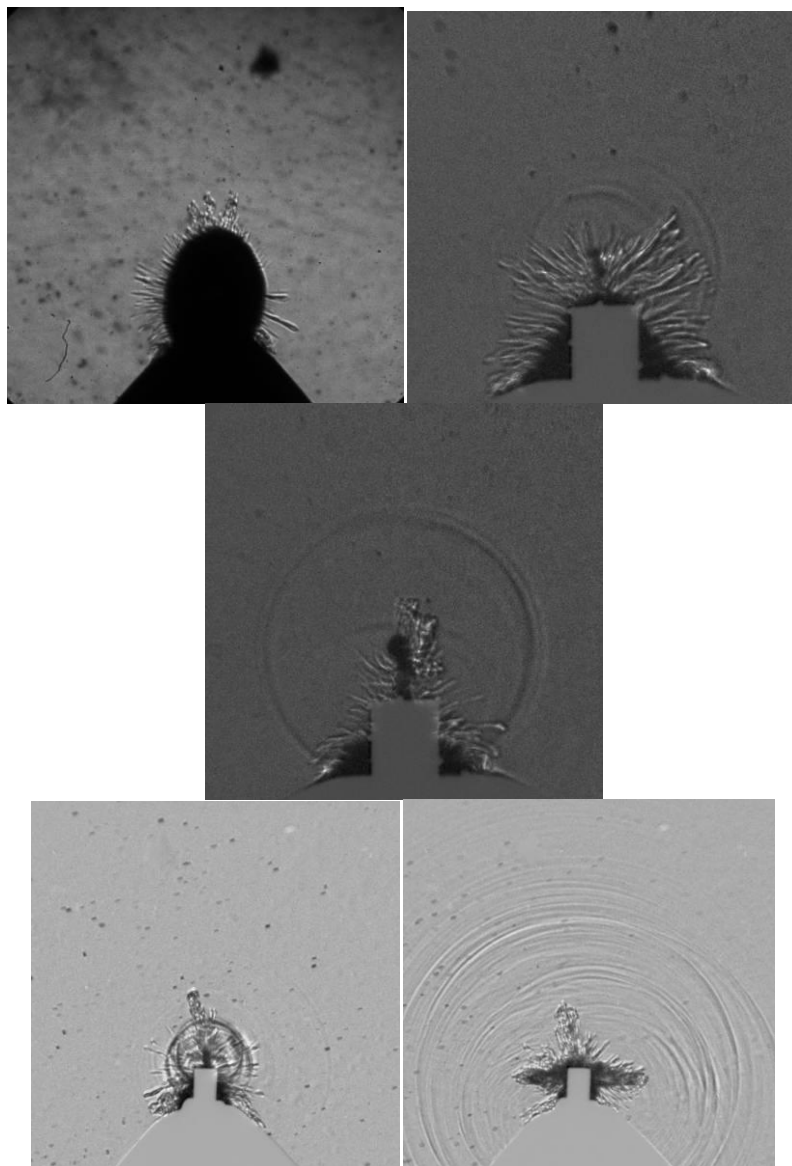


fig 5.12 collapse of the vapor layer and shock wave emission, pin is 500 μ m diameter

The layer reaches a **maximal expansion length** depending on the duration of applied voltage pulse. On fig 5.12 we can see that the layer **collapses back** toward the metal electrode and leaves some hot water “fingers”. At the maximum collapse of the vapour layer shock waves

are emitted. The center of the **shock waves** is often a gas pillar structure at the maximum collapse.

The layer can then restart to **expand again** if the applied voltage pulse is long enough. Several growth and collapse cycles can occur. Only the first growth is quite reproducible. We systematically observed that the following nucleations of the layer is quite perturbed if there is plasma initiation.

5.1.5 Conclusions on the QUB low voltage saline discharge

The discharge ignition follows the nucleation of a gas **layer around the high voltage electrode**. The nucleation follows a joule heating mechanism.

The discharge bridges the gas gap and uses the water interface as a water electrode. The discharge is continuous for voltage above inception voltage. Sodium emission is very strong compared to OH and O lines. The sodium line is likely to originate from the sodium metal deposited on the metal electrode surface and strongly heated by the plasma filament root (hot cathode spot).

Ignition occurs at **maximum expansion** where the pressure inside the gas cavity is minimum. The cavity growth is faster when there is a discharge compared to pure **resistive heating**. The propagation of the discharge inside the liquid is not observed: the plasma follows the gas layer motion.

This discharge presents similarities to the high voltage positive discharge in the sense that there is **nucleation of gas phase prior to the discharge ignition**. There are similarities with the high voltage negative discharge in the fact that fluid motion is of particular importance for the discharge propagation. However, the interface motion is here one order of magnitude below the discharge described in the following section.

5.2 The HV point to plane negative mode

In this section we present the morphology, initiation, and propagation of the point to plane at negative high voltage. The approach is similar to the chapter on the positive polarity discharge. Emphasis has been made on the specific difference of this negative mode compared to the positive mode.

The slow negative mode was obtained by applying the positive high voltage pulse on the plane electrode because the power supply we have is not reversible. However the electric field is not exactly the same because of the boundary conditions. The electric field lines do not connect exactly the same way between the positive needle setup and the positive plane setup because of surrounding ground potential. To be more accurate, the HV setup could have been modified by placing the spark gap switch between the high voltage capacitor and the ground to obtain transient voltage reversal. In such a voltage reversal setup, the spark needs to be discharge into ground through and inductive resistance.

5.2.1 Morphology

The negative mode is much **less luminous** and this could explain why this structure has been qualified as non emitting streamers by some authors [Kolb]. The time resolved emission of the discharge could be recorded only because we used a short focal quartz lens length for maximum light collection solid angle, a wide open iris, and maximum intensification.

The first obvious difference between the positive mode and the negative mode is the visual **morphology difference**. At first on emission imaging the negative mode appears less filamentary and has a more glow-like appearance. A closer observation with higher time resolution and

higher spatial resolution shows that in fact the plasma has also a **filamentary shape**. Compared to positive mode, branching is much more important here and presents a fractal pattern with at least 3 or 4 levels as shown in **fig 5.13**. The **filaments are very numerous and tiny** at the extremity of the main branches. The emission intensity is proportional to the filament thickness as shown in **fig 5.13**. The more thick filaments that support the children filaments are more luminous. In fact this filamentary structure is observed through a deformed interface with a lot of ripple and a **bubbly shape**. This explains why the filamentary shape of the discharge appears less sharp compared to the positive mode.

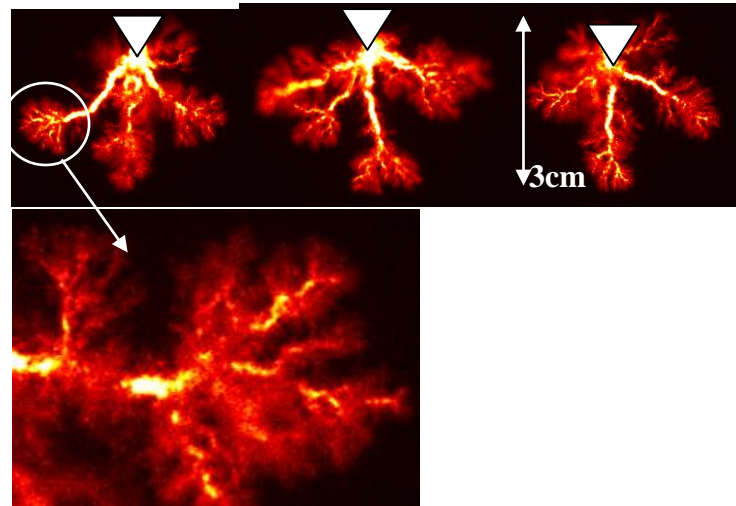


fig 5.13 emission imaging in negative polarity, 1 μ s iCCD gate, 15 μ s delay, different shots, zoom on a branch extremity. image size is 2cm

The gas/liquid interface is not well described when using the emission imaging. The schlieren imaging allowed to clearly observe the boundary of the plasma discharge. It is quite trivial to say the discharge has a **fractal pattern**, however the fractal dimension is quite useless from the physical point of view. We observed that the interface is more defined in the shadow imaging that in the schlieren imaging as shown in **fig 5.14**. The **wavenumber of the interface** is not easily seen with 1:1 magnification ratio obtained with an achromatic doublet with 75cm focus length. Thus a 1:5 magnification was attempted with the use of a third focusing lens of 10cm focus length. The magnification was in fact better achieved with a single achromatic doublet of 50cm focus length as in **fig 5.17** or a single 7cm achromatic doublet as in **fig 5.21**.

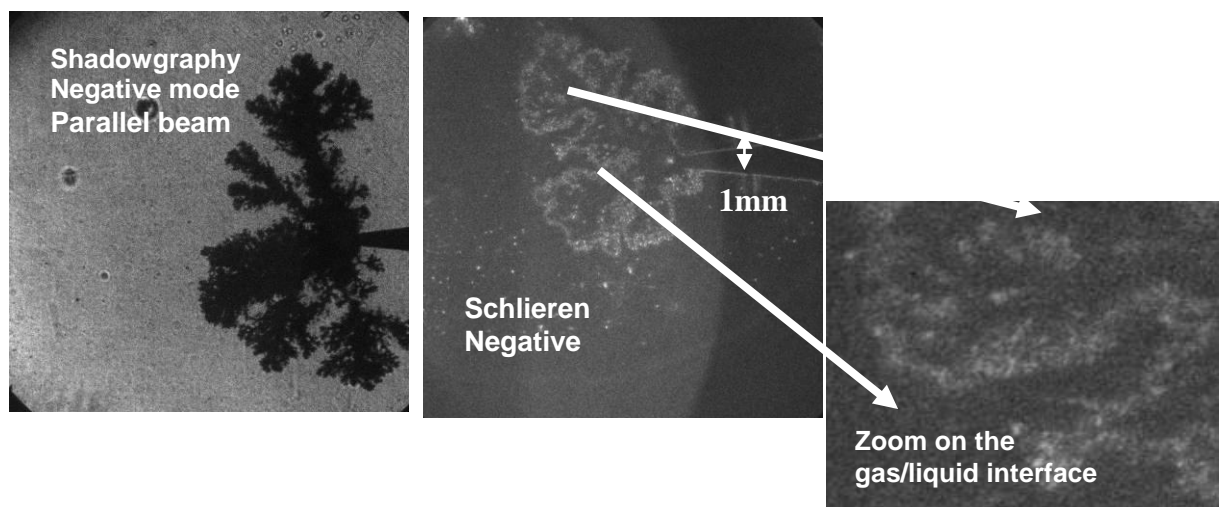


fig 5.14 shadow imaging vs schlieren imaging in negative polarity, scale is the same as in fig 5.26

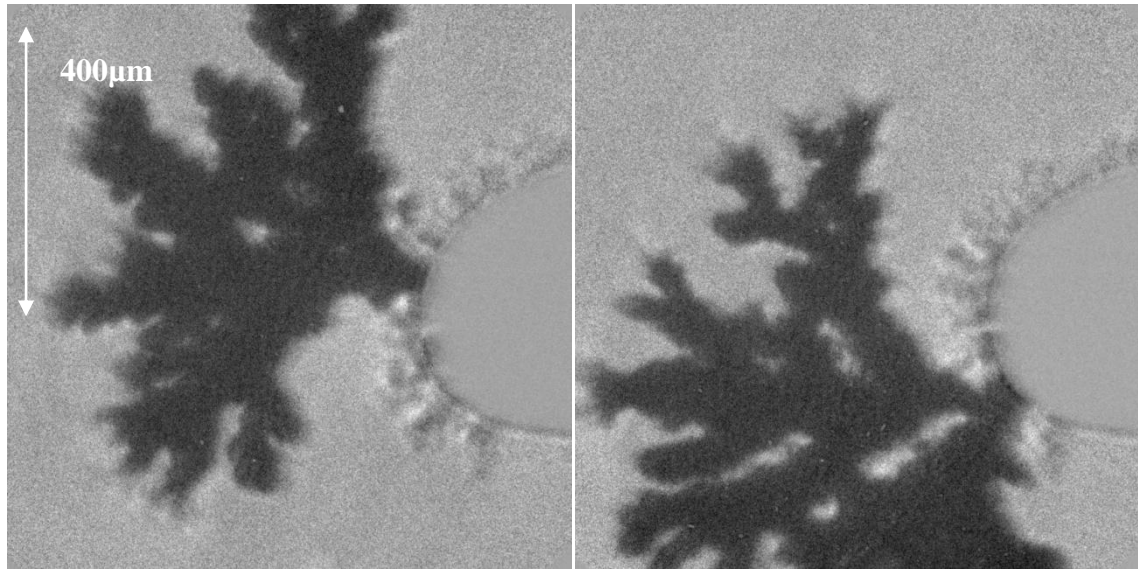


fig 5.15 shadow image, 1µs gate, 5µs delay, the morphology of the channels is clearly seen, the typical wavelength of the gas/liquid interface can be identified to the channel diameter.

The **wavelength of the interface does not increase with time during the propagation** as shown in fig 5.25. The fine structure of the gas/liquid interface is present from the very start of the propagation on shadow images as shown in fig 5.21. The gas/liquid interface morphology suggests an interface instability mechanism. The growth of the gas channels does not happen in the post discharge as in the positive mode but during the propagation. Indeed, the **timescale of the negative discharge allows hydrodynamic phenomenon like interface instability to develop**. On the hundreds of microseconds timescale, **interface instability** has time to develop, this interface instability can have a thermal origin or an electrostatic origin as discussed in a previous chapter. The thermal assumption could be eliminated by checking the gas temperature inside bubble and compare to the available electrostatic pressure on the gas/liquid interface. Additional spectroscopic measurements are thus required.

Due to the liquid conductivity the interface is likely to be charged by adsorbed negative ions since charge removal by the liquid is slower than the incoming flux of charged particles that the plasma filament is able to supply. The charged interface is repelled from the point electrode by the negative applied voltage. The interface charging is able to explain both the propagation and the morphology of the discharge. The charged interface in a radial electric field is unstable as discussed in [Chadband] [Melcher1969] [Vega2003]. This electrostatic instability is an electrohydrodynamic (EHD) instability because of interface charging and electric field normal to the interface. The electrostatic nature of this interface instability is further suggested by the discharge current spikes (reilluminations) in fig 5.35 and fig 5.36 that indicate some charge deposition process close to the interface, electric field screening, and charge removal as described in a following section.

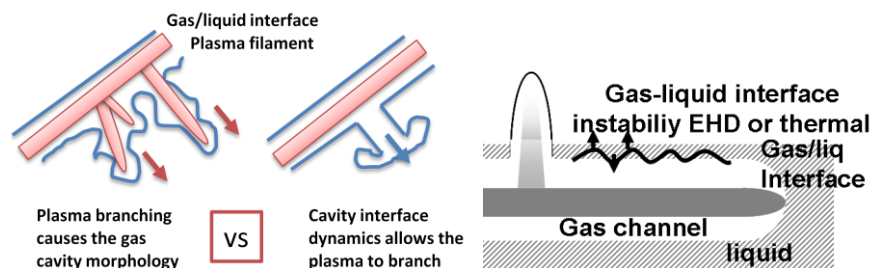


fig 5.16 gas/liquid interface motion because of interface EHD instability.

The **growth rate of this interface instability and the wavenumber** should be tested by changing the liquid **viscosity** and **surface tension**. The **charge removal** at the interface due to the liquid ionic conductivity means that conductivity is a good experimental parameter to test this **EHD instability assumption**.

We also observed that the morphology is deeply affected when changing the liquid conductivity. The discharge appears less filamentary and the wavenumber decreases roughly by a factor two from distilled water to tap water (factor two in two decades of conductivity) as shown in **fig 5.17**.

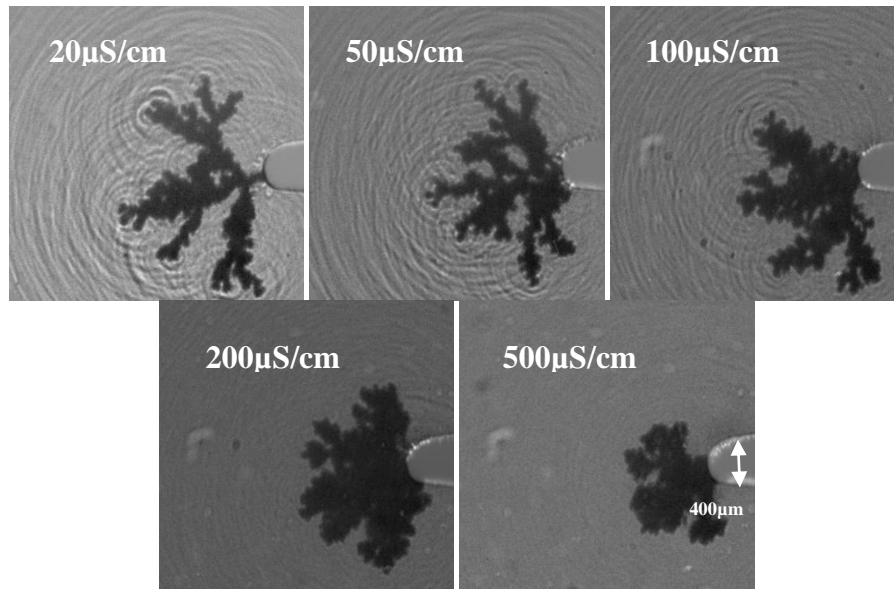


fig 5.17 influence of the water conductivity on the discharge morphology, respectively 20 μ S/cm, 50 μ S/cm, 100 μ S/cm, 200 μ S/cm, and 500 μ S/cm, (20ns gate, 40kV), pin is 400 μ m diameter.

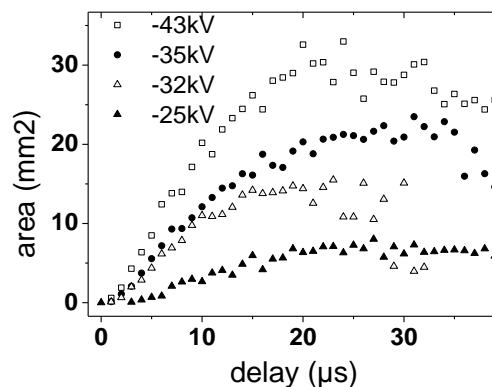


fig 5.18 area increase as a function of time, for different applied voltage from -25kV to -43kV.

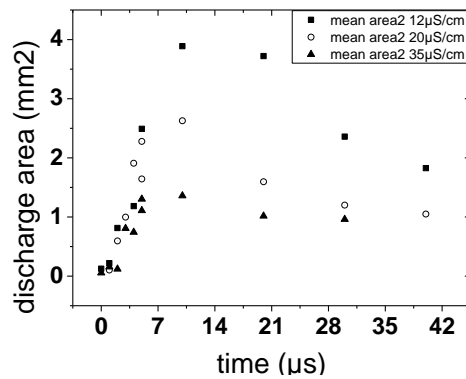


fig 5.19 area increase as a function of time for different water conductivities.

The **discharge area** (projection on 2D) has been measured with the script illustrated in fig 5.23 during the propagation as a function of the applied voltage and the water conductivity. The area roughly measures the volume of gas. We tried to extract a quantitative information on the discharge branching by plotting the ratio of the area to the perimeter on emission images. In fact this should be tested with shadow images instead. **The area growth rate does not seem to depend on the water conductivity but depends clearly on the applied voltage.** At same time the propagation velocity is not changed by the applied voltage as indicated by fig 5.27. It means that a larger amount of charges is deposited on the interface but that the interface area is also increased, thus the resulting charge density stays the same and thus the propagation velocity remains constant as discussed in the following.

5.2.2 Initiation

As in the case of the positive mode, a study of the time delay to breakdown can be used to study the initiation time delay (statistical time lag) and the propagation velocity (formative time lag). This time to breakdown is clearly seen on applied voltage waveform on fig 5.20: the breakdown empties the storage capacitor of the power supply. This kind of plots gives information about a maximum boundary for the propagation velocity and allows to determine the distribution function of the initiation delay. Here on fig 5.20 the large jitter to breakdown is not due to the jitter of the initiation delay but to the 3D propagation of the filaments and the fact that there are only a few large main branches at low water conductivity.

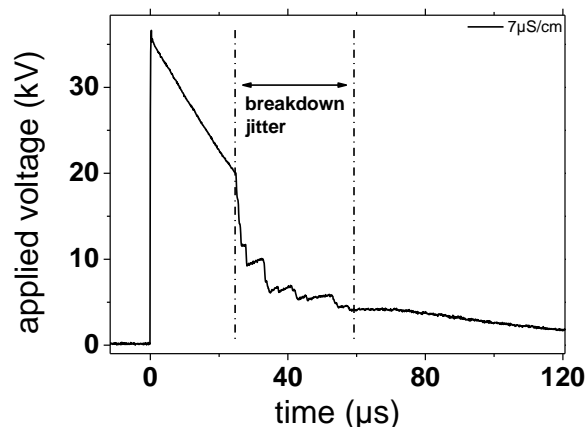


fig 5.20 accumulated voltage waveform over 100 shots, the breakdown occurs with some distribution over time depending on the initiation delay, the 3D propagation, and the propagation velocity (which is constant)

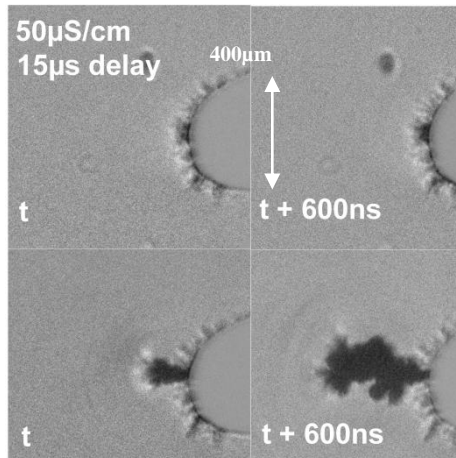


fig 5.21 pairs of shadow images taken on the same single shot (during the same applied voltage pulse), negative polarity, initiation

In fig 5.21 a zoom on the high voltage point is made. The discharge initiation exhibits the **gas cavity** originating from a more tiny root. This **root** does not expand during the whole duration of the propagation and is always of this typical size.

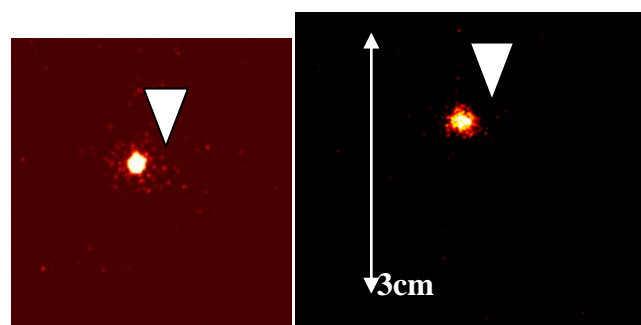
Additional pattern can be distinguished all around the point. Those **tiny dark filaments aside form the discharge** does not grow and do not evolve into additional discharge during the pulse. It is likely to be hot water jet or EHD liquid flow. The pattern of tiny filaments is more intense at larger liquid conductivity. This corroborates the hot water jet hypothesis.

5.2.3 Imaging the propagation of the negative discharge

5.2.3.1 Time resolved emission/schlieren/shadow

With the 2 iCCD setup working on emission imaging, some fine details of the propagation of the negative mode can be observed. The plasma discharge begins at the high voltage point and has a spherical shape. No sub-structure can be observed on this spatial resolution. Then some filaments begin to grow in a tree-like fashion on a hemispheric shape. The propagation follows the Laplacian electric field lines and is in this respect quite similar to the secondary mode of the positive polarity. The filaments appear to be slower, much less intense, and with very large radius. The number of the initial main filaments is not very important, the number of filaments will go increasing during the propagation. The number of main branches increases during the propagation as they split (branching) as shown in emission imaging in **fig 5.22**.

Some **spots** of bright intensity emission are often observed on some particular branch or at the extremity of one branch or simultaneously at the extremity of several branches.



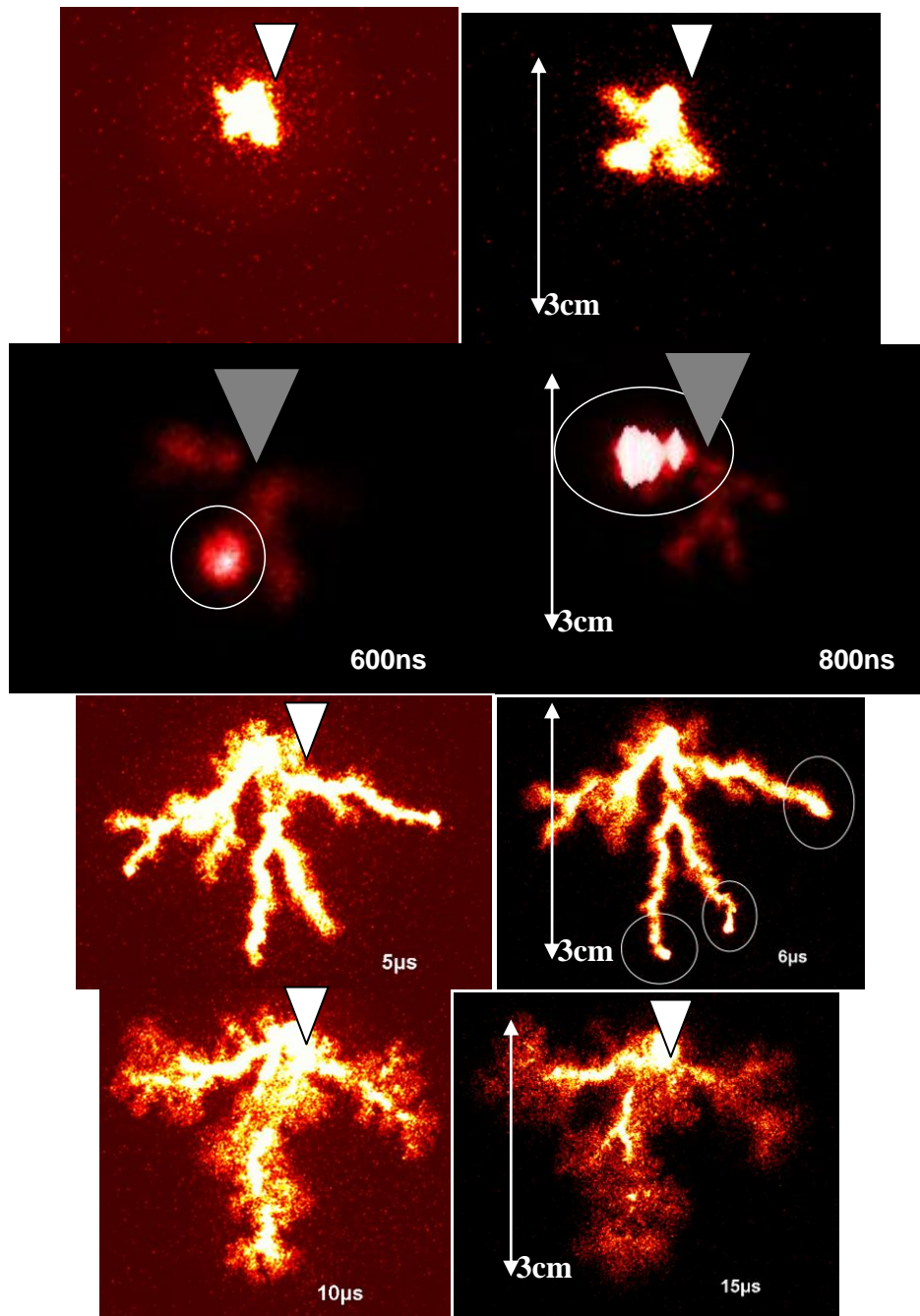


fig 5.22 two iCCDs emission imaging setup at negative voltage polarity

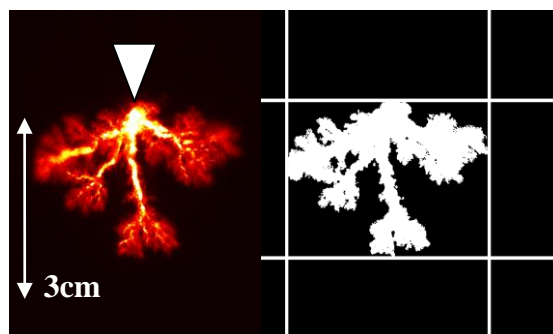


fig 5.23 emission image of the negative polarity and image post-treatment binarisation in Matlab

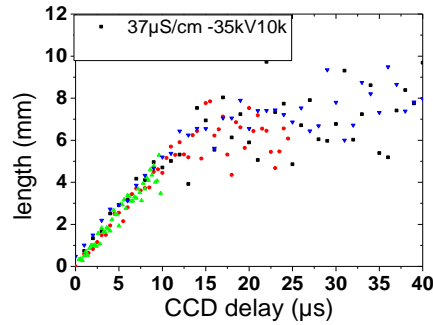


fig 5.24 velocity growth , each datat point is taken on a different shot with single iCCD setup, this plot illustrates the reproducibility.

As in the case of the positive mode, the maximum extension of the discharge structure illustrated in **fig 5.23** is measured as a function of the iCCD delay to obtain **fig 5.24**. In the case of the negative polarity no accumulation of images is required: the **velocity-growth plot fig 5.24** has a very low scattering because the initiation delay jitter is one order of magnitude less than the propagation duration unlike in the case of the positive mode. The **linear growth** of the discharge during the propagation is very clear and reproducible even with just the single iCCD setup as shown in **fig 5.24**. With the 2 iCCD setup the instantaneous velocity is the same and is of **400-500m/s**. There is a weak but significant increase of the discharge size during the “stopping” phase after the main phase of the discharge propagation. The discharge presents then **two propagation stages** at two separated velocity. This very slow propagation is in the **10m/s** range.

The gas cavity growth does not seem to fully stop during the postdischarge as shown in **fig 5.24**. This expansion velocity in the post discharge is consistent with a channel thermal expansion. The same order of velocity is found for the channel expansion in the positive mode in the post discharge.

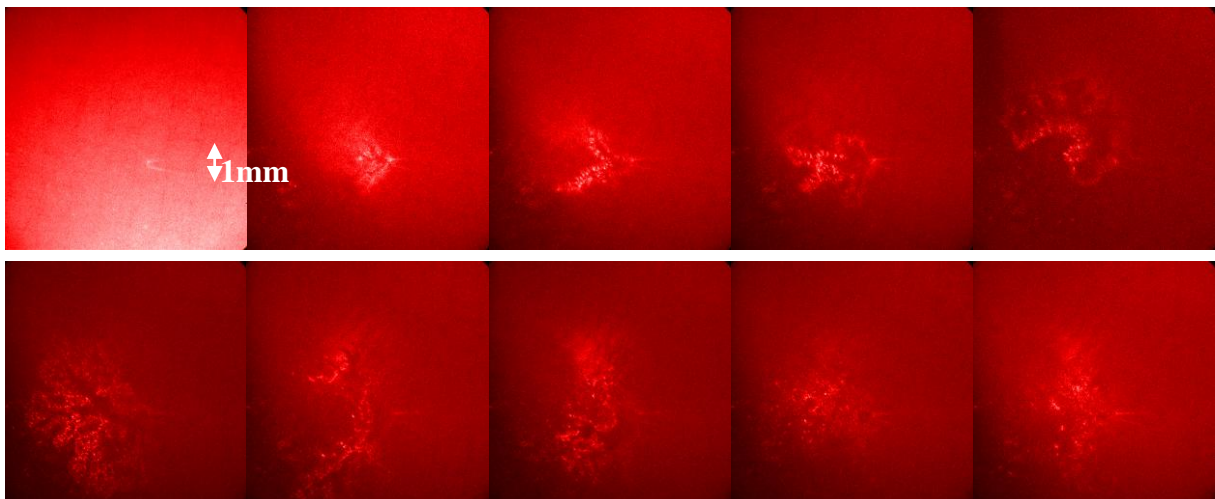


fig 5.25 time resolved schlieren imaging in negative voltage polarity, 1μs gate, 1μs step, scale is the same as in fig 5.26, 40kV, 10μS/cm

At first the propagation of the gas cavity was measured with the schlieren diagnostic as in **fig 5.25**. In the following we will keep on with shadow diagnostic. With shadow imaging the gas structure can be observed very clearly. The shadow imaging in **fig 5.26** confirmed the propagation velocity value measured with the emission imaging setup. In addition, the **post discharge** expansion and dilatation of the gas channels can clearly be seen. The **dilatation of the channel** is followed by the **fragmentation** of the finest channels first. The gas cavity of the negative mode fragments on the same timescale as the positive mode, the fragmentation is

faster for the small diameter channels, the fragmentation mechanism is likely to be the same. The discharge releases a **cloud of microbubbles** in the liquid and those bubbles rise due to Archimedes forces. Some filaments roots can fragment before the extremity of the filament in **fig 5.26**. It could be quite interesting to check if the propagation of this severed branch continues. It would mean that the propagation does not need necessarily some power income from the pin unlike the positive discharge secondary mode.

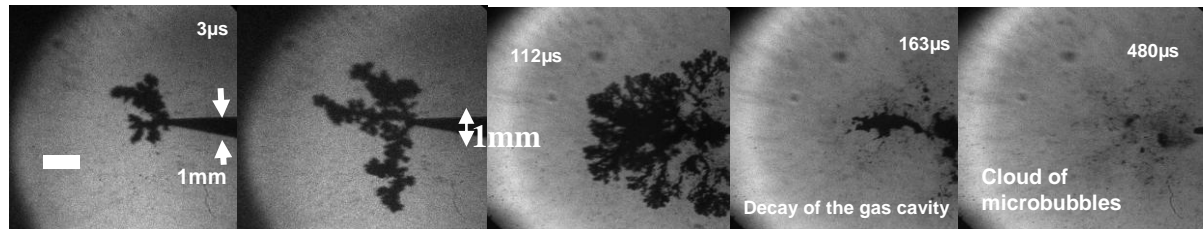


fig 5.26 time resolved shadow imaging in negative polarity, branched gas cavity propagation (plasma discharge propagation) and fragmentation on hundreds of μs timescale

5.2.3.2 Influence of the applied voltage on the propagation velocity

On **fig 5.27** the discharge length is plotted as a function of time for different applied voltages. The **voltage has no clear influence on the propagation velocity**. This **does not corroborate the charged interface mechanism where the interface is repelled by the negative voltage** at the point electrode.

It is possible that the voltage between the propagating charged interface and the point stays the same. In fact **the charge density deposited on the interface** is exactly the charge required to **screen the electric field inside the gaseous cavity and extinguish the plasma** as described in the section dedicated to the plasma current waveform. The surface of the gas/liquid interface increases during the propagation but at the same time the “gap” increases also. Surface increases faster. The resulting capacitance of the gas/liquid interface in respect with the point electrode increases during the propagation. The total amount of charges Q deposited on this interface S must thus increase during the propagation in order to still screen the voltage. However the **surface charge density q decreases as $1/R$** . According to this electrical screening and pushing, the **pushing force should be proportional V^2/R^2** . One can argue that the filamentary shape of the discharge can be of particular importance here since it invalidates the assumption on the charge deposited and the assumed **spherical cavity** used in the previous estimate. **Only the tip of filament will be charged** and repelled. The charged surface S' will thus be smaller and so will be the total charge deposited Q' . However, the **field to screen remains the same**, the charge density still decreases as $1/R$ during the propagation. The overall behaviour of the filamentary cavity should remain the same compared as a spherical cavity. Only the discharge current is modified since the total charge to deposit is changed.

We assumed that the cavity is like a plane capacitor in respect with the point electrode, a spherical approximation described in a previous approximation for the cavity capacitance in respect to the point leads to the same behaviour, the dependence as a function of R is just not linear.

A charged interface on a **spherical cavity** will produce a different **field ahead of the cavity** on the liquid side compared to a **charged filaments tips**. This value of the field can be relevant for the propagation of the discharge. Moreover, it is unlikely that the cavity is expanding with **constant gas mass**, there should be some **vaporization process** going on. The discharge propagation mechanism is thus not only due to the repelling of the charged interface but also to some etching or vaporization process. The deposited charges at the interface **screen the electric field** within the cavity but lead to high electric field in the liquid ahead of the filament. This high

electric field creates local joule heating by conduction of solvated ion. The recombination of charges can also produce gaseous products and participates to the gas production process.

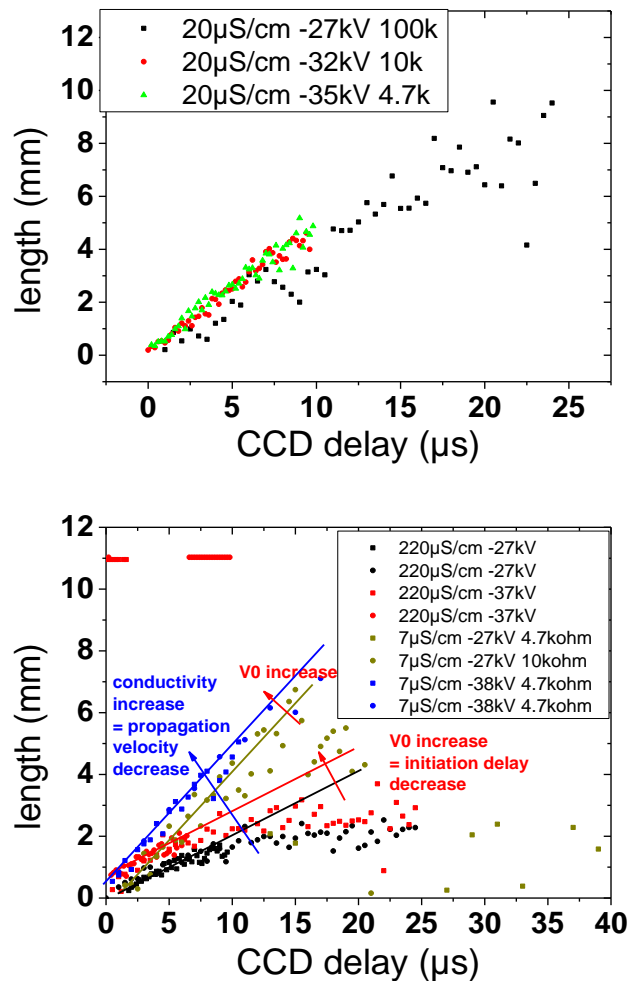


fig 5.27 propagation velocity determined with single iCCDs setup in emission imaging for different applied voltage

There is an influence of the applied voltage on the initiation delay of the discharge. **The discharge ignites earlier at larger applied voltage.** This behaviour is similar to the positive polarity case described in the previous chapter.

5.2.3.3 Influence of ionic conductivity on the stopping length and the propagation velocity

As in the positive polarity case, the ionic conductivity has the side effect to decrease the applied voltage halfwidth as shown in **fig 5.28**. The stopping length of the discharge decreases accordingly because the voltage falls below a threshold voltage as discussed in a positive polarity section. The **stopping length** is changed when the **pulse duration** is changed with all other experimental parameters identical as shown in **fig 5.29**. The stopping length is related to a **threshold voltage** at the tip required to sustain the discharge propagation.

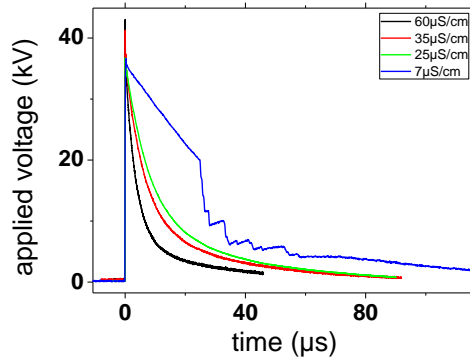
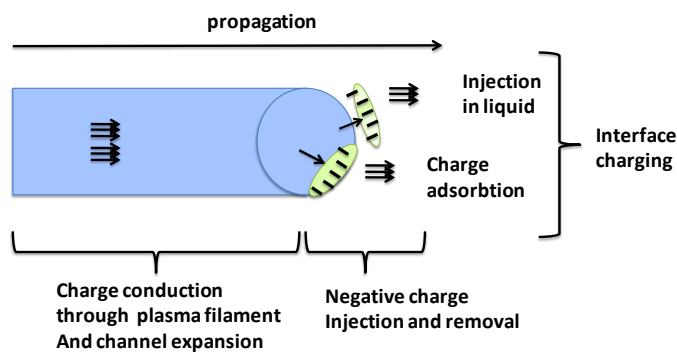


fig 5.28 voltage waveforms for different liquid conductivities, (inverted curves: applied voltage is negative)

The voltage decrease rate shown on fig 5.28 has no clear influence as in the case of the positive discharge. fig 5.30 shows that the **propagation velocity decreases with an increase of the liquid ionic conductivity**. The liquid conductivity influences the joule heating by conduction of solvated ions in the liquid ahead of the plasma filaments. Consequently a larger liquid conductivity would lead to a larger propagation velocity which is not the case.

It also influences the **removal rate of adsorbed negative ions on the gas/liquid interface**. It is not sure if the ions are stored on the liquid side or on the gas side of the interface. The ions can be adsorbed in the gas side as in the case of DBD discharge in gases where charges are adsorbed in the dielectric. Those charges incoming from the plasma can be physically adsorbed or stay in place because of polarisation of the material and attraction force due to the image charge. The charge deposited in the negative polarity should be negative and attached to heavy negative ions on the interface or dissolved into the liquid (which implies that the solvation time is faster than the removal time by conduction at solvated ionic mobility). This homocharge removal can be done by conduction or recombination. In both cases the low ionic conductivity prevents this charge recombination. The recombination occurs because of reaction of the negative ion adsorbed on the interface with a neutral molecule (charge exchange) or a positive ion. The removal by conduction is associated to the solvation of the adsorbed ion and its removal by conduction. The conduction process leading to **vanishing of the adsorbed charges occurs in a microsecond timescale** for typical mobility of $10\text{m}^2/\text{V}/\text{s}$ and field of $500\text{kV}/\text{cm}$ at the tip of the filament. This removal rate is consistent with the **period between two current peaks** required to have a potential difference between the interface and the point electrode sufficient to initiate a new gas phase streamer inside the cavity. This field should be close to the breakdown field observed in humid air at atmospheric pressure which is of some tens of kV/cm . In fact the exact pressure inside the cavity is not known, it should be close to atmospheric given the propagation timescale. The exact composition can differ from $\text{O}_2/\text{H}_2/\text{H}_2\text{O}_{\text{vap}}$ mixture because excited species do not have time to recombine completely from one peak to another peak.



The value of the field on the liquid side ahead of the adsorbed charges at the filament tip can be estimated by knowing the **surfactic charge** and the diameter of the filament. The diameter of the filament is typically $30\mu\text{m}$. At 1cm from the point electrode and 40kV applied voltage the surface charge density is $40\mu\text{C}/\text{m}^2$. Such a charge at the head of the filaments generates typically some tens of kV/cm $50\mu\text{m}$ ahead in the liquid. This value is required to estimate the removal rate of the adsorbed charges. The field ahead of the filament due to the adsorbed charges is also relevant for propagation mechanisms based on vaporization or charge acceleration ahead of the plasma filament tip.

Even if the surfactic **charge on the interface stays the same for different liquid conductivities** since it is associated to field screening, a lower recombination rate or removal rate will lead to slower decay of this charged interface. The **repelling/pushing of the interface due to electrostatic pressure** has the same amplitude but applies during a longer time. At this point one needs to understand how the charges are deposited on the interface and what is the deposition rate. A larger removal at the interface needs more plasma current to charge the interface at a surface charge value required for field screening.

A second important notion is that **charges can be deposited by discrete pulses** and not continuously, this can lead to a stepwise propagation instead of a continuous propagation. A pulsed charge deposition induces a pulsed pushing force, the propagation is thus stepwise. The removal rate of adsorbed charges dictates the **duration of the pushing periods**. The **duration of the pause periods** is dictated by the value of the electric field to screen and the interface capacitance. The **duty cycle** of pushing and pause phases leads a modification of the mean propagation velocity of the cavity. This explains why the **mean propagation velocity** decreases at larger liquid conductivity.

A closer examination of the behaviour of the **plasma current** as a function of the liquid conductivity is required here to corroborate the charged interface mechanism.

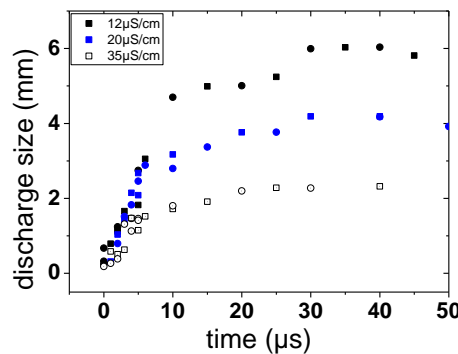


fig 5.29 stopping length depending on the liquid conductivity due to shorter pulse duration of fig 5.28.

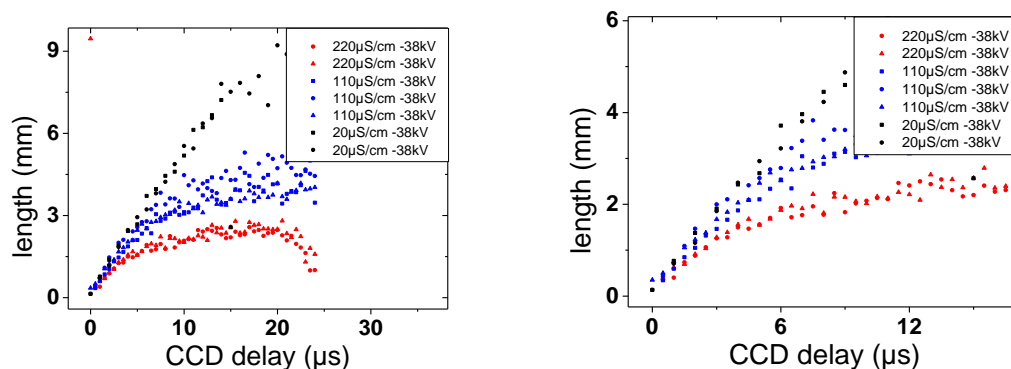


fig 5.30 velocity-growth for several conductivity, the propagation velocity remains constant across the gap until some transition, there is no real stopping length but rather a slower propagation, the initial velocity decreases slightly at high conductivity.

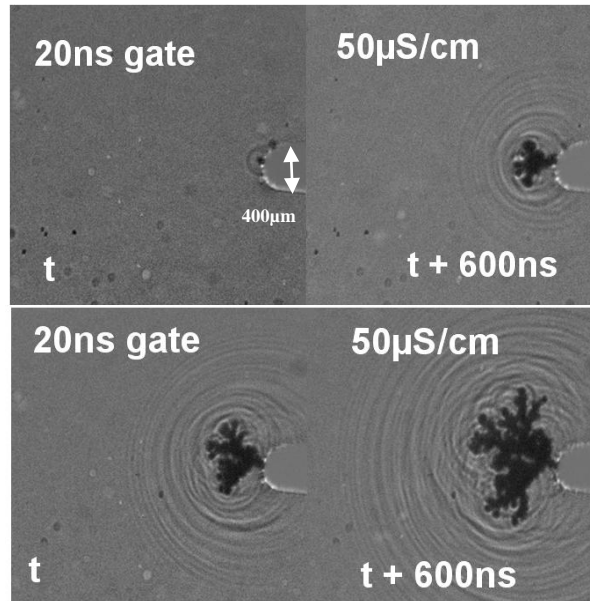


fig 5.31 shadow image of the negative plasma discharge in water, pair of images taken on the same single shot (20ns gate, 40kV), pin is 400μm diameter.

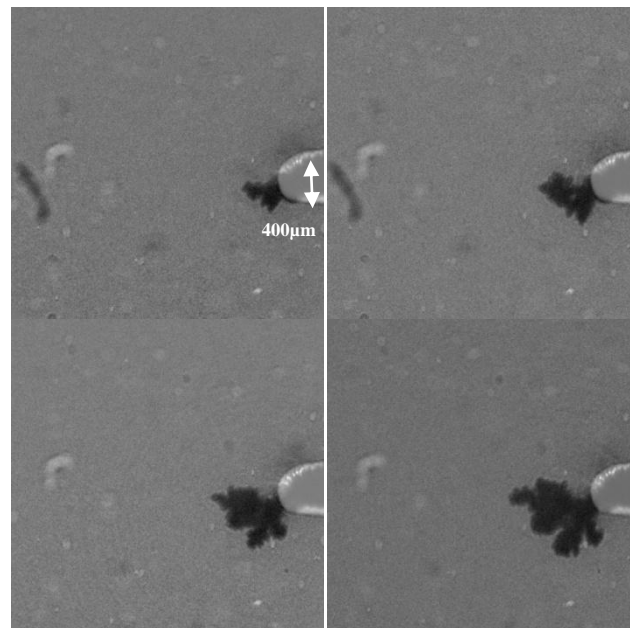


fig 5.32 pair of shadow image taken on the same single shot at negative polarity, for 500μS/cm water conductivity, pin is 400μm diameter.

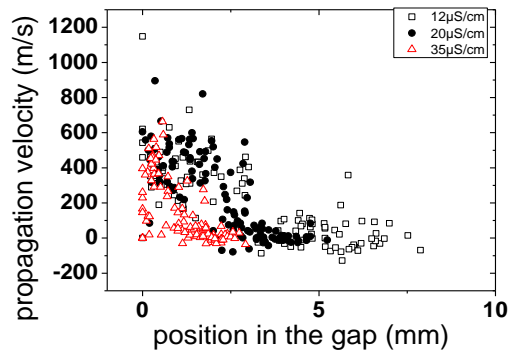


fig 5.33 propagation velocity determined with two iCCDs setup in emission imaging for different water conductivities.

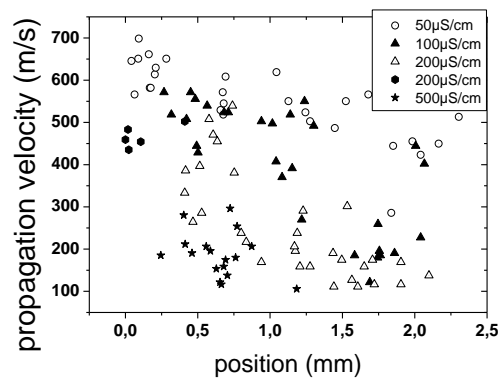


fig 5.34 propagation velocity determined with two iCCDs setup in shadow imaging and single shot images for different liquid conductivities .

5.2.4 Discharge current and reilluminations in the negative mode

The discharge current has a **resistive component** that follows the voltage pulse shape according to the reactor resistivity with is dictated by: the gap, the electrode surface, and the liquid ionic conductivity. The **plasma current is superimposed on this resistive component and is composed of current spikes** as shown in fig 5.35.

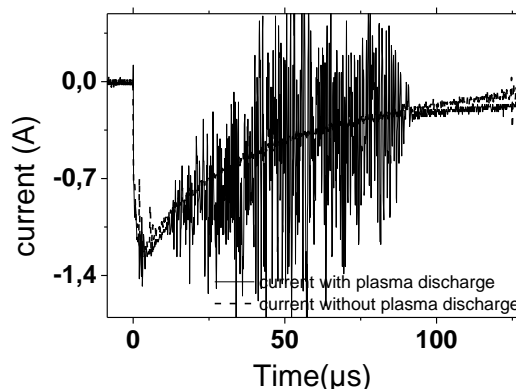


fig 5.35 current waveform without plasma and with plasma in negative voltage polarity, the waveform without plasma was obtained with voltage level just below plasma initiation threshold.

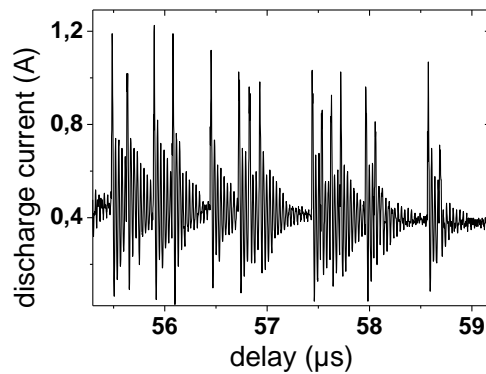


fig 5.36 current waveform for distilled water, zoom at the end of the pulse, chaotic repetition of spikes there is no long range regular frequency during the applied voltage pulse because of the superposition of each peak train emitted.

Those current impulsions have a typical **ringing shape**. The peak amplitude is of some Amps with 20ns duration, the ringing has a typical **LC damped** shape that lasts some hundreds of nanoseconds as shown in **fig 5.37**. The ringing itself can be physical and occur in the discharge or comes from the current detection circuit. Anyway this ringing is widely observed in gas phase discharges and DBDs. It most likely comes from a **LC resonance**. The L and C values come respectively from the probe inductance and the **stray** capacitance of the BNC cable between the probe and the scope.

In fact the **peak amplitude of some amperes** is very similar between the second mode of the positive discharge and this negative discharge and it is very possible that the propagation velocity difference is due to the duty cycle: the negative discharge has long pauses between two current impulsions and thus does not lead to a continuous pulse. A careful imaging analysis is required to distinguish if the propagation is stepwise and is correlated to the current peaks.

In the negative mode there is a **complete correlation between the discharge current spikes and the streak signal** during one shot. **Each plasma emission is associated with a current pulse**. The 2D iCCD images in **fig 5.37** prove that the whole gaseous structure is turned on and off periodically. The structure is turned on at a current spike and immediately turned off between spikes. **All the plasma discharge emits and not just a single filament** as in the reilluminations at positive polarity described in the previous chapter. The charges are thus deposited on the gas/liquid interface in a single pulse on the entire cavity surface.

The amplitude of this pulse should depend on the **amount of charge to deposit** which is dictated by the voltage and the **cavity capacitance**. The cavity capacitance is related to the cavity surface and the cavity "radius". A current of 1A during 20ns at 40kV is associated to an energy of **0.8mJ**, this energy leads to an interface capacitance of **1pF**. In plane to plane approximation it gives **1000mm²** for a 1cm discharge radius. Such a value is much higher than values that can be extrapolated from the projections in **fig 5.18** and **fig 5.19** with typically 20mm². It means that the criterion of roughness used for automatic binarisation in the data processing of **fig 5.18** and **fig 5.19** is not accurate and does not indicates the real value of the cavity surface.

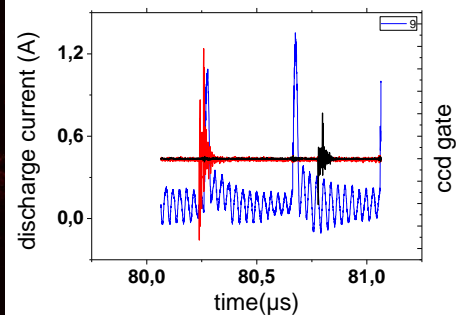
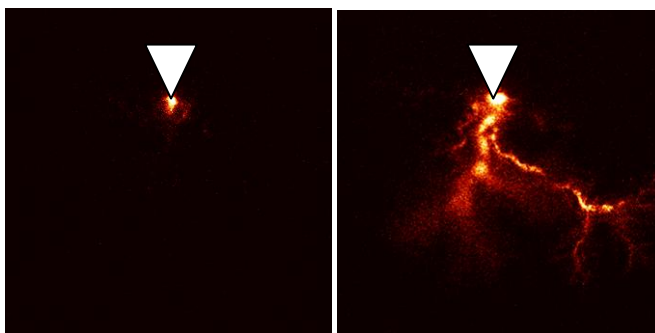
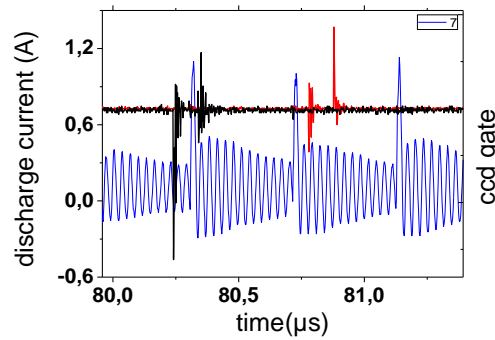
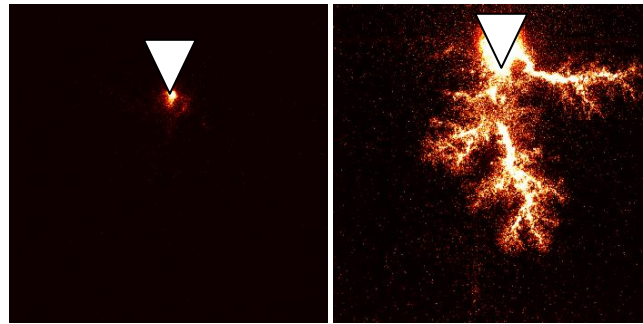


fig 5.37 reillumination in the negative mode, in fact the propagation is a succession of discrete plasma current impulsion superimposed on a resistive current baseline, the plasma is emitting only during the plasma current peaks, iCCD gates are marked by the red or black brackets

Those current impulsions are separated with some **frequency pattern**. Most of the time there is no clean frequency to identify as shown on **fig 5.36** but peaks **volbulations** can be observed on some shots. This pattern is not reproducible from one shot to another, but a general behaviour can be observed: the frequency decreases at low voltage at the end of the pulse. The frequency is high at the beginning of the pulse. Consequently the current peaks should be related to an electrical field screening and unscreening like Trichel pulses. Trichel pulses are a self pulsing regime where charges are injected into the medium faster than they can be removed. The pulsed nature of the current is the main clue for a charge deposition process on the gas/liquid interface of the cavity.

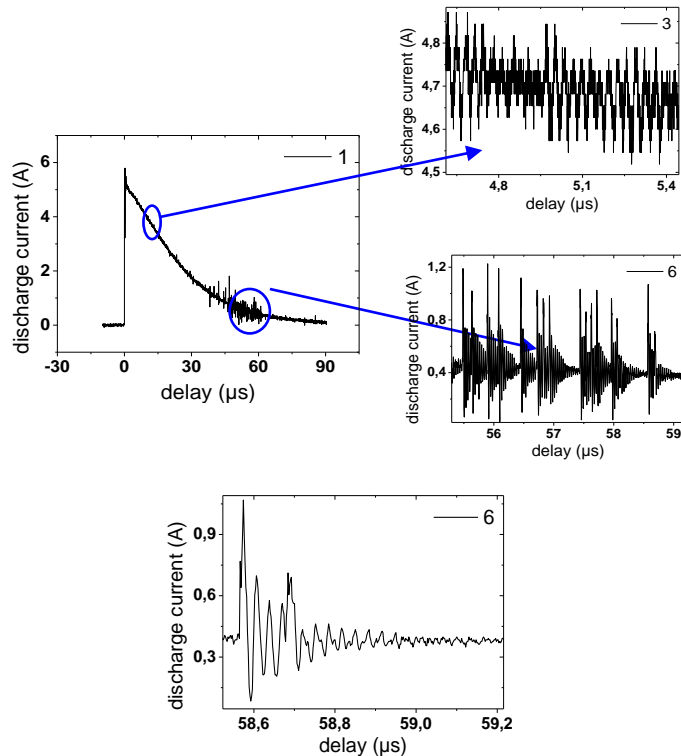


fig 5.38 the current spikes have ringing shape due to detection circuit response, the peaks are clearly distinguished at the end of the applied voltage pulse, the current peaks repetition frequency decreases with decreasing the applied voltage (with also means they are decreasing as the discharge propagates)

A single current peak is associated to many filaments and is equivalent to a transferred charge of **40nC**. There is thus some kind of synchronisation of all the filaments at all the branching nodes. Given the timescale of the pulse which lasts only **20ns** one can invoke a gas phase streamer occurring between the charged interface and the point electrode. In gas phase the typical value of transferred charges in a DBD is of 4nC per filament, thus the observed value of 40nC (~10 filaments) supports the gas phase streamer assumption. The stored charge on the interface is of negative polarity as mentioned above and the discharge reinitiates when the charge has decayed and the electric field is not screened any more. If the current peak really stops because of deposited charges screening the field inside the cavity, then the role of this gas phase streamer is to deposit a new amount of charges on the gas/liquid interface of the cavity. It would be a **negative streamer**. The propagation velocity of this fast discharge of 20ns inside the cavity has not been resolved in the present thesis. The divergent nature of the negative gas phase streamer explains why the plasma filament split at each branching node. Here there is probably no need to invoke photoionization or photodesorption processes to explain the “synchronisation” of all the cavity filaments during one current peak. Here we can also conclude that the cavity morphology dictates the plasma branching. the branching is explained by the interface motion instability or processes inside the liquid ahead the plasma filament tips.

The gaseous structure does not change much from one peak to the other or at least this changing was not resolved with emission imaging. The 2iCCD setup working in emission imaging in **fig 5.37** was not sufficient to discriminate a step propagation associated with the current peak. This has been further investigated with 2iCCDs shadow imaging.

5.2.5 Shock wave emission

Surprisingly the **negative mode also emits some shock waves**. They are **emitted from the tip of each main propagating filament** as can be seen on **fig 5.39**. However, the mean

propagation velocity of the **discharge is subsonic** as shown in the previous section. The waves are not emitted from the sides of the filaments.

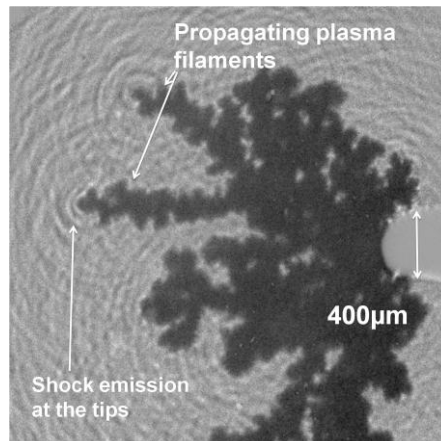


fig 5.39 shock wave emission at the tip of the propagating filaments in negative polarity, shadow image, high voltage tip on the right is 400μm diameter, (30ns gate, 30μs delay, 40kV, 1.4cm gap)

We carefully checked that experimental setup was exactly the same and the resolution and the contrast of the images was also identical to the study of the shock waves emitted with the positive discharge. This means that the **shock wave magnitude is lower in the case of the negative polarity**. The fact that there are shock waves in the negative polarity is quite surprising since the measured propagation velocity is in the range of 400-500m/s which is subsonic.

Those shock waves have a **circular pattern** and are emitted mainly at the propagating extremity of the filaments. The shock wave emission should be related to a fast or violent event during the propagation. It can be related to the discharge current impulsions. Thus it is likely that the negative mode has a stepwise propagation with **supersonic propagation phases and long pause phases** as discussed in the previous section dealing with the plasma current peaks. The shock waves are concentric and their center does not move much because the mean propagation velocity of the discharge is slower than the propagation velocity of the discharge. There are thus no shock wave tubes and cones as in the positive mode.

5.3 Conclusions on the negative polarity modes

5.3.1 On the low voltage saline discharge (QUB)

One can consider that the low voltage **QUB discharge** is a low voltage and high conductivity limiting case of the negative discharge where the cavity is **pushed only by thermal pressure and vaporization**. The driving force is not electrostatic pressure because of the large water conductivity that does not allow charge build-up at the interface. There are no filaments observed in the QUB discharge and the morphology of the high voltage negative discharge is less filamentary as the water conductivity is increased. The propagation velocity of the QUB discharge is of some **tens of m/s** whereas the HV discharge propagation velocity decreases as the water conductivity increases. The respective propagation mechanisms are not necessarily different between those two discharges and there can be a gradual change from low voltage /large conductivity and HV/low conductivity. The **driving mechanism can move gradually from an electrostatic pressure to thermal pressure/vaporization**. Intermediate case at medium water conductivity and medium voltage should be studied to really determine if those two discharges are really different modes.

5.3.2 On the point to plane HV discharge (Palaiseau)

The growth of the high voltage **negative discharge** is dictated by a **charged interface that explains both the morphology and propagation**. Propagation occurs because the **charged interface is repelled by the point electrode**. The **interface instability dictates the discharge channel thickness and branching through a EHD interface instability**.

The discharge current is not continuous and is correlated to a **DBD-like behaviour** of the discharge. The current peaks repetition rate is voltage and conductivity dependant. This supports the charged interface mechanism.

The **water conductivity has a clear influence on the discharge morphology and on the discharge propagation velocity**. At higher conductivity, the filaments are thinner, the gas cavity is less filamentary (or there are more filaments in a smaller volume) and propagation is more difficult. This further supports the charged interface interpretation.

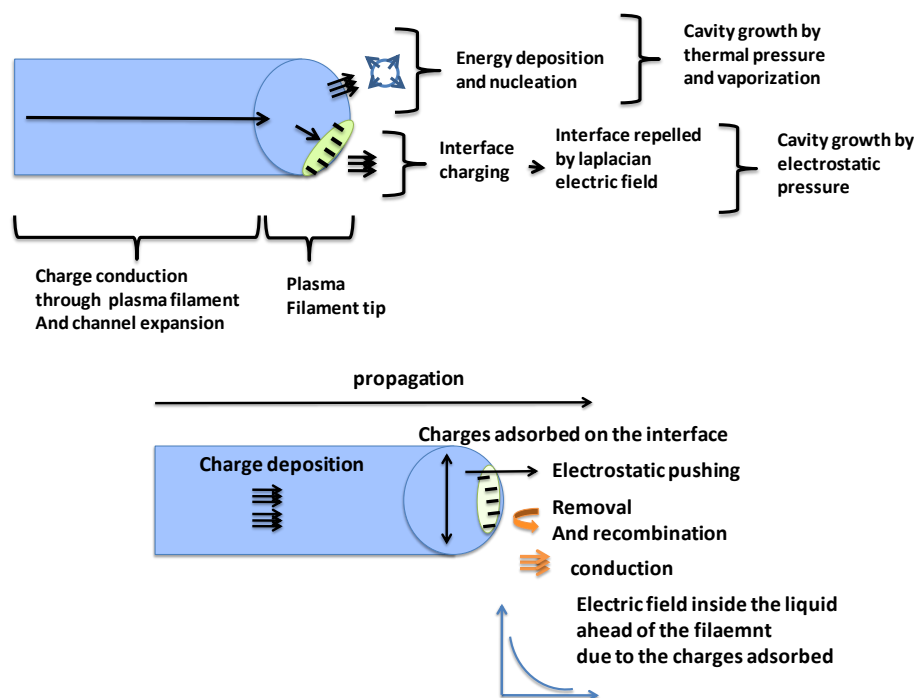
A closer examination of the **discharge morphology** at low water conductivity and large magnification shows that the filaments are clearly defined. It is difficult to assimilate them only to the result of an interface instability.

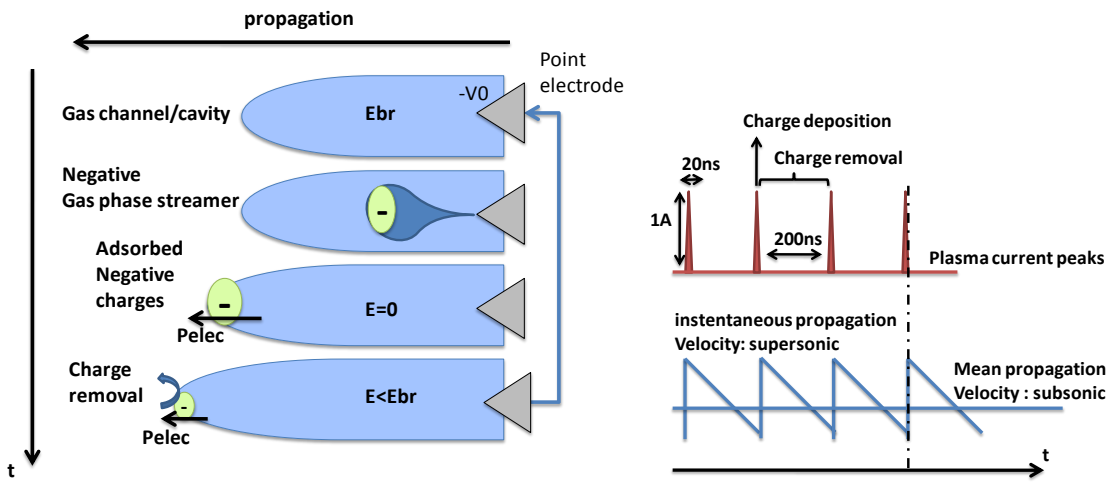
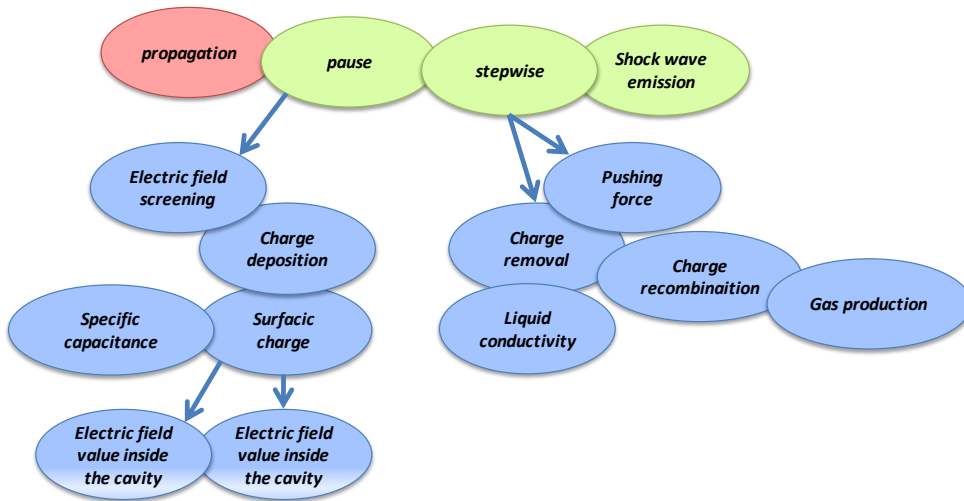
The behaviour of the **propagation velocity as a function of applied voltage** is surprising and is not consistent with a charged interface mechanism since it should depend on the square root of the applied voltage (inertia limited case). However, the applied voltage parameter needs to be investigated over a larger range and with a square waveform instead of a RC decay.

The fact that the **propagation remains constant across the gap** is a serious objection to the charged interface mechanism since the discharge radius should grow as $t^{1/2}$ (inertia limited case).

The **presence of adsorbed charge on the interface** lead to an instability as mentioned previously but also leads to **recombination processes** and **high electric field** region in the liquid ahead of the filament. This can contribute to **gas production**.

The **radius of the filament can be of particular importance to explain the propagation of this negative mode and the differences observed between the positive and the negative mode**.





6 General conclusions on the negative and the positive modes

The present thesis has **characterised different modes of plasma discharge inside water**. **Electrical and fast imaging** has been performed to achieve a detailed **time resolved study** of the discharge. We **focused on the water conductivity** which is an **unusual parameter** for discharge inside liquid and a very relevant parameter for chemical applications.

The combinations of **shadow measurement** and **spectroscopic measurements** have allowed to give some **insight on the physical mechanisms responsible for the discharge propagation inside a dense medium**.

In **positive polarity** the **shock wave** emission pattern indicates that the “continuous” phase preceding the **reilluminations** of the propagation is stepwise on the subnanosecond level. These reilluminations present a **DBD-like behaviour**. **Two modes can be identified during the continuous propagation: primary mode and secondary mode**. Those two modes have filamentary shape and exhibit branching. They can be distinguished by the current amplitude and the propagation velocity: respectively 100mA 3km/s, 10A 30km/s. The shock wave pattern emitted by the plasma structure during its propagation suggests that this continuous phase is in fact stepwise on a subnanosecond timescale. The shocks also give some insight on the **gas pressure** inside the gas channels that can be estimated to be in the range of **hundreds of bars**. The **rate of energy deposition** in the liquid ahead of the tip of the plasma filaments is responsible for this high pressure. Conversely this high pressure will have an influence on the plasma parameters in the filaments and its ability to supply energy from the point

Both positive and negative modes present some general similarities. The negative discharge is also filamentary as in the positive mode but the propagation mechanism is radically different since negative charges are deposited on the gas/liquid interface of the cavity whereas in positive polarity electrons are extracted from the liquid.

The water conductivity does not have the same influence on both modes. **The propagation is not modified in positive polarity whereas it slows down at higher conductivity in the case of negative polarity**.

The propagation velocity difference observed between the positive and the negative mode can result from a **difference of mechanism or a difference of morphology**. As shown in shadow images, the **diameter of the channels** is below 10nm for the positive discharge and tens of nanometers for the negative discharge. The **field amplification at the tip of the filament** is thus very different between the two and explains why the positive discharge is able to etch the liquid faster. The origin of the channel radius difference originates from the divergent or the convergent flux of electrons. This field amplification difference between the two modes induces a different rate of energy deposition and thus leads to a different pressure conditions at the nucleation site in front of the advancing channel and in the channel column itself.

Let us conclude by saying that this thesis represents a particularly detailed set of experiments and made a significant contribution to better understand the physics of the plasma state inside liquids.

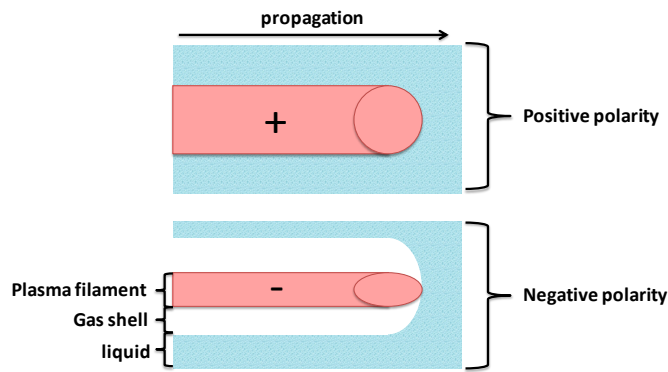


fig 6.1 the positive discharge directly in contact with the liquid, the plasma channel radius and the gas channel radius are almost identical, on the contrary for the negative discharge the plasma pulses occur in a gaseous cavity

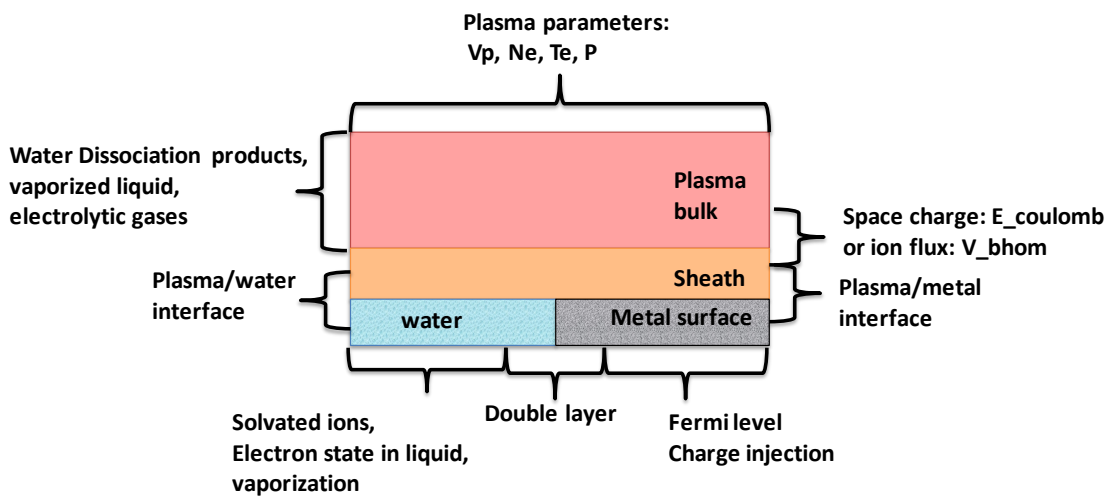


fig 6.2 the plasma/liquid interface differs from plasma/metal interface, it includes vaporization/etching/interface motion processes, charge injection/adsorption/removal, the conduction of charges and electronic states inside a liquid are also very different from a metal.

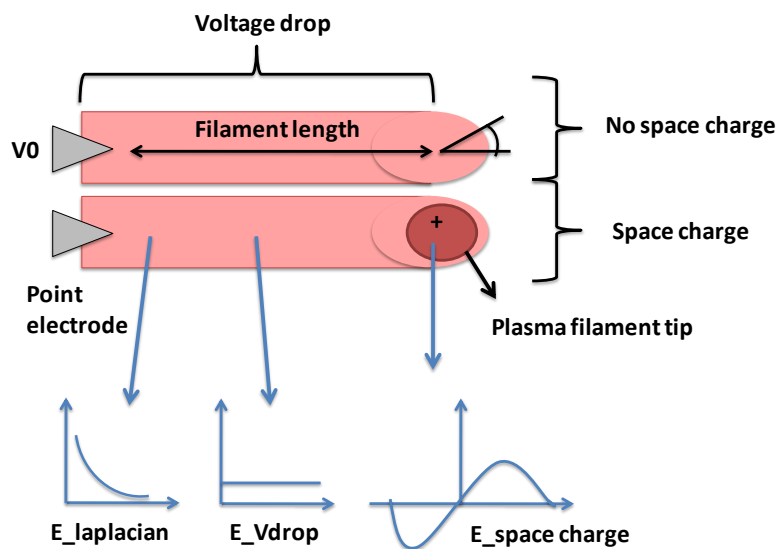


fig 6.3 presence of absence of space charge or adsorbed charges at the tip of the plasma filament, the electric field in the liquid ahead of the channel can be of primary importance for the propagation, its value depends if the plasma channel can be considered as a resistive conductor extending the point electrode potential or if there is a space charge at the filament tip.

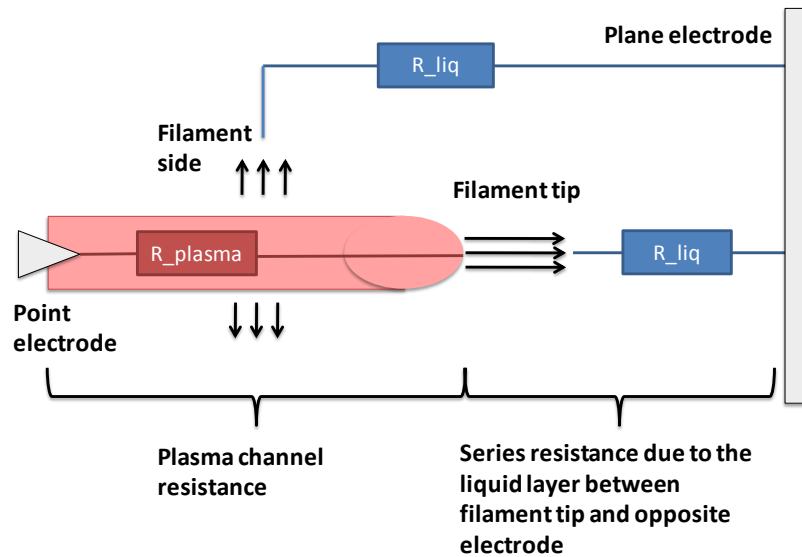


fig 6.4 the energy deposition at the plasma/liquid interface on the sides and at the tip of the filament is also limited by the plasma channel resistance and the liquid conductivity that constitutes a series resistance with the plasma filament. Filamentation process can be explained by: active head (adsorbed charges, sheath, or space charge) at the tip of the plasma filament, or interface instability (EHD, Taylor), or more efficient propagation with a lower radius of curvature of the tip of the plasma filament.

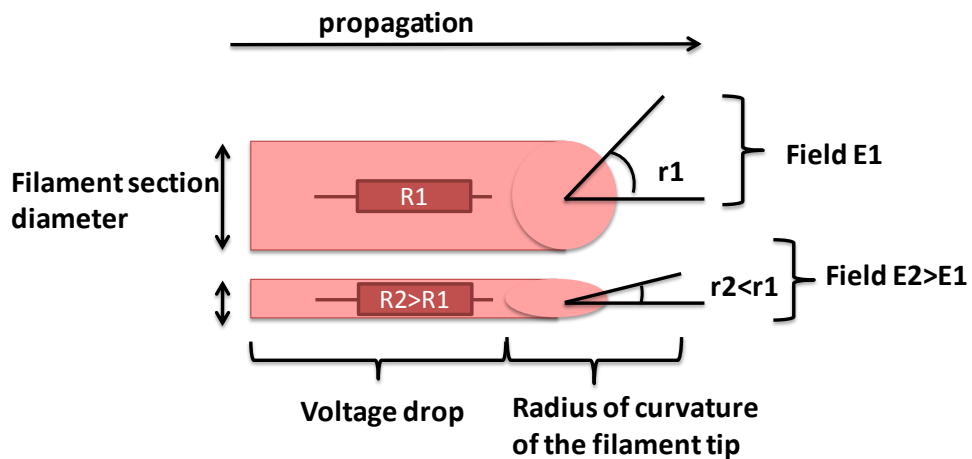


fig 6.5 channel diameter is of primary importance for the electric field value in the liquid ahead of the filament, the channel diameter is linked to the radius of curvature at the filament tip, channel diameter is a morphological properties that can influence the propagation.

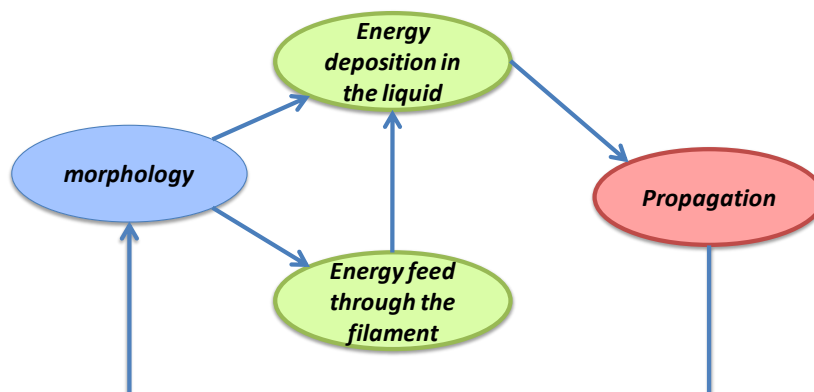


fig 6.6 discharge morphology is linked to the discharge propagation

7 references

Warning: lots of references are extracted from the recent book of Ushakov and are thus simply referenced as [Ushakov] inside the above report and not by the original author of each figure within this review.

[Ushakov]

Vasily Y. Ushakov et al

Impulse Breakdown of Liquids
Power Systems, Springer, 2007

This book is a review (mostly from Russian publications) about discharges inside dielectric liquids.

Other reference books:

[Raizer] Gas discharge Physics, Y.P.Raizer, Springer, 1991

[Lieberman] Principle of plasma discharges and material processing, Michael A. Lieberman,
Allan J. Lichtenberg

[Bluhm] pulsed power systems, Hansjoachim Bluhm, Springer, 2006

[Mesyats] pulsed power, Gennady A. Mesyats, Springer, 2005

NRL Pulsed power formulary

[Kuffel] High voltage engineering fundamentals, E. Kuffel, W.S. Zaengl, J. Kuffel 2nd edition,
2000

[Martin] Advances in Pulsed Power Technology, T.H. Martin, M. Williams, University of
Newcastle, NSW, Australia; M. Kristiansen, Texas Technical
University, Lubbock, USA, 1996

[Zeldovich] Physics of shock waves and high temperature hydrodynamic phenomena,
Ya.B.Zeldovich, Yu.P.Raizer, Academic presse New York and London, 1966.

The following are the main references read during the present PhD thesis and invoked in the present PhD report.

7.1 Plasma discharges inside water and liquids dielectrics

Ph.D. Thesis

Analysis of chemical reactions in pulsed streamer
discharges: an experimental study

MAYANK SAHNI

Department of Chemical Engineering of The Florida
State University
2006

Ph.D. Thesis

Water treatment by pulsed streamer corona
discharge

Petr LUKEŠ

Institute Of Chemical Technology, Prague
2001

Ph.D. Thesis

Etude expérimentale des phénomènes induits dans un
liquide par une injection fortement localisée d'énergie

Rachid QOTBA

université Joseph Fourier Grenoble 1
2005

Ph.D. Thesis

Contribution à l'étude de plasmas d'arc immergé,
applications à la décontamination et à la gazeification
d'effluents organiques aqueux

Université de Limoges

Nicolas BOUDESOCQUE

2007

Ph.D. Thesis

Modélisation de la décharge positive dans les grands
intervalles d'air

Issouf FOFANA

Ecole Centrale De Lyon
1996

Ph.D. Thesis

Contribution a l'étude des phénomènes de préclaquage dans les diélectriques liquides - modeles de génération et de propagation des streamers
NGnui Thomas AKA
Ecole Centrale De Lyon
2000

Ph.D. Thesis

caracterisation des décharges glissantes se propageant aux interfaces liquide-solide sous différentes formes de tension, relation entre propriété des matériaux et dimension fractale
lazhar Kebbabi
Ecole Centrale De Lyon
2006

Ph.D. Thesis

Chemical processes in aqueous phase pulsed electrical discharges: fundamental mechanisms and applications to organic compound degradation
SELMA MEDEDOVIC
Department of Chemical and Biomedical Engineering
The Florida State University
2007

[Abou-Ghazala2002]

A. Abou-Ghazala, S. Katsuki, Karl H. Schoenbach, F. C. Dobbs, and K. R. Moreira
Bacterial Decontamination of Water by Means of Pulsed-Corona Discharges
IEEE Transactions On Plasma Science 2002

[Adelhelm1999]

Christel Adelhelm, Britta Bergfeldt, Volker Neubert, Detlef Rusch, Christoph Schultheiss, Ralf Straessner
Inertisation of municipal solid waste incinerator ashes with electrodynamically generated, underwater shockwaves
IEEE 1999

[Aka-Ngnui]

T. Aka-Ngnui and A. Beroual
Modelling of Positive Streamers Propagation in Transformer Oil

[Aka-Ngnui2001]

T. Aka-Ngnui and A. Beroual
Modeling of branching streamers propagating within dielectric liquids
Annual Report Conference on Electrical Insulation and Dielectric Phenomena 2001

[Aka-Ngnui2002]

T. Aka-Ngnui, A. Beroual and Ph. Auriol
A Predicting Model for Branching Streamers Propagating in Liquid Dielectrics using a Computation Electrical Network
ICDL 2002

[Akiyama2000]

H. Akiyama

Streamer Discharges in Liquids and their Applications
IEEE Transactions on Dielectrics and Electrical Insulation 2000

[Akiyama2002]

H. Akiyama, S. Katsuki, T. Namihira, K. Ishibashi and N. Kiyosaki
production of large, volume discharges in water and their industrial applications
IEEE Transactions on Dielectrics and Electrical Insulation 2002

[An2007]

Wladimir An, Kurt Baumung, and Hansjoachim Bluhm
Underwater streamer propagation analyzed from detailed measurements of pressure release
JOURNAL OF APPLIED PHYSICS 2007

[Anpilov2002]

A.M. Anpilov, E.M. Barkhudarov, N. Christofi, V.A. Kopev, I.A. Kossyi, M.I. Taktakishvili and Y. Zadiraka
Pulsed high voltage electric discharge disinfection of microbially contaminated liquids
Letters in Applied Microbiology 2002

[Appleton]

A.T. Appleton, P. Lukes, W.C. Finney and B.R. Locke
study of the effectiveness of different hybrid pulsed corona reactors in degrading aqueous pollutants

[Ataka1996]

Ken-ichi Ataka, Takao Yotsuyanagi, and Masatoshi Osawa
Potential-Dependent Reorientation of Water Molecules at an Electrode/Electrolyte Interface Studied by Surface-Enhanced infrared Absorption Spectroscopy
J. Phys. Chem. 1996

[Atrazhev]

V.M. Atrazhev
Review of investigations of streamers in dense gases and liquids by computer simulation
IEEE

[Atrazhev 1991]

V. M. Atrazhev, E. G Dmitriev and I. T. Iakubov
The Impact Ionization and Electrical Breakdown Strength for Atomic and Molecular Liquids
IEEE transactions on Electrical Insulation Vol. 26 No. 4, August 1991

[Atrazhev1998]

V. M. Atrazhev I. V. Timoshkin
Transport of Electrons in Atomic Liquids in High Electric Fields
IEEE Transactions on Dielectrics and Electrical Insulation 1998

[Babaeva2008]

Natalia Yu. Babaeva and Mark J. Kushner

Consequences of inhomogeneities on branching of streamers in high pressure gases
Escampig 2008

[Baerdemaeker2005]

F. De Baerdemaeker, M. Monte, and C. Leys
Capillary Underwater Discharges
IEEE TRANSACTIONS ON PLASMA SCIENCE 2005

[Baerdemaeker2006]

F. De Baerdemaeker, M. Simek, J. Schmidt, C. Leys
Time resolved optical and electrical characteristics of capillary underwater discharges 2006

[Baerdemaeker2006]

F. De Baerdemaeker, M. Simek, M. Clupek, P. Lukes, C. Leys
Hydrogen peroxide production in capillary underwater discharges
Czech. J. Phys. 2006

[Baerdemaeker2007]

F De Baerdemaeker, M. Simek, J Schmidt and C Leys
Characteristics of ac capillary discharge produced in electrically conductive water solution
Plasma Sources Sci. Technol. 2007

[Beroual]

A. Beroual and C. Hrosseau
Step Propagation of Filamentary Streamers in Dielectric Liquids

[Beroual1988]

A. Beroual, C. Marteau and R. TobazCon
Behavior of Streamers in Liquids under Step Voltages in Point-Plane Geometry
IEEE Transactions on Electrical Insulation 1988

[Beroual1988]

Beroual, C. Marteau and R. Tobazeon.
Measurement of the Charge of a Single or of a Series of Streamers in Liquids Subjected to a Voltage Step A.
IEEE transactions on Electrical Insulation 1988

[Beroual1993]

A. Beroual
spectral analysis of light emitted by streamers and gas chromatography in liquid dielectric
Jpn J Appl Phys 1993

[Beroual1998]

A. Beroual
Propagation and Structure of Streamers in liquid Dielectrics
IEEE Electrical Insulation Magazine 1998

[Beroual2002]

A. Beroual,
influence of additives and hydrostatic pressure on streamers initiation and dielectric strength of liquids
annual report conference on electrical insulation and dielectric phenomena 2002

[Bonifaci1995]

N. Bonifaci, A. Denat, V. M Atrazhev
Onset Voltage for Corona Pulses in Gaseous A under High Pressure and in Liquid A
IEEE Transactions on Dielectrics and Electrical Insulation 1995

[Bonifaci1997]

N. Bonifaci, A. Denat and B. Malraison
Transport phenomena in point-plane geometry in dense argon
Journal of Electrostatics 1997

[Bonifaci2006]

N. Bonifaci, A. Dena, P.E. Frayssines
Application de la spectroscopie demission a l'etude des decharges electriques dans les liquides
Journal of Electrostatics 2006

[Bonifaci2008]

Z. Li, N. Bonifaci, A. Denat, V.M. Atrazhev, V.V. Atrazhev
Ionization and charge transport phenomena in liquid helium induced by corona discharge
Journal of Electrostatics 2008

[Boussaton2005]

M.P. Boussaton, S. Coquillat, S. Chauzy, J.F. Georgis
Influence of water conductivity on micro-discharges from raindrops in strong electric fields
Atmospheric Research 2005

[Briggs1994]

A. C. T. Briggs, A. Beroual, and F. Buret
The Dynamics of dc Predisruption in Liquid Insulating Media
IEEE Transactions on Dielectrics and Electrical Insulation Vol. 1 No. 3, June 1994

[Brosseau]

C.Brosseau, A.Beroual
prebreakdown phenomena in a dielectric liquid.

[Brosseau1993]

C.Brosseau, A.Beroual
Optical investigation of high-field conduction and prebreakdown phenomena in a dielectric liquid.
1993

[Brosseau1994]

C. Brosseau and A. Beroual
Optical Investigation of High-field Conduction and Prebreakdown in a Dielectric Liquid
IEEE Transactions on Dielectrics and Electrical Insulation 1994

[Bruggeman2006]

P. J. Bruggeman and C. A. Leys
Electrical breakdown of a bubble in a water-filled capillary
Journal Of Applied Physics 99, 2006

[Bruggeman2007]

- P. Bruggeman, C. Leys, J. Vierendeels**
experimental investigation of DC electrical breakdown of long vapour bubble in capillaries
J Phys D appl phys 2007
- [Bruggeman2007]**
Peter Bruggeman, Leigh Graham, Joris Degroote, Jan Vierendeels and Christophe Leys
Water surface deformation in strong electrical fields and its influence on electrical breakdown in a metal pin–water electrode system
J. Phys. D: Appl. Phys. 2007
- [Bruggeman2007]**
P. Bruggeman, J. Degroote, C. Leys, J. Vierendeels
Plasma characteristics in air and vapor bubbles in water.
ICPIG 2007
- [Bruggeman2008]**
Peter Bruggeman, Jingjing Liu, Joris Degroote, Michael G Kong, Jan Vierendeels and Christophe Leys
Dc excited glow discharges in atmospheric pressure air in pin-to-water electrode systems
J. Phys. D: Appl. Phys. 2008
- [Bruggeman2009]**
Peter Bruggeman, Daan Schram, Manuel A Gonzalez, Robby Rego, Michael G Kong and Christophe Leys
Characterization of a direct dc-excited discharge in water by optical emission spectroscopy
Plasma Sources Sci. Technol. 2009
- [Bruggeman2009]**
Peter Bruggeman and Christophe Leys
TOPICAL REVIEW Non-thermal plasmas in and in contact with liquids
J. Phys. D: Appl. Phys. 2009
- [Brujan2006]**
Emil-Alexandru Brujan And Alfred Vogel
Stress wave emission and cavitation bubble dynamics by nanosecond optical breakdown in a tissue phantom
J. Fluid Mech. 2006
- [Carnell1997]**
M. T. Carnell, S. J. Barrington, and D. C. Emmony
A phase-inverting parabolic concentrator for the generation of negative waves in water
J. Acoust. Soc. Am. 1997
- [Cevallos2003]**
Michael D. Cevallos, James C. Dickens, Andreas A. Neuber, Mark A. Haustein, and Hermann G. Krompholz
Self electrical breakdown in biodegradable oil
IEEE 2003
- [Chadband1965]**
W. G. Chadband, G. T. Wright
A pre-breakdown phenomenon in the liquid dielectric hexane
BRIT. J. APPL. PHYS., 1965
- [Chadband1985]**
W. G. Chadband and T. M. Sufian
experimental support for a model of positive streamer propagation in liquid insulation
IEEE Transactions on Electrical Insulation 1985
- [Chadband1988]**
W. G. Chadband
The Ubiquitous Positive Streamer
IEEE Transactions on Electrical Insulation 1988
- [Chadband1991]**
W G Chadband
Electrical breakdown-from liquid to amorphous solid
J. Phys. D: Appl. Phys. 1991
- [Chadband]**
W.G. Chadband
electrical breakdown of liquid insulation
- [Chadband]**
W.G. Chadband
the positive streamer as the link between breakdown processes in gases and liquids
IEEE
- [Chadband]**
W.G. Chadband
From bubbles to breakdown, or vice-versa
- [Champion2003]**
C Champion
Theoretical cross sections for electron collisions in water: structure of electron tracks
Phys. Med. Biol. 2003
- [Date2006]**
H. Date, K.L. Sutherland, T. Hayashib, Y. Matsuzakic, Y. Kiyanagi
Inelastic collision processes of low-energy protons in liquid water
Radiation Physics and Chemistry 2006
- [Date2007]**
H. Date, K.L. Sutherland, H. Hasegawa, M. Shimozuma
Ionization and excitation collision processes of electrons in liquid water
Nuclear Instruments and Methods in Physics Research B 2007
- [Denaro1958]**
A. R. Denaro and A. Hickling
Glow-Discharge Electrolysis in Aqueous Solutions
Journal Of The Electrochemical Society 1958
- [Denat1988]**
A. Denat, J. P. Gosse, and B. Gosse
Electrical Conduction of Purified Cyclohexane in a Divergent Electric Field
IEEE Transactions on Electrical Insulation 1988

[Denat2002]

A. Denat, F. Jomni, F. Aitken and N. Bonifaci
Thermally and Electrically Induced Bubbles in Liquid Argon and Nitrogen
IEEE Transactions on Dielectrics and Electrical Insulation 2002

[Denat]

Denat
High field conduction and prebreakdown phenomena in dielectric liquids.
IEEE

[Devins1982]

J. C. Devins and S. J. Rzad
Streamer propagation in liquids and over Liquid-solid interfaces
IEEE Transactions on Electrical Insulation Vol. EI-17 No.6, 1982

[Dumitrescu2001]

L. Dumitrescu, O. Lesaint, N. Bonifaci, A. Denat, P. Notingher
Study of streamer inception in cyclohexane with a sensitive charge measurement technique under impulse voltage
Journal of Electrostatics 2001

[Dyakonov1988]

M I Dyakonov, V Yu Kachorovskii
Theory of streamer discharge in semiconductors
1988

[Ershov]

A.P. Ershov, A.L. Kupershtokh
Fluctuation model of liquid dielectrics breakdown with incomplete charge relaxation

[Farzaneh2004]

M Farzaneh and I Fofana
Experimental study and analysis of corona discharge parameters on an ice surface
J. Phys. D: Appl. Phys. 2004

[Felici]

N. J. Felici
Blazing a Fiery Trail with the Hounds
IEEE Transactions on Electrical Insulation 1988

[Fofana1998]

I. Foffana, A. Beroual
predischarge models in dielectric liquids
Jpn J Appl Phys vol 37 1998

[Forster1985]

E. O. Forster
The 1985 j. B. Whitehead memorial lecture: Critical assessment of the electrical breakdown Process in dielectric fluids
IEEE Transactions on Electrical Insulation 1985

[Frayssines2002]

P.E. Frayssines, O. Lesaint, N. Bonifaci, A. Denat, F. Devaux

Prebreakdown and Breakdown Phenomena Under Uniform Field in Liquid Nitrogen
ICDL 2002

[Frayssines2002]

P E Frayssines, N Bonifaci, A Denat and O Lesaint
Streamers in liquid nitrogen: characterization and spectroscopic determination of gaseous filament temperature and electron density
J. Phys. D: Appl. Phys. 2002

[Frayssines2003]

P. E. Frayssines, O. Lesaint, N. Bonifaci, A. Denat, F. Devaux
Prebreakdown and Breakdown Phenomena Under Uniform Field in Liquid Nitrogen and Comparison with Mineral Oil
IEEE Transactions on Dielectrics and Electrical Insulation 2003

[Fry1999]

L. H. Fry, P. Adair, Jr., R. Williams
Long life sparker for pulse powered underwater acoustic transducer
IEEE 1999

[Gao2001]

Jinzhang Gao, Zhongai Hu, Xiaoyan Wang, Jingguo Hou, Xiaoquan Lu, Jingwan Kang
Oxidative degradation of acridine orange induced by plasma with contact glow discharge electrolysis
Thin Solid Films 2001

[Gao2003]

Jinzhang Gao, Yongjun Liu, Wu Yang, Lumei Pu, Jie Yu and Quanfang Lu
Oxidative degradation of phenol in aqueous electrolyte induced by plasma from a direct glow discharge
Plasma Sources Sci. Technol. 2003

[Gavrilov1994]

I. M. Gavrilov, V. R. Kukhta, V. V. Lopatin, P. G. Petrov
Dynamics of Prebreakdown Phenomena in a Uniform Field in Water
IEEE Transactions on Dielectrics and Electrical Insulation 1994

[Gerhold1988]

J. Gerhold
Helium Breakdown near the Critical State
IEEE Transactions on Electrical Insulation 1988

[Glaze1982]

William H. Glaze, Gary R. Peyton, Simon Lin, R. Y. Huang, and Jimmie L. Burieson
Destruction of Pollutants in Water with Ozone in Combination with Ultraviolet Radiation.
Environ. Sci. Technol. 1982

[Gogate2004]

Parag R.Gogate, Aniruddha B.Pandit

A review of imperative technologies for wastewater treatment I: oxidation technologies at ambient conditions

Advances in Environmental Research 2004

[Graham2007]

W.G. Graham and K R Stalder

Plasmas in saline solution

Journal of Physics: Conference Series 2007

[Grymonpre2001]

David R. Grymonpré, Amit K. Sharma, Wright C.

Finney, Bruce R. Locke

The role of Fentons reaction in aqueous phase pulsed streamer corona reactors

Chemical Engineering Journal 2001

[Grymonpre2003]

David R. Grymonpre, Wright C. Finney, Ronald J.

Clark and Bruce R. Locke

Suspended Activated Carbon Particles and Ozone Formation in Aqueous-Phase Pulsed Corona Discharge Reactors

Ind. Eng. Chem. Res. 2003

[Haidara1991]

M. Haidara, A. Denat

Electron Multiplication in Liquid Cyclohexane and Propane An Estimation of the Ionization Coefficient

IEEE transactions on Electrical Insulation 1991

[Hancock2003]

Patrick Hancock, Randy Curry and Kenneth

McDonald

Megawatt, Pulsed Ultraviolet Photon Sources For Microbial Inactivation

IEEE 2003

[Hart1962]

Edwinj. Hart, J. W. Boag

Absorption Spectrum of the Hydrated Electron in Water and in Aqueous Solutions

1962

[Hayashi2000]

D Hayashi, W F L M Hoeben, G Dooms, E M van

Veldhuizen, W R Rutgers and G M W Kroesen

Influence of gaseous atmosphere on corona-induced degradation of aqueous phenol

J. Phys. D: Appl. Phys. 2000

[He2005]

Zhengguang He, Junshen Liu, Weimin Cai

The important role of the hydroxy ion in phenol removal using pulsed corona discharge

Journal of Electrostatics 63 2005

[Hemmert2003]

D. Hemmert, K. Shiraki, T. Yokoyama, S. KatsukiS, H.

Bluhm, and H. Akiyama, H. Ito and Y. Imaizumi

optical diagnostics of shock waves generated by a pulsed streamer discharge in water

IEEE Transactions on Dielectrics and Elctrical Insulation 2003

[Hirai1999]

N.Hirai. K.Arii. Kikuchi, T.Masaoka and H.Nitanda

measurement of hole mobility in dielectric liquids

J. Phys. D: Appl. Phys. 1999

[Hiroki2002]

Akihiro Hiroki, Simon M. Pimblott, and Jay A.

Laverne

Hydrogen Peroxide Production in the Radiolysis of Water with High Radical Scavenger Concentrations

J. Phys. Chem. A, 106, 2002

[Hoeben]

W F L M Hoeben, E M van Veldhuizen, W R Rutgers

and G M W Kroesen

Gas phase corona discharges for oxidation of phenol in an aqueous solution

[Hoeben2000]

W F L M Hoeben, E M van Veldhuizen, W R Rutgers, C

A M G Cramers and G M W Kroesen

The degradation of aqueous phenol solutions by pulsed positive corona discharges

Plasma Sources Sci. Technol. 2000

[Holzer2006]

Frank Holzer and Bruce R. Locke

Influence of Electrode Geometry and Material on the Discharge in the Gas and Liquid Phases of a Hybrid

Series Reactor

[Ihara1999]

Satoshi IHARA, Tomoaki MIICHI, Saburoh SATOH,

Chobei YAMABE and Eiji SAKAI

Ozone Generation by a Discharge in Bubbled Water

Jpn. J. Appl. Phys. Vol. 1999

[Ingebrigtsen2007]

S Ingebrigtsen, L E Lundgaard and P-O Åstrand

Effects of additives on prebreakdown phenomena in liquid cyclohexane: II. Streamer propagation

J. Phys. D: Appl. Phys. 2007

[Ingebrigtsen2008]

S Ingebrigtsen, N Bonifaci, A Denat and O Lesaint

Spectral analysis of the light emitted from streamers in chlorinated alkane and alkene liquids

J. Phys. D: Appl. Phys. 2008

[Jomni1997]

F. Jomni, A. Denat

Viscosity Effect on the Dynamics of Small Bubbles Generated by Electrical Current Pulse in Viscous Insulating Liquids

IEEE Annual Report - Conference on Electrical Insulation and Dielectric Phenomena, 1997

[Jonah1976]

C. D. Jonah, M. S. Matheson, J. R. Miller, and E. J. Hart
Yield and Decay of the Hydrated Electron from 100 ps to 3 ns
The Journal of Physical Chemistry 1976

[Jonah1977]
Charles D. Jonah; John R. Miller, and Max S. Matheson
The Reaction of the Precursor of the Hydrated Electron with Electron Scavengers
The Journal of Physical Chemistry 1977

[Jones1994]
H. M. Jones and E. E. Kunhardt
The Influence of Pressure and Conductivity on the Pulsed Breakdown of Water
IEEE Transactions on Dielectrics and Electrical Insulation 1994

[Jones1995]
H M Jones and E E Kunhardt
Development of pulsed dielectric I breakdown in liquids
J. Phys. D Appl. Phys. 1995

[Jones1996]
H. M. Jones and E. E. Kunhardt
Evolution of Cathode Initiated Pulsed Dielectric Breakdown in Polar and Nonpolar Liquids
ICDL 1996

[Jones1996]
H. M. Jones and E. E. Kunhardt
Nanosecond Pre-Breakdown and Breakdown Phenomena in Water: Influence of Pressure, Conductivity, and Ionic Sheath Formation
ICDL 1996

[Joshi1995]
A.A. Joshi, B.R. Locke, P. Arce, W.C. Finney
Formation of hydroxyl radicals, hydrogen peroxide and aqueous electrons by pulsed streamer corona discharge in aqueous solution
Journal of Hazardous Materials 1995

[Joshi2003]
R. P. Joshi, J. Qian, J. Kolb, K. H. Schoenbach
model analysis of breakdown in high-voltage, water-based switches
IEEE Transactions on Dielectrics and Electrical Insulation 2003

[Joshi2003]
R. P. Joshi, J. Qian, S. Katsuki, K. H. Schoenbach, E. Schamiloglu
Electrical Conduction in Water Revisited: Roles of Field-Enhanced Dissociation and A Reaction-Based Boundary Condition
IEEE Transactions on Dielectrics and Electrical Insulation 2003

[Joshi2004]

R. P. Joshi, J. Qian, G. Zhao, J. Kolb, and K. H. Schoenbach, E. Schamiloglu and J. Gaudet
Are microbubbles necessary for the breakdown of liquid water subjected to a submicrosecond pulse
Journal Of Applied Physics 2004

[Joshi2007]
K N Joshipura, Sumona Gangopadhyay, C G Limbachiya and Minaxi Vinodkumar
Electron impact ionization of water molecules in ice and liquid phases
Journal of Physics: Conference Series 2007

[Kabashima2001]
Hajime Kabashima, Hisahiro Einaga, and Shigeru Futamura
Hydrogen Generation from Water, Methane, and Methanol with Nonthermal Plasma
IEEE 2001

[Kao1958]
H. Sueda and K. C. Kao
Determination of electric field distributions along fluid-solid dielectric interfaces using a schlieren technique
IEEE Transactions on Electrical Insulation 1958

[Kao1976]
Kwan C. Kao
Theory of High-Field Electric Conduction and Breakdown in Dielectric Liquids
IEEE Transactions On Electrical Insulation 1976

[Katsuki2002]
Sunao Katsuki, Hidenori Akiyama, Amr Abou-Ghazala and Karl H. Schoenbach
Parallel Streamer Discharges Between Wire and Plane Electrodes in Water
IEEE Transactions on Dielectrics and Electrical Insulation 2002

[Katsuki2002]
S. Katsuki, S. Xiao, R.P. Joshi, M. Laroussi, and K.H. Schoenbach
Electrical breakdown of sub-millimeter water gaps
IEEE Transactions on Electrical Insulation 2002

[Katsuki2002]
S. Katsuki
bacterial decontamination of water by means of pulsed corona discharges
IEEE Transactions on Electrical Insulation 2002

[Kattan1991]
R. Kattan, A. Denat and N. Bonifaci
Formation of Vapor Bubbles in Non-polar Liquids Initiated by Current Pulses
IEEE Transactions on Electrical Insulation 1991

[Kebbabi2006]
L Kebbabi and A Beroual

Fractal analysis of creeping discharge patterns propagating at solid/liquid interfaces: influence of the nature and geometry of solid insulators
J. Phys. D: Appl. Phys. 2006

[Kim2006]

M. Kim and R. E. Hebner
Initiation from a Point Anode in a Dielectric Liquid
IEEE Transactions on Dielectrics and Electrical Insulation 2006

[Klimkin]

V.F.Klimkin
super high speed anode prebreakdown phenomena in liquid dielectrics under uniform fields

[Klimkin]

V.F.Klimkin
on mechanisms to increase electric strength of n-hexane in micron gaps

[Klimkin]

V.F.Klimkin
a pulsed electrical breakdown in n-hexane under uniform field

[Klimkin]

V.F.Klimkin
multiframe high speed laser schlieren system for observations of prebreakdown phenomena in nanosecond region

[Klimkin1993]

V.F. Klimkin, A.L. Kupershtokh
Statistical lag time in fluctuation model of liquid dielectric breakdown and experimental results
1993

[Klimkin1999]

V. F. Klimkin
Bubble Generation Model for Initiating Breakdown from Anode in n-Hexane with Quasi-Uniform Electrical Fields
Proceedings of 13th International Conference on Dielectric Liquids 1999

[Kolb2003]

J. Kolb, S. Kono, S. Xiao, B. Goan, XP. Lu, C. Bickes, M. Laroussi, R.P. Joshi, K.H. Schoenbach
water and propylene carbonate as storage and switching media in pulsed power systems
IEEE Transactions on Dielectrics and Electrical Insulation 2003

[Kolb2008]

J F Kolb, R P Joshi, S Xiao and K H Schoenbach
Streamers in water and other dielectric liquids
J. Phys. D: Appl. Phys. 2008

[Korobeynikov1992]

S.M.Korobeynikov
Bubble model of pulse breakdown in liquids
1992

[Krasucki1966]

Z. Krasucki
Breakdown of liquid dielectrics
1966

[Krcma]

František Krcma, Zdenka Stará
The Investigation of Chemical Processes Initiated by the Diaphragm Discharge in Liquids

[Kukhta1996]

Kukhta V., Lopatin V.
Discharge propagation in water in non-uniform field.
ICDL 1996

[Kukhta1998]

Kukhta V.R., Lopatin V.V.
Inception and development prebreakdown cavities in water
Proceedings ICDL 1998

[Kuraica2004]

Milorad M. Kuraica, Bratislav M. Obradovic, Dragan Manojlovic, Daliborka R. Ostojic, Jagos Puric
Ozonized water generator based on coaxial dielectric-barrier-discharge in air
Vacuum 73 2004

[Kuretz]

V. Kuretz, G. Filatov, A. Yushkov
Initiation of Electric Discharge in High-Conducting Mediums
Pulsed power applications, poster session

[Kuskova1998]

N. I.Kuskova, S. I. Tkachenko
To the theory of the streamer discharge in condensed media
IEEE International Symposium on Electrical Insulation, Arlington, Virginia, USA, June 7-10, 1998

[Kusic2005]

Hrvoje Kusic, Natalij Koprivana, Bruce R. Locke
Decomposition of phenol by hybrid gas/liquid electrical discharge reactors with zeolite catalysts
Journal of Hazardous Materials 2005

[Laroussi]

Dr.Mounir Laroussi, et al
Energy Storage and Electrical Breakdown in Liquids
Second Annual Review on Compact Portable Pulsed Power

[Larsson2001]

A. Larsson, A. Sunesson, J. Garmer and S. Kroll
Laser-Triggered Electrical Breakdown in Liquid Dielectrics Imaging of the Process by the Shadowing Technique
IEEE Transactions on Dielectrics and Electrical Insulation 2001

[Laverne1993]

Jay A. Laverne and Hiroko Yoshida

Production of the Hydrated Electron in the Radiolysis of Water with Helium Ions
J. Phys. Chem. 1993

[Leckbee]

**Joshua Leckbee, Randy Curry, and Ken McDonald
Ray Cravey and Allen Grimmis**

An advanced model of a high pressure liquid dielectric switch for directed energy applications
Journal of chemical chemistry

[Lee2003]

Han Y. Lee, Han N. Choi, Yoon J. Jung and Han S. Uhm, Bang K. Kang

Sewage sludge treatment by arc discharge
2003

[Lee2006]

Changha Lee, Yunho Lee, Jeyong Yoon

Oxidative degradation of dimethylsulfoxide by locally concentrated hydroxyl radicals in streamer corona discharge process
Chemosphere 2006

[Lehr2003]

JM Lehr, JE Maenchen, JR Woodworth, WA Johnson

Multi-megavolt water breakdown experiments
IEEE 2003

[Lesaint1991]

O. Lesaint, P. Gournay and R. TobazCon

Investigations on Transient Currents Associated with Streamer Propagation in Dielectric Liquids
IEEE Transactions on Electrical Insulation 1991

[Lesaint1994]

O. Lesaint and P. Gournay

Initiation and Propagation Thresholds of Positive Prebreakdown Phenomena in Hydrocarbon Liquids
IEEE Transactions on Dielectrics and Electrical Insulation 1994

[Lesaint1998]

O. Lesaint and G. Massala

Positive Streamer Propagation in Large Oil gaps
Experimental Characterization of Propagation Modes
IEEE Transactions on Dielectrics and Electrical Insulation 1998

[Lesaint2000]

O Lesaint and M Jung

On the relationship between streamer branching and propagation in liquids: influence of pyrene in cyclohexane
J. Phys. D: Appl. Phys. 2000

[Lewis1994]

T. J. Lewis

Basic Electrical Processes in Dielectric Liquids
IEEE transactions on Dielectrics and Electrical Insulation 1994

[Lewis1996]

T. J. Lewis, J. P. Llewellyn, M. J. van der Sluijs, J. Freestone and R. N. Hampton

A new model for electrical ageing and breakdown in dielectrics
International Conference on Dielectric Materials Measurements & Applications 1996

[Lewis1998]

T. J. Lewis

A New Model for the Primary Process of Electrical Breakdown in Liquids
IEEE Transactions on Dielectrics and Electrical Insulation June 1998

[Lewis2002]

T. J. Lewis

The Electrode-Liquid Interface under High Fields
ICDL 2002

[Lewis2003]

T. J. Lewis

Breakdown Initiating Mechanisms at Electrode Interfaces in Liquids
IEEE Transactions on Dielectrics and Electrical Insulation 2003

[Li2006]

Jie Li, Masayuki Sato, Takayuki Ohshima

Degradation of phenol in water using a gas-liquid phase pulsed discharge plasma reactor
Thin Solid Films 2006

[Lisitsyn1999]

Igor V. Lisitsyn Hiroaki Nomiya, Sunao Katsuki, and Hidenori Akiyama

Streamer discharge reactor for water treatment by pulsed power
Review Of Scientific Instruments 1999

[Lisitsyn1999]

I. V. Lisitsyn, H. Nomiya, S. Katsuki, H. Akiyama

Thermal Processes in a Streamer Discharge in Water
IEEE Transactions on Dielectrics and Electrical Insulation 1999

[Lisitsyn1999]

I.V. Lisitsyn, H. Nomiya, S. Katsuki

Water treatment by pulsed streamer discharges
IEEE 1999

[Lih98]

D. Lih and JS. C. Kao

The Energy Distribution of Dipoles and Its Relation to The behaviour of Solids
IEEE Transactions on Electrical Insulation 1998

[Locke2006]

B. R. Locke, M. Sato, P. Sunka, M. R. Hoffmann, J.-S. Chang

Electrohydraulic Discharge and Nonthermal Plasma for Water Treatment
Ind. Eng. Chem. Res. 2006

[Lojewsk1999]

D. Lojewsk, M. Kristiansen, L. Hatfield, and G. Engelt
Experimental investigations of high voltage breakdown in water
1999

[Lukes2002]

P. Lukes, M. Clupek, P. Sunka, V. Babick, V. Janda
effect of ceramic composition on pulse discharge induced processes in water using ceramic-coated wire to cylinder electrode system
Czechoslovak Journal of Physics 2002

[Lukes2005]

Petr Lukes and Bruce R. Locke
Degradation of Substituted Phenols in a Hybrid Gas-Liquid Electrical Discharge Reactor
Ind. Eng. Chem. Res. 2005

[Lukes2005]

Petr Lukes, Martin Clupek, Vaclav Babicky, Vaclav Janda and Pavel Sunka
Generation of ozone by pulsed corona discharge over water surface in hybrid gas-liquid electrical discharge reactor
J. Phys. D: Appl. Phys. 2005

[Lukes2005]

Petr Lukes and Bruce R Locke
Plasmachemical oxidation processes in a hybrid gas-liquid electrical discharge reactor
J. Phys. D: Appl. Phys. 2005

[Lukes2005]

P. Lukes, V. Babicky, M. Clupek and P. Sunka
Bipolar high voltage pulse power generator
2005 Pulsed Power Conference poster session

[Magureanu]

M. Magureanu, N.B. Mandache
Corona discharge for oxidation of organic compounds in water

[Malik2001]

Muhammad Arif Malik, Abdul Ghaffar and Salman Akbar Malik
Water purification by electrical discharges
Plasma Sources Sci. Technol. 2001

[Malik2002]

Muhammad Arif Malik, Ubaid-ur-Rehman, Abdul Ghaffar and Kurshid Ahmed
Synergistic effect of pulsed corona discharges and ozonation on decolorization of methylene blue in water
Plasma Sources Sci. Technol. 2002

[Malik2003]

Muhammad Arif Malik
Synergistic effect of plasmacatalyst and ozone in a pulsed corona discharge reactor on the decomposition of organic pollutants in water

Plasma Sources Sci. Technol. 2003

[Malik2005]

Muhammad Arif Malik, Yasushi Minamitani, Shu Xiao, Juergen F. Kolb, Karl H. Schoenbach,
Streamers in Water Filled Wire-Cylinder and Packed-Bed Reactors
IEEE Transactions On Plasma Science 2005

[Massala1998]

G. Massala and O. Lesaint
Positive Streamer Propagation in Large Oil Gaps
Electrical Properties of Streamers
IEEE Transactions on Dielectrics and Electrical Insulation 1998

[Massala2001]

G Massala and O Lesaint
A comparison of negative and positive streamers in mineral oil at large gaps
J. Phys. D: Appl. Phys. 2001

[Maximov2006]

A. I. Maximov · L. A. Kuzmicheva · A. Y. Nikiforov, J. V. Titova
The Observation of Plasma Structures in Electrolyte Solution
Plasma Chem Plasma Process 2006

[Melcher1969]

J. R. Melcher
electrohydrodynamic charge relaxation and interfacial perpendicular field instability
the physics of fluids 1969

[Miichi2000]

T. Miichi , S. Ihara, S. Satoh, C. Yamabe
Spectroscopic measurements of discharges inside bubbles in water
Vacuum 2000

[Mizeraczyk2006]

J. mizeraczyk, M. Dors, E. Metel, Y.S. Mok
Gas phase corona discharge for phenol oxidation in water
2006

[Munoz2007]

Muñoz, J. C. Oller, F. Blanco, J. D. Gorfinkiel, P. Limão-Vieira, and G. García
Electron-scattering cross sections and stopping powers in H₂O
PHYSICAL REVIEW A 2007

[Munoz]

A. Munoz, F. Blancob, G. Garcia, P.A. Thorne, M.J. Brungere,
J.P. Sullivand, S.J. Buckman
Single electron tracks in water vapour for energies below 100 eV

[Namihira2003]

T. Namihira, D. Wang, T. Takashima, S. Katsuki and H. Akiyama

water purification using pulsed streamer discharges in micro-bubbled water
IEEE Transactions on Dielectrics and Electrical Insulation 2003

[Namihira2005]

t. namihira, t. yamaguchi, k. yamamoto, j. choi, t. kiyon, t. sakugawa, S. Katsuki and H. Akiyama
characteristics of pulsed discharge plasma in water
IEEE Transactions on Dielectrics and Electrical Insulation 2005

[Niemeyer1983]

L Niemeyer and F Pinnekamp
Leader discharges in SF₆,
J. Phys. D: Appl. Phys. 1983

[Niemeyer1984]

L.Niemeyer
fractal dimension of dielectric breakdown
physical review letters 1984

[Nikiforov2007]

A Yu Nikiforov and Ch Leys
Influence of capillary geometry and applied voltage on hydrogen peroxide and OH radical formation in ac underwater electrical discharges
Plasma Sources Sci. Technol. 2007

[Njatawidjaja2005]

Ellyana Njatawidjaja, Anto Tri Sugiarto, Takayuki Ohshima, Masayuki Sato
Decoloration of electrostatically atomized organic dye by the pulsed streamer corona discharge
Journal of Electrostatics 2005

[Norgard2003]

P. Norgard, R. Curry, K. McDonald
A high pressure, rep-rate liquid-dielectric switch test stand
2003

[Perkowski2002]

Jan Perkowski, Stanisław Ledakowicz
Decomposition of Anthraquinone Dye in the Aqueous Solution by Ozone, Hydrogen Peroxide or UV Radiation
Fibres & Textiles in Eastern Europe 2002

[Perkowski2003]

Jan Perkowski, Lech Kos
Decolouration of Model Dyehouse Wastewater with Advanced Oxidation Processes
Fibres & Textiles in Eastern Europe 2003

[Pompili2005]

M. Pompili, C. Mazzetti, R. Bartnikas
Partial Discharge Pulse Sequence Patterns and Cavity Development Times in Transformer Oils under ac Conditions

IEEE Transactions on Dielectrics and Electrical Insulation 2005

[Qian2005]

J. Qian, R. P. Joshi, J. Kolb, and K. H. Schoenbach, J. Dickens, et al
Microbubble-based model analysis of liquid breakdown initiation by a submicrosecond pulse
Journal Of Applied Physics 2005

[Ridah1988]

S. Ridah
Shock waves in water
J. Appl. Phys. 64 1988

[Rodríguez-Méndez2006]

B. G. Rodríguez-Méndez, et al
A model of plasma discharges in pre-arcing regime for water treatment
IASTED international conference 2006

[Sadeghzadeh-Araghi1991]

M. Sadeghzadeh-Araghi, M. I. Qureshi, W. G. Chadband, P. K. Watson
Measurement of the Growth of Cavities and of EHD Instabilities during the Negative-point Breakdown of Silicone Fluids
IEEE transactions on Electrical Insulation 1991

[Sahni2006]

Mayank Sahni, Bruce R. Locke
Degradation of chemical warfare agent simulants using gas-liquid pulsed streamer discharges
Journal of Hazardous Materials 2006

[Schaffer2002]

Chris B. Schaffer, Nozomi Nishimura, Eli N. Glezer, Albert M.-T. Kim, and Eric Mazur
Dynamics of femtosecond laser-induced breakdown in water from femtoseconds to microseconds
Optics Express 201 2002

[Schoenbach2008]

Karl Schoenbach, Juergen Kolb, Shu Xiao, Sunao Katsuki, Yasushi Minamitani, and Ravindra Joshi
Electrical breakdown of water in microgaps
Plasma Sources Sci. Technol. 2008

[Sekiguchi2004]

Hidetoshi Sekiguchi, Kazunori Yamagata
Effect of liquid film on decomposition of CFC-12 using dielectric barrier discharge
Thin Solid Films 2004

[Sengupta1997]

Susanta K. Sengupta, Ashok K. Sfvastava, Rajeshwar Singh
Contact glow discharge electrolysis: a study on its origin in the light of the theory of hydrodynamic instabilities in local solvent vaporisation by Joule heating during electrolysis
Journal of Electroanalytical Chemistry 1997

[Sengupta1999]

Susanta K. Sengupta, Rajeshwar Singh, and Ashok K. Srivastava

A Study on the Origin of Nonfaradaic Behavior of Anodic Contact Glow Discharge Electrolysis, The Relationship Between Power Dissipated in Glow Discharges and Nonfaradaic Yields
J. Electrochem. Soc 1998

[Stalder2005]

Kenneth R Stalder, Donald F McMillen, JeanWoloszko
Electrosurgical plasmas
J. Phys. D: Appl. Phys. 2005

[Stara2005]

Z. Stará, F. Krcma

Influence of OH radicals on Organic Dyes in DC Diaphragm Discharge in Water Solutions
ICPIG 2005

[Strauss1999]

M. Strauss, M. Friedman, E. Gurewitz, P. Amendt, R. A. London, M. E. Glinsky

Two-Dimensional Rayleigh Model of Vapor Bubble Evolution
Photonics West Symposium San Jose, 1999

[Stricklett1991]

K. L. Stricklett, C. Fenimore, E. F. Kelley, H. Yamashita, A. L. Wintenber, I. Alexeff

Observation of Partial Discharge in Hexane under High Magnification
IEEE transactions on Electrical Insulation 1991

[Sugiarto2001]

Anto Tri Sugiarto, Masayuki Sato and Jan D Skalny

Transient regime of pulsed breakdown in low-conductive water solutions
J. Phys. D: Appl. Phys. 2001

[Sugiarto2002]

Anto Tri Sugiarto, Takayuki Ohshima, Masayuki Sato

Advanced oxidation processes using pulsed streamer corona discharge in water
Thin Solid Films 2002

[Sugiarto2003]

Anto Tri Sugiarto, Shunsuke Ito, Takayuki Ohshima, Masayuki Sato,, Jan D. Skalny

Oxidative decoloration of dyes by pulsed discharge plasma in water
Journal of Electrostatics 2003

[Sun1997]

Bing Sun, Masayuki Sato, J. Sid Clements

Optical study of active species produced by a pulsed streamer corona discharge in water
Journal of Electrostatics 1997

[Sun1998]

B. Sun, M. Sato,, A. Harano, J.S. Clements

Non-uniform pulse discharge-induced radical production in distilled water

Journal of Electrostatics 1998

[Sun1999]

Bing Sun, Masayuki Sato and J S Clements

Use of a pulsed high-voltage discharge for removal of organic compounds in aqueous solution, review
J. Phys. D: Appl. Phys. 1999

[Sun2000]

B Sun, M sato, Clements

Oxidative Processes Occurring When Pulsed High Voltage Discharges Degrade Phenol in Aqueous Solution
Environ. Sci. Technol. 2000

[Sunka1999]

P Sunka, V Babicky, M C lupek, P Lukes, M Simek, J Schmidt and M Cernak

Generation of chemically active species by electrical discharges in water
Plasma Sources Sci. Technol. 1999

[Sunka2002]

P. Sunka, M. Fuciman, V. Babickj, M. Clupek, J. Bene, I PouEkovi, J. SouEek

Generation of focused shock waves by multi-channel electrical discharges in water
IEEE 2002

[Sunka2004]

Pavel Sunka, Václav Babický, Martin C lupek, Jirí Benes, and Pavla Poucková

Localized Damage of Tissues Induced by Focused Shock Waves
IEEE Transactions On Plasma Science 2004

[Sunka2004]

P. Sunka, V. Babicky, M. Clupek, M. Fuciman, P. Lukes, M. Simek, J. Benes, B. Lockey, Z. Majcherovaz

Potential applications of pulse electrical discharges in water
acta physica slovacica 2004

[Sunka2005]

P. Šunka, V. Babický, M. Clupek, P. Lukeš, M. Šimek and B. R. Locke

Potential applications of pulse electrical discharges in water
ICPIG 2005

[Tezuka1999]

M. Tezuka, M. Iwasaki

Liquid-phase reactions induced by gaseous plasma. Decomposition of benzoic acids in aqueous solution
Plasmas & ions 1999

[Thomas1964]

J. K. Thomas, Sheffield Gordon, and Edwin J. Hart

The Rates of Reaction of the Hydrated Electron in Aqueous Inorganic Solutions
The Journal of Physical Chemistry

[Tobazkon1994]

- R. Tobazkon**
Prebreakdown Phenomena in Dielectric Liquids
IEEE Transactions on Dielectrics and Electrical
Insulation 1994
- [Tomita2001]**
Y. Tomita, M. Tsubota and N. An-naka
Energy evaluation of shock wave emission and bubble
generation by laser focusing in liquid nitrogen
CAV2001
- [Toney1994]**
M F Toney
voltage dependant ordering of water molecule at an
electrode electrolyte interface
letters to nature nature 328 1994
- [Touya2006]**
**G Touya, T Reess, L Pecastaing, A Gibert and P
Domens**
Development of subsonic electrical discharges in
water and measurements of the associated pressure
waves
J. Phys. D: Appl. Phys. 2006
- [Tsukamoto2002]**
tsukamoto, namihira
an analysis of pulsed streamer discharge using a high
speed camera
IEEE Transactions on Dielectrics and Elctrical
Insulation 2002
- [Vaught1995]**
A. Vaught, T.W. Jing, S.M. Lindsay
Non-exponential tunneling in water near an electrode
Chemical Physics Letters 1995
- [Vega2003]**
F. Vega, A.T. Perez
Corona-induced electrohydrodynamic instabilities in
low conducting liquids
Experiments in Fluids 2003
- [Wanga2006]**
Huijuan Wanga, Jie Lib and Xie Quana
Decoloration of azo dye by a multi-needle-to-plate
high-voltage pulsed corona discharge system in water
Journal of Electrostatics 2006
- [Watson1965]**
D. B. Watson, W. Heyes, K. C1. Kao, J. H. Calderwood
Some Aspects of Dielectric Breakdown of Solids
IEEE Transactions On Electrical Insulation 1965
- [Watson1985]**
P. K. Watson
Bubble growth following a localized electrical
discharge and its relationship to the breakdown of
triggered spark gaps in liquids
IEEE Transactions on Electrical Insulation 1985
- [Watson1988]**
P. Keith Watson and W. G. Chadband
The Dynamics of Pre-Breakdown Cavities in Viscous
Silicone Fluids in Negative Point-Plane Gaps
IEEE Transactions on Electrical Insulation 1988
- [Watson1991]**
**P. Keith Watson, W. G. Chadband, M. Sadeghzadeh-
Araghi**
The Role of Electrostatic and Hydrodynamic Forces in
the Negative-point Breakdown of Liquid Dielectrics
IEEE Transactions on Electrical Insulation 1991
- [Watson]**
**P. Keith Watson. Towfick Sufian, W.G. (Bill)
Chadband**
A thermal model of positive pre-breakdown
streamers in insulating liquids
- [Watson]**
**P. Keith Watson, Towfick Sufian2,W .G.
(Bill)Chadband, isanao Yamashita**
The growth and collapse of streamer channels in
insulating liquids
- [Wen2002]**
Yuezhong Wen, Xuanzhen Jiang, and Weiping Liu
Degradation of 4-Chlorophenol by High-Voltage Pulse
Corona Discharges Combined with Ozone
Plasma Chemistry and Plasma Processing 2002
- [Wen2005]**
**Yue Zhong Wen, Hui Jun Liu, Wei Ping Liu and Xuan
Zhen Jiang**
Degradation of Organic Contaminants in Water by
Pulsed Corona Discharge
Plasma Chemistry and Plasma Processing 2005
- [Wetz2003]**
**D. Wetz, K. Truman, J. Dickens, J. Mankowski, and A.
Neuber**
Short pulse electric field sterilization of liquid media
IEEE 2003
- [Wolozko2002]**
Jean Wolozko, Kenneth R. Stalder, Ian G. Brown
Plasma Characteristics of Repetively-Pulsed Electrical
Discharges in Saline Solutions Used for Surgical
Procedures
IEEE Transactions On Plasma Science 2002
- [Woodworth2003]**
**J. R. Woodworth, J. Lehr, P. A. Miller, B. Aragon, J.
Elizondo-Decanini, W. Fowler, J. E. Maenchen, G. S.
Sarkisov, J. Corley, K. Hodge, S. Drennan, D. Guthrie,
G. Mowrer, M. Navarro, D. L. Johnson**
Optical diagnostics of 4-MV water switches in the 220
test facility
IEEE 2003
- [Xiao2004]**
S. Xiao, J. Kolb, S. Kono, S. Katsuki
High Power Water Switches: Postbreakdown
Phenomena and Dielectric Recovery

IEEE Transactions on Dielectrics and Electrical Insulation 2004

[Yamada1990]

Hiroshi Yamada, Tadashi Sato and Tamiya Fujiwara
High-speed photography of prebreakdown phenomena in dielectric liquids under highly non-uniform field conditions
J. Phys. D: Appl. Phys. 1990

[Yamatake2004]

Atsushi YAMATAKE, Koichi YASUOKA and Shozo ISHII
Ozone Generation by a DC Driven Micro-Hollow Cathode Discharge in Nitrogen-Mixed Oxygen Flow
Japanese Journal of Applied Physics 2004

[Yamatake2006]

Atsushi Yamatake, Jeremy Fletcher, Koichi Yasuoka, Shozo Ishii
Water Treatment by Fast Oxygen Radical Flow With DC-Driven Microhollow Cathode Discharge
IEEE Transactions On Plasma Science 2006

[Yamatake2006]

Atsushi YAMATAKE, et al
Characteristics of Pulsed Arc Electrohydraulic Discharge for Eccentric Electrode Cylindrical Reactor using Phosphate-Buffered Saline Water
Japanese Journal of Applied Physics 2006

[Yan2005]

Jian-hua Yan, Chang-ming Du, Xiao-dong Li, Xiao-dan Sun, Ming-jiang Ni, Ke-fa Cen1 and Bruno Cheron
Plasma chemical degradation of phenol in solution by gas-liquid gliding arc discharge
Plasma Sources Sci. Technol. 2005

[Yang2005]

Bin Yang, Minghua Zhou, Lecheng Lei

Synergistic effects of liquid and gas phase discharges using pulsed high voltage for dyes degradation in the presence of oxygen
Chemosphere 2005

[Yan2006]

Keping Yan, Ruinian Li, Tianle Zhu, Hongdi Zhang, Xiaotu Hu, Xuedong Jiang, Hui Liang, Ruichang Qiu, Yi Wang
A semi-wet technological process for flue gas desulfurization by corona discharges at an industrial scale
Chemical Engineering Journal 2006

[Yanshin]

E. V. Yanshin, S. M. Korobeynikov, I. T. Ovchinnikov, S. G. Sarin, K. V. Yanshin, V. M. Kopylov, and A. V. Klepikov
Physical processes limiting the pulse energy release in liquid dielectrics

[Yerokhin1999]

A.L. Yerokhin, X. Nie, A. Leyland, A. Matthews, S.J. Dowey
Review : Plasma electrolysis for surface engineering
Surface and Coatings Technology 1999

[Zakharov2007]

A G Zakharov, A I Maksimov, Yu V Titova
Physicochemical properties of plasma - solution systems and prospects for their use in technology
Russian Chemical Reviews 2007

[Zhang2005]

C.H. Zhang, T. Namihira, T. Kiyan, K. Nakashima, S. Katsuki, H. Akiyama, H. Ito and Y. Imaizumi
Investigation of shockwave produced by large volume pulsed discharge under water
IEEE Transactions on Dielectrics and Electrical Insulation 2005

7.2 Streamers in gases, DBD, ozone production

Phd thesis

Etude experimentale des décharges électriques impulsives nanoseconde à pression atmosphérique, application au traitement des effluents gazeux et à la décontamination de surface
Julien Jarrige
Université De Rouen
2008

[Babaeva1997]

Natalya Yu. Babaeva and George V. Naidis
Dynamics of Positive and Negative Streamers in Air in Weak Uniform Electric Fields
IEEE Transactions On Plasma Science 1997

[Babaeva2004]

N Yu Babaeva, J K Lee and H C Kim

Non-stationary charging of a dust grain in decaying streamer-channel plasma
Plasma Sources Sci. Technol. 2004

[Bastien1979]

F Bastien and E Marode
The determination of basic quantities during glow-to-arc transition in a positive point-to-plane discharge
J. Phys. D: Appl. Phys., Vol. 12, 1979

[Bourdon2007]

A Bourdon, V P Pasko, N Y Liu, S Celestin, P Segur and E Marode
Efficient models for photoionization produced by non-thermal gas discharges in air based on radiative transfer and the Helmholtz equations
Plasma Sources Sci. Technol 2007

[Dong2003]

Lifang Dong, Zengqian Yina, Xuechen Lia, Zhifang Chaia, Long Wang

Spatiotemporal dynamics of discharge filaments in dielectric barrier discharges
Journal of Electrostatics 2003

[Dyakonov1989]

M.I.Dyakonov

Streamer discharge in homogeneous field
Sov phys jetp 1989

[Ebert2005]

U Ebert, C Montijn, T M P Briels, W Hundsdorfer, B Meulenbroek, A Rocco and E M van Veldhuizen

The multiscale nature of streamers
Plasma Sources Sci. Technol. 2006

[Eliasson1987]

B.Eliasson, M.hirth, U.Koge Ischatz

Ozone synthesis from oxygen in dielectric barrier discharge
J phys D appl phys 1987

[Golubovskii2002]

Yu B Golubovskii, V A Maiorov, J Behnke and J F Behnke

Influence of interaction between charged particles and dielectric surface over a homogeneous barrier discharge in nitrogen
J. Phys. D: Appl. Phys. 2002

[Guaitella2006]

O Guaitella, F Thevenet, C Guillard and A Rousseau

Dynamic of the plasma current amplitude in a barrier discharge: influence of photocatalytic material
J. Phys. D: Appl. Phys. 2006

[Hammer2004]

Th. Hammer, Th. Kappes, M. Baldauf

Plasma catalytic hybrid processes: gas discharge initiation and plasma activation of catalytic processes
Catalysis Today 2004

[Held2000]

B. Held

Analytic calculations of ozone concentration in an oxygen-fed DBD cylindrical ozonizer
Eur. Phys. J. AP 2000

[Holzer2002]

F. Holzer, U. Roland, F.-D. Kopinke

Combination of non-thermal plasma and heterogeneous catalysis for oxidation of volatile organic compounds Part 1. Accessibility of the intra-particle volume
Applied Catalysis B: Environmental 2002

[Kogelschatz1999]

Ulrich Kogelschatz, Baldur Eliasson and Walter Egli

From ozone generators to at television screens: history and future potential of dielectric-barrier discharges

Pure Appl. Chem 1999

[Kozlov2001]

K V Kozlov, H-EWagner, R Brandenburg and P Michel

Spatio-temporally resolved spectroscopic diagnostics of the barrier discharge in air at atmospheric pressure
J. Phys. D: Appl. Phys. 2001

[Kulikovskiy1997]

A A Kulikovskiy

Positive streamer between parallel plate electrodes in atmospheric pressure air
J. Phys. D: Appl. Phys. 1997

[Kulikovskiy]

A.A.Kulikovskiy

Numerical modeling of positive streamer in air in nonuniform fields: Efficiency of radicals production

[Kulikovskiy1998]

A. A. Kulikovskiy

Positive streamer in a weak field in air: A moving avalanche-to-streamer transition
Physical Review E 1998

[Kogelschatz2003]

Ulrich Kogelschatz

Dielectric-barrier Discharges: Their History, Discharge Physics, and Industrial Applications
Plasma Chemistry and Plasma Processing 2003

[Kogelschatz1999]

Ulrich Kogelschatz, Baldur Eliasson and Walter Egli

From ozone generators to at television screens: history and future potential of dielectric-barrier discharges
Pure Appl. Chem 1999

[Kulikovskiy1997]

Andrei A. Kulikovskiy

Production of Chemically Active Species in the Air by a Single Positive Streamer in a Nonuniform Field
IEEE Transactions On Plasma Science 1997

[Liu2007]

Ningyu Liu, Sébastien Célestin and Anne Bourdon, Victor P. Pasko, Pierre Ségur, Emmanuel Marode

Application of photoionization models based on radiative transfer and the Helmholtz equations to studies of streamers in weak electric fields
Applied Physics Letters 2007

[Meek1940]

J.M.Meek

a theory of spark discharge
physical review 1940

[Pancheshnyi2005]

S. Pancheshnyi, M. Nudnova, and A. Starikovskii

Development of a cathode-directed streamer discharge in air at different pressures: Experiment and comparison with direct numerical simulation
Physical Review E 2005

[Peyrous1981]

R Peyrous and R-M Millot

Ozone generation in oxygen by corona discharges in a point-to-plane gap subjected to a chopped DC positive voltage
J. Phys. D: Appl. Phys. 1981

[Roland2005]

U. Roland, F. Holzer, F.-D. Kopinke

Combination of non-thermal plasma and heterogeneous catalysis for oxidation of volatile organic compounds Part 2. Ozone decomposition and deactivation of γ -Al₂O₃
Applied Catalysis B: Environmental 2005

[Roland2005]

U. Roland,, F. Holzer, A. Popp, F.-D. Kopinke

Combination of non-thermal plasma and heterogeneous catalysis for oxidation of volatile organic compounds Part 3. Electron paramagnetic

resonance (EPR) studies of plasma-treated porous alumina
Applied Catalysis B: Environmental 2005

[Serdyuk2001]

Yu V Serdyuk, A Larsson, S M Gubanski and M Akyuz

The propagation of positive streamers in a weak and uniform background electric field
J. Phys. D: Appl. Phys. 2001

[Staack2006]

David Staack, Bakhtier Farouk, Alexander F Gutsol and Alexander A Fridman

Spectroscopic studies and rotational and vibrational temperature measurements of atmospheric pressure normal glow plasma discharges in air
Plasma Sources Sci. Technol. 2006

[Starikovskaia2001]

S M Starikovskaia, N B Anikin, S V Pancheshnyi, D V Zatsepin, and A Yu Starikovskii

Pulsed breakdown at high overvoltage: development, propagation and energy branching
Plasma Sources Sci. Technol. 2001

7.3 Soft matter, bubble motion

[Chen1998]

X. M. Chen and A. Prosperetti

Thermal processes in the oscillations of gas bubbles in tubes
J. Acoust. Soc. Am. September 1998

[Devins1959]

Charles Jr Devin

Survey of Thermal, Radiation, and Viscous Damping of Pulsating Air Bubbles in Water
The Journal Of The Acoustical Society Of America
Volume 31, Number 12 December, 1959

[Howkin1965]

S. D. Howkins

Measurements of the Resonant Frequency of a Bubble near a Rigid Boundary
The Journal Of The Acoustical Society Of America
1965

[Hao2000]

Y. Hao, A. Prosperetti

The collapse of vapor bubbles in a spatially non-uniform flow
International Journal of Heat and Mass Transfer 2000

[Jordan2004]

P.M. Jordan, C. Feuillade

On the propagation of harmonic acoustic waves in bubbly liquids
International Journal of Engineering Science 2004

[Laakkonen2005]

Marko Laakkonen, Pasi Moilanen, Juhani Aittamaa

Local bubble size distributions in agitated vessels
Chemical Engineering Journal 2005

[Leighton1987]

Timothy G Leighton and Alan J Walton

An experimental study of the sound emitted from gas bubbles in a liquid
Eur. J. Phys. 1987

[Leroy2002]

Valentin Leroy, Martin Devaud and Jean-Claude Bacri

The air bubble: experiments on an unusual harmonic oscillator
Am. J. Phys. 2002

[Leroy2005]

V. Leroy, M. Devaud, T. Hocquet, and J.-C. Bacri

The bubble cloud as an N-degree of freedom harmonic oscillator
Eur. Phys. J. E 2005

[Oguz1998]

H. N. Oguz and A. Prosperetti

The natural frequency of oscillation of gas bubbles in tubes
J. Acoust. Soc. Am. 1998

[Payne2005]

Edward M. B. Payne, Suhith J. Illesinghe, and Andrew

Symmetric mode resonance of bubbles attached to a rigid boundary
Ooi, Richard Manasseh
J. Acoust. Soc. Am. 2005

[Prosperetti 1974]

Andrea Prosperetti

viscous and nonlinear effects in the oscillations of drops and bubbles
phd thesis
california institute of technology 1974

[Prosperetti 1974]

Andrea Prosperetti

Nonlinear oscillations of gas bubbles in liquids:
steady-state solutions
J. Acoust. Soc. Am. 1974

[Prosperetti 1977]

Andrea Prosperetti

Thermal effects and damping mechanism in the forced radial oscillations of gas bubbles in liquids
J. Acoust. Soc. Am. 1977

[Piñeiro2001]

Ángel Piñeiro, Pilar Brocos, Ramón Bravo, Alfredo Amigo

A comprehensive approach to the surface tension of binary liquid mixtures
Fluid Phase Equilibria 182 2001

[Rath1981]

H. J. RATH

On the stability of gas bubbles oscillating non-spherically in a compressible liquid

7.4 Electrotechnical

Ph.D. Thesis

Contribution à l'étude et à la réalisation de commutateurs et de générateurs haute tension transitoires

Jérôme BAC

Université De Pau Et Des Pays De L Adour
2005

[Davanloo1998]

Farzin Davanloo, Carl B. Collins, and Forrest J. Agee
High-Power, Repetitive-Stacked Blumlein Pulsers

Commutated by a Single Switching Element
IEEE Transactions On Plasma Science 1998

[Davanloo]

F.Davanloo, R.P.Krause, J.D.Bhawalkar, C.B.Collins
a novel repetitive stacked blumlein pulse power source

[Deepak2001]

Deepak K Gupta And P I John

Design and construction of double-Blumlein HV pulse power supply
Sadhana 2001

[Efanov1997]

V.M.Efanov, V.V.Karavaev, A.F.Kardo-Sysoev, G.Tchashnikov

Journal of Engineering Mathematics 1981

[Strasberg1956]

M.Strasberg

Gas Bubbles as Sources of Sound in Liquids
The Journal Of The Acoustical Society Of America
1956

[Strasberg1953]

I, Strasberg

The Pulsation Frequency of Nonspherical Gas Bubbles in Liquids
The Journal Of The Acoustical Society Of America
1953

[Walton2005]

Alan J. Walton, May Glover Gunn, and George T. Reynolds

The Quality Factor of Oscillating Bubbles as an Indication of Gas Content With Particular Reference to Methane
IEEE Journal Of Oceanic Engineering 2005

Fast ionization dynistor (fid) - a new semiconductor superpower closing switch
IEEE 1997

[Katsuki2001]

S. Katsuki, D. Takano, T. Namihira, and H. Akiyama, T. Majima

Repetitive operation of water-filled Blumlein generator
Review Of Scientific Instruments 2001

[Milovanovic]

Ivana Milovanovic, Uroš Mitrovic, Nebojša Malešević, Jovan M. Cvetic

Development of Rotary Spark Gap for a Tesla Coil Apparatus

[MacGregor]

S. J. MacGregor, S. M. Turnbull, F.A. Tuema, O. Farish
Increasing the performance of high pressure spark gap switches

[Pecastaing2003]

L. Pecastaing, T. Rees, J. Paillol, A. Gibert, and P. Domens

Voltage gain optimization of transmission line transformers
Eur. Phys. J. AP 2003

[Rishi2004]

Rishi et al

A transmission line based compact repetitive and portable cascaded blumlein pulser
IEEE 2004

[Rim2003]

Geun-Hie Rim, Evgeny P. Pavlov, Hong-Sik Lee, Jongsoo S. Kim, and Young-Wook Choi
Pulse Forming Lines for Square Pulse Generators
IEEE Transactions On Plasma Science 2003

[Roche]

Dr. Stephan Roche
Solid State Pulsed Power Systems

[Rossi2002]

José Osvaldo Rossi, Mário Ueda, and Joaquim José Barroso
Design of a 150-kV 300-A 100-Hz Blumlein Coaxial Pulser for Long-Pulse Operation
IEEE Transactions On Plasma Science 2002

[Rossi2003]

J.O. Rossi, M. Ueda, J.J. Barroso
A 150kV/300A/1 μ s coaxial blumlein pulser
IEEE 2003

[Rossi]

J.O. Rossi, M. Ueda And J.J. Barroso Design and Construction of a150kV/300A/1 μ s Blumlein Pulser

[Rossi2006]

José O. Rossi, Member, IEEE, Joaquim J. Barroso, and Mário Ueda
Modeling of Wound Coaxial Blumlein Pulsers
IEEE Transactions On Plasma Science 2006

[Sevick2004]

Jerry Sevick
A Simplified Analysis of the Broadband Transmission Line Transformer
Bell Laboratories 2004

[Sundararajan2005]

Raji Sundararajan, G. R. Nagabhusana, N. K. Kishore, Esaki Soundarajan
Influence of Peaking Capacitors in Reducing Rise Times of High-Voltage Nanosecond Pulses
IEEE Transactions On Industry Applications 2005

[Trask2006]

Chris Trask,
Transmission Line Transformers: Theory, Design and Applications — Part 2
Sonoran Radio Research 2006

[Verma2006]

Rishi Verma, A Shyam And Kunal G Shah
Design and performance analysis of transmission line-based nanosecond pulse multiplier
Sadhana 2006

[Wilson]

C.R.Wilson, G.A.Erickson, and P.W.Smith
Compact, repetitive, pulsed power generators based on transmission line transformers

[Xiao]

S. Xiao, J. Kolb, S. Kono, S. Katsuki, R. P. Joshi, M. Laroussi, and K. H. Schoenbach
High power, high recovery rate water switch